JAERI-M--91-062

JP9105202

JAERI - M
91-062

NEANDC(J)-162 U
INDC(JPN)-151 L

PROCEEDINGS OF THE SECOND SPECIALISTS' MEETING ON NUCLEAR DATA FOR FUSION REACTORS

March 1991

(Eds.) Yutaka NAKAJIMA and Hiroshi MAEKAWA

日 本 原 子 力 研 究 所
Japan Atomic Energy Research Institute

JAERI-M レポートは、日本原子力研究所が不定期に公刊している研究報告書です。
入手の問合わせは、日本原子力研究所技術情報部情報資料課（〒319-11 茨城県那珂郡東海村）あてに、お申し込みください。なお、このほかに財団法人原子力弘済会資料センター（〒319-11 茨城県那珂郡東海村日本原子力研究所内）で複写による実費頒布をおこなっております。

JAERI-M reports are issued irregularly.

Inquiries about availability of the reports should be addressed to Information Division Department of Technical Information, Japan Atomic Energy Research Institute, Tokai-mura, Naka-gun, Ibaraki-ken 319-11, Japan.

編集兼発行　日本原子力研究所
印　　刷　　

JAERI-M 91-062

Proceedings of the Second Specialists' Meeting on Nuclear Data for Fusion Reactors

(Eds.) Yutaka NAKAJIMA and Hiroshi MAEKAWA

Japanese Nuclear Data Committee
and
Japanese Research Committee on Reactor Physics
Tokai Research Establishment
Japan Atomic Energy Research Institute
Tokai-mura, Naka-gun, Ibaraki-ken

(Received March 6, 1991)

This report consists of the Proceedings of the Second Specialists' Meeting on Nuclear Data for Fusion Reactors. The meeting was held on December 20 - 21, 1990, at the Tokai Research Establishment, Japan Atomic Energy Research Institute with the participation of forty-odd specialists, who were the evaluators of the fusion related data in JENDL-3, the members of Working Groups on Nuclear Data for Fusion, on Activation-Cross-Section Data and on Fusion Neutronics Integral Test in the Japanese Nuclear Data Committee, and the members of the Subcommittee on Fusion Reactor in the Japanese Research Committee on Reactor Physics. The First Specialists' Meeting was held on July 23 ~ 25, 1985 with the participation of twenty-odd specialists. The presentations and discussions of the First Meeting were compiled in the Proceedings (JAERI-M 86-029) and have been very useful for the evaluation of JENDL-3 and the study on fusion neutronics. The main object of the Second Meeting was to review the evaluated data of JENDL-3 and the results of integral tests, and to contribute the discussions and conclusion of the meeting for the development of JENDL and promotion of research in fusion neutronics. After the general review of the evaluation work, the results of benchmark tests were presented for the following subjects, which were followed by the lively discussions among the evaluators and users for each subject:

(1) nuclear data relevant to blanket materials of fusion reactors

(2) nuclear data relevant to structural materials

(3) gamma-ray production data

(4) activation cross section data.

The discussion was at coalescing and the research for the main nuclides relevant to the fusion reactors was supposed to be very close to being complete.

Organizing Committee

Hiroshi	MAEKAWA (Chairman)	(JAERI)
Akira	HASEGAWA	(JAERI)
Kazuaki	KOSAKO	(JAERI)
Koichi	MAKI	(JAERI)
Yutaka	NAKAJIMA	(JAERI)
Yukio	OYAMA	(JAERI)

Keywords: Proceedings, Nuclear Data, Fusion Reactor, Benchmark Test, JENDL, Evaluation

JAERI－M 91－062

第２回核融合炉核データ専門家会議報文集

日本原子力研究所東海研究所
シグマ研究委員会・炉物理研究委員会
（編）中島　豊・前川　洋

（1991年３月６日受理）

本報文集は，第２回核融合炉核データ専門家会議の報文及び討論内容を収録したものである。専門家会議は，1990年12月20日と21日の両日日本原子力研究所東海研究所において40数名の専門家の出席のもとに開催された。出席した専門家は，JENDL－３の核融合炉に関連する核種の核データの評価者，シグマ研究委員会核融合炉核データワーキンググループ，放射化断面積ワーキンググループと核融合ニュートロニクス積分テストワーキンググループのメンバー及び炉物理研究委員会核融合炉専門部会のメンバーであった。第１回会合は，1985年７月23～25日20数名の専門家の出席のもとに開催され，会議での発表と討論は，報文集(JAERI－M 86－029)にまとめられ，JENDL－３の評価と核融合炉ニュートロニクスの研究の進展に大いに役立った。今回の会議の主要目的は，核融合炉関連核種に関するJENDL－３の評価データをレビューし，ベンチマークテストの結果を評価者と利用者の両者で検討し，JENDLと核融合炉中性子工学の研究の発展に役立てる事にあった。

核融合炉ブランケット関連核種，構造材核種，ガンマ線関連データ，放射化断面積等の評価データに関する，JENDL－３核データの総合的なレビューとそれに関連するベンチマークテストの結果が報告された後，活発な討論が行われた。評価者と利用者の両者の討論はかつてなくかみ合っており，この分野に関連する研究は完熟に近づいている事をうかがわせた。

第２回核融合炉核データ専門家会議幹事会

前川　洋（幹事長）	（日本原子力研究所）
大山　幸夫	（日本原子力研究所）
小迫　和明	（日本原子力研究所）
中島　豊	（日本原子力研究所）
長谷川　明	（日本原子力研究所）
真木　紘一	（日本原子力研究所）

東海研究所：〒319－11　茨城県那珂郡東海村白方字白根２－４

Contents

目　　次

1. Nuclear Data for Fusion Reactors and Development of JENDL-3

1.1 Background and Scope of the Specialists' Meeting on Nuclear Data for Fusion Reactors

Hiroshi MAEKAWA
Department of Reactor Engineering
Japan Atomic Energy Research Institute
Tokai-mura, Naka-gun, Ibaraki-ken, 319-11 Japan

Circumstances of Data Testing

First I would like to describe briefly how this meeting came about. In May 1983, a tentative nuclear data file for fusion neutronics study was requested to the Japanese Nuclear Data Committee. Because JENDL-2 was prepared mainly for fission reactor and its accuracy was not enough for fusion neutronics. Especially, there are problems in the nuclear data above 5 MeV.

In December 1983, JENDL-3PR1, having 8 nuclei of ^{6}Li, ^{7}Li ^{9}Be, ^{12}C, ^{16}O, Cr, Fe and Ni, was completed. Three nuclei of ^{6}Li, ^{7}Li and ^{12}C were re-evaluated in March 1985. Both nuclear data files were used for the analyses of experiments relevant to fusion neutronics at FNS/JAERI and OKTAVIAN/Osaka University.

In July 1985, the first Specialists' Meeting on Nuclear Data for Fusion Neutronics was held at JAERI Tokai Research Establishment. The proceedings was published as JAERI-M 86-029. The meeting was very fruitful and full of suggestions.

The working group of fusion neutronics integral test was starting in April 1987 for the data testing of JENDL-3. A tentative version was released in April 1987 as JENDL-3T Rev. 0. The file has 32 nuclei For the data testing, the cross section library FSX125/J3T for ANISN/DOT codes was prepared and distributed in October 1987. The library has 125-group for neutron and 16 nuclei. The results of integral test was reported at the 1987 Seminar on Nuclear Data (JAERI-M 88-065). At the Seminar, many groups pointed out the problem of Be and Pb nuclear data. A technical meeting was held to discuss the problems in mainly Be and Pb data in December 1987.

In March 1988, the revised version was released as JENDL-3T Rev. 1. This version is just the same as JENDL-3. For the data testing, the cross section library FUSION-J3 for ANISN/DOT codes was prepared and distributed to users in October 1989. The library, whose structure is 125-group for neutron and 40-group for gamma-ray, has 40 nuclei. Some of data testing results were reported at the 1989 Seminar on Nuclear Data (JAERI-M90-025). The cross section library FSXLIB for the Monte Carlo code MCNP was distributed to users in April 1990. The library has 48 nuclei.

Purpose of Meeting

The purpose of this meeting is to discuss frankly among the specialists, i.e., evaluators, experimentists, data testing groups and users such as fusion reactor designers, basing on the results of data testing for JENDL-3 in order to contribute the fusion neutronics and next stage following to JENDL-3.

Scope of Meeting

Following discussions are expected in the meeting:

(1) Status and problems of JENDL-3.
- ·Nuclei relevant to fusion blanket
- ·Nuclei relevant to structure material
- ·Gamma-ray data
- ·Activation cross section data
- ·Nuclear data for radiation damage

(2) How to improve the data in JENDL-3 from those in JENDL-3PR1, -3PR2 and -3T.

(3) Differences between JENDL-3 and the other files such as ENDF/B-IV.

(4) Necessity of special file for fusion neutronics.
- ·ENDF/B-VI format, double differential cross section (DDX)
- ·Nuclear data relevant to material development (> 20 MeV)
- ·Nuclear data relevant to safety

1.2 Review of JENDL-3 Evaluation Work

Tsuneo NAKAGAWA
Tokai Research Establishment
Japan Atomic Energy Research Institute
Tokai-mura, Naka-gun, Ibaraki-ken 319-11

Before completion of final JENDL-3, tentative versions, JENDL-3PR1 and JENDL-3PR2, were made for use in fusion neutronics in 1983 and 1985, respectively, and JENDL-3T was compiled for benchmark tests of JENDL-3 in 1987. JENDL-3PR1 contains the data for eight nuclides important for fusion neutronics, and JENDL-3PR2 the revised data of three nuclides. Evaluation for these preliminary files is briefly reviewed in this talk.

1. Introduction

The second version of Japanese Evaluated Nuclear Data Library (JENDL-2)[1] was released in December 1982. As is described in Chapter 2, however, JENDL-2 is not applicable to fusion neutronics. Therefore, JENDL-3PR1 was made in order to answer to the requirements from fusion community in Japan. This tentative version consists of only the data of eight nuclides (^{6}Li, ^{7}Li, ^{9}Be, ^{12}C, ^{16}O, Cr, Fe and Ni) important for fusion neutronics. After some tests of JENDL-3PR1, the data were partly modified to JENDL-3PR2. The next tentative version was JENDL-3T which was compiled for wide benchmark tests for various application fields.

Finally, JENDL-3[2] was completed and released in 1989, after modification of JENDL-3T data according to the benchmark tests and by adding data of many nuclides. In this talk, a review of evaluation work for the above mentioned eight nuclides will briefly made.

2. JENDL-2

Evaluation and compilation work of JENDL-2 was finished in December 1982, and its first revision was made in 1984, by modifying some trivial mistakes and adding descriptive information in File 1(MF=1). The purpose of JENDL-2 had been application for fast and

thermal reactors, shielding calculations and for fusion neutronics. Benchmark tests of JENDL-2 confirmed the applicability of JENDL-2 to the fast and thermal reactors, and shielding calculations. However, it was revealed by the benchmark tests that JENDL-2 was not able to be used for the fusion neutronics calculations because the JENDL-2 data were not reliable above about 5 MeV.

Measurement of double differential neutron emission cross sections (DDX) was started in 1981 at the Osaka University by using the intense 14-MeV neutron source facility of OKTAVIAN[3]. The measured DDX data were extensively compared with various evaluated data. Figure 1 shows an example of the DDX for natural lithium. In comparison with the experimental data[4], the JENDL-2 data seem to be too small and its shape is not good in the entire energy region of secondary neutrons. The reason of this disagreement is that JENDL-2 gives only an evaporation spectrum for the inelastic scattering in the continuum and ignores discrete inelastic scattering cross sections to highly excited levels.

Disagreements of JENDL-2 and measured cross sections were also found for some important reactions around 14 MeV. Furthermore, in the case of ^{16}O, JENDL-2 dose not contain any evaluated data and use of ENDF/B-IV was recommended.

For structural material nuclides, almost the same problems were found. Figure 2 is a comparison of the DDX measured at OKTAVIAN[4] with evaluated data. The DDX calculated from JENDL-2 is too small in the secondary neutron energy region from 4 to 13 MeV. The cross section of the inelastic scattering to the first excited level of ^{56}Fe is shown in Fig. 3. JENDL-2 is too small above 4 MeV. The reason of these disagreements is quite obvious. The evaluation for JENDL-2 did not take into account the contributions of direct and preequilibrium processes for the inelastic scattering. Only calculations with optical and statistical models were made for almost all nuclides.

3. JENDL-3PR1

It was pointed out as a result of comparison of the DDX data that JENDL-2 was not applicable to the fusion neutronics calculations. However, in JAERI, the Japan-USA Joint Mock-up Experiment of Fusion Blanket was scheduled to start in 1983 by using JAERI Fusion Neutronics Source (FNS). For the analysis of its experimental results, a reliable evaluated data set was urgently required. Therefore, revision work

of JENDL-2 data for selected nuclides which were important for fusion neutronics was made by the member of JAERI Nuclear Data Center and Japanese Nuclear Data Committee (JNDC). The evaluation was made for only eight nuclides (^{6}Li, ^{7}Li, ^{9}Be, ^{12}C, ^{16}O, Cr, Fe and Ni), and evaluated data were compiled in the ENDF-5 format as JENDL-3PR1 (JENDL-3 preliminary version 1) which was released at the end of 1983.

The data of lithium isotopes were evaluated by Shibata[5,6]. The neutron spectra from the inelastic scattering in the continuum were calculated with the three-body phase space model. The DDX calculated from JENDL-3PR1 is given in Fig. 1. JENDL-3PR1 reproduced the structure at 9 MeV, while the values were still too small. The energy-angle correlation data were also given in File 6 (MF=6) of the ENDF-5 format. Photon-production data were newly evaluated.

A new evaluation of ^{9}Be and ^{12}C data was also made by Shibata[7,8]. The ^{9}Be(n,2n) reaction was treated as a sequential reaction. In the case of ^{12}C, only one level was considered in JENDL-2, while three levels up to 9.63 MeV were taken into account in JENDL-3PR1. Photon-production data were given for the both nuclides.

The data of ^{16}O were evaluated by Working Group on Nuclear Data for Fusion[9]. Below 3 MeV, the R-matrix theory was used to calculate the total and elastic scattering cross sections. Above 3 MeV, many experimental data were available to decide the evaluated cross section curves. The inelastic scattering cross section was calculated with the statistical model. The coupled-channel theory was partly applied. The other partial cross sections were based on available experimental data.

The re-evaluation for structural materials was performed by Kikuchi et al.[10] Since the time was not enough to make a full evaluation, they modified the inelastic scattering data of JENDL-2 by adding their results obtained from theoretical calculation with ECIS[11] for the direct process and with GNASH[12] for the preequilibrium process. The calculation was made for only main isotopes; ^{52}Cr, ^{56}Fe and ^{58}Ni. The result for the inelastic scattering to the first level of ^{56}Fe is shown in Fig. 3. JENDL-3PR1 is superior to the JENDL-2 data above 4 MeV and agreed very well with the experimental data of Hyakutake et al.[13] at 14 MeV. The angular distributions are shown in Fig. 4. A very good agreement with experimental data is found in the case of JENDL-3PR1. Therefore, the DDX data were also very much

improved as shown in Fig. 2.

4. JENDL-3PR2

As shown above, JENDL-3PR1 is much better than JENDL-2. However, after careful comparison with new experimental data measured at OKTAVIAN[3] and Tohoku University[14], the following problems were pointed out for ^{6}Li, ^{7}Li and ^{12}C.

1) More high energy excited levels should be taken into consideration.
2) Neutron spectra are not good enough.
3) The cross section of ^{6}Li(n,2n) is about 20-% larger than experimental data at 14 MeV.
4) The angular distributions of inelastically scattered neutrons should not be isotropic in the center-of-mass system. And so on.

According to these suggestions, improvement of the data for ^{6}Li, ^{7}Li and ^{12}C was made and JENDL-3PR2 was editted in 1985.

The data of lithium isotopes were revised by Chiba[15] on the basis of the DDX data measured at OKTAVIAN and Tohoku University. In order to reproduce a tendency of energy-angle correlation found in the measured DDX, pseudo-level representation was adopted for the continuum inelastic scattering which is a break-up reaction as ^{6}Li(n,n'd)α and ^{7}Li(n,n't)α, respectively. The cross section values were also modified for the ^{7}Li(n,n't)α and ^{6}Li(n,2n) reactions. Figure 5 gives an example of DDX. JENDL-3PR2 shows excellent agreement with the experimental data[14]. The data of ^{12}C were modified by Shibata so as to reproduce well the experimental data of DDX.

5. JENDL-3T

Evaluation work for important nuclide data had been finished, and JENDL-3T which was a temporary version for benchmark tests was compiled in 1987. In JENDL-3T, the data of lithium isotopes and ^{12}C were slightly modified from JENDL-3PR2. The data of Cr, Fe and Ni were completely replaced with new evaluations[16] made by Asami for Cr, by Iijima and Yamakoshi for Fe and by Iijima for Ni. The new evaluations were made by using GNASH, DWUCK[17] and PEGASUS[18], and recent experimental data. For the final JENDL-3, the DWUCK calculation for direct process was replaced with a coupled-channel calculation with ECIS as

is explained by Asami[19].

JENDL-3T contained the data for about 70 nuclides. Benchmark tests for fusion neutronics was performed by Fusion Neutronics Integral Test Working Group, and its results were presented by Maekawa[20] at the 1987 Seminar on Nuclear Data. By this tests, re-evaluation of ^{9}Be and Pb data was strongly recommended.

6. JENDL-3

According to the results of the benchmark tests for fusion neutronics, fast and thermal reactors, shielding, etc., the JENDL-3T data were modified partly. Then, JENDL-3[2] was released at the end of 1989. In the case of light nuclides, the data modified are those of ^{9}Be(n,2n), inelastic scattering of ^{7}Li, total cross section of ^{12}C and ^{16}O. The data of structural materials were also slightly modified. Details of the JENDL-3 data will be described by Chiba[21] for light nuclides and Pb, by Asami[19] for structural materials, at this Meeting.

In December 1990, evaluation and compilation work of fission product nuclide data was completed, and the first modification was made for the JENDL-3 general purpose file. Finally, JENDL-3 contains the data for 324 nuclides in the ENDF-5 format.

7. Conclusion

Evaluation work of ^{6}Li, ^{7}Li, ^{9}Be, ^{12}C, ^{16}O, Cr, Fe and Ni for the preliminary files of JENDL-3 was reviewed. The data have been revised every two years, by mainly taking account of DDX data measured at Osaka University and Tohoku University, and results of benckmark tests. As a result, JENDL-3 has become a reliable data set for fusion neutronics applications.

As one of JENDL special purpose files, a file for fusion neutronics is being made in the Nuclear Data Center, JAERI. This file is compiled in the ENDF-6 format by giving data in File 6 (MF=6) so as to reproduce energy-angle correlation. At the same time, modification of JENDL-3 data will be performed for some nuclides which do not reproduce well the measured DDX data. The nuclides stored in this file will be determined by taking account of discussions at this Meeting.

References

1) (Ed.) Nakagawa T.: "Summary of JENDL-2 General Purpose File", JAERI-M 84-103 (1984).

2) Shibata K., Nakagawa T., Asami T., Fukahori T., Narita T., Chiba S., Mizumoto M., Hasegawa A., Kikuchi Y., Nakajima Y., and Igarasi S.: "Japanese Evaluated Nuclear Data Library, version-3", JAERI 1319 (1990).

3) Takahashi A.: Proc. of Specialist's Meeting on Nuclear Data for Fusion Neutronics", JAERI-M 86-029, p.99 (1986).

4) Takahashi A., Yamamoto J., Oshima K., Ueda M., Fukazawa M., Yanagi Y., Miyaguchi J., and Sumita K.: "Measurements of Double Differential Neutron Emission Cross Sections for Fusion Reactor Candidate Elements", OKTAVIAN Report A-83-03 (1983).

5) Shibata K.: "Evaluation of Neutron Nuclear Data of ^{6}Li for JENDL-3", JAERI-M 84-198 (1984).

6) Shibata K.: "Evaluation of Neutron Nuclear Data of ^{7}Li for JENDL-3", JAERI-M 84-204 (1984).

7) Shibata K.: "Evaluation of Neutron Nuclear Data for ^{9}Be for JENDL-3", JAERI-M 84-226 (1984).

8) Shibata K.: "Evaluation of Neutron Nuclear Data for ^{12}C", JAERI-M 83-221 (1983).

9) Shibata K.: private communication (1984).

10) Kikuchi Y., Shibata K., Asami T., Sugi T., Yamakoshi H., and Kitajima N.: J. Nucl. Sci. Technol., 22, 499 (1985).

11) Raynal J.: "Computing as a Language of Physics", Trieste, 1971, p.281 (1972).

12) Young P.G., and Arthur E.D.: "GNASH: A Preequilibrium, Statistical Nuclear-Model Code for Calculation of Cross Sections and Emission Spectra", LA-6947 (1977).

13) Hyakutake M., Matoba M., Tonai T., Niidome J., and Nakamura S.: J. Phys. Soc. Japan, 38, 606 (1975).

14) Chiba S., Baba M., Nakashima H., Ono M., Yabuta N., Yukinori S., and Hirakawa N.: J. Nucl. Sci. Technol., 22, 771 (1985).

15) Chiba S., and Shibata K.: "Revision and Status of the Neutron Nuclear Data of ^{6}Li and ^{7}Li", JAERI-M 88-164 (1988).

16) Iijima S., Asami T., Shibata K., and Yamakoshi H.: Proc. of Int. Conf. on Nuclear Data For Science and Technol., May 30-June

3, 1988, Mito, p.627 (1988).
17) Kunz P.D.: unpublished.
18) Iijima S., Sugi T., Nakagawa T., and Nishigori T.: Proc. of the 1986 Seminar on Nuclear Data, JAERI-M 87-025, p.337 (1987).
19) Asami T.: presented at this Meeting.
20) Maekawa H.: Proc. of the 1987 Seminar on Nuclear Data, JAERI-M 88-065, p.198 (1988).
21) Chiba S.: presented at this Meeting.
22) Iguchi T., Oyama Y., Nakada T., Doi T., and Kikuchi Y.: private communication (1984).
23) Chiba S.: Proc. of Specialists' Meeting on Nuclear Data for Fusion Neutronics, JAERI-M 86-029, p.32 (1986).

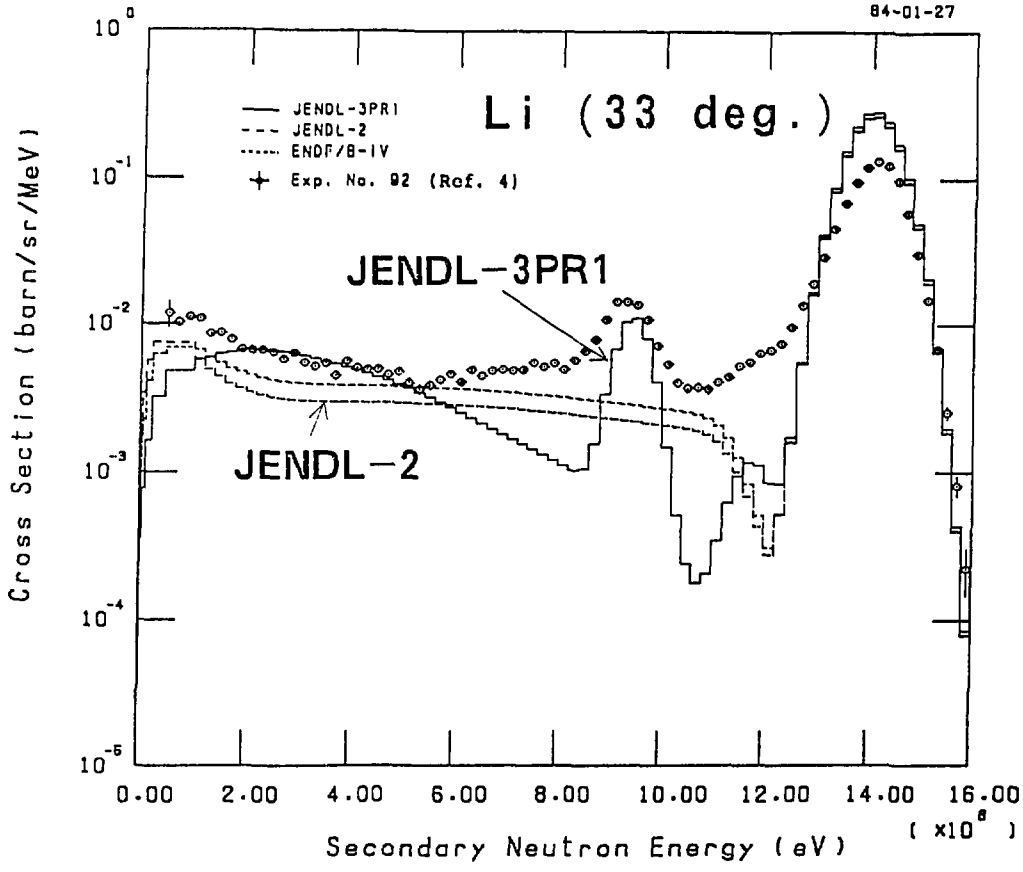

Fig. 1 Double-differential neutron emission cross section of natural lithium at the incident neutron energy of 14.8 MeV and the scattered angle of 33 degrees. Experimental data were those measured at OKTAVIAN[4]. This graph was made by Iguchi et al.[22]

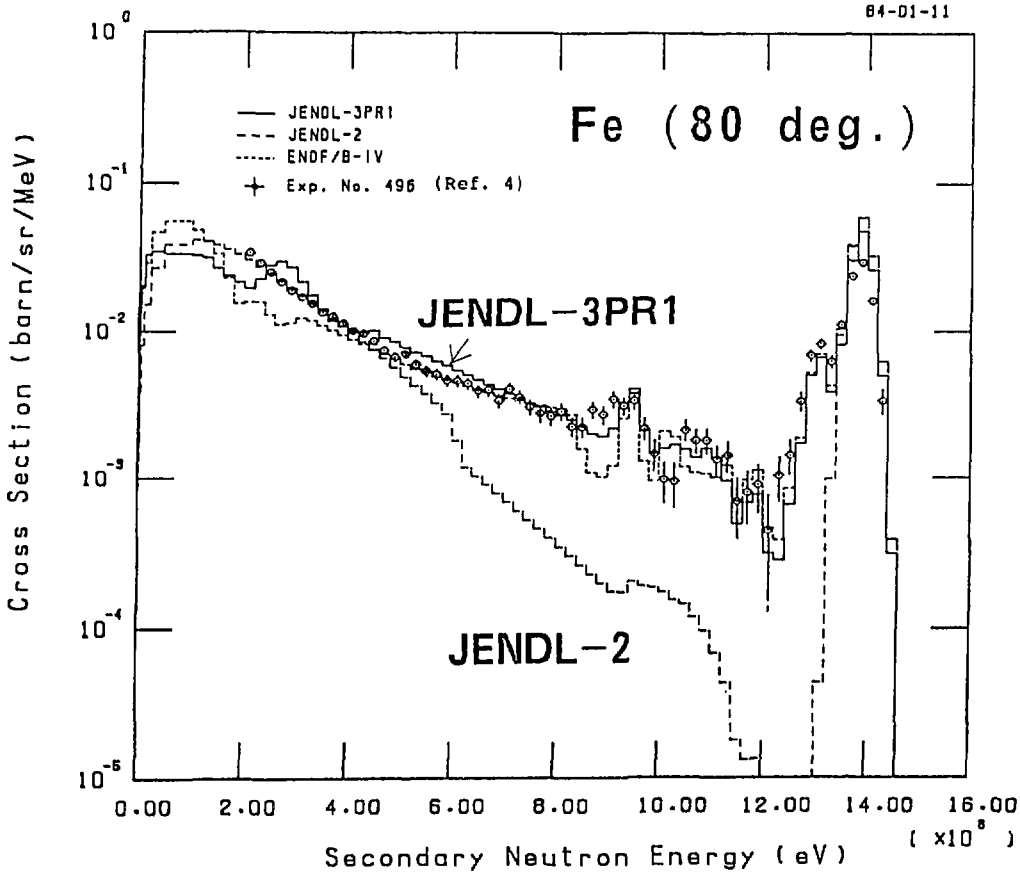

Fig. 2 Double-differential neutron emission cross section of natural iron at the incident neutron energy of 14.25 MeV and the scattered angle of 80 degrees (taken from Ref. 22).

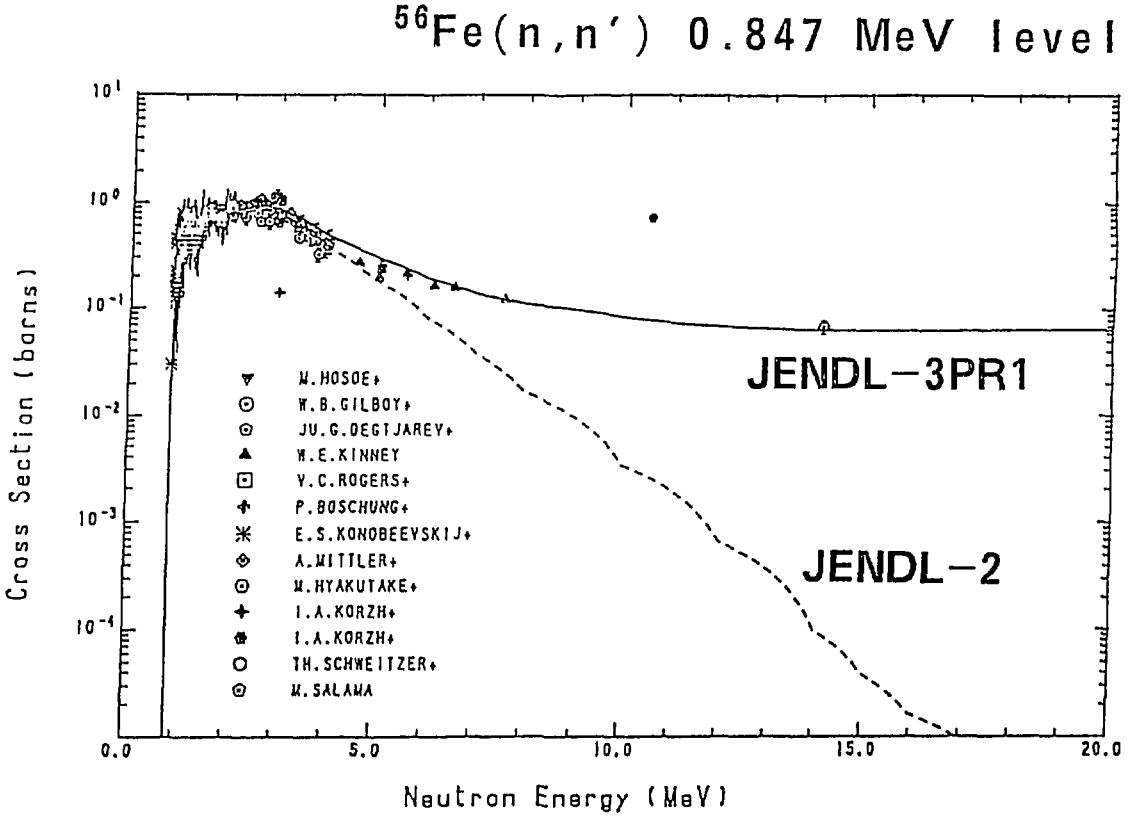

Fig. 3 ^{56}Fe inelastic scattering cross section to the 0.847 MeV level.

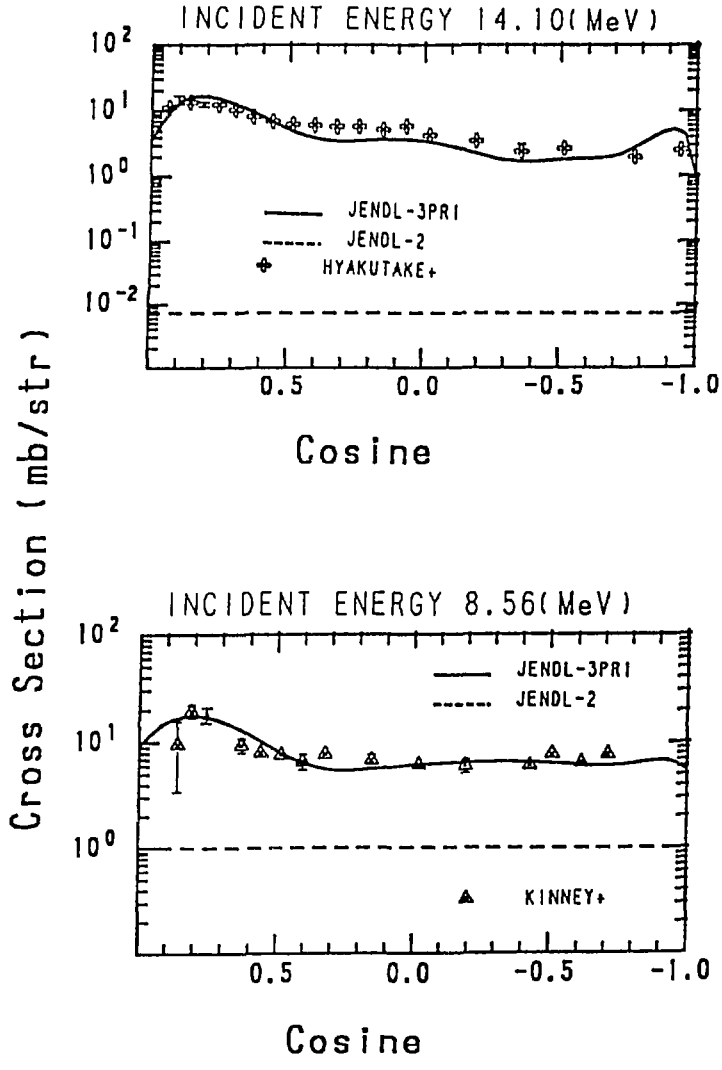

Fig. 4 Angular distributions of inelastically scattered neutrons from $^{56}Fe(n,n')$ reaction to the 0.847 MeV level, at the incident neutron energies of 8.56 and 14.1 MeV.

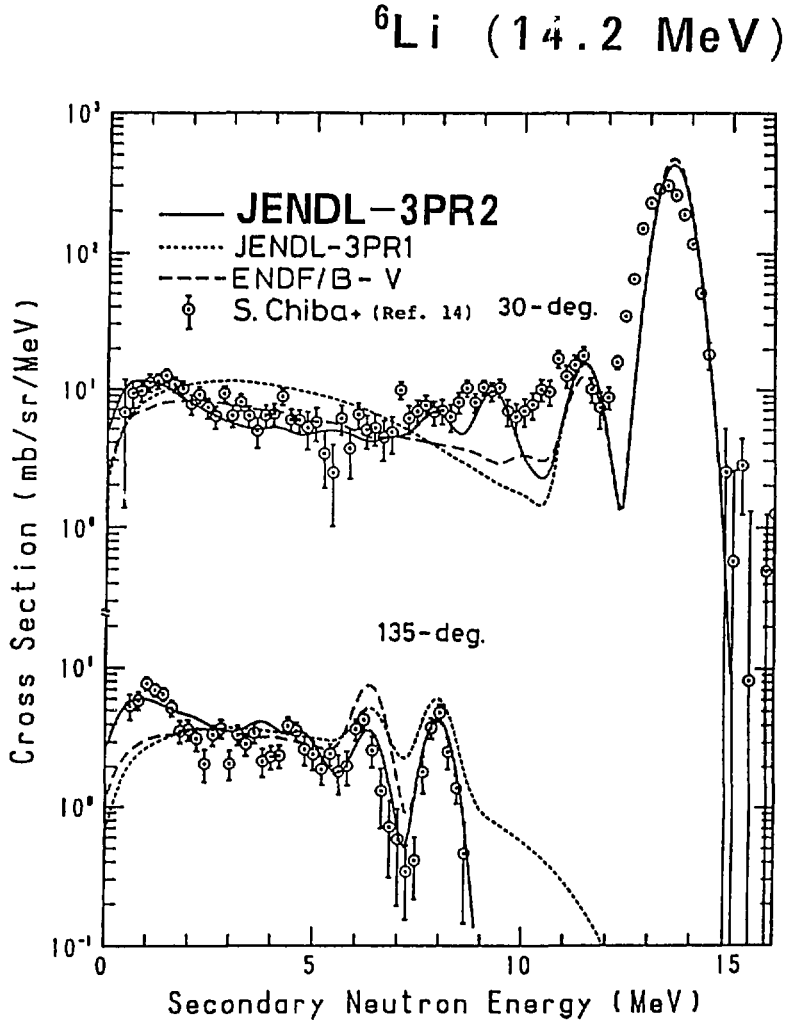

Fig. 5 Double-differential neutron emission cross section of ^{6}Li at the incident neutron energy of 14.2 MeV. (taken from Ref. 23).

2. Preparation of Reactor Constants

2.1 JSSTDL-295n-104γ; a Common Nuclear Group Cross-Section Library Based on JENDL-3 Nuclear Data File

Akira HASEGAWA

Shielding Laboratory, Department of Reactor Engineering

Tokai Research Establishment,
Japan Atomic Energy Research Institute,
Tokai-mura, Naka-gun, Ibaraki-ken, 319-11 Japan

abstract

JSSTDL 295n-104γ : a common group cross-section library system has been developed in JAERI to be used in fairly wide range of applications in nuclear industry. This system is composed of a common 295n-104γ group cross-section library based on JENDL-3 nuclear data file and its utility codes. Target of this system is mainly focused to the criticality or shielding calculations in fast and fusion reactors. Group structure is defined so as to cover almost all group structures currently used in Japan. Neutron cross-sections and photon production cross-sections are processed by Prof. GROUCH-G/B code system and γ ray transport cross-sections are generated by GAMLEG-JR. In this paper, outline of the JSSTDL library system is presented with some emphases on the design philosophy. Effects of self-shielding factor (f-table) is also shown in conjunction with the analysis of the ASPIS natural iron deep penetration experiment. Without considering resonance self-shielding effect in resonance energy region for resonant nuclides like iron, the results is completely missled in the attenuation profile calculation in the shields.

keywords: group constants library, JSSTDL system, JENDL-3, fast reactor, fusion reactor, shielding, self-shielding factor, iron, deep penetration, attenuation profile, calculation, ASPIS.

1. Out line of JSSTDL-295n-104γ common group cross-section library

This library is a common group cross-section library recently developed in JAERI by the author under the cooperation of Working Group on Standard Group Constants affiliated by the Committee of Group Constants of JNDC (Japanese Nuclear Data Committee). This work was promoted by Nakazawa Committee's recommendation /1/ deserted to the JNDC (Proposal on Post-JENDL-3 Activity Programme for JNDC, 1986) defining the working frame of JNDC after JENDL-3 project was completed. In this recommendation, it was writ-

ten that JNDC should supply commonly usable group cross-section library for primary data users like fast or fusion reactor designers in no delay of JENDL-3 release. Such a system has been requested for many years by various nuclear data users, particularly nuclear design group. Up to now shielding and criticality calculations have been performed in different calculation paths using the different group constants libraries, i.e., in different group structures and data sources due to the characteristics of the calculations involved. Finer group structure is inevitably necessary for the shielding or fusion reactor calculations but relatively coarse group structure is sufficient for the criticality calculations. Hence there have been many requests for supplying a common library applicable both for the criticality and shielding or fusion calculations. Users are also very keen for using the latest nuclear data.

Responding to these requests, specifications of the common group constants were decided. In Table 1.1 specification of JSSTDL system is shown. Most users insist to maintain their own group structure which has been so far used. Therefore a universal group structure was decided to cover almost all group structures used in Japan, as seen in Table 1.2 ~ 1.3, so as to produce their own required group structure library from a master library. It was also decided to prepare a library for design codes most frequently used such as ANISN /2/, DOT /3/ or MORSE /4/. Resonance self-shielding factors were also considered for primary reactions. Scattering matrices were calculated up to P5 components and were stored independently for elastic and inelastic scatterings so as to use the different self-shielding factors. For secondary γ production cross sections, data are stored for the following 4 reactions, i.e., total, capture((n,γ) MT:102 only), fission(MT:18), other than capture and fission ((n,n'),(n,p),(n,α),...), to reflect self-shielding factor for capture and fission reactions in neutrons. Gamma transport cross-section are generated by GAMLEG-JR /5/.

Table 1.1 Group cross-section library processing specification

Group structure	neutron:295 gamma:104
Weighting spectrum	Maxwellian from 1.0E-5 to 0.3224 eV the rest is 1/E.
Resonance reconstruction tolerance	0.1%
Self-shielding factor	
Temperature grid	300 600 900 2100 Kelvin
σ_0 grid	0 0.1778 1 10 10^2 10^3 10^4 10^5 10^6 barn
Self-shielding factor reaction	total, elastic, capture, fission.
Anisotropic Pl order	5

A utility routine was developed to enhance portability of this system to other sites or machines. Routines for group collapsing and for generating region dependent macro-scopic cross sections were also developed and released with the library. In the Table 1.4, all of the routines developed are shown.

Up to now, 63 nuclides were processed and stored for JSSTDL library from JENDL-3 general purpose file /6/. Gamma data are furnished for 32 nuclides out of 63 processed nuclides. Almost all nuclides available of γ production data in JENDL-3 were processed. Detailed list of processed nuclides are given in Table. 1.5 ~ 1.6. For the processing of JENDL-3 neutron and γ production cross-section, Prof.GROUCH-G/B /7/ system and its utility codes were fully used. Actual processing codes used are shown in Fig.1.1.

Table 1.2 Neutron group boundaries considered in JSSTDL system

Library name	groups
JSD-100	100
JSD-1000	100
BERMUDA-121	121
FNS-125	125
VITAMIN-C	171
VITAMIN-J(E+C)	175
GICX-42	42
ABBN-25	25
JFS-New	70
GAM-123(fast only)	92
MGCL-137(fast only)	91
WIMS-69(fast only)	28

Table 1.3 Gamma group boundaries considered in JSSTDL system

Library name	groups
CSEWG-94	94
LANL-12	12
STEINER-21	21
STRAKER-22	22
LANL-48	48
LANL-24	24
BERMUDA-36	36
HONEYCOMB-15	15

Table 1.4 Developed utility codes for JSSTDL system

code		
neutron-lib.	gamma-lib.	comment
CONVJSS	CONVJGG	format conversion code Binary <==> EBCDIC
CONDNSJ	CONDNSJG	collapsing code to any broad group 295 <==> User specified group (JSD100, BERMUDA-125, etc)
NACROJ	MACROJG	region dependent macro-scopic cross section creation for ANISN,DOT,MORSE code.

Table 1.5 JSSTDL-295 PROCESSED NUCLIDES
as of 1990 Nov.22

order	gamma	Z	ch	A	MAT	NCODE	comment
1	G	1	H	1	3011	117	
2		1	H	2	3012	127	
3		2	He	3	3021	237	
4		2	He	4	3022	247	
5	G	3	Li	6	3031	367	
6	G	3	Li	7	3032	377	
7	G	4	Be	9	3041	497	
8	G	5	B	10	3051	507	
9	G	5	B	11	3052	517	
10	G	6	C	12	3061	607	
11	G	7	N	14	3072	707	
12	G	8	O	16	3081	807	
13		9	F	19	3091	907	
14	G	11	Na	23	3111	1107	
15	G	12	Mg	0	3120	1207	
16	G	13	Al	27	3131	1307	
17	G	14	Si	0	3140	1407	
18		15	P	31	3151	1507	
19		16	S	0	3160	1607	
20		19	K	0	3190	1907	
21	G	20	Ca	0	3200	2007	
22	G	22	Ti	0	3220	2207	
23		23	V	51	3231	2307	
24	G	24	Cr	0	3240	2407	
25	G	25	Mn	55	3251	2557	
26	G	26	Fe	0	3260	2607	
27	G	28	Ni	0	3280	2807	
28	G	29	Cu	0	3290	2907	
29		31	Ga	0	3100	3108	ENDF/B-VI
30	G	40	Zr	0	3400	4007	
31	G	41	Nb	93	3411	4137	
32	G	42	Mo	0	3420	4207	
33		48	Cd	0	3480	4807	
34	G	63	Eu	0	3630	6307	
35	G	72	Hf	0	3720	7207	
36	G	73	Ta	81	3731	7307	
37	G	74	W	0	3740	7407	
38	G	82	Pb	0	3820	8207	
39	G	83	Bi	209	3831	8397	

Table 1.6 JSSTDL-295 PROCESSED NUCLIDES
as of 1990 Nov.22 (continued)

order	gamma	Z	ch	A	MAT	NCODE	comment
40		90	Th	232	3905	9027	
41		92	U	233	3922	9237	
42		92	U	234	3923	9247	
43	G	92	U	235	3294	9257	
44		92	U	236	3925	9267	
45	G	92	U	238	3926	9287	
46		93	Np	237	3931	9377	
47		93	Np	239	3932	9397	
48		94	Pu	236	3941	9467	
49		94	Pu	238	3942	9487	
50	G	94	Pu	239	3934	9497	
51		94	Pu	240	3944	9407	
52		94	Pu	241	3945	9417	
53		94	Pu	242	3946	9427	
54		95	Am	241	3951	9517	
55		95	Am	242m	3953	9597	
56		95	Am	243	3954	9537	
57		96	Cm	242	3962	9627	
58		96	Cm	243	3963	9637	
59		96	Cm	244	3964	9647	
60		96	Cm	245	3965	9657	
61		96	Cm	246	3966	9667	
62		96	Cm	247	3967	9677	
63		96	Cm	248	3968	9687	

n.b.
gamma: G means data given
Z : atomic number
ch : chemical symbol
A : mass number
MAT : MAT number of JENDL-3
CODE : code number in JSSTDL lib.

JAERI-M 91-062

2. Effect of Self-shielding factor on the analysis of natural iron deep penetration shielding experiment performed by ASPIS facility

To demonstrate the effect of self-shielding factor for resonant nuclide, we performed an analysis of axial attenuation profile for ASPIS deep penetration experiment measured for natural iron block. This experiment was selected because it was designed to provide information of benchmark quality for the testing of data and calculational methods for deep-penetration profiles by natural iron shielding material.

Experimental configuration is as follows, a low-power natural uranium converter plate, driven by the source reactor NESTOR, provided a large thin disc source of fission neutrons is placed at the interface of a graphite moderator and extensive iron shield (= 140 cm thickness). Analyses are made for the axial attenuation measurements with three threshold detectors and one low-energy activation detector, and for the spectrometer measurements at four selected positions in the iron shield.

Calculational model and analysis

As for the calculational model, we closely follow the model in the report of M. D. Carter et al. /8/. However some modifications were made. Converter plate region is simulated rather in a straight way, i.e., it is composed from 5 regions as represented by Al-Fe-U-Fe-Al layers. Used configuration is shown in Fig.2.1 together with the detailed model of the converter plate in the upper part of the figure. The volume distributed sources (equivalent radius is 59.3 cm and thickness 0.318 cm) were treated as cross products of energy and space(in radial direction only). For energy dependence of fission emitted neutrons, ENDF/B-V U-235 data was used. Average values of each functional data were calculated and inputted on each mesh points of the fuel region.

For Fe natural cross-sections in the test region, which is thought as nearly pure material, following three methods are used to check self-shielding effects for the resonance cross-sections.

CASE 1: exact weighted cross-sections, this means that group cross-sections are generated by $1/\sigma_t$ (Fe) weighting, i.e. fully shielded cross-sections including higher Pl matrices (using special option of PROF-GROUCH-G/B). For the macro cross-section generation for DOT code, GLIB.MAKE -MACROX utilities were used.

CASE 2: self-shielding effect is automatically considered by JSSTDL system.

CASE 3: no self-shielding effect is considered.

For the energy groups, BERMUDA 121 /9/ group structure was adopted, which is defined as follows, from 16.487 MeV to 1.054 MeV (1-44 groups) lethargy increment(Δ u) is 0.0625, from 1.054 MeV to 19.304 keV (45-76 groups) Δ u is 0.125, for the rest of energy down to 0.32241 eV Δ u is 0.250 and one thermal group down to 1.0E-5 eV. This energy group structure is sufficiently detail for the ASPIS analysis. Anisotropy were included up to P5. Calculations were performed by DOT3.5 with S48 P5 R-Z: 53x92 meshes.

Results and discussions

The results are shown in Fig.2.2 ~ 2.3 for transmitted fluxes and it's C/E at 114cm depth position in the natural iron shields. And in Fig.2.4 ~ 2.5 axial attenuation profile of Rh-103 (n,n') reaction rate is shown. Circle marks in figures show experimental results. Triangle, plus, cross marks show CASE 1(exact weighting), CASE 2(self-shielding), CASE 3(no self-shielding) results respectively. From Fig.2.2 ~ 2.3, CASE 1 is the best, the next is CASE 2, the worst is the CASE 3. In this depth position, i.e., about one meter depth, the results of CASE3 (no self-shielding effect) is completely deviate from experiments. The difference is nearly factor 10, i.e., magnitude of order is different. The same tendency is seen in the axial attenuation profile for Rh-103 (n,n') given in Fig. 2.4 ~ 2.5. From these results, it is concluded that the best is using exact weighted cross-sections. But this method is very expensive, because every time we must generate group cross-sections using the quite-time consuming processing code for each nuclides and for each region. From the results shown above we conclude that self-shielding factor method is rather convenient even though it is not superior to the exact weighting method. No self-shielding factor results are completely bad. We cannot use the library without self-shielding factor for the resonant nuclides.

3. Conclusion

Newly developed JSSTDL library system was introduced. This system is composed of a common 295n-104γ group cross-section library based on JENDL-3 nuclear data file and its utility codes. The target of this system is focused to the criticality or shielding calculations in fast and fusion reactors. Group structure is defined so as to cover almost all group structures currently used in Japan. Neutron cross-sections and photon production cross-sections were processed by Prof. GROUCH-G/B code system and γ ray transport cross-sections are generated by GAMLEG-JR.

As seen from ASPIS deep penetration analysis, self-shielding effects from the iron nuclide are very large. At about one meter penetration depth, the spectrum is underestimated by factor 10 in the resonance energy range if no self shielding effect is considered. This might happen to mislead the required shield for the actual reactor shielding design.

We must pay attention resonance structures for the resonant nuclide in the structure materials or shielding materials if the sensitive energy range is concerned to the resonance energies of these materials. In other wards, group constants libraries without self-shielding factor table can not be applicable to the shielding applications as for as resonance nuclides are concerned. In the criticality calculation, this is a very common knowledge.

This library system has been fully applied for the benchmark test of JENDL-3. We confirmed the applicability of this system to the fast reactor calculations both for criticality and shielding and also to the fusion neutronics calculations. This system: 295n-104γ JSSTDL library is now available through JNDC Nuclear Data Center with the associated utility codes in FORTRAN source. The package includes also 100n-40γ library for the users of shielding fields.

For future plan, more nuclides will be processed and stored according to the user's requests not only from JENDL-3 but also from ENDF/B-VI or ENDL data files. Gamma production data are relatively poor in JENDL-3 because not so many nuclides are evaluated. The requests for the nuclides not available in JENDL are very strong for some γ production data. We are now starting for making a complete set of the neutron and gamma coupled group constants library of JENDL-3 by substituting γ production data not available in JENDL-3 for the data from the other data files.

JSSTDL system is just the requested one from the user's side. To accept user's common requests for the group-constants, such as applicable to widely used transport code, consistent with user's required group-structures, the latest nuclear data source,..., JSSTDL library system was developed and released through JNDC Nuclear Data Center.

Today JENDL-3 is a common treasure for all of the persons involved in nuclear industries of JAPAN. Therefore we should bring up JENDL-3 as a common knowledge for all of the persons involved. We hope that JSSTDL library system becomes a platform for the users of JENDL-3 and also discussions on the problems encountered in JENDL-3 are going on along with this library.

References

/1/ Nakazawa M. et al.: "Proposal on Post-JENDL-3 Activity Programme for Japanese Nuclear Data Committee",JAERI-M 87-025 pp9 (1987).

/2/ Engle W.W.Jr: "A Users Manual for ANISN A One Dimensional Discrete Ordinates Transport Code With Anisotropic Scattering", K-1963 (1967).

/3/ Rhodas W.A. and Mynatt F.R. :'The DOT-III Two Dimensional Discrete Ordinate Transport Code,' ORNL-TM-4280 (1973).

/4/ Straker E.A., Stevens P.N., Irving D.C. and Cain V.R. :' The MORSE Code - A Multigroup Neutron and Gamma Ray Monte Carlo Transport Code,' ORNL-4585 (1970).
/5/ Koyama K. et al. :"RADHEAT-V3",JAERI-M 7155 (1977).
/6/ Shibata K., Nakagawa T., Asami T., et al. :"Japanese Evaluated Nuclear Data Library, Version-3 -JENDL-3-",JAERI-1319 (1990).
/7/ Hasegawa A. :"Development of a Processing Code System Prof. GROUCH-G/B", unpublished work (1986).
/8/ Carter M. D., McCracken A.K. and Packwood A. : 'The Winfrith Iron Benchmark Experiment, A Compilation of Previously Published Results for use in the International Comparison of Shielding Data-Sets Sponsored by NEA,' AEE Winfrith (1982).
/9/ Suzuki T., Hasegawa A., Mori To. and Ise T. : ' BERMUDA-2DN : A Two-Dimensional Neutron Transport Code,' (in japanese), JAERI-M 82-190 (1982).

process	CODE used	Process comments
pre-processing	LINAER	linearlized data generation
	RECENT-J	resonance reconstruction for 0. K
	SIGMA1	Doppler broadened cross-section
Processing	Prof. GROUCH-G/B	group averaging process self-shielding factor cal. group transfer matrices cal.
post-processing	GLIBMK	group library compilation

Fig. 1.1 Processing out-line for group cross-section library generation

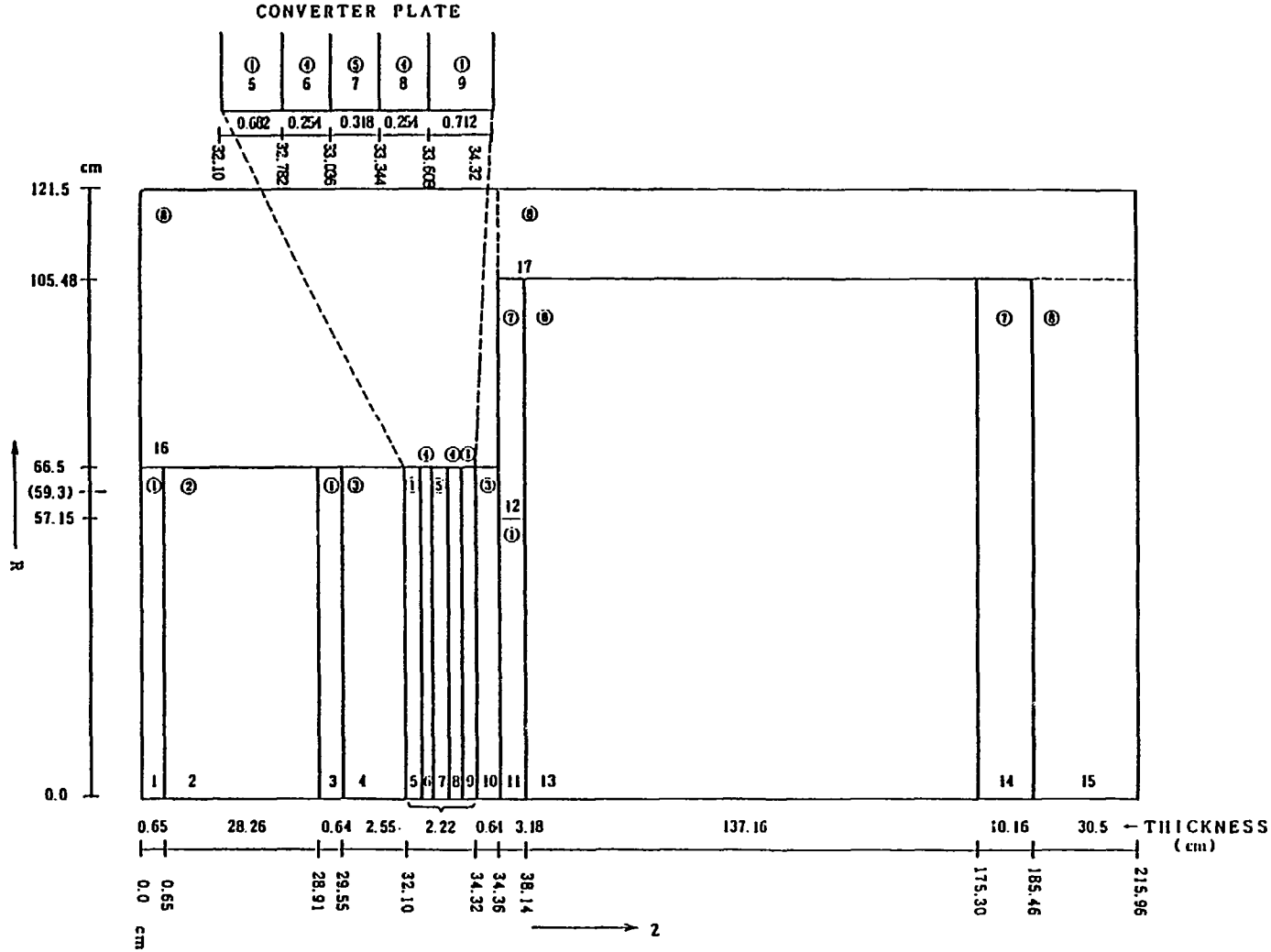

Fig. 2.1 R-Z geometrical model for transport calculation of DOT3.5

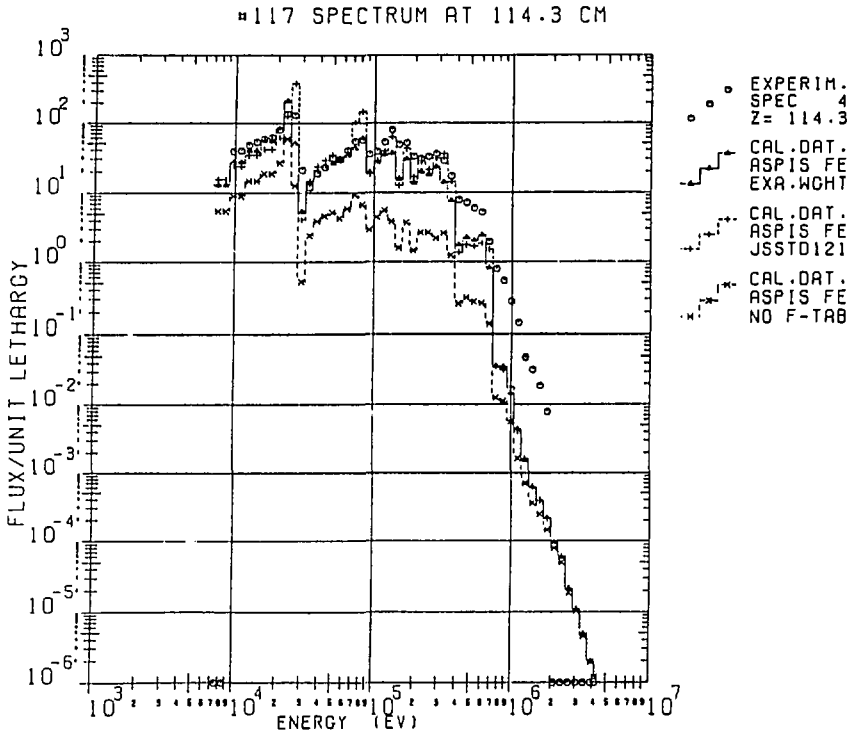

Fig. 2.2 Transmitted Spectrum in natural iron block at 114.3 cm position

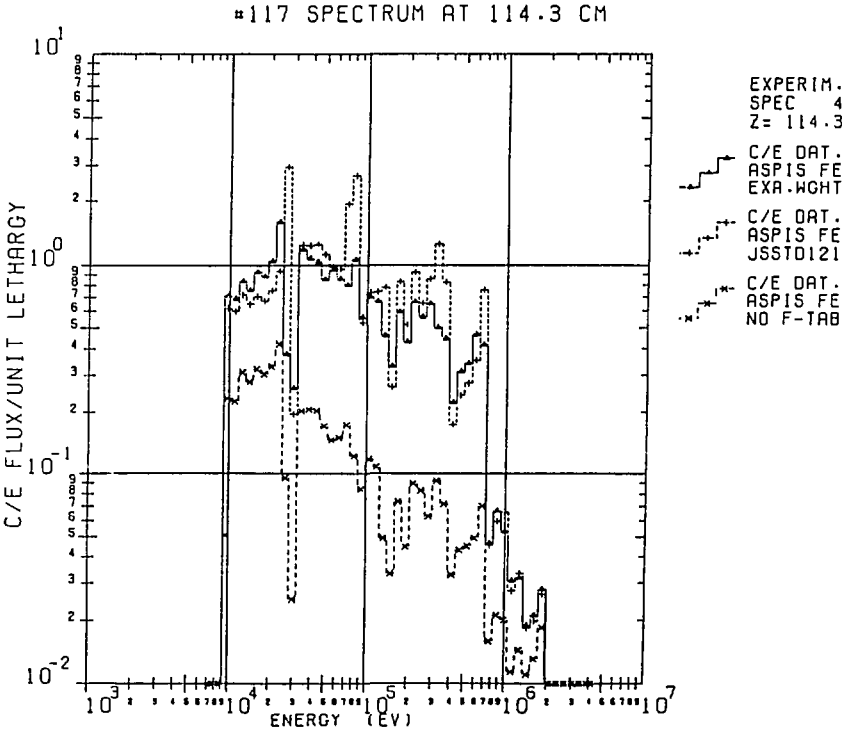

Fig. 2.3 C/E values of transmitted Spectrum in natural iron block at 114.3 cm position

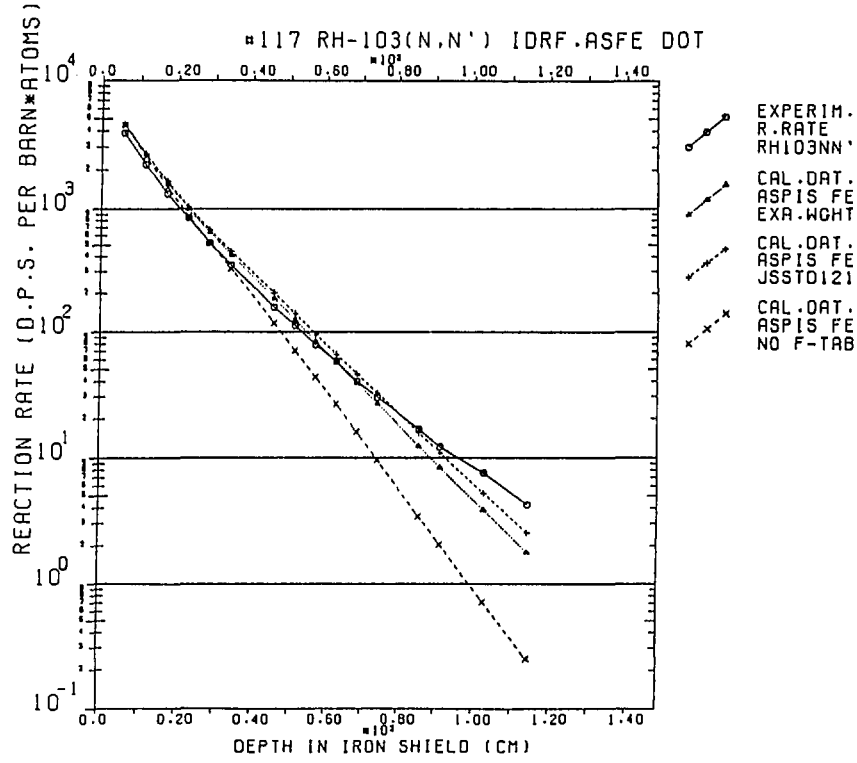

Fig. 2.4 Rh-103 (n,n') reaction rate axial attenuation profile

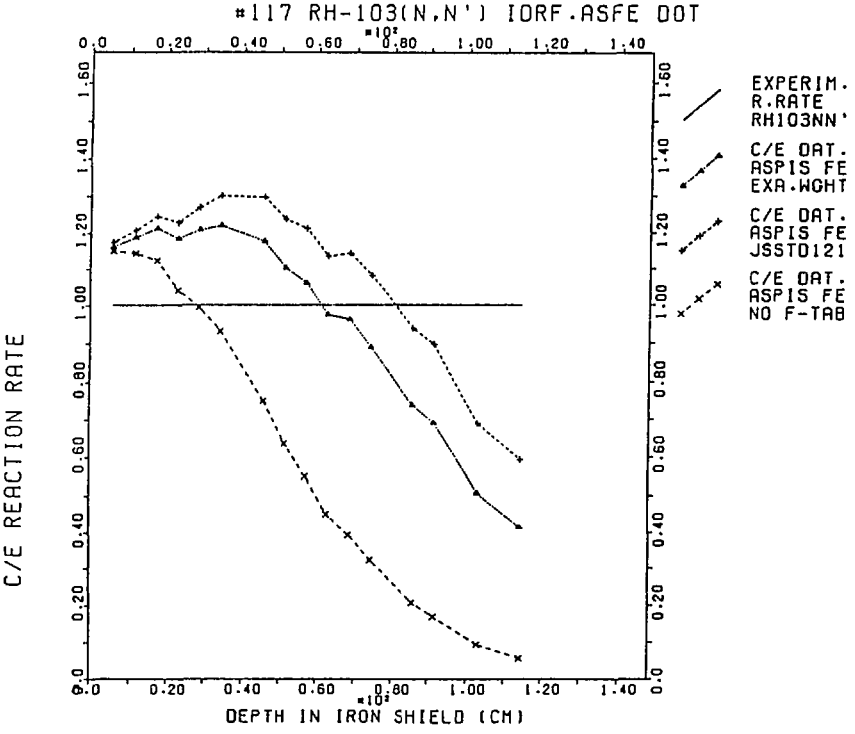

Fig. 2.5 C/E values of Rh-103 (n,n') reaction rate axial attenuation profile

2.2 MCNP Cross Section Library Based on JENDL-3

K. Kosako
Department of Reactor Engineering
Japan Atomic Energy Research Institute
Tokai-mura, Naka-gun, Ibaraki-ken

The MCNP cross section library was produced from JENDL-3. This consists of a pointwise neutron interaction data and a directory table, and can reduce uncertainty due to processing of evaluated nuclear data compared to past P_L type processing. The nuclear data processing is performed by NJOY and MACROS codes. The MCNP library has high precision enough to calculate accurately neutron transport. The confirmation for processing the nuclear data file to the MCNP library was discussed.

1. Introduction

Nuclear design of fusion reactor as ITER/FER is now going on. The prediction accuracy in calculation for design element is required to be high quality. As a result, it is essential to verify the precision and the applicable range of calculation method used in nuclear design.

Generally, the verification in fusion neutronics calculations is obtained through by analyses of various benchmark experiments. Those calculations involve cross section library, transport calculation, and comparison with experimental result. Though it is difficult to separate quantitatively uncertainties for the transport calculation from the cross section, it is very important to reduce uncertainty for cross section library.

The uncertainties included in cross section library are inadequacy of the data format, evaluation uncertainty, and processing algorithm of evaluated nuclear data. The ENDF data format[1] and evaluated nuclear data are not discussed here. The uncertainty discussed here is of processing of evaluated nuclear data for making a library used in the calculations. To reduce it, the less approximation to evaluated nuclear data are necessary.

The MCNP[2] cross section library is made up considering to reduce the uncertainty for processing of evaluated nuclear data. The MCNP library is faithful to the ENDF format and its representation, and can reproduce the cross section with similar precision to the evaluated nuclear data. Therefore, the analysis with this library can exclude the uncertainty due to nuclear data expression.

The latest evaluated nuclear data file, JENDL-3[3], was developed mainly fusion reactor application. The MCNP library based on JENDL-3 is expected to be able to analyze more accurately benchmark problems in comparison with past libraries.

2. MCNP Code and Cross Section Library

The MCNP code is a general purpose 3-dimensional Monte Carlo code. The main features of this code are as follows: 1) coupling of neutron and photon transport calculations, 2) usage of pointwise cross section, 3) geometry definition by surface and cell, and 4) many useful tally options. At present, MCNP is used as one of the most accurate transport calculation code in the world.

The MCNP cross section library consists of a nuclear data table file and a directory data table file. The cross section data are stored in the former file with 5 types. The necessary information to refer a nuclear data table is stored in the latter file. The types of nuclear data table are a pointwise (continuous energy) neutron interaction data, a multigroup (discrete reaction) neutron data, a photon interaction data, a neutron dosimetry cross section, and a neutron thermal $S(\alpha,\beta)$ table. Especially, the pointwise data is provided faithfully to ENDF format. The stored formats of nuclear data table are BCD, binary and ACE. The binary format is usually used because of computer resources.

The above MCNP library is produced from the evaluated nuclear data files, e.g., JENDL-3, by the nuclear data processing code system, NJOY[4], and by the compiling and editing code of MCNP library, MACROS[5]. The processing flow is shown in Fig. 1. The NJOY treats resonance parameter, Doppler broadening, generation of pointwise data, etc., and provides the ACE type cross section data. The MACROS compiles them from any ACE type data to the MCNP cross section library (pointwise neutron interaction data and directory table).

Here we discuss the precision of the MCNP library in comparison to

multigroup data. A multigroup cross section library is generally used in reactor design and analyses, because this library has a merit of shortening computation time. While the cross section of MCNP is pointwise with continuous energy and given for each reaction type, the multigroup one is an energy-averaged cross section in each energy group and gathered up all reactions into scattering matrix, total cross section and absorption cross section. For example, the total cross sections of MCNP and 125-group in high energy are shown for iron in Fig. 2 and 3, respectively. The MCNP library represents finely peaks and dips, but the multigroup library smears the fine structure.

The angular distribution is represented by 32 equal-probability bins for the MCNP library, while the multigroup library generally used the Legendre expansion in 5 orders except the codes using DDX format. The JENDL-3, however, is given by high order of Legendre expansion in higher energy, so the P-5 multigroup library cannot represent sufficiently angular distribution probability as shown in Fig. 4, in contrast to the MCNP case shown in Fig. 5.

The energy distribution is given almost by the same as ENDF format for the MCNP except tabulated energy distribution, but the multigroup library given by the scattering matrix.

The applied example of MCNP library is shown in Fig. 6. This figure compares the MCNP calculation, DOT3.5[6] with multigroup library to the experimental value. The experiment is for a pure iron cylinder of 95 cm in thick and 50 cm in radius. The result of MCNP is satisfactory on the whole. Though the multigroup result needs to consider the effects of self-shielding factor and Legendre expansion, the MCNP result does not require to consider these effects.

3. Processing for JENDL-3 and its confirmation

The NJOY system had to be modified for some points in JENDL-3 processing. The main modifications were performed to the following: 1) processing of any numbers in NK sections for tabulated energy distribution (MF=5, LF=1), 2) processing of Reich-Moore resonance cross section, 3) conversion from LO=2 to LO=1 of photon production (MF=12), 4) fitting of tabulated angular distribution (MF=4), and 5) addition of interpolation mode.

The produced MCNP cross section library based on JENDL-3 is a set of

FSXLIB (pointwise neutron interaction data) and FSXDIR (directory table). The FSXLIB is written in binary format and a direct access file. The FSXDIR is in BCD format and a direct access file, but the general directory table corresponding to FSXDIR is a sequential file. Number of nuclide stored in library is 48. These nuclides are relevant to blanket components, construction materials, basic fissionable materials, and other important materials.

for confirm after how the present processing was well performed, the plots of energy differential cross sections for each reaction, angular distribution, and energy distribution give good confidence. The processed data in MCNP library and the data in evaluated nuclear data file are plotted as shown in Fig. 5. However, the energy distribution has not been obtained at present. This is planned in the further confirmation.

4. Summary

The pointwise neutron interaction data of MCNP library was produced from JENDL-3 with similar precision to the evaluated nuclear data. The use of this library can reduce the uncertainty with nuclear data processing.

The features of MCNP library were described and the higher precision of MCNP library was explained in comparison with the multigroup library. The produced library was checked by comparison of plotted data with the original evaluated nuclear data.

The current problems for MCNP library are mainly as follows: 1) complete confirmation of pointwise data processing to the original nuclear data file, 2) too enormous energy points in some nuclides, and 3) impossibility of complete processing for MF=6 in ENDF-6 by recent NJOY.

References

1) BNL: "ENDF/B-IV: Evaluated Nuclear Data File, Version-IV" (1975).
BNL: "ENDF/B-V: Evaluated Nuclear Data File, Version-V" (1979), and its documentation, "ENDF/B Summary-Documentation, third edition (ENDF/B-V)", BNL-17541 (ENDF-201) (1979).
2) Briesmeister J. F. (edited): "MCNP - A General Monte Carlo Code for Neutron and Photon Transport", LA-7396-M, revised 2, (1986).
3) Shibata K., et al.: "JENDL-3: Japanese Evaluated Nuclear Data

Library, Version-3", JAERI-1319 (1990).

4) MacFarlane R. E., et al.: "The NJOY Nuclear Data Processing System", LA-9303-M (ENDF-324) (1982).

5) Kosako K., et al.: "Neutron Cross Section Libraries for Analysis of Fusion Neutronics Experiments", JAERI-M 88-076 (1988) (in Japanese).

6) Rhodes W. A. and Mynatt F. R.: "The DOT-III Two Dimensional Discrete Ordinates Transport Code", ORNL/TM-4280 (1973).

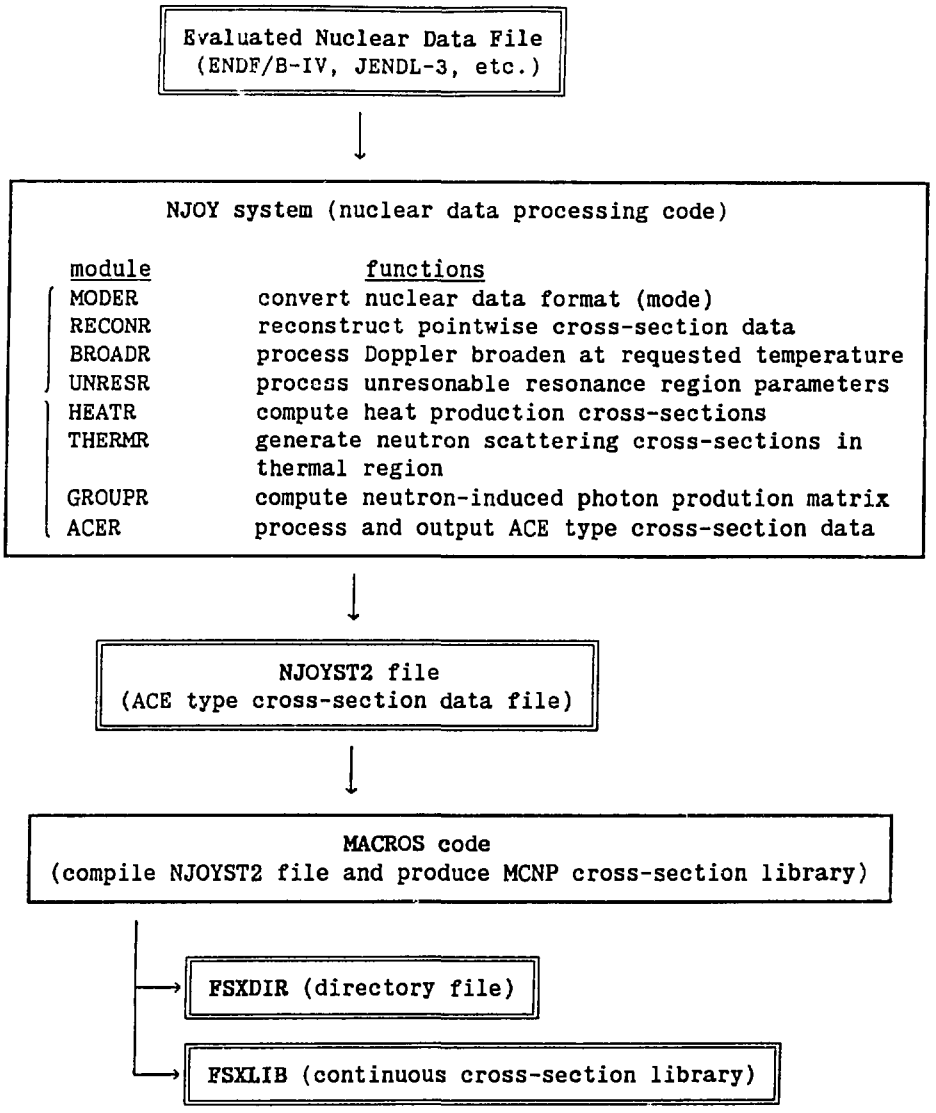

Fig. 1 The processing flow to produce a continuous energy cross section library of MCNP code.

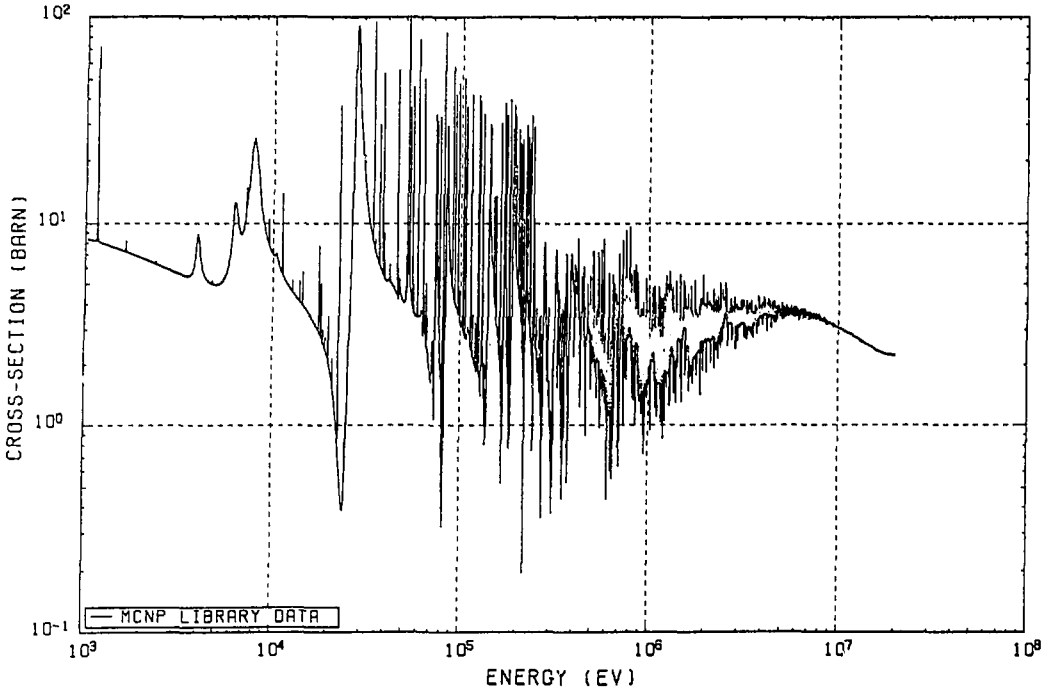

Fig. 2 The total cross section of neutron for Fe-0 (JENDL-3) in MCNP library.

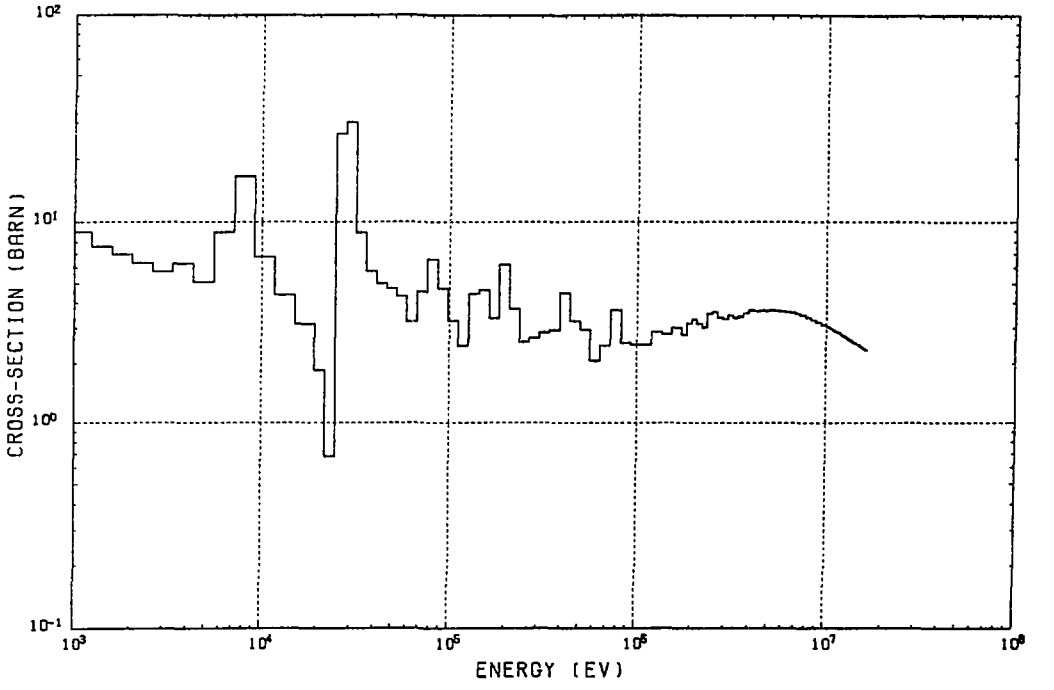

Fig. 3 The total cross section of neutron for Fe-0 (JENDL-3) in 125-group library.

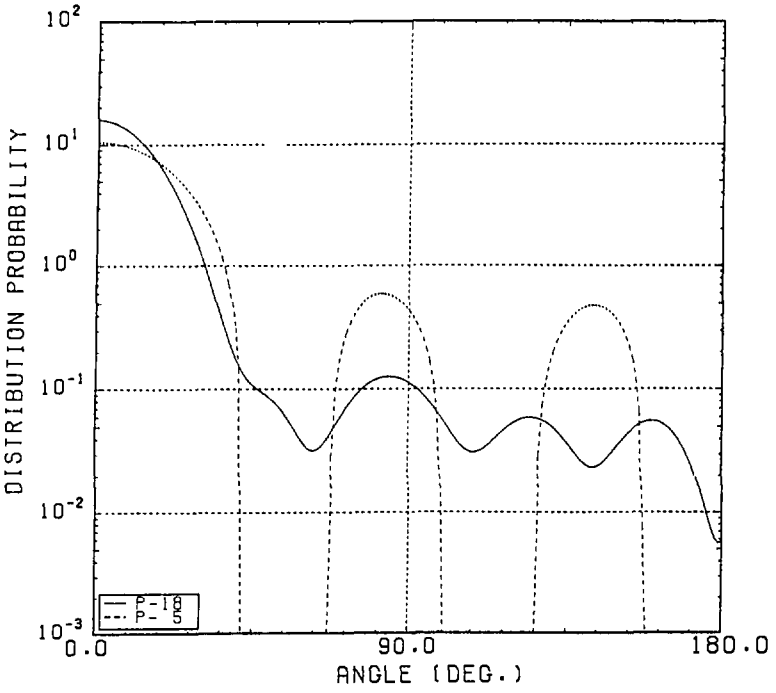

Fig. 4 The angular distributions of elastic scattering to 14 MeV incident neutron for Cu-0 (JENDL-3) compared with evaluated nuclear data and P-5 expansion.

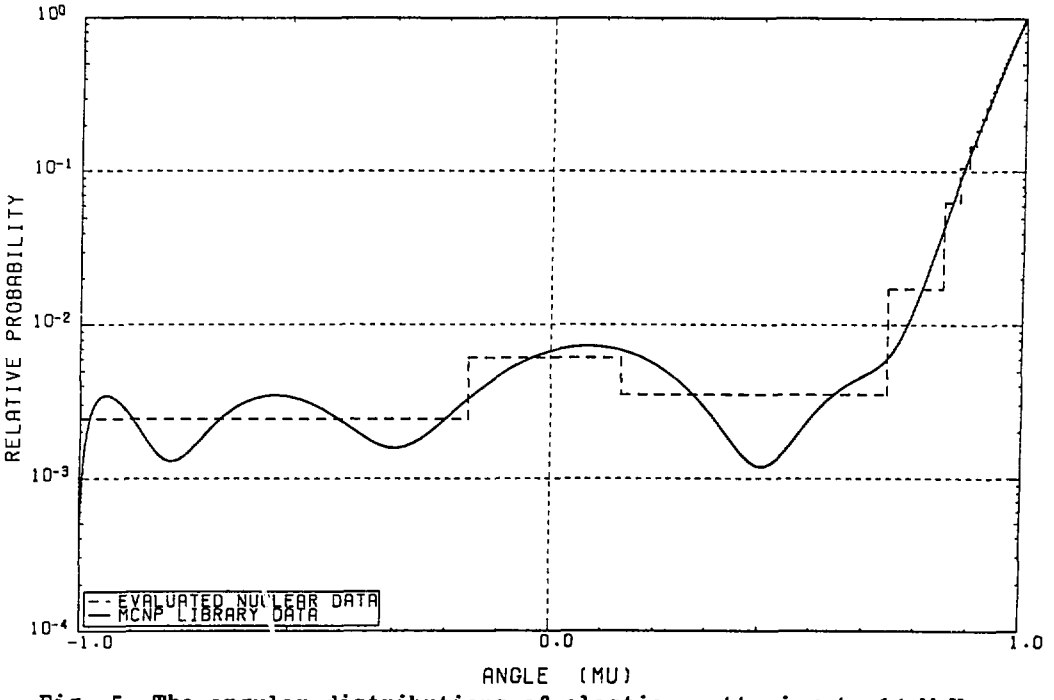

Fig. 5 The angular distributions of elastic scattering to 14 MeV incident neutron for Cu-0 (JENDL-3) compared with evaluated nuclear data and MCNP library.

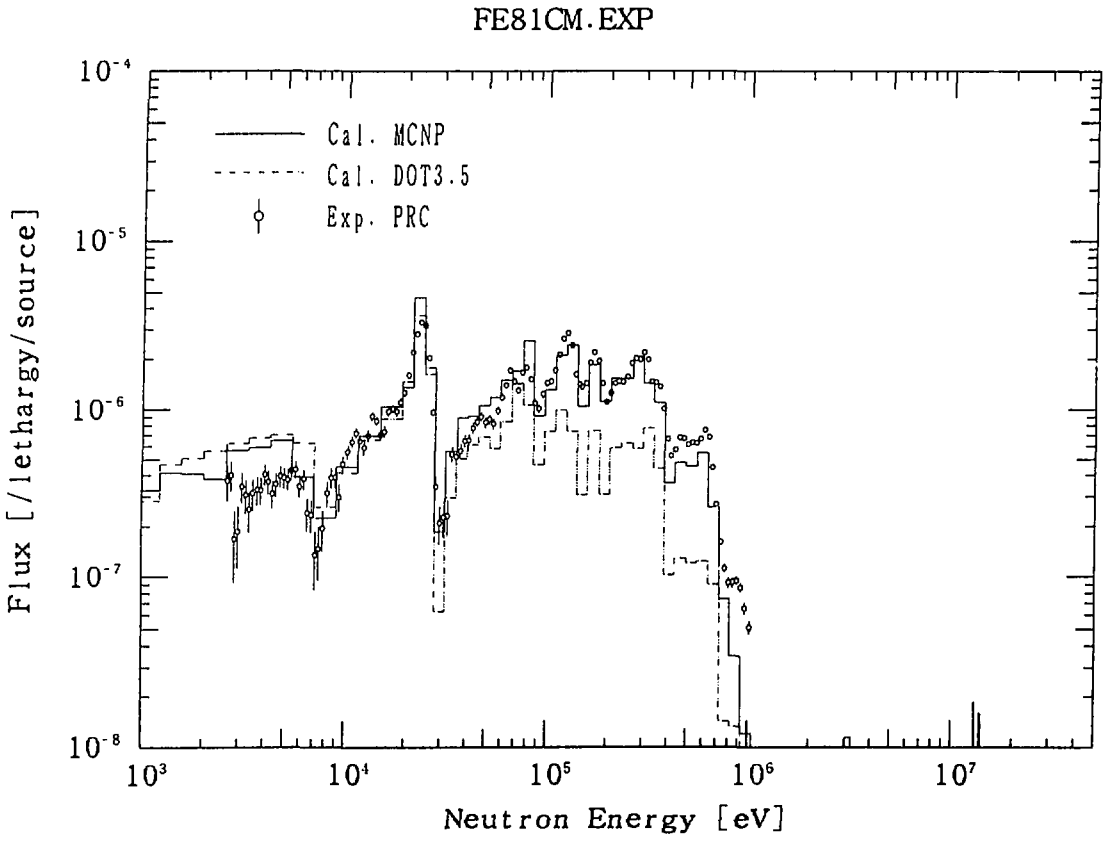

Fig. 6 The neutron spectra at 81 cm from iron cylinder surface.

3. Nuclear Data Relevant to Blanket Materials (Mainly Light Nuclides)

3.1 Review of JENDL-3 Data for Blanket Materials – ^{6}Li, ^{7}Li, ^{9}Be, ^{12}C, ^{14}N, ^{16}O and Pb –

Satoshi CHIBA

Nuclear Data Center
Japan Atomic Energy Research Institute
Tokai, Ibaraki, Japan

A brief review about the JENDL-3 data for some blanket materials of D-T fusion reactors, especially those of light nuclides, is described. Changes made from JENDL-3T to JENDL-3 are summarized, and the status of the double-differential neutron emission cross sections and some important reaction cross sections in JENDL-3 is described. A future plan to further improve the JENDL data will be also mentioned.

1. Brief Chronological Review

After JENDL-2 was released in 1982, great efforts were made to improve accuracy of the evaluated data for the incident neutron energy above several MeV. For some light and structural materials, a preliminary version, called JENDL-3PR1[1] was made in 1983. For light elements, this became the base of the JENDL-3 data. However, because some drawbacks were pointed out both from integral and differential experiments, JENDL-3PR1 was updated to JENDL-3PR2 in 1985[2], to JENDL-3T in 1987[3] and finally to JENDL-3 in 1989[4]. The following table summarizes the main evaluator(s) for each version of JENDL.

	JENDL-2 (1982)	JENDL-3PR1 (1983)	JENDL-3PR2 (1985)	JENDL-3T (1987)	JENDL-3 (1989)
^{6}Li	Komoda(N)	Shibata(N)	Chiba(M)		
^{7}Li	Shibata(N)	Shibata(N)	Chiba(M)	Chiba(M)	Chiba(M)
^{9}Be	Shibata(N)	Shibata(N)			Shibata(M)
^{12}C	JENDL-1	Shibata(N)	Shibata(M)		Shibata(M)
^{14}N	not given	not given	not given	JNDC(N)	
^{16}O	ENDF/B-IV	JNDC(N)		Chiba(M)	Shibata(M)
Pb	Asami(N)			Mizumoto(N)	Mizumoto(M)

(N) : New evaluation, (M) : Modification

In the light mass region, theoretical calculations are difficult to apply with high accuracy. Therefore, the improvements of the JENDL data were mainly made by taking account of newly measured differential data. For example, the JENDL-3PR1 data for ^{6}Li, ^{7}Li and ^{12}C were modified considering the double-differential cross sections (DDX) measured in Japan. In other words, the JENDL data in the light mass region were gradually updated considering then-up-to-date data. The results of integral experiments also played an important role to "guide" the modification work.

2. Changes Made from JENDL-3T to JENDL-3

In the light mass region, no big change was made going from JENDL-3T to JENDL-3, except for ^{9}Be where the JENDL-3T data could not reproduce measured DDX data well[5]. The following summarizes changes for the light mass region from JENDL-3T to JENDL-3:

a) The total cross section of ^{7}Li was slightly (~ 3% at 14MeV) enhanced above 10MeV.
b) The total cross section of ^{16}O was slightly lowered in the MeV region.
c) DDX of ^{9}Be was modified by adding the three-body simultaneous break-up mode for the ^{9}Be(n,2n)^{8}Be reaction.
d) ^{9}Be(n,n') and (n,2n) cross sections were modified considering newly measured experimental data.
e) ^{12}C(n,n') cross section was modified considering new experimental data.

The data for Pb were modified greatly, because it could not reproduce the measured DDX and energy dependence of the (n,2n) reaction cross section. In JENDL-3T, the data for Pb were mainly calculated by the GNASH code[6]. This program uses the Gilbert-Cameron type level density formula[7] for continuous levels. This, however, did not reproduce measured DDX and energy dependence of the (n,2n) reaction cross section, with the level density parameters determined to reproduce the neutron resonance properties. For JENDL-3, therefore, Mizumoto used the Ignatyuk level density formula[8] where energy dependence of the level density parameter could be incorporated. This led to a change in "shapes" of DDX and in energy dependence of the (n,2n) reaction cross sections, and agreement of the calculated and experimental data was greatly improved.

3. Status of JENDL-3

3.1 DDX

In Figures 1, 2 and 3, DDX data of ^{9}Be, ^{7}Li and natural lead calculated from JENDL-3, respectively, are compared with the experimental data measured at 14MeV[9,10]. Except for the very low energy region of backward angles, the JENDL-3 data can reproduce the measured DDX of ^{9}Be very well, as shown in Fig. 1. Drawbacks of JENDL-3T data, which in this case were almost equivalent to those of JENDL-3PR1, were almost completely resolved in JENDL-3. DDX of ^{7}Li is also almost perfectly reproduced by JENDL-3, while the ENDF/B-VI[11] slightly underestimates DDX in the mid-energy region. Figure 3 shows DDX of elemental lead. In the mid-energy range, the JENDL-3 data understimates the DDX.

3.2 ^{7}Li(n,n't)α reaction cross section

The ^{7}Li(n,n't)α reaction cross section is shown in Fig. 4. In this figure, only experimental data measured after 1980 are shown. The JENDL-3 data are very close to those of ENDF/B-VI above 10MeV. The ENDF/B-VI data are several percent higher than JENDL-3 around 6MeV, and has a peculiar shape near the threshold energy.

3.3 ^{9}Be(n,2n)2α reaction cross section

This cross section is given in Fig. 5. In the whole energy region, JENDL-3 is very close to ENDF/B-VI, despite the scatter of the available experimental data.

3.4 Pb(n,2n) reaction cross section

Figure 6 shows the (n,2n) reaction cross section of elemental lead. Mizumoto averaged several available data and obtained a value of 2.184b at 14MeV. Then, he normalized his calculation using Ignatyuk level density formula to this value. As a result, the JENDL-3 data are different from the experimental data measured by Frehaut et al.[12] in the whole energy region. However, the energy dependence of the cross section became much similar to Frehaut et al.'s data, compared with the JENDL-3T evaluation.

4. Future Plan

The JENDL-3 data have very high accuracy for fusion neutronics purposes, especially below 15MeV. However, of course, the JENDL-3 data are not perfect. For example, the DDX data of ^{14}N cannot reproduce the measured data. Very recently, Asami has modified the $^{14}N(n,n')$ data, using the pseudo-level representation[13]. The result is compared in Fig. 7 with JENDL-3 and experimental data measured by Baba et al[14]. Drawbacks of JENDL-3 are almost resolved in his new evaluation. The ^{14}N data of JENDL-3 will be replaced by this evaluation in near future.

As mentioned in chapter 1, the evaluations and upgrades for light nuclides were mainly made a-posteriori way. So far, it has been working well. However, accurate theoretical calculations are strongly desired especially because the range of the nuclear data is extending toward higher energy, where available experimental data become extremely sparse. Few-body nature of the light nuclides has to be considered by solving rigorous Faddeev or Yakubovsky equations[15]. However, they seem to be too complicated to apply in a routine data evaluation work at first glance. Other simpler approaches, e.g., the final-state interaction model, sequential decay model, impulse approximation, coupled-channel approach with microscopic form-factors, etc., might have to be used approximately, supplementing each other.

The JENDL-3 data do not have file 6 (MF=6), the energy-angle distribution of secondary particles. However, it has been pointed out that the energy-angle correlation should be considered explicitely at least for neutron emitting reactions, even for medium- and heavy-mass nuclides. A work on this direction has already been started, and methods of calculation and compilation of the DDX are now being investigated[16].

5. Concluding Summary

In this paper, a brief review about the status of JENDL-3 for some D-T fusion reactor blanket materials was made. First, a brief chronological review was given, which was followed by an explanation of the status of JENDL-3, especially of DDX. JENDL-3 data is now considered to have very high accuracy below 15MeV. It has to be noticed that experimental data, both differential and integral, measured in Japan played an important role in improving JENDL. However, calculational method in higher energy range must be explored as an urgent task.

Acknowledgement

The author is grateful to Drs. T.Nakagawa, T.Fukahori, M.Mizumoto and K.Shibata for their helps and useful comments.

References

1) Shibata, K.: "Summary of Evaluated Nuclear Data for ^{6}Li, ^{7}Li, ^{12}C and ^{16}O in JENDL-3PR1", JAERI-memo 59-062, private communication (1984).
2) Igarasi, S. and Asami, T.(Ed.): "Proceedings of Specialists' Meeting on Nuclear Data for Fusion Neutronics", JAERI-M 86-029 (1986).
3) Asami, T., Nakagawa, T., Mizumoto, M., Narita, T., Shibata, K., Chiba, S., Fukahori, T., Hasegawa, A. and Igarasi, S.: "STATUS OF JAPANESE EVALUATED NUCLEAR DATA LIBRARY VERSION 3", Proc. Nucl. Data for Sci. and Tech., Mito, p.533, Saikon Publ. (1988).
4) Shibata, K., Nakagawa, T., Asami, T., Fukahori, T., Narita, T. Chiba, S., Mizumoto, M., Hasegawa, A., Kikuchi, Y., Nakajima, Y. and Igarasi, S.: "Japanese Evaluated Nuclear Data Library, Version-3", JAERI 1319 (1990).
5) Shibata, K.: "Evaluation of Neutron Nuclear Data of ^{9}Be for JENDL-3", JAERI-M 84-226 (1984).
6) Young, P.G. and Arthur, E.D.: "GNASH: A Preequilibrium, Statistical Nuclear-Model Code for Calculation of Cross Sections and Emission Spectra", LA-6947 (1977).
7) Gilbert, A. and Cameron, A.G.:Canad. J. Nucl. Phys. 43, 1446(1965).
8) Ignatyuk, A.V.: "STATISTICAL PROPERTIES OF EXCITED ATOMIC NUCLEI", INDC(CCP)-233/L, IAEA (1985).
9) Takahashi, A.: "Double Differential Neutron Emission Cross Sections at 14 MeV Measured at OKTAVIAN", JAERI-M 86-029, p.99 (1986).
10) Takahashi, A., Ichimura, E., Sasaki, Y. and Sugimoto, H.: "DOUBLE AND SINGLE DIFFERENTIAL NEUTRON EMISSION CROSS SECTIONS AT 14.1 MEV : Vol. 1", OKTAVIAN Report A-87-03, Osaka University, (1987).
11) Evaluated Nuclear Data File, Version VI, National Nuclear Data Center, Brookhaven National Laboratory (1990).
12) Frehaut, J., Bertin, A., Bois, R. and Jary, J.: "Status of (n,2n) Cross Section Measurements at Bruyeres-le-Chatel", Proc. of Symposium on Neutron Cross Sections from 10-50MeV, USA, BNL, Upton, N.Y., 12-14 May 1980, p.399.
13) Kanda, Y., Murata, T., Nakajima, Y. and Asami, T.: "Reevaluation of

the DDX Data of ^{14}N in JENDL-3", Proc. of 1990 Seminar on Nuclear Data, JNDC, to be published.

14) Baba, M., Ono, M., Yabuta, N., Kikuti, T. and Hirakawa, N.: Radiation Effects 92, 223 (1986).

15) e.g., Glöckle, W.: "The Quantum Mechanical Few-Body Problem", Springer-Verlag (1983).

16) Yu, B., Fukahori, T. and Chiba, S.: private communication (1991).

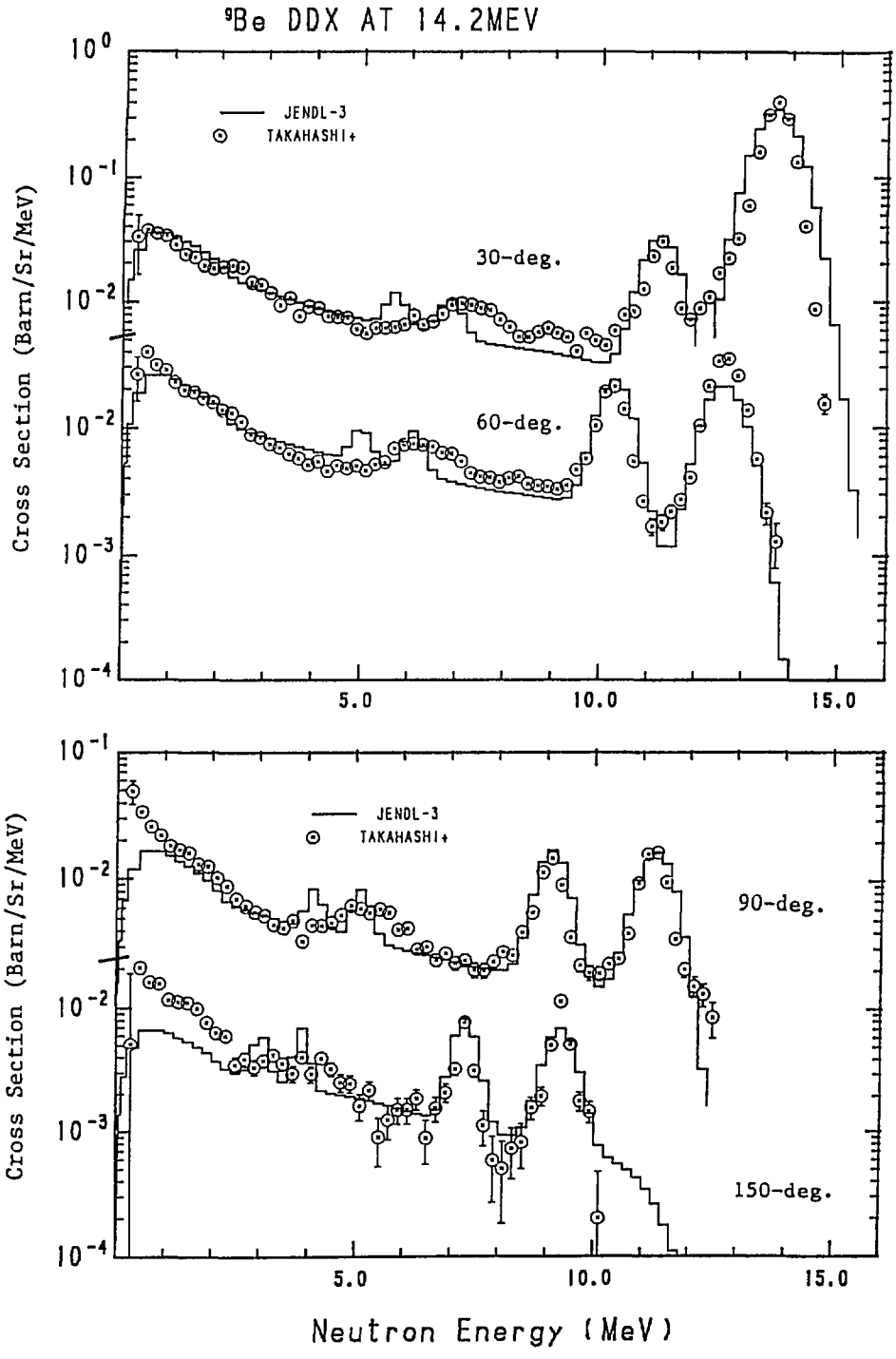

Fig. 1 DDX of ^{9}Be at 14.2MeV

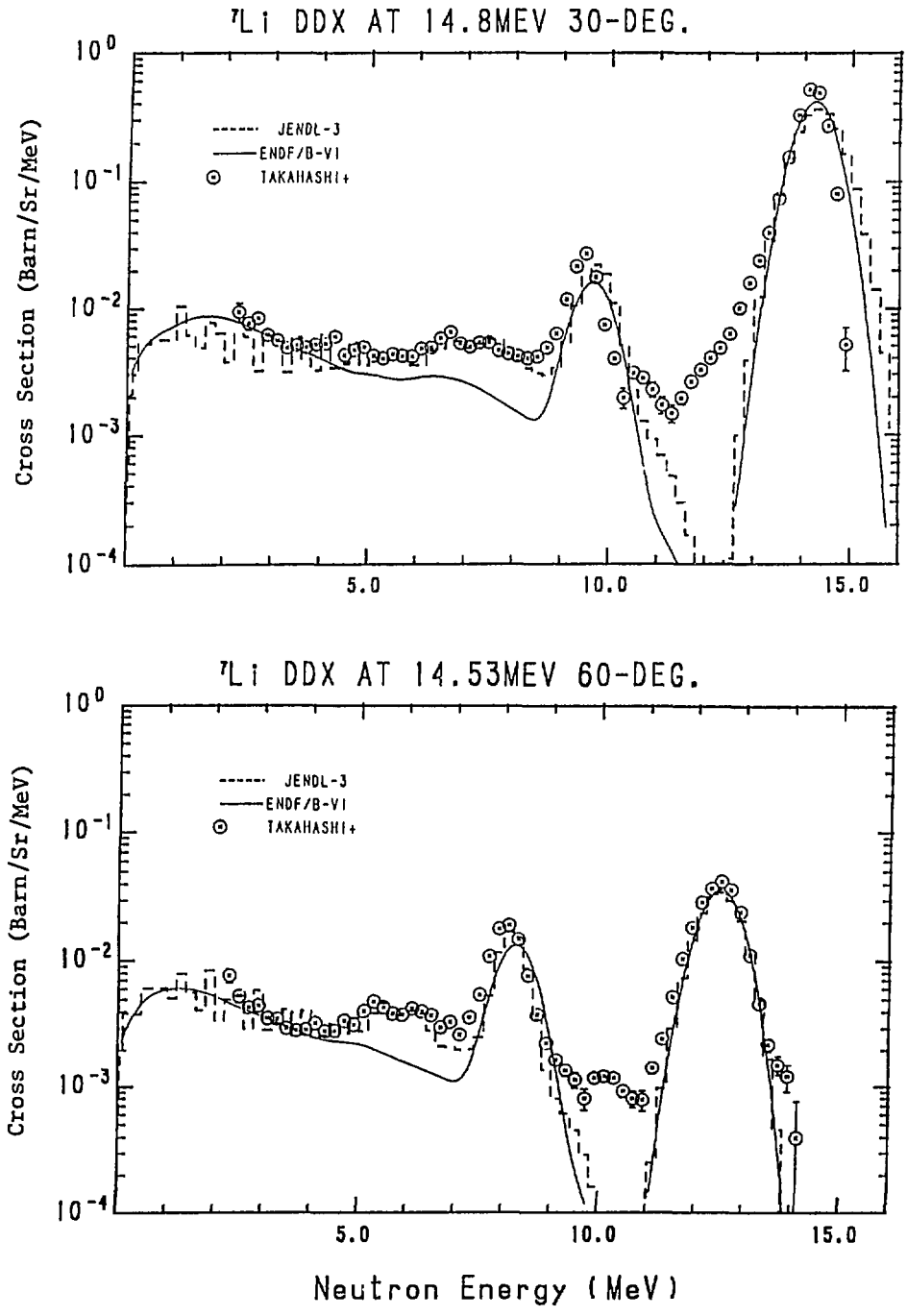

Fig. 2 DDX of ^{7}Li at 14MeV

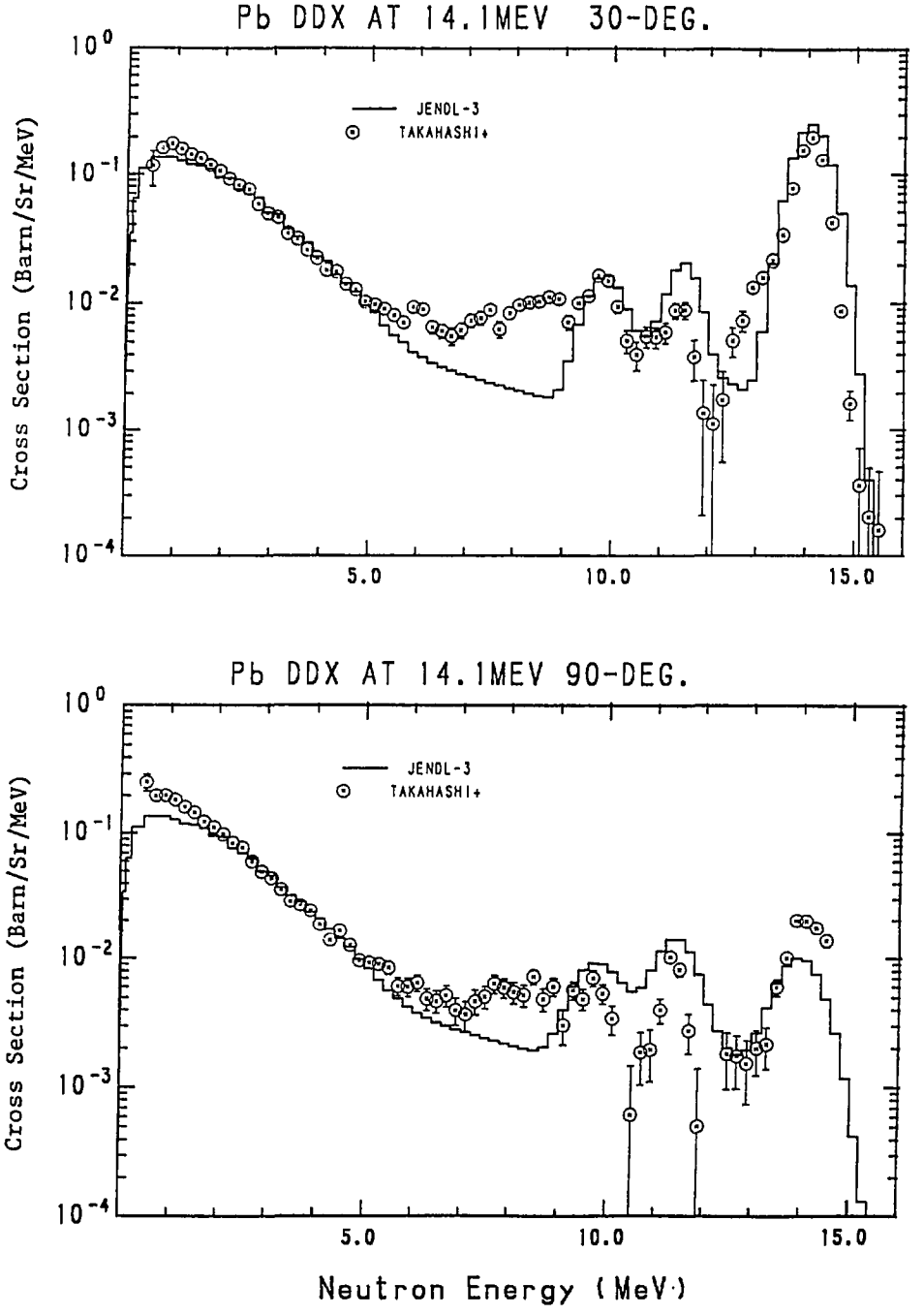

Fig. 3 DDX of elemental lead at 14.1MeV

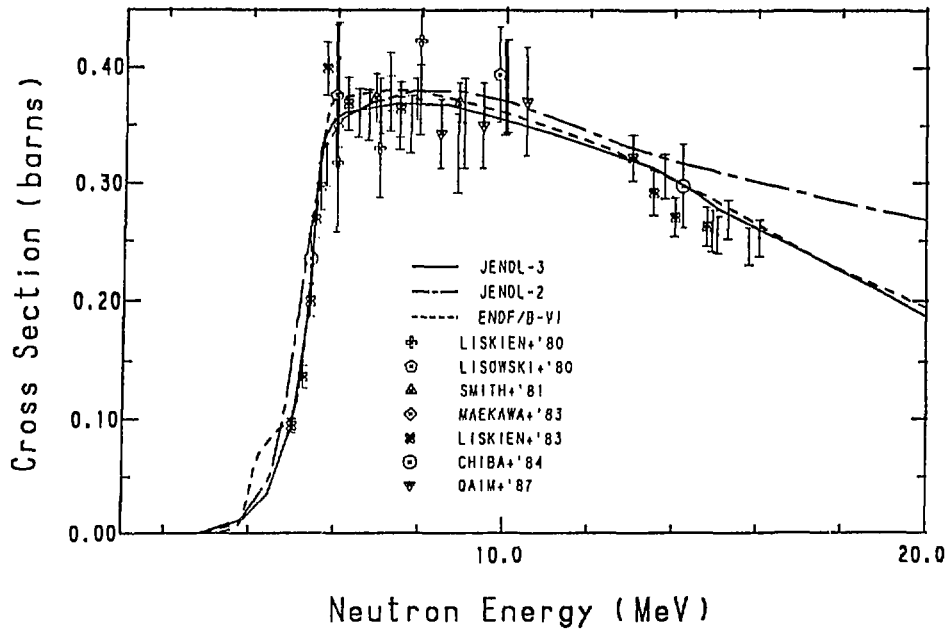

Fig. 4 $^{7}Li(n,n't)\alpha$ reaction cross section

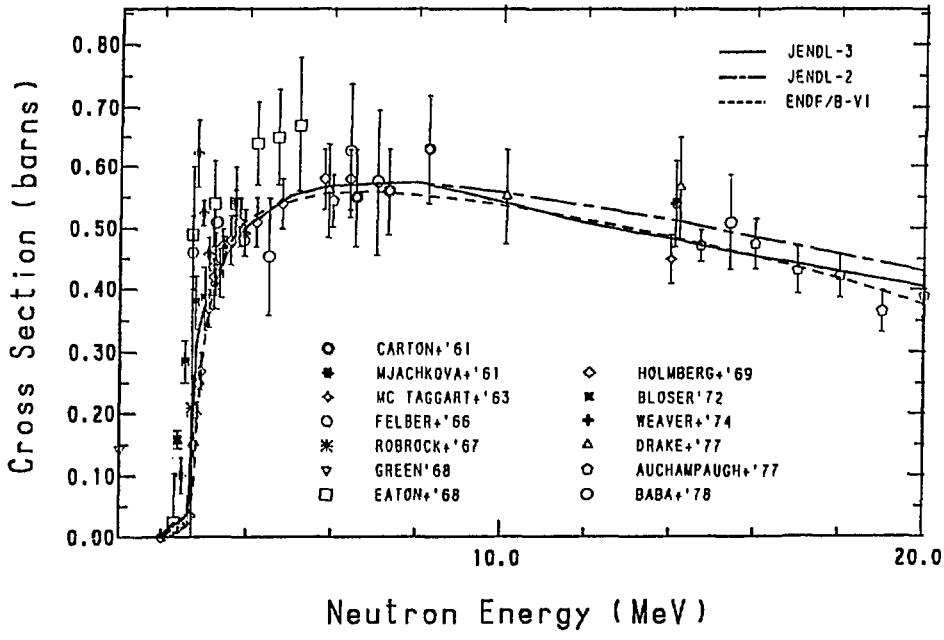

Fig. 5 $^{9}Be(n,2n)$ reaction cross section

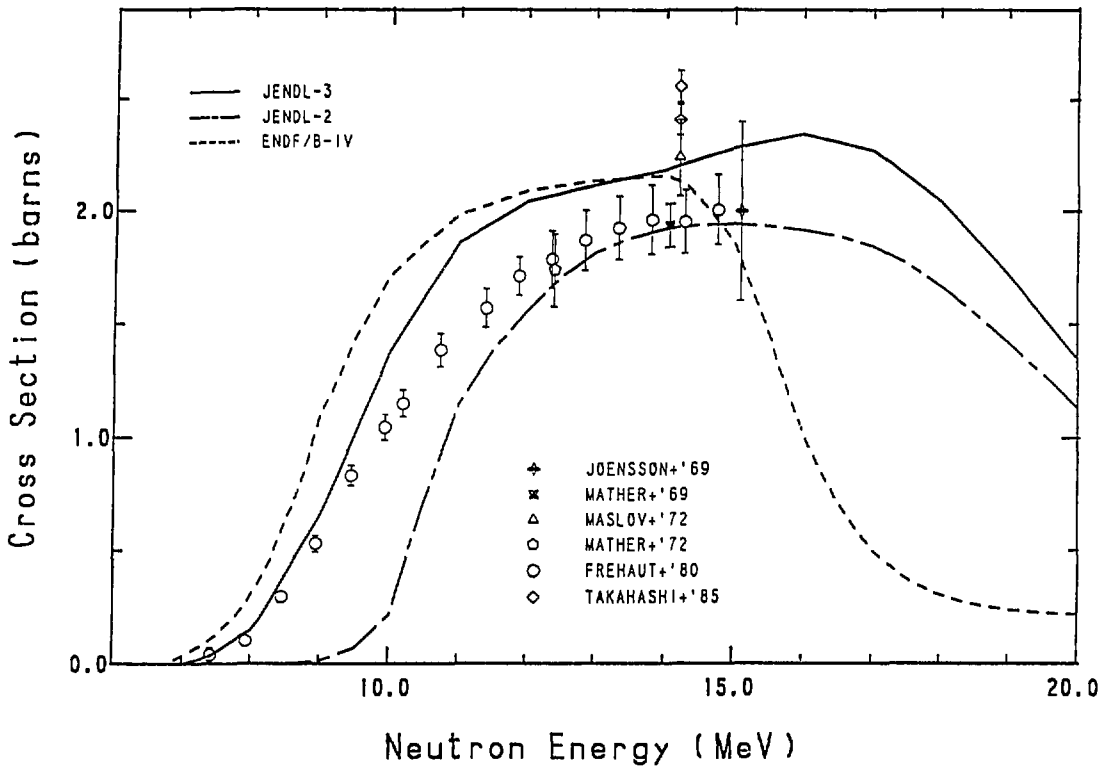

Fig. 6 Pb(n,2n) reaction cross section

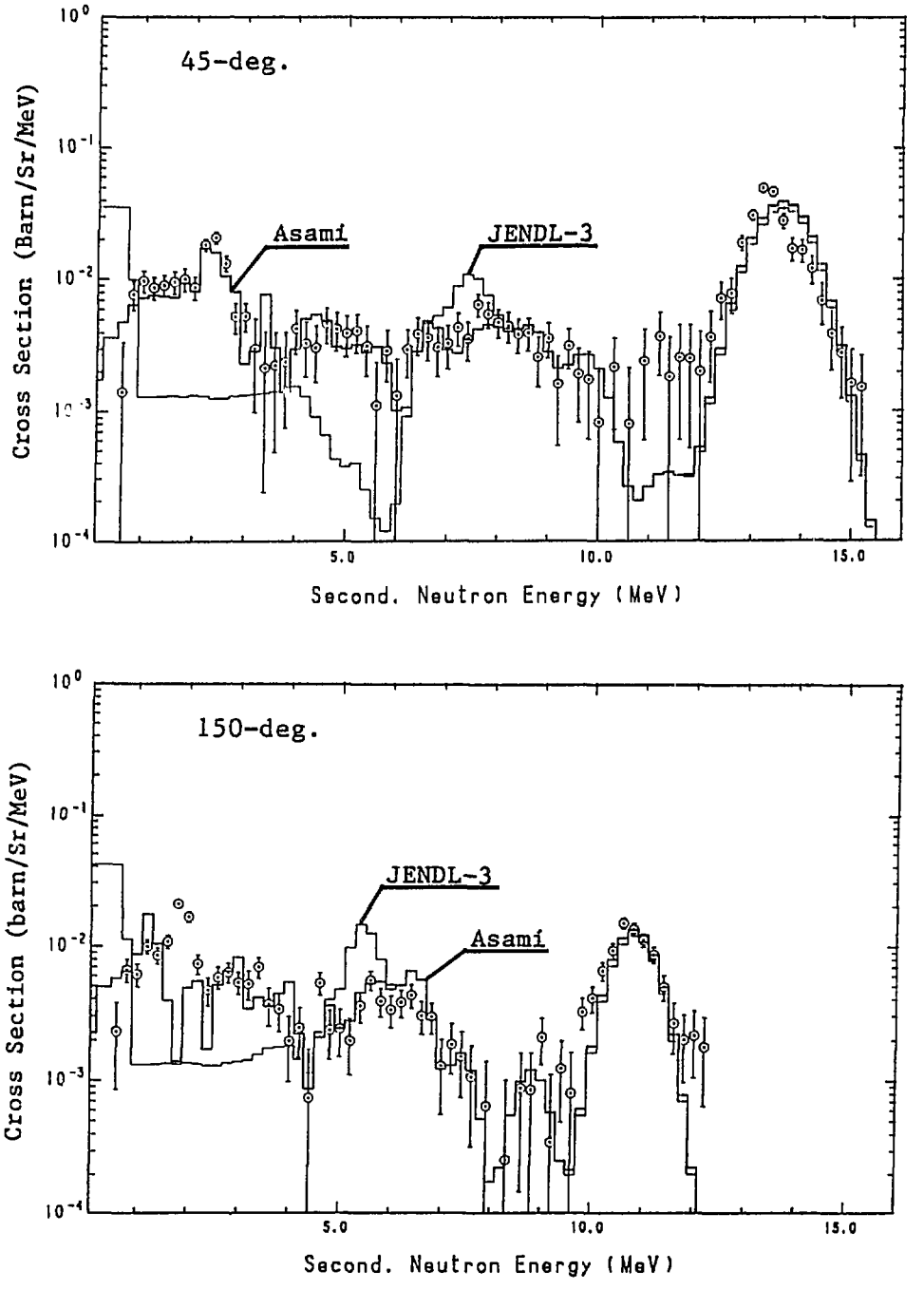

Fig. 7 DDX of ^{14}N at 14.2MeV

3.2 Summary of Discussion on the Data Status of Blanket-relevant Nuclei

M.Baba
Department of Nuclear Engineering, Tohoku University
Sendai 980, Miyagi-ken

In this session, the results of analyses for various integral experiments were presented and discussed to assess the status of JENDL-3 data for nuclei relevant to fusion reactor blanket, i.e., ^{6}Li, ^{7}Li, Be, C, N, O, F and Pb. The detailed description for analyses are presented separately in this proceedings, and this report presents a brief summary of the discussion.

The analyses were presented for the following integral experiments using 14 MeV incident neutrons:

1) LLNL pulsed sphere experiments; ^{6}Li, ^{7}Li, Be, C, O and Pb,
2) TOF experiments for angular flux from slab assemblies at FNS, JAERI; Li_2O, Be, C, N, O and Pb,
3) TOF experiments for neutron leakage spectrum from spherical assemblies at OKTAVIAN, Osaka university; LiF, CF_2,
4) Reaction rate measurements in Li_2O and Li_2O/Be assembly at FNS,
5) Neutron multiplication measurement for Be bulk at Kurchatov institute.

These integral data will provide useful data base for benchmark of the adequacy of evaluated data concerning 1)secondary neutron angular distribution (SAD) and energy distribution (SED) for 14 MeV primary neutrons, 2)the cross sections at lower energy region, and for 3)the total cross section and SAD of elastic scattering around 14 MeV, since neutrons undergo multiple-scattering and deep-penetration in massive assembly used for these integral experiments. The experiments 1-3 will be especially sensitive to SAD and SED for 14 MeV neutron induced reaction. Double-differential neutron emission data were also referred in the discussion.

Through the presentation and discussion, it was shown that the analyses using the JENDL-3 data reproduce generally well the experimental results. However, significant discrepancies were reported between experiments and analyses for the following cases: a) neutron spectrum from ^{6}Li, liquid nitrogen, LiF, CF_2, and Pb assemblies, b)tritium production rate in Li_2O/Be assembly, and for c)neutron fluxes around 14 MeV in thick assembly of Li and C.

In the discussion, qualitative conclusions were drawn for some cases. For example, in the case of ^{6}Li and Pb, the problems will be attributed mainly to the inelastic-scattering cross section and/or SED for 14 MeV neutrons rather than cross sections at lower energy region, since DDX data show similar discrepancies. Similarly, it is likely that the discrepancy observed for liquid nitrogen assembly is attributed to the cross section or SAD for elastic-scattering, and those for LiF and CF_2 assemblies are due to inadequate SED and/or SAD of F for 14 MeV neutrons.

For b) and c), however, straightforward diagnostic is not possible because of complex configuration of the assembly and correlation between the effects of neutron transmission and scattering for light elements. Therefore, sensitivity analyses were recommended to point out the origin of the problems. Of course, sensitivity analyses will be valuable for the case a).

It was pointed out that the internal consistency of the experimental data is important and should be checked for use in nuclear data assessment based on integral data. In some cases, discrepancy between the analyses using Monte-Carlo and discrete-ordinate methods was pointed out.

For further discussion, analyses considering energy-angle correlation between SAD and SED were requested as well as the precautions mentioned above.

4. Nuclear Data Related to Structural Materials (Mainly Medium Weight Nuclides)

4.1 A Review of JENDL-3 Structural Material Data

S. Iijima* and T. Asami**

* Nuclear Engineering Laboratory, Toshiba Corporation
** Nuclear Energy Data Center

The status of the JENDL-3 data for structural materials of Cr, Fe and Ni are described briefly. Especially the outline of the data revisions from JENDL-3T to JENDL-3 are given. The JENDL-3 data for Cr, Fe and Ni are discussed for the double differential ones for neutron emission and the some threshold reactions, and the problems to be resolved are also discussed.

1. Introduction

The evaluated data of JENDL for the structural materials of Cr, Fe, Ni and so on have been revised so much through JENDL-3PR1,-3PR2[1] and -3T[2] to JENDL-3[3]. The structural material data in JENDL-3PR1 and -3PR2 were compiled in revising partially the ones in JENDL-2[4]. The whole reevaluation for Cr, Fe and Ni was made for JENDL-3T in the point of view for the urgent uses in fusion neutronics, and the evaluated data for photon production were adopted newly. These structural material data of JENDL-3T were compiled in JENDL-3 after the minor changes.

In this paper a general review of these data is given as well as the data revision from JENDL-3T to JENDL-3, from the viewpoint of fusion neutronics. The structural material data of JENDL-3 are compared with of the other libraries, especially ENDF/B-VI. The problems from the work on the international comparison of the structural material data are also described.

2. Outline of the Data Evaluation for Cr, Fe and Ni in JENDL-3

The data reevaluations of Cr, Fe and Ni were performed in almost the same manner. For the resonance parameters the new evaluated data from recent measurements were added to, and the data for high-energy neutrons

were reevaluated carefully.

The data with very few or no experimental ones were obtained from theoretical calculations. The threshold reaction cross sections were calculated mainly with the GNASH code[4], and some data were with the PEGASUS code[5]. The calculations for the elastic and inelastic scattering and capture data were made with the CASTHY code[6]. For some levels the direct components of the inelastic scattering were calculated with the DWUCK code[7] or the ESCIS code[8]. the photon productions and the DDX data were evaluated based on the calculations with the GNASH code.

The general descriptions of the data evaluation for these materials are given in the File 1 in JENDL-3[3]. In this paper, our discussions are limited to the data revised in the course from JENDL-3T to -3. An outline of the data revision is shown in Table 1.

3. General Aspects of JENDL-3 Structural Material Data

In the reevaluations for JENDL-3 the data revised widely are the resonance parameters, the inelastic scatterings and the threshold reactions, and the ones evaluated newly are the photon productions. Among those, the data important for the fusion research are the DDX ones for neutron emissions, the threshold reactions including the activation cross sections and the photo production ones. Since the data for the activations and the photo productions will be discussed in this proceedings later, we concern only with the data for the threshold reactions and the DDX for neutron emission. The status of JENDL-3 for these data are discussed for each material below.

Cr : Figure 1 shows the (n,α) cross sections of the Cr element for JENDL-3T, JENDL-3 and ENDF/B-VI. In JENDL-3 these cross sections were slightly modified at near the threshold to give a good fit to the experimental data.

The DDX data of JENDL-3 for neutron emissions are compared with the experimental ones of Tohoku university[9] at 30, 80 and 150 degrees in Figs. 2(a), 2(b) and 2(c), respectively. The evaluated data at the forward angle are in good agreement with the experimental ones. However, the data at 80 degrees are rather lower. The data at the backward angle are slightly higher and have a different shape from the experimental ones. From these comparisons it is shown that the spectral shape of JENDL-3 for

the continuum of the inelastic scattering (MF=5, MT=91) has some problems. This problem would be solved only with the full description of kinematics by the use of the File 6 of the ENDF/B format. Baba et al.[9] have measured the angle-integrated double-differential neutron spectra and discussed the problems in JENDL-3T

Fe : The (n,2n) cross sections of ^{56}Fe element are compared between JENDL-2, -3 and ENDF/B-VI as well as the experimental ones in Fig. 3. Above about 15 MeV, there are some discrepancies between JENDL-3 and ENDF/B-VI.

As shown in Table 1 the (n,p) cross sections of ^{54}Fe are slightly modified at JENDL-3. Figure 4 shows the (n,p) cross-section data of ^{54}Fe in comparing the evaluated ones with the experimentals. In the range between 7 and 13 MeV there are some discrepancies among the experimental ones and also among the evaluated data libraries.

For the (n,α) cross sections of ^{56}Fe, the International Task Force has pointed out[10] that there have been large discrepancies around 10 MeV among the evaluated data libraries.

In Figs. 5(a) to 5(c) the DDx data at 14.1 MeV for JENDL-3T and JENDL-3 at the angles of 30, 80 and 150 degrees are compared with the experimental ones of Tohoku university[9]. These figures are shown that the JENDL-3T data were revised slightly for the 3- level of the ^{56}Fe 4.51 MeV and so on. Takahashi et al.[11] have discussed on the Fe DDX data of JENDL-3T and pointed out their discrepancies. The JENDL-3 Data are generally in good agreement with the experimental ones and overcome the above discrepancies almost. However, the File 6 descriptions for the evaluated DDX data would be necessary to give a good fit to the experimental ones.

Ni : The (n,α) cross sections of the Ni element for JENDL-3 are compared with the ENDF/B-VI ones in Fig. 6. The ENDF/B-VI data deviate much from both the JENDL-3 and the experimental ones. This shows that there are some problems in the (n,α) cross sections of ^{58}Ni and ^{60}Ni.

Figures 7(a), 7(b) and 7(c) show the DDX data of JENDL-3 at 30, 80 and 150 degrees, respectively, in comparing with the ones in JENDL-3T and ENDF/B-VI. The JENDL-3 data are generally in good agreement with the experimentals. However, the JENDL-3 data at the forward angle are slightly lower than the experimental ones.

4. Discussions

The JENDL-3 data for structural materials were examined in the points of view for fusion neutronics. Generally the data for Cr, Fe and Ni are revised satisfactorily for wide uses. However, the (n,α) cross sections of Fe and Ni have some discrepancies between the libraries.

The DDX data of JENDL-3 for Cr, Fe and Ni generally reproduce the experimental ones. However, the DDX evaluated data should be compiled in using the File 6 format of the ENDF/B for further revision of these data.

The international task force has now made the comparison of the evaluated data between the major libraries in the world. We expect that this comparison work would resolve the discrepancies between the libraries in near future.

References

1) Kikuchi, Y. et al.: J. Nucl. Sci. Tech. 22, 499 (1985).
2) Asami, T. : JAERI-M 88-065 (1988) p.4.
3) Shibata, K. et al. : JAERI 1319 (1990).
4) Nakagawa, T. (ed.) : JAERI-M 84-103 (1984).
4) Young, P.G. and Arthur, E.D. : LA-6947 (1977).
5) Iijima, S. : JAERI-M 87-025, p.337 (1987).
6) Igarasi, S. : J. NUcl. Sci. Tech. 12, 67 (1975).
7) Kunz, P.D. : unpublished.
8) Fukahori, T. and Tazaki, I. : JAERI-memo 62-453 (1988) (unpublished).
9) Baba, M. et al. : 88Mito (1988) p.291.
10) Working Group of a joint NEACRP/NEANDC Task Force on Intercomparison of the Evaluated Files for ^{52}Cr, ^{56}Fe and ^{58}Ni, (1990).
11) Takahashi, A. et al. : 88Mito (1988) p.205.

Table 1 The outline of the data revision for chromium, iron and nickel in the course of the version-up from JENDL-3T to JENDL-3.
The MT and MF numbers listed here show the data with some revisions in JENDL-3T.

Chromium

	Cr-nat	^{50}Cr	^{52}Cr	^{53}Cr	^{54}Cr
MAT	3240	3241	3242	3243	3244
MF MT					
3	107	107			
15	102				

Evaluator: T. Asami (Nuclear Energy Data Center)

Iron

	Fe-nat	^{54}Fe	^{56}Fe	^{57}Fe	^{58}Fe
MAT	3260	3261	3262	3263	3264
MF MT					
2	151				151
3	4	4	4		
	51,58,61,63-65, 70,73-74	51-54, 59,68	51-54, 77		
	103	103	103		
4	55,58,61, 63-65,74	51-54, 59,68	51-54 77		

Evaluator: S. Iijima (Nuclear Engineering Laboratory, Toshiba Corp.)
H. Yamakoshi (Ship Research Institute)

Table 1 (continued)

Nickel

	Ni-nat	^{58}Ni	^{60}Ni	^{61}Ni	^{62}Ni	^{63}Ni
MAT	3280	3281	3282	3283	3284	3285
MF	MT					
2	151	151				
3	4	4	4			
	56,59-63, 69-70	51-53, 55,65	51-54, 61			
4	56,59-63	51-53, 55	51-54			
13	3					
15	3					
	102					

Evaluator: S. Iijima (Nuclear Engineering Laboratory, Toshiba Corp.)

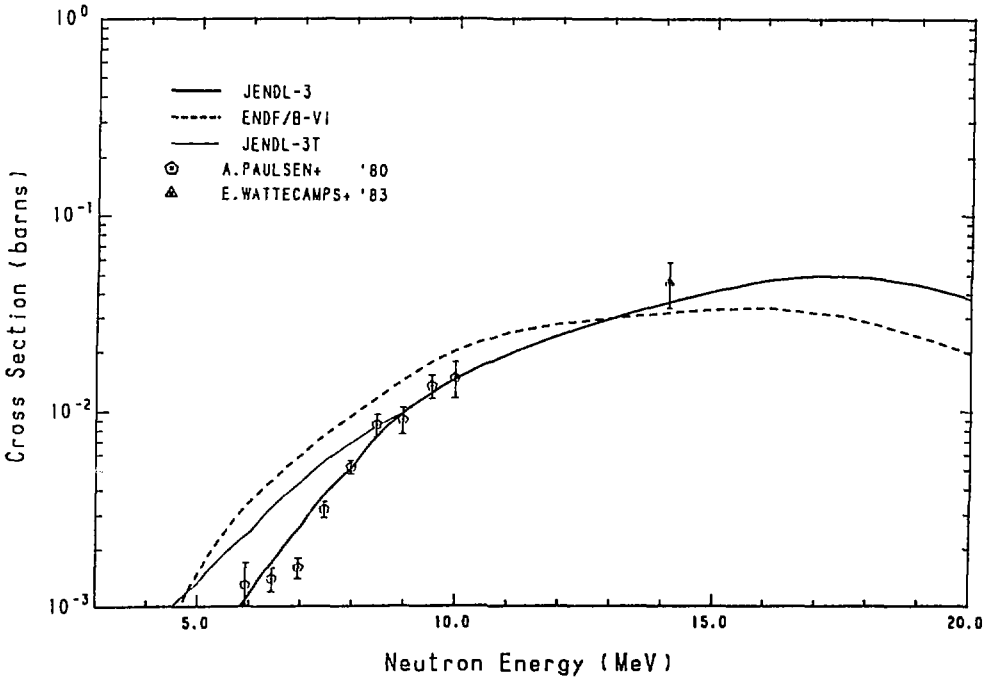

Fig. 1 The (n,α) cross sections of the Cr element for JENDL-3T, -3 and ENDF/B-VI.

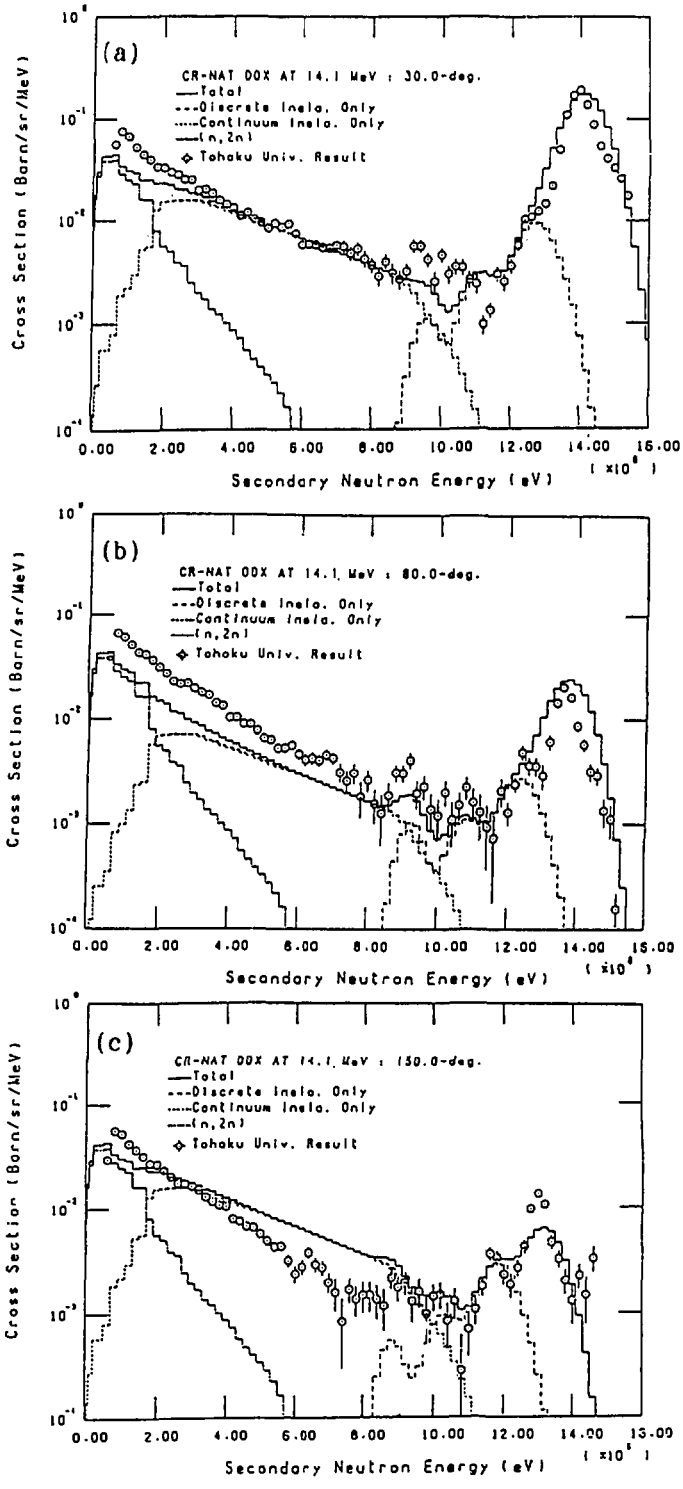

Fig. 2

The DDX data for neutron emission of the Cr element for 14.1 MeV neutrons, at the laboratory angles of (a) 30, (b) 80 and (c) 150 degrees. The JENDL-3 (JENDL-3T) data are compared with the experimental ones of Tohoku university. These figures are taken from ref(8).

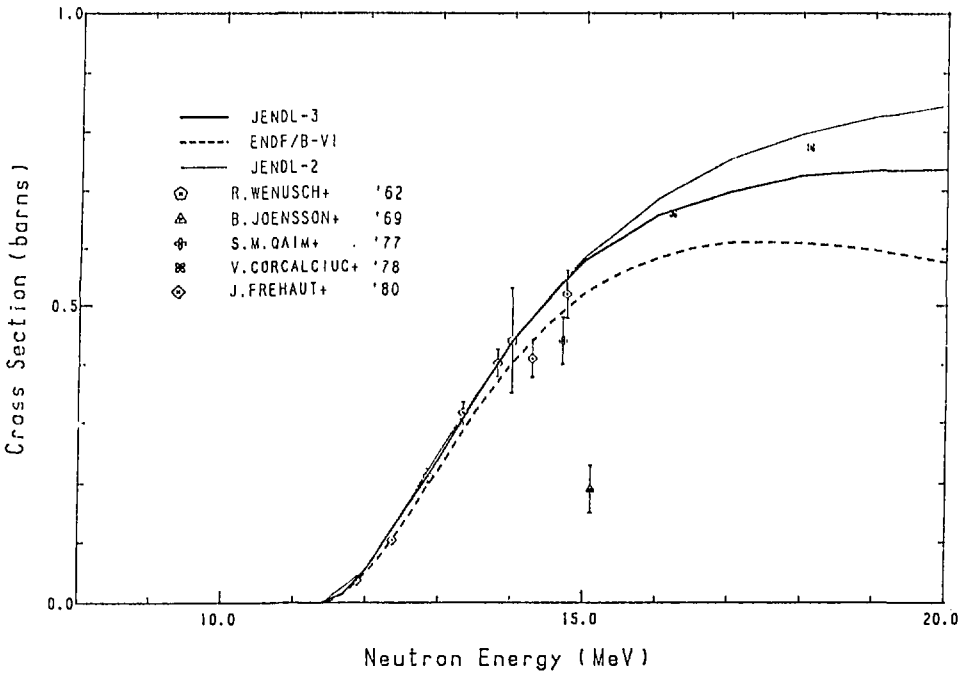

Fig. 3 The (n,2n) cross sections of ^{56}Fe.

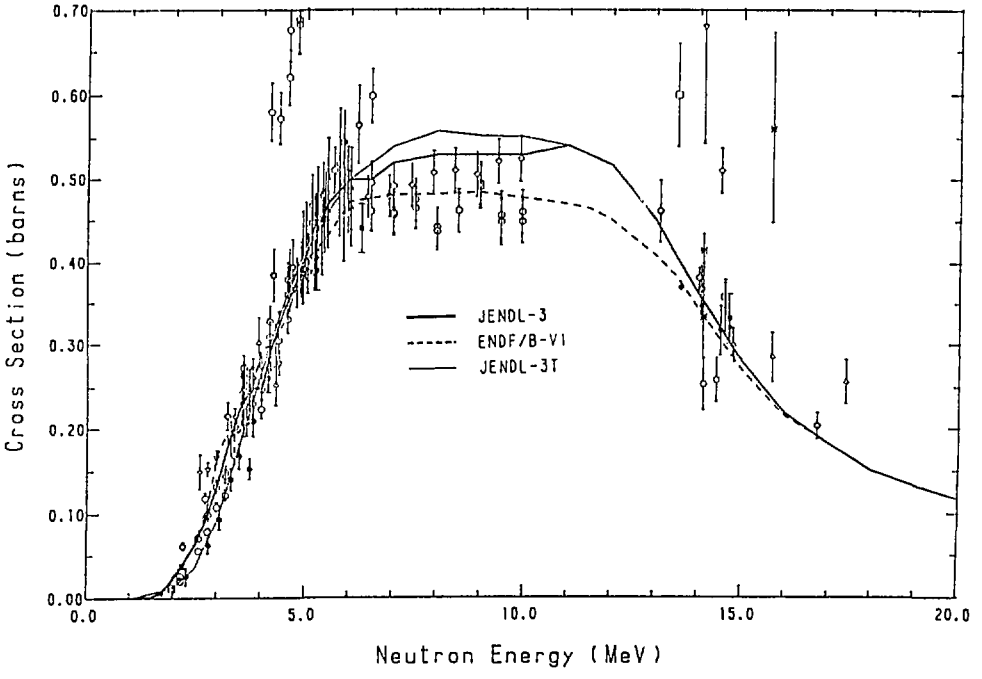

Fig. 4 The (n,p) cross sections of ^{54}Fe.

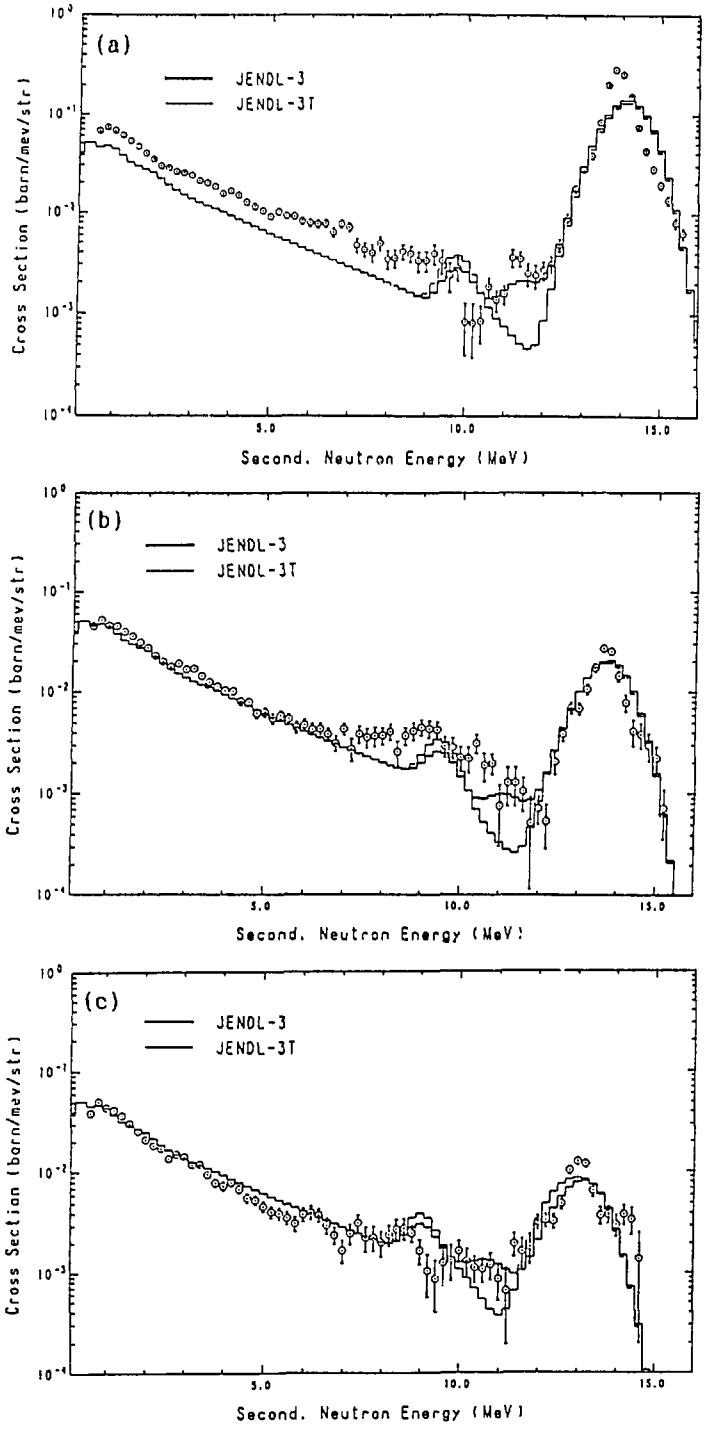

Fig. 5

The DDX data for neutron emission of the Fe element for 14.1 MeV neutrons, at the laboratory angles of (a) 30, (b) 80 and (c) 150 degrees. The JENDL-3 (JENDL-3T) data are compared with the experimental ones of Tohoku university[9].

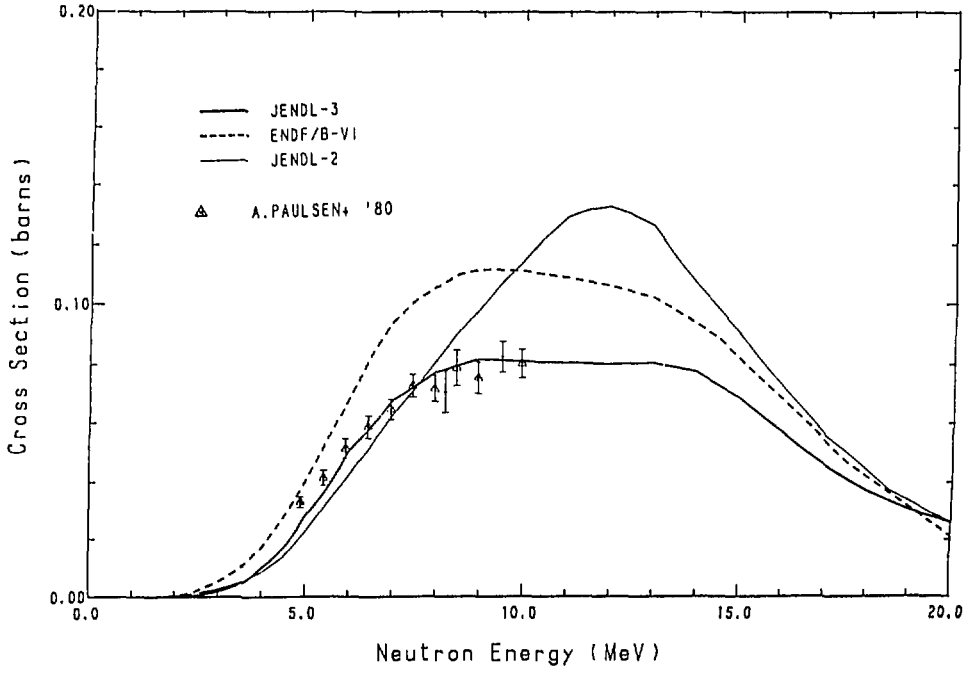

Fig. 6 The (n,α) cross section of the Ni element.

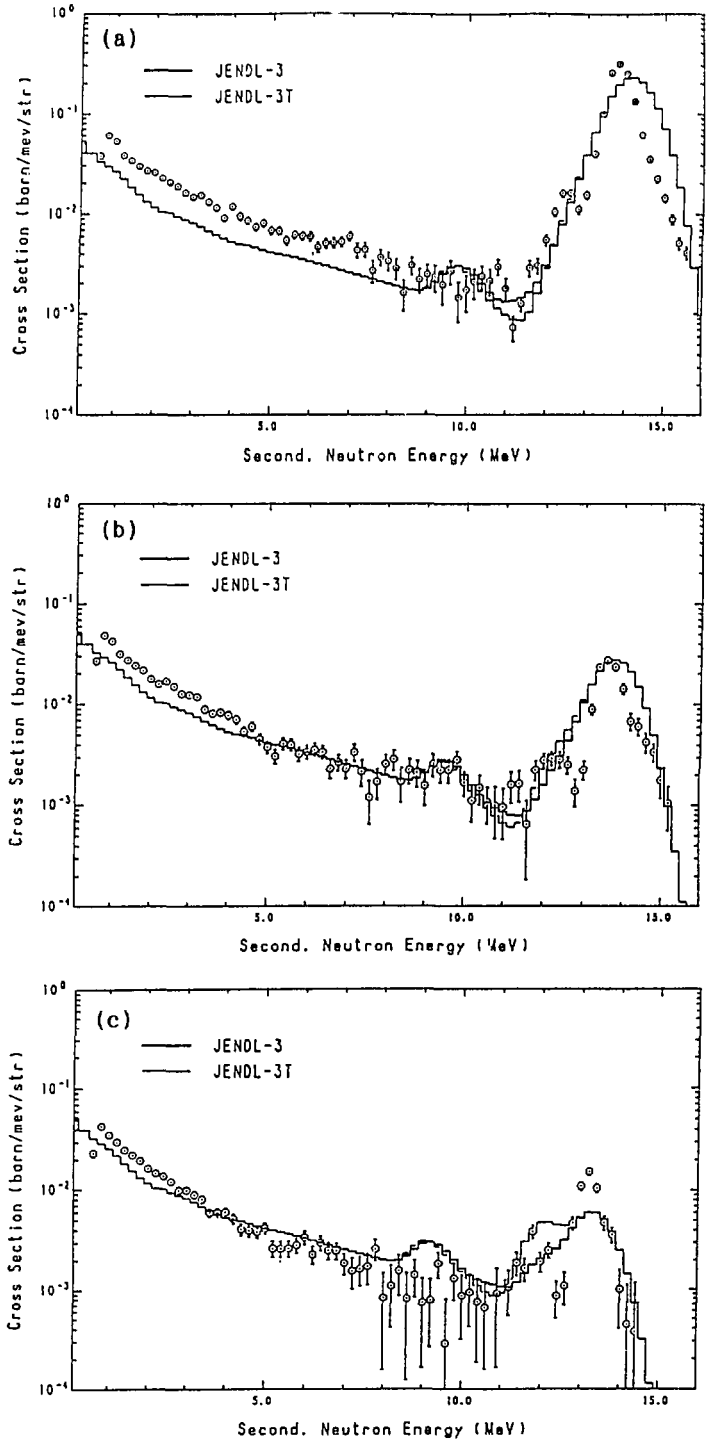

Fig. 7

The DDX data for neutron emission of the Ni element for 14.1 MeV neutrons, at the laboratory angles of (a) 30, (b) 80 and (c) 150 degrees. The JENDL-3 (JENDL-3T) data are compared with the experimental ones of Tohoku university[9].

4.2 Main Discussion on the Data Status of Strucutral Material Nuclides

Y. Kanda
Department of Energy Conversion Engineering,
Kyushu University
Kasuga, Fukuoka 816, Japan

Medium heavy nuclides discussed in this session are contained in major candidates for structural materials of fusion reactors. Since they are irradiated with primary fast neutrons produced in fusion reactions their nuclear data decisively affect design of reactors. Neutron transport is the main nuclear process to be considered in massive materials in order that it determines neutron energy and spacial distribution which results in the nuclear effects in the fusion reactor blanket such as induced activities and heating. The nuclear data concerning the process are the double differential cross section (DDX). Therefore, the DDX for the medium heavy nuclides are mainly discussed in this session.

After the presentations about the evaluations, integral experiments, and comparisons between experiment and calculation which can be found individually in this report, we are enthusiastic about the discussion on the disagreement between evaluation and DDX measurement and between calculation and integral experiment. The remarkable disagreement in common for the interesting nuclides is in the secondary neutron energy range of approximately 8～12 MeV where the inelastically scattered neutrons are predominant and the secondary neutron yields are minimum for the 14 MeV incident neutrons. Concerning the issues the following two reasons are emphasized:

(1) The recommended inelastic scattering cross sections must be insufficiently and unwilling given in JENDL-3 by the evaluators because the number of energy levels used for the inelastic scattering is limited in the ENDF/B-VI Format.

(2) There can be large experimental uncertainties for some nuclides because of low secondary neutron yield in this energy region.

5. Analyses of Engineering Benchmark Experiments

5.1 Integral Test of JENDL-3 through Analysis of Fusion Blanket Experiment Phase IIB

M. Nakagawa
Japan Atomic Energy Research Institute
Tokai-mura, Naka-gun, Ibaraki-ken

Neutronics parameters measured in the JAERI-US fusion blanket experiment Phase IIB have been analysed based on JENDL-3 and compared with the results by JENDL-3/PR1. The differences in C/E values are small for the tritium production rates by lithium 6 but amount to several percent for the threshold reaction rates between both nuclear data files. The integral test of the cross sections used in the transport calculations and the reaction cross sections are separately performed at the present work.

1. Introduction

For the integral test of JENDL-3, the fusion blanket neutronics experiments have been analysed and the results obtained by JENDL-3 and JENDL-3/PR1 are compared[1]. The Phase IIB is one of the fusion blanket experiment series performed in a frame of the JAERI-USDOE collaborative program[2]. In the Phase II experimental systems, the lithium oxide test region and the neutron source are contained by the lithium carbonate region which is enclosed by a polyethylene layer. The 5 cm thick beryllium multiplier and the thin stainless steel first wall were placed at the inner surface of the system. The measured parameters are tritium production rates by lithium 6(T_6) and lithium 7(T_7), reaction rate distributions, neutron spectrum and etc. The detail of the measurements and the results are described in Ref(3). The analysis of Phase II has been performed based on JENDL-3/PR1 and the results are described in Ref(4). At the present work, JENDL-3 was used for an integral test and the dependence of C/E values on nuclear data was investigated. The calculation methods are almost the same as those used in the previous analysis. The 125 group double differential cross sections have been produced from JENDL-3 by the processing code PROF-DD[5] . The angular meshes consist

of the 20 equal cosine bins with $\Delta\mu$ = 0.1. The calculation model is briefly illustrated in Fig.1 which presents the vertical cross sectional view of the Phase IIB system. 14 MeV neutrons are generated at the rotating neutron target(RNT) by (d,t) reactions. Reaction rates analysed here were measured along the central axis in the test channel. The calculations were performed by the Monte Carlo method using the GMVP[6] code.

2. Tritium Production Rates

The comparison of T_6 between the measured values and the calculated one is shown in Fig.2. In these calculations, JENDL-3/PR1 was commonly used as the $^{6}Li(n,\alpha)t$ reaction cross section. That of JENDL-3 was also used but the results are quite similar between both files. At the neighborhood of the surface of beryllium zone, the statistical uncertainties are too large to form a conclusion. Both files show a common trend that the C/E values drop below 0.8 at the behind of the beryllium zone. This was one of the most important discrepancies observed in the Phase IIB analysis when JENDL-3/PR1 was used, and is still not resolved even if JENDL-3 was used. In the deeper zone, the C/E values agree with each other within the statistical uncertainties. Therefore, it can be said that both files would give quite similar T_6 in the Li_2O system.

The results for T_7 are shown in Fig.3. JENDL-3 gives larger values by about several percent over the whole region. It should be noted that the differences come from those in the neutron fluxes. When the $^{7}Li(n,n',\alpha)t$ cross sections in each files are respectively used, JENDL-3 gives larger T_7 by 3-4% than JENDL-3/PR1 because this cross section of JENDL-3 is larger in the energy region above 12 MeV. In conclusion, JENDL-3 reduces the discrepancy in a prediction of T_7.

3. Reaction Rate Distributions

Various reaction rates have been measured using activation foils. Those include threshold reactions such as $^{27}Al(n,\alpha)^{24}Na$, $^{58}Ni(n,2n)^{57}Ni$, $^{58}Ni(n,p)^{58}Co$, $^{93}Nb(n,2n)^{92}Nb$, $Ti(n,xp)^{46}Sc$, $Ti(n,xp)^{47}Sc$, $Ti(n,xp)^{48}Sc$ and $^{115}In(n,n')^{115}In^{*}$. At the first, neutron fluxes were calculated by both JENDL-3 and JENDL-3/PR1, and then the reaction rates were calculated using the FNS file[7] The results for the $Al(n,\alpha)$ reaction are shown in Fig.4. The C/E values obtained by both files are close to unity at the surface of the test region and gradually lower with increase of the distance from the front surface. Such a trend is similar with t[illegible] cases

of $^{7}Li(n,n',\alpha)$ reaction. JENDL-3 shows a better agreement compared with JENDL-3/PR1. The C/E curves for Nb(n,2n), Ti(n,xp)^{47}Sc and In(n,n') are shown in Figs.5, 6 and 7, respectively. In the case of Ti(n,xp)^{47}Sc, a trend of the C/E curves is slightly different from the cases mentioned above. The calculations fairly underestimate the reaction rates even at the surface of the test region. The energy dependence of this reaction cross sections may be inadequate.

Since the In(n,n') reaction has a low threshold energy, the reaction rate has a high sensitivity even at a few hundred keV region. Therefore, the differences in the C/E values which increase up to 10% at the maximum would be mainly attributed to the differences in the low energy part of neutron spectra. With respect to $^{197}Au(n,\gamma)^{198}Au$ reaction which shows a high sensitivity at the eV region, the C/E values obtained by both files are close with each other in the region, z > 20cm as seen in Fig.8. The statistical uncertainties are large in the front region but they become smaller in the deeper region. Such a trend is consistent with the case of T_6.

In JENDL-3, activation cross sections are also evaluated and compiled in the dosimetry files. Some reaction rates have been calculated using these new data and compared with the results by the FNS or ENDF-B/IV or V where the neutron fluxes were obtained by the transport calculations using JENDL-3.

The C/E curves for $^{93}Nb(n,2n)^{92}Nb$ are compared in Fig.9. JENDL-3 gives smaller C/E values by 5 - 10%. The deviations from unity at the front surface(z= -5.0cm) are small for both files but the discrepancy by JENDL-3 increases much more with the distance from the front surface. The groupwise cross sections of Nb(n,2n) for metastable state are compared in Fig.10 where JENDL-3 gives smaller values below 13 MeV. Measurements of this cross sections are being carried out at JAERI and the results would be reflected in JENDL-3 in near future. The reaction rates for Ni(n,2n) are compared in Fig.11. JENDL-3 gives smaller C/E values by about 10%. The reaction cross sections are compared in Fig.12 which shows a considerable disagreement over the whole region. Further measurements and evaluations should be done to reduce such a discrepancy.

References

1) Nakagawa M., Mori T. and Kaneko K.: "Production of Multi-group Double Differential Form Cross Section Library Using JENDL-3 and Benchmark Test of Fusion Neutronics Problem," JAERI-M 90-097 (1990) (in Japanese)
2) Nakamura T. et al.: Fusion Technol.,10, 541 (1986)
3) Oyama Y. et al.: "Phase IIA and IIB Experiments of JAERI/U.S.DOE Collaborative Program on Fusion Blanket Neutronics- Neutronics Experiment on Beryllium Configuration in a Full Coverage Blanket Geometry," JAERI-M 89-215 (1989)
4) Nakagawa M. et al.: "JAERI/U.S. Collaborative Program on Fusion Blanket Neutronics - Analysis of Phase IIA and IIB Experiments," JAERI-M 89-154 (1989)
5) Mori T., Nakagawa M. and Sasaki M.: "One-, Two-, and Three-Dimensional Transport Codes Using Multi-Group Double-Differential Form Cross Sections," JAERI-1314 (1988)
6) Nakagawa M., Mori T. and Sasaki M.,: 1st Int. Conf. Supercomputing in Nuclear Applications, BS103, Mito (1990)
7) Ikeda Y. et al.: "Activation Cross Section Measurements for Fusion Reactor Structural Materials at Neutron Energy from 13.3 to 15.0 MeV Using FNS Facility," JAERI 1312 (1988)

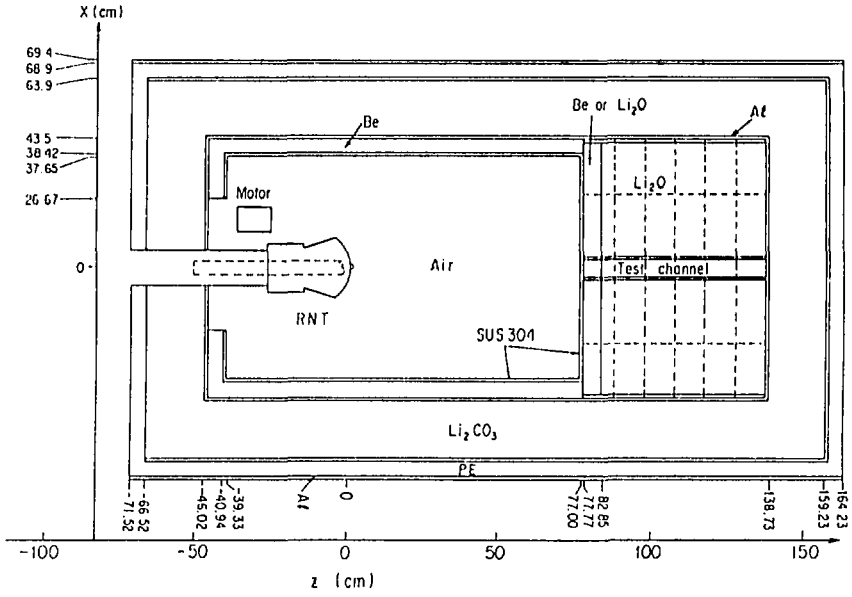

Fig.1 Calculational model of Phase IIB experimental system

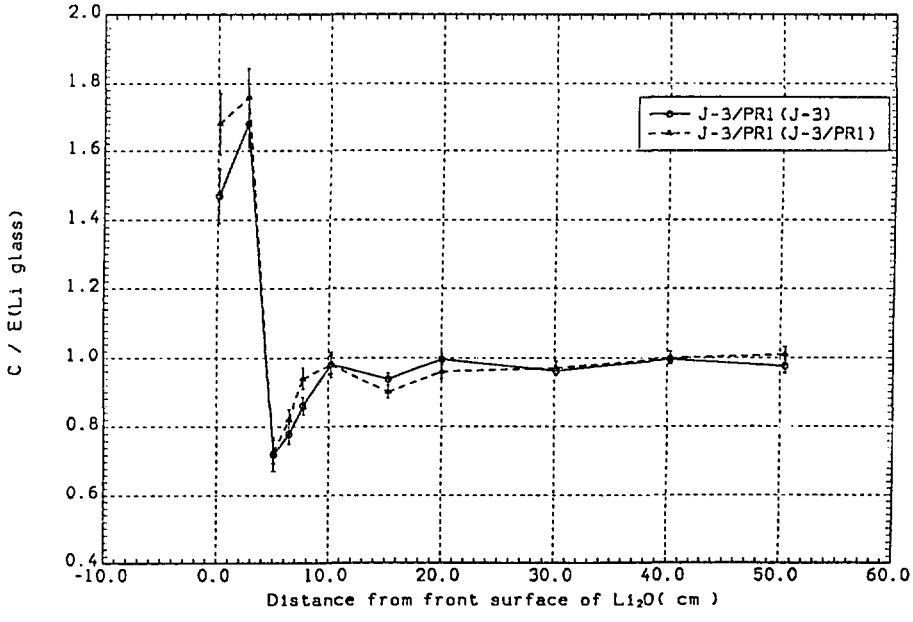

Fig.2 C/E values of tritium production rates by ^{6}Li

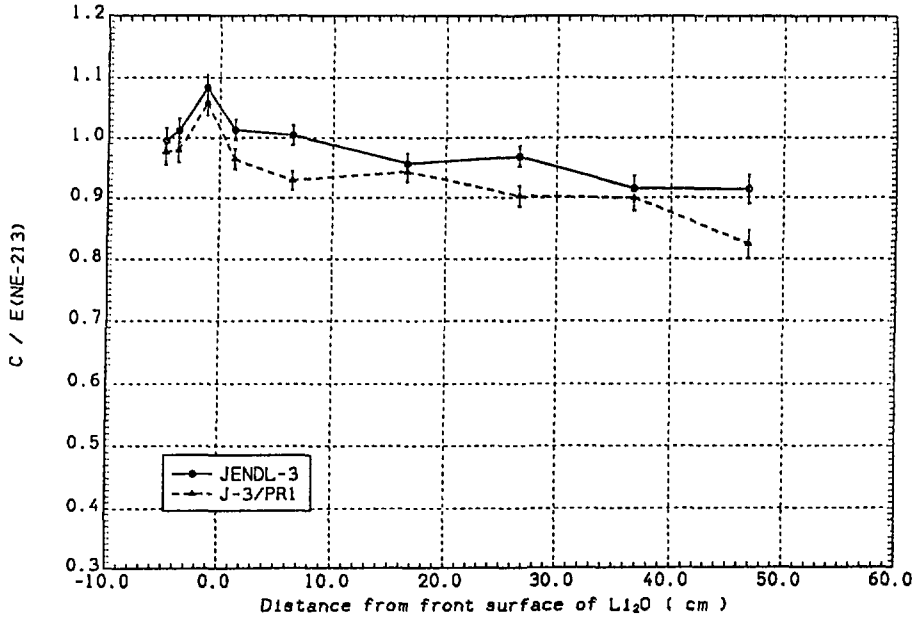

Fig.3 C/E values of tritium production rates by ^{7}Li

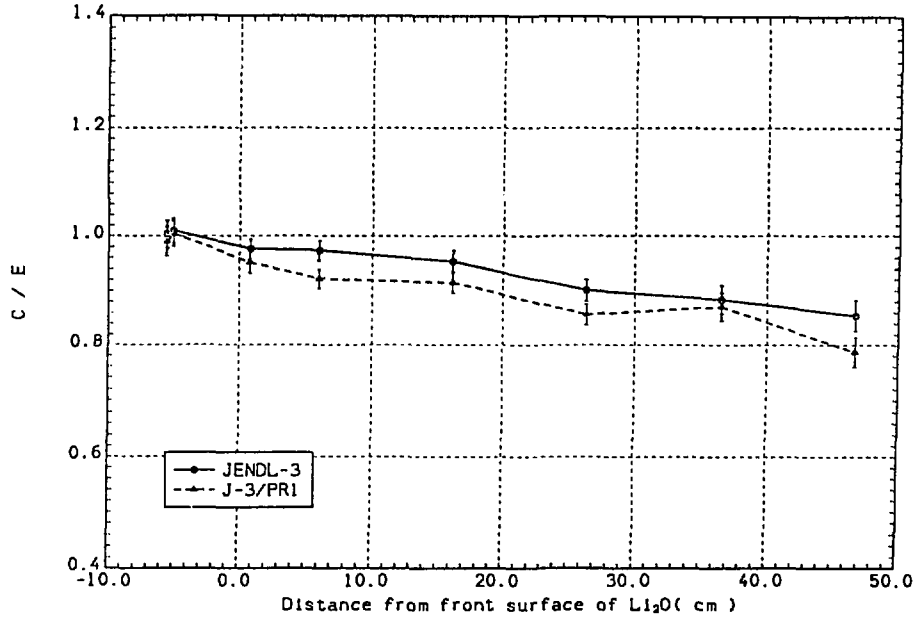

Fig.4 C/E values of $^{27}Al(n,\alpha)^{24}Na$ reaction rates

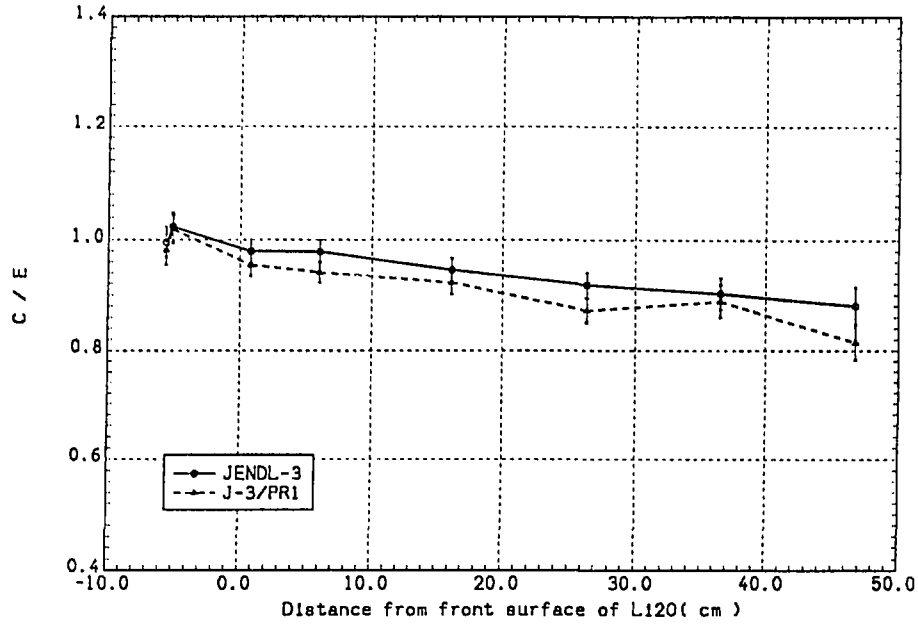

Fig.5 C/E values of $^{93}Nb(n,2n)^{92}Nb$ reaction rates

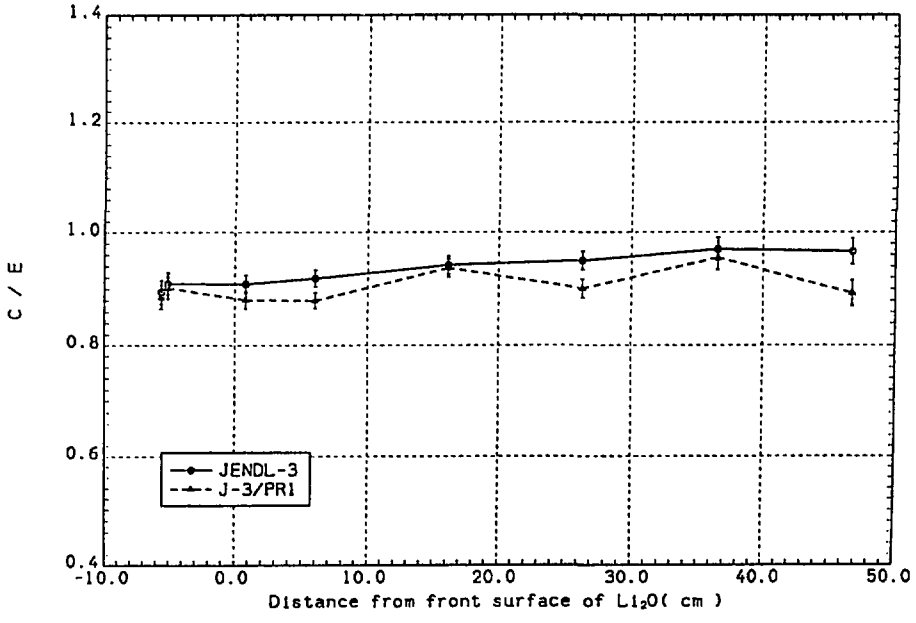

Fig.6 C/E values of $Ti(n,xp)^{47}Sc$ reaction rates

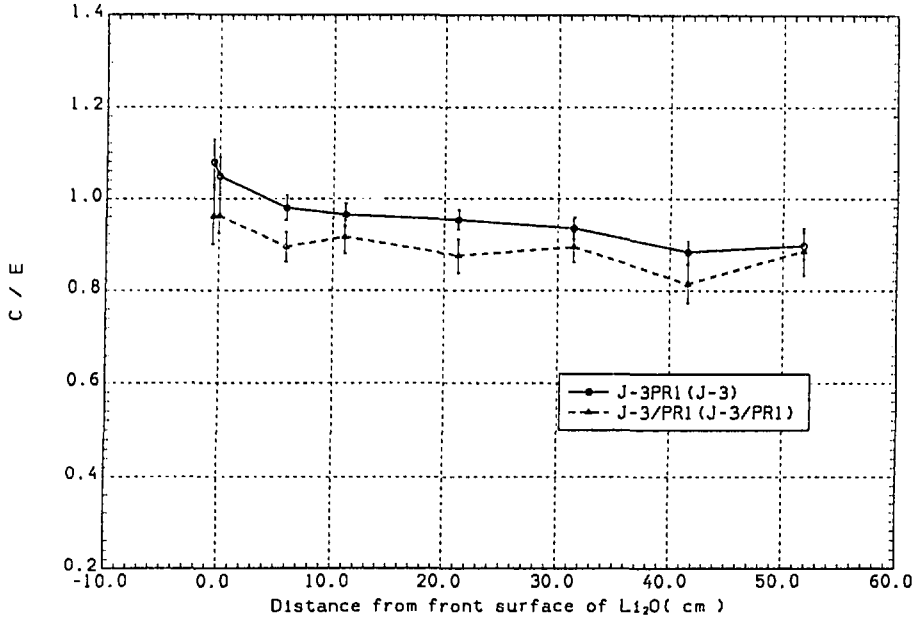

Fig.7 C/E values of $^{115}In(n,nn')^{115}In^{*}$ reaction rates

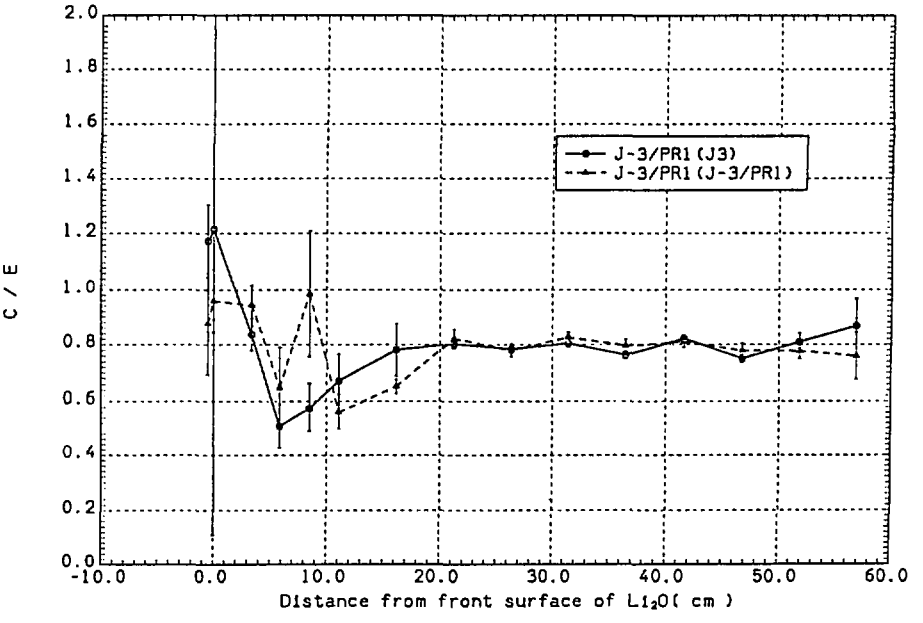

Fig.8 C/E values of $^{197}Au(n,\gamma)^{198}Au$ reaction rates

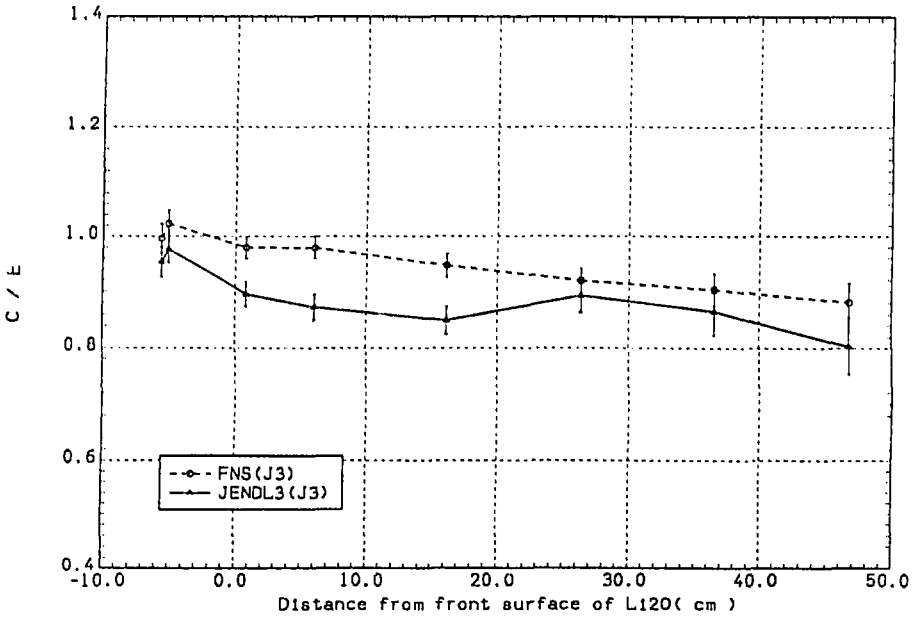

Fig.9 C/E values of $^{93}Nb(n,2n)^{92}Nb$ reaction rates based on the transport calculation by JENDL-3

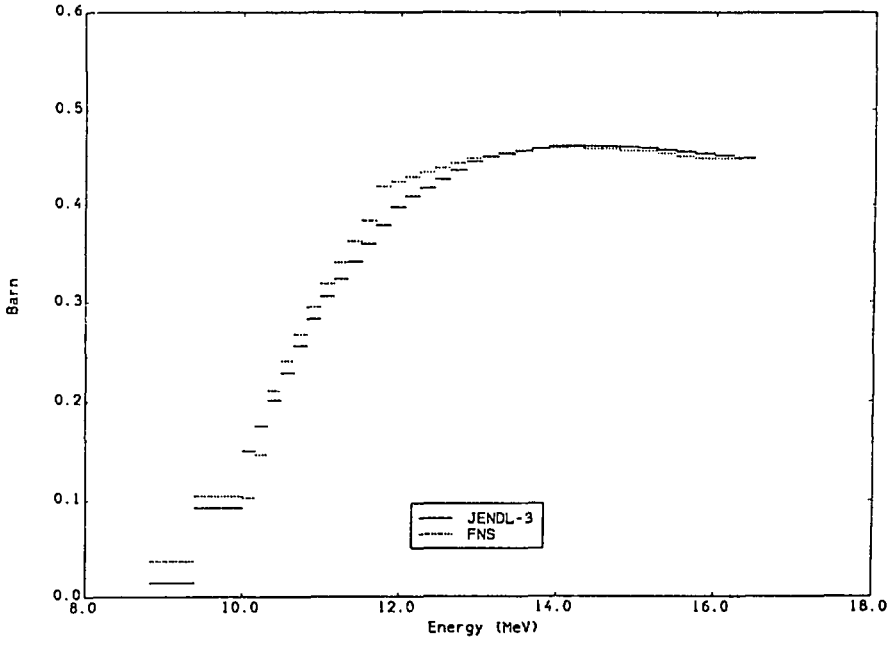

Fig.10 Comparison of (n,2n) cross sections of ^{93}Nb

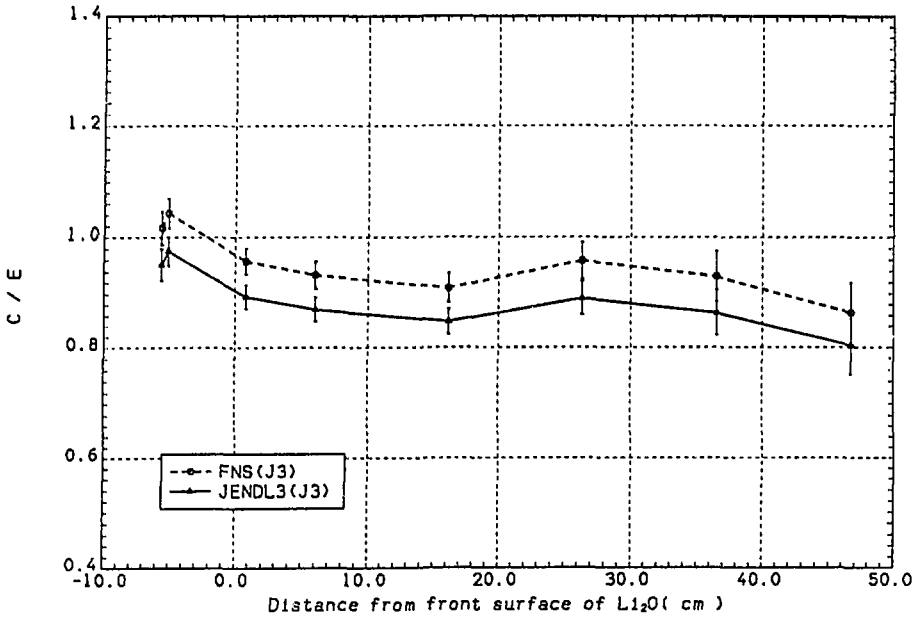

Fig.11 C/E values of $^{58}Ni(n,2n)^{57}Ni$ reaction rates based on the transport calculation by JENDL-3

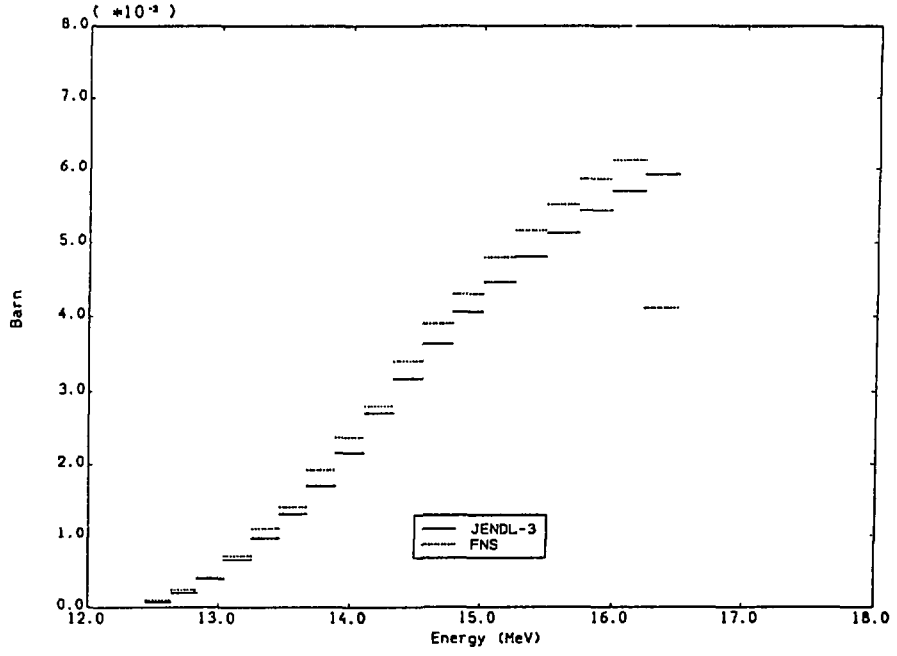

Fig.12 Comparison of (n,2n) cross sections of ^{58}Ni

5.2 Tritium Breeding Ration in Li, Li-C, Pb-Li, Pb-Li-C, Be-Li, Be-Li-C Spheres Measured by TLD or Li Pellets

J. Cetnar, T. Iguchi, M. Nakazawa,
[1]K. Sugiyama, [2]A. Takahashi, [2]K. Sumita
and [3]Inter-university research group, Japan
University of Tokyo, Bunkyo-ku, Tokyo 113

Several experiments were carried out to measure tritium breeding ratio (TBR) in various lithium spheres combined with lead or beryllium neutron multiplier and optionally graphite reflector. The tritium production rate distributions inside the lithium spheres were measured with Li_2CO_3 pellets or LiF TLDs. Determination of TBR from TLD measurements was done using the least squares method employing covariance matrixes of nuclear data. The measured values of TBR do not differ much from theoretical ones. In cases of the systems with multiplier and reflector, total TBR in lithium zone significantly exceeds 1.0 level.

1. Introduction

One of the main goals of a fusion reactor system is to achieve self-sufficiency of tritium production in the blanket. To accomplish this goal, a series of integral experiments were carried out to measure TBR in lithium spherical assemblies. We investigated various types of the blanket starting from bare lithium sphere. The main effort was done towards systems with a neutron multiplier as the most promising ones. A design of a fusion reactor blanket with neutron multipliers has been suggested in order to achieve TBR greater than 1.0. On the progress of our research work a graphite reflector was added to the systems to improve TBR by a neutron leakage reduction. The measured values of TBR is to be compared with theoretical ones obtained by neutron transport calculation using the ANISN code with the nuclear library JENDL-3.

2. Outline of the experiment

The experiments were held in the 14MeV neutron source facility "OKTAVIAN" at Osaka University. The neutron source strength was of order 10^9 n/s and for its measurement the 'Large Solid Angle Activation Foil Method' [1] has been applied. In reported experiments

---

[1]Tohoku University, Sendai 980,
[2]Osaka University, Suita 565,
[3]S.Iwasaki, N.Matsuyama, J.R.Dumais, M.Sakuma (Tohoku U.), J.Kaneko, K.Harada, P.Strasser (U. of Tokyo), S.Itoh (Nagoya U.), J.Yamamoto and K.Yamanaka (Osaka U.)

lithium carbonate pellets (Li_2CO_3) and LiF TLDs namely UD136N combined with UD137N were used to measure local tritium production rate (TPR). However, to obtain TPR from TLD measurements as well as total TBR from TPR some support from neutron transport calculation is necessary. This calculation was done using the ANISN code with the nuclear library JENDL-3. The number of neutron groups is equal to 125 and the order of Legendre expansion of anisotropic scattering equals 5. A complex uncertainty analysis employing covariances matrixes was developed to obtain proper error estimation of the TBR measurements. Calculations and measurements of TBR were carried out for the following structures of the spherical assemblies:

1. Li(50cm)
2. Li(50cm)+C(20cm)
3. Pb(10cm)+Li(40cm)
4. Pb(10cm)+Li(40cm)+C(20cm)
5. Be(11.65cm)+Li(40cm)
6. Be(11.65cm)+Li(40cm)+C(20cm).

Fig.1 presents the systems with the neutron multiplier and the graphite reflector.

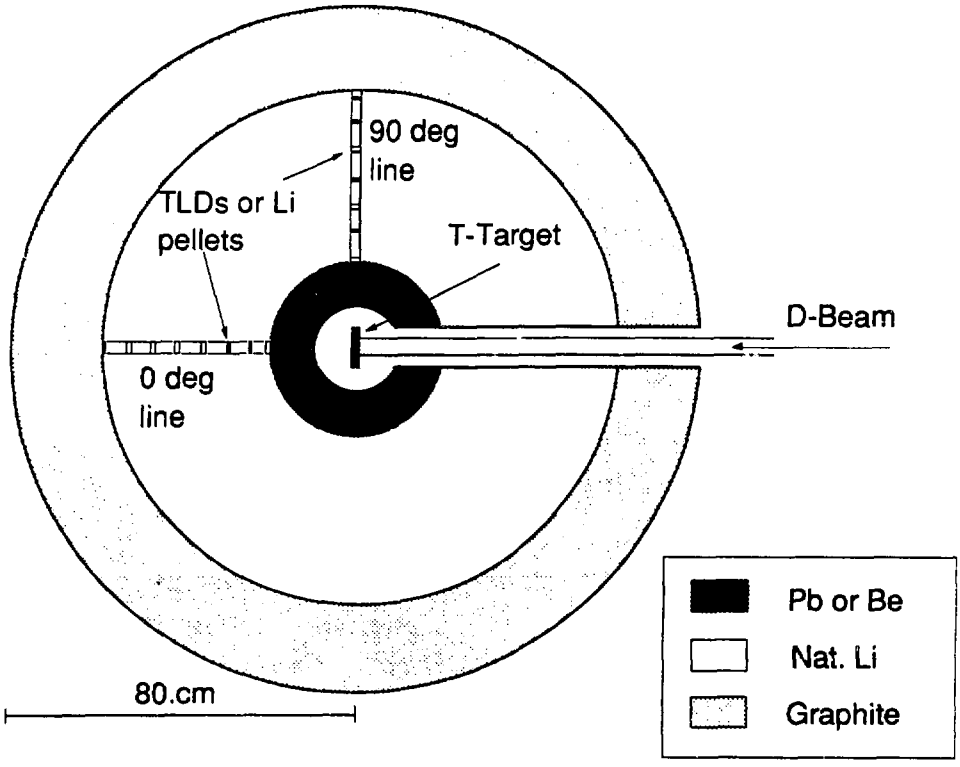

Fig.1 Pb(Be)-Li-C combined spherical system

3. Methodology of TBR estimation

The direct measurement of local TPR by lithium carbonates pellets is widely known. This technique was applied to bare Li(50cm) assembly as well as to Pb(10cm)+Li(40cm) one. Derivation of TBR by integrating the local TPR over the whole lithium zone was assisted by its theoretical distribution to overcome problems with step space dependencies of measured values. In case of TLD application to TBR measurements, additional effort is necessary to obtain local TPR from TLD measurements. This technique was used for remaining systems. Now this method will be briefly described.

Idea of the measurement is based on the fact that TLDs UD-136N and UD-137N consist of the same material apart from isotope of lithium. In the former case it is ^{6}Li, in the latter ^{7}Li. Detectors of ^{6}Li are sensitive for neutrons mainly due to reaction $^{6}Li(n,\alpha)T$, thus the response function to neutrons is similar to tritium production cross section. Both detectors has the same sensitivity for gamma radiation. If we take difference of responses from UD-136N and UD-137N, it will be the response only for neutrons. In this case the presence of gamma radiation will not disturb the measurement. But since the difference response function of TLDs (TLDD response function) differs from the tritium production cross section (Fig. 2), an influence of a neutron spectrum uncertainty on the TPR derivation from TLD responses must be of concern. For this purpose the neutron spectrum is treated as a variable. When the neutron flux and cross sections are presented in the group structure one can write equations:

$$TPR=\sum \phi \cdot \Sigma_{TP} \qquad (1)$$

$$TLDD=\sum \phi \cdot f_{TLDD} \qquad (2)$$

where ϕ is the neutron flux at measured point, Σ_{TP} is the macroscopic tritium production cross section and f_{TLDD} is the difference of TLDs response function. To solve the equations (1) and (2) the general least squares method was used. Generally, it minimizes function (3) conserving side equations (1) and (2) expressing TPR and TLDD responses at each point of measurement.

$$M=[\vec{y}-\vec{y}^{m}]^{T} \cdot \mathbf{G}_{y} \cdot [\vec{y}-\vec{y}^{m}] \qquad (3)$$

where $\vec{y}$ and $\vec{y}^{m}$ denote true and measured values vectors, $\mathbf{G}_{y}$ is the weight matrix equal to reverse covariance matrix of measurements.

During the experiment, TLD responses in lithium zone and source strength were measured. Measured values of TLD response functions with their covariance matrixes were prepared from direct measurements [2], [3].

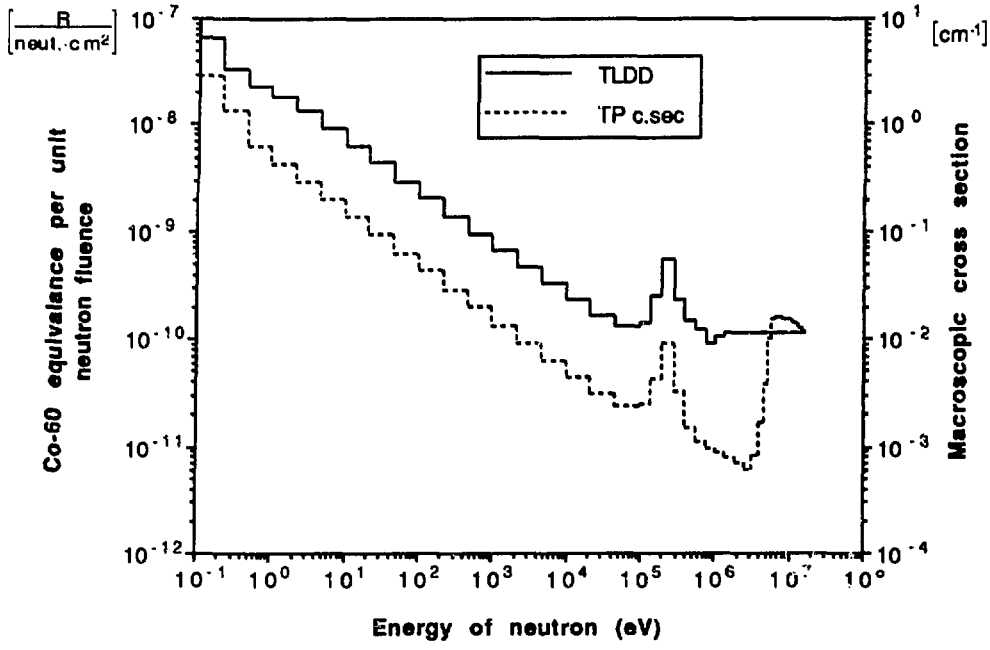

Fig.2 TLD difference response function and macroscopic tritium production cross section in natural lithium

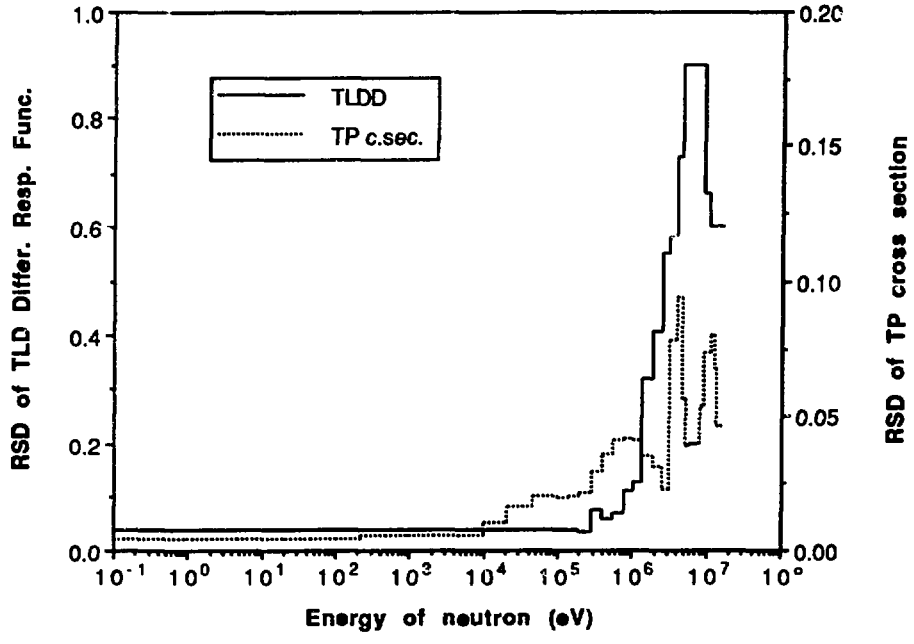

Fig.3 Relative standard deviation of TLD difference response function and TP cross section

Macroscopic tritium breeding cross section and its covariance matrix were prepared from $^{6}Li(n,\alpha)T$ and $^{7}Li(n,n'\alpha)T$ cross section and uncertain data from [4] (Fig. 3). Neutron flux obtained from transport calculation is treated as a measured one but uncertainty of these data was chosen large since direct measurement of flux is not performed. This treatment gives us an information about the impact of flux spectrum uncertainty on the final uncertainty of TBR. It can be also noticed that this method imposes some correlation of TPR measured in different points what is physically understandable due to a fact that mean free path of neutrons in the system is comparable with the size of the lithium zone.

The neutron spectrum is treated as uncertain to take into consideration errors imposed by differences between shape of TLDD response function and tritium production cross section. Condition of the positive value of neutron spectrum sets limit on relative standard deviation. It was chosen equal to 80% and correlations between group values were set at the level leading to TBR uncertainty obtained only from transport calculation equal to about 40%. This way final TBR uncertainty derived from TLD measurements is not strongly affected by additional a priori information concerning neutron spectrum.

4. Results and discussion

Theoretical values of TBR from $^{6}Li(n,\alpha)T$ and $^{7}Li(n,n'\alpha)T$ reactions calculated using ANISN with JENDL-3 library are presented in Table 1.

Table 1 TBR in Lithium spherical assemblies

	T6	T7	Total
Li	0.205	0.467	0.672
LiC	0.542	0.488	1.03
PbLi	0.366	0.161	0.527
PbLiC	0.92	0.19	1.11
BeLi	0.691	0.244	0.935
BeLiC	1.20	0.25	1.45

It can be noticed that tritium production by ^{6}Li isotope is strongly gained in the systems with a neutron multiplier and reflector. In all cases of systems with the reflector, the theoretical TBR is above 1.0. The strongest and most promising is the case with the beryllium multiplier. Experimental data concerning the Li-C blanket are shown on Fig. 4, the next Be-Li on Fig. 5, Pb-Li-C on Figs. 6 and 7, and Be-Li-C on Fig. 8 and 9. Fig. 10 presents C/E ratio concerning measurements using TLD. Values of TBR measured with lithium pellets in Li and Pb-Li spheres fit very well to theoretical ones (Table 2). The differences are smaller than uncertainties of the measurements. The main source of error in this case is the neutron source strength estimation (Table 3).

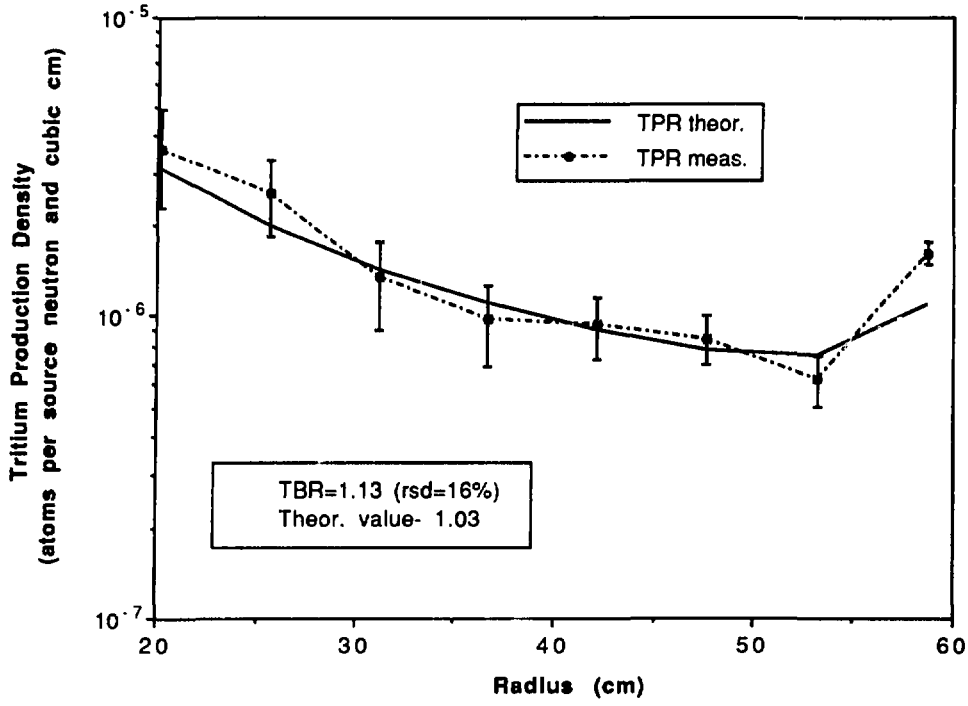

Fig.4 Tritium Production Rate in the Li-C blanket

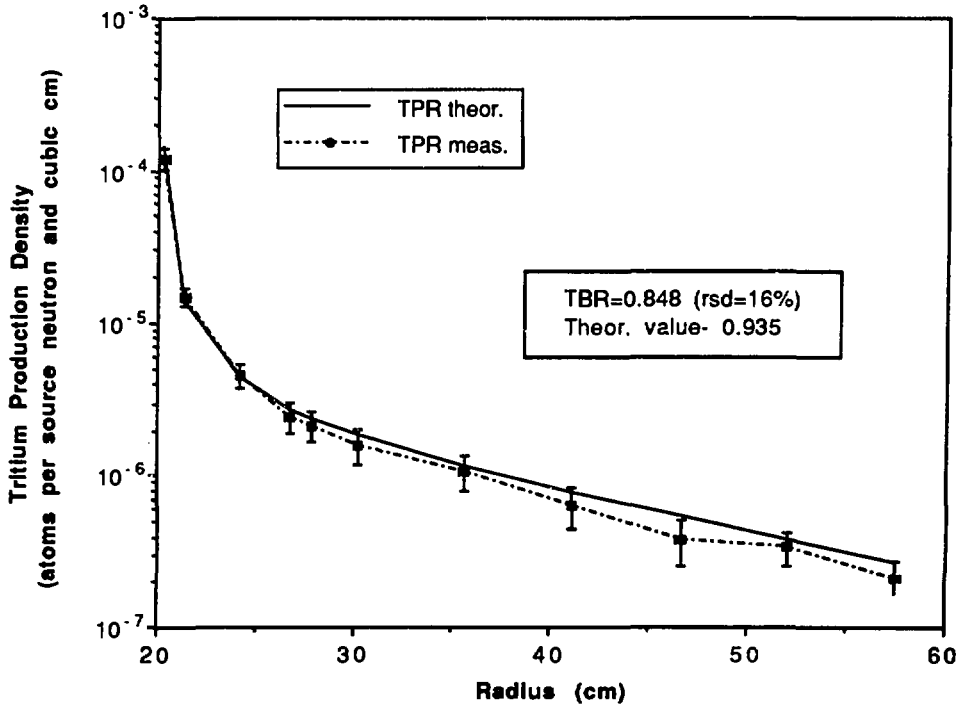

Fig.5 Tritium Production Rate in the Be-Li blanket

Table 2 Comparison of TBR experimental and theoretical values.

	TBR Exp.	TBR Theor.	C/E	RSD
Li	0.685	0.672	0.98	5.6%
LiC	1.13	1.03	0.91	16%
PbLi	0.530	0.527	0.99	6.0%
PbLiC	1.16	1.11	0.96	8.5%
BeLi	0.848	0.935	1.1	16%
BeLiC	1.51	1.45	0.96	9.1%

Table 3 Partial errors forming uncertainty of total TBR [%]

	Source strength	Detectors meas.	TPR cross sec.	TLD resp.funct.	Neutron spectrum
Li	5.3	1.0			
LiC	2.6	8.0	1.5	7.0	10.0
PbLi	5.3	2.0			
PbLiC	3.0	2.0	1.0	5.0	6.0
BeLi	2.6	9.0	1.0	6.0	9.0
BeLiC	2.5	3.5	1.0	4.5	6.0

In the Li-C blanket case the experimental TBR is higher than theoretical one but uncertainty is rather high (Table 2). In this type of blanket without any neutron multiplier the neutron spectrum is rather hard. This creates significant errors due to the neutron spectrum uncertainty linked with higher errors of the TLD difference response function and its shape differing from the tritium production cross section (Figs. 2, 3).

Measured value of TBR in the Pb-Li-C blanket is slightly greater than calculational one mainly in the outer Li region. It can be resulted from better reflection of neutrons than theoretically predicted. The final value of TBR is about 1.16 with relative standard deviation equal to 8.5% what means that the real value of TBR is greater than 1.0 with probability about 95%.

The data from experiments with the Be multiplier show that the thermal neutron flux after passing the beryllium zone is significantly lower than theoretical one, since the epithermal and medium energy range neutron flux can be higher. This reflects lower TPR in the part of lithium zone facing Be layer and higher TPR in the middle part. In outer part of the Be-Li blanket without presence of the reflector, the TPR distribution underestimates calculational one. This also points out that neutron spectrum is moved towards higher energies increasing the neutron leakage. Moreover the neutron multiplication in the beryllium zone can be higher than the result from the JENDL-3 based theoretical calculations. Results obtained for the Be-Li-C blanket are optimistic since TBR is about 1.5 level.

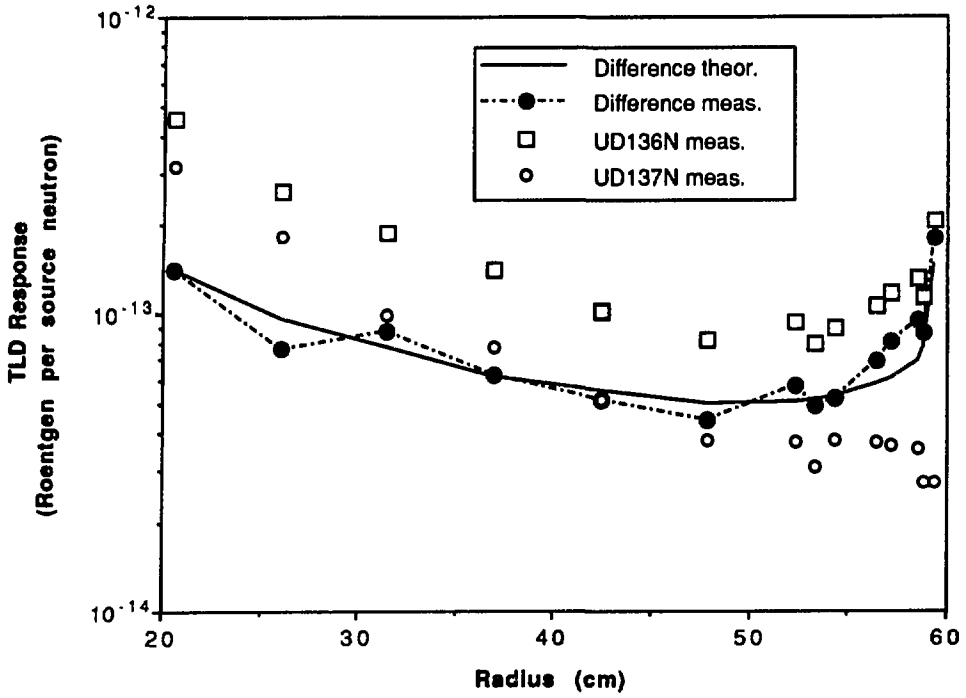

Fig.6 Theoretical and measured responses of UD136N, UD137N and their difference in the lithium zone of Pb-Li-C blanket

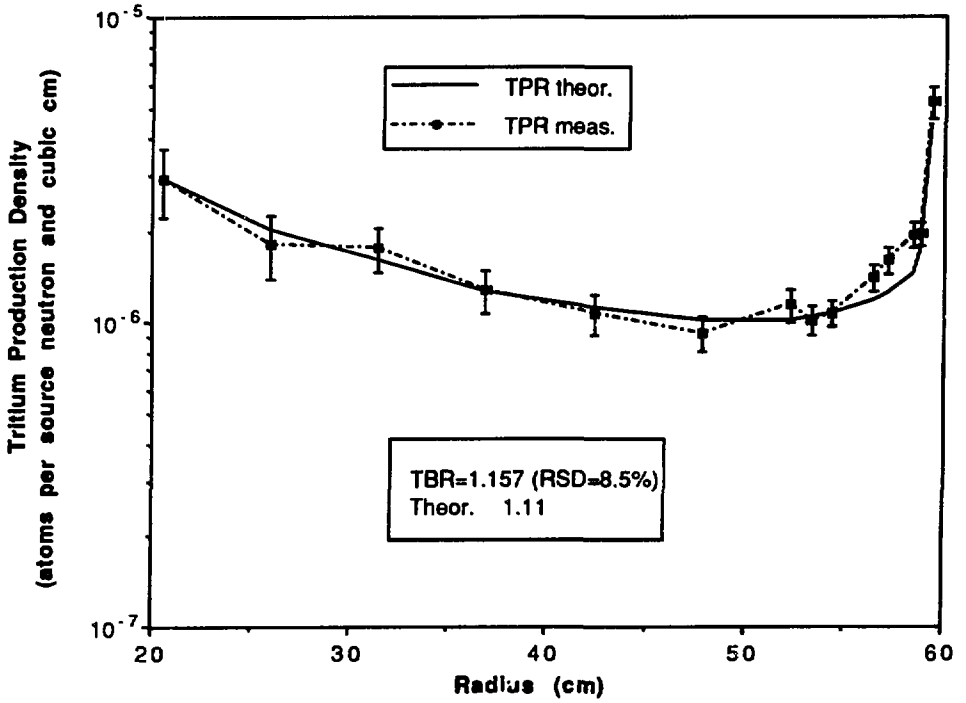

Fig.7 Tritium Production Rate in the Pb-Li-C blanket

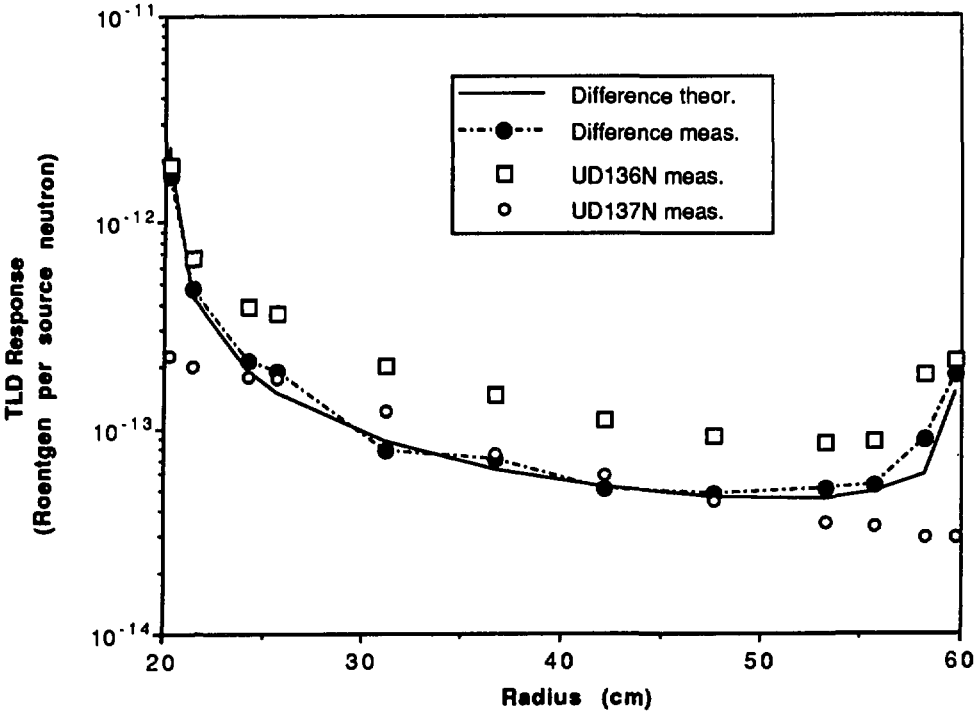

Fig.8 Theoretical and measured responses of UD136N, UD137N and their difference in the lithium zone of Be-Li-C blanket

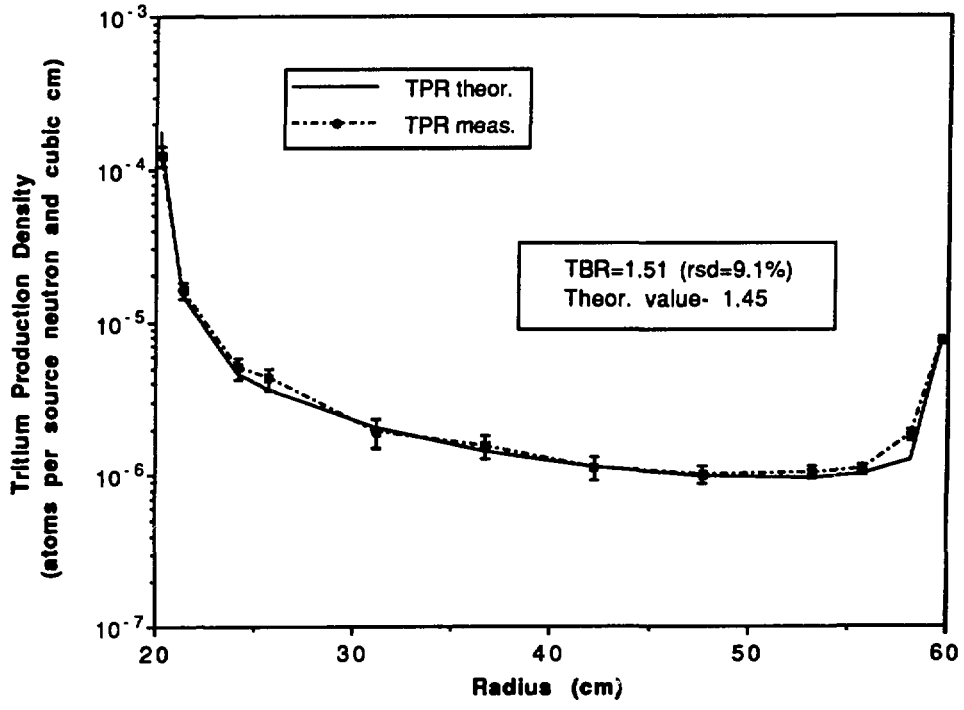

Fig.9 Tritium Production Rate in the Be-Li-C blanket

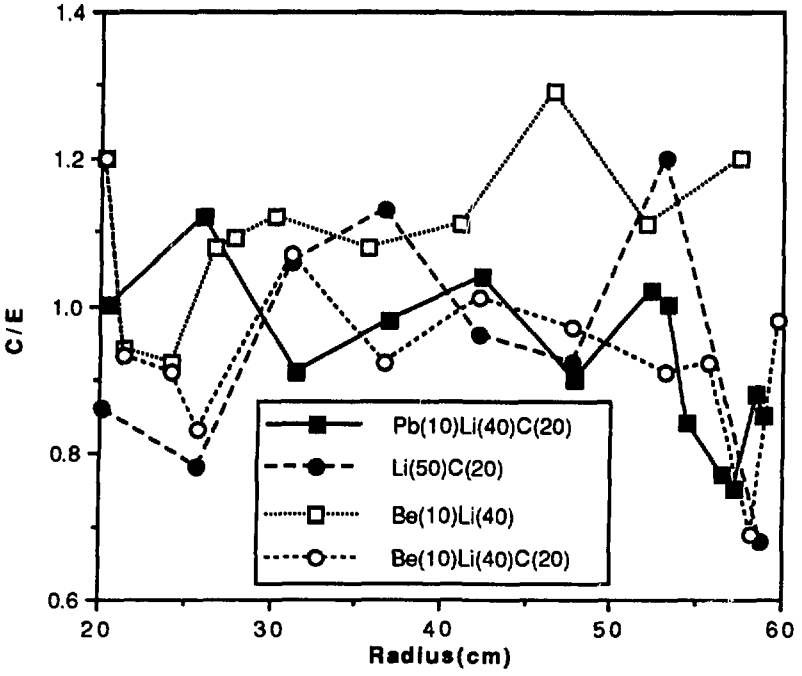

Fig.10 Ratio C/E of TPR derived from TLD measurements

5. Conclusions

Data obtained in the present experiments show quite good fitting to theoretical values. The experimental TPR in the vicinity of Pb reflector is higher than calculational one. All systems with the reflector give TBR above 1.0 level. In case of the Pb-Li-C and Be-Li-C blankets the TBRs are significantly higher than 1.0 with good uncertainties of the measurements. The neutron production in Be can be slightly higher comparing with JENDL-3 based calculations.

References

1) T. Iguchi and M. Nakazawa: New Large Solid Angle (4π) Activation Foil Method for Absolute Measurement of D-T Neutron Source Intensity, Journal of Nuclear Science and Technology Vol. 24, No. 11 (1987)

2) H. Hashikura, K. Haikawa, S. Tanaka and S. Kondo: Calculation of Neutron Response of Thermoluminescent Dosimeters, Journal of the Faculty of Engineering, the University of Tokyo (B) Vol. XXXIX, No.1 (1987)

3) Private communication

4) K. Furuta, Y. Oka and S. Kondo: Evaluation of Covariance Data for ^{6}Li and ^{7}Li Cross Section in JENDL3-PR1, UTNL-R-0167 (VIII 1984)

5.3 Measurement and Analysis of Time-Dependent Tritium Production Rates in Lithium Spheres with Be and Pb Neutron Multiplier

A. Takahashi, K. Yamanaka, K. Yoshioka, K. Sumita and K. Sugiyama*

Osaka University, *Tohoku University

Abstract: To assess uncertainties of nuclear data for breeding and multiplying elements, integral neutronics experiments using Li-spheres with Be and Pb multipliers were carried out to measure time-dependent tritium production rates which approximately reflected energy profiles of T-6 in the systems. Time dependent analyses were made using the newly evaluated nuclear data file JENDL-3.

1. Introduction

Tritium breeding with self-sufficiency is one of key issues for nuclear performances of fusion reactor blankets. It must be compatible with other key issues like shielding optimization, easy extractkion and minimum inventory of tritium, heat extraction with conventional coolant, and so on. To improve the predictability of breeding performance in design studies, uncertainties arising from nuclear data accuracies and geometrical blanket configurations have to be resolved. To study problems on nuclear data, the inter-university team has undertaken a series of integral neutronics experiments using a large sphere of natural lithium[1], two-layered spherical shell of Pb-Li[2], three layered spherical shell of Pb-Li-C[3] and three-layered spherical shell of Be-Li-C[4]. Many experimental techniques have been employed in the experiments to measure tritium production rate distributions, other reaction rate distributions, in-system and leakage neutron spectra. In the mean time of the program, newly evaluated nuclear data files like JENDL-3[5] and ENDF/B-VI have been completed. Now it is time to assess these newly evaluated nuclear data files using the accumulated integral data in the inter-university program. In this paper, we pick up the newest data of time-dependent tritium production rates to compare with the time-dependent Sn calculations using the nuclear data from JENDL-3.

2. Methods

Detailed description of spherical assemblies is given elsewhere[1,2,3,4].

Schematic drawings of spherical assemblies are shown in Figs.1-3, respectively for the Pb-Li, the Pb-Li-C and the Be-Li-C system.

Since the thermal blanket concept based on neutron multiplication and tritium production by the $^{6}Li(n,t)$ reaction is a current design trend, accuracies of Be(n, 2n) and Pb(n,2n) data are of interest concerning the effects on tritium production performance by Li-6. Considering the difference of neutron flux spectra between the model blanket which is simplified for integral experiments and the blankets of experimental fusion reactors[6], information on the energy profiles of tritium production rates in the systems is interested because if we know disagreements between experiment and calculation in some energy region of the profile of the model blanket we can extrapolate the difference to the energy profile of the real reactor blanket so as to estimate the TBR uncertainty of experimental reactor. To measure directly the energy profile of TPR (tritium production rate) is a difficult task. Instead, we can measure the time profile of TPR supposing that the experimental system is a neutron slowing down spectrometer which gives us a definite relationship, almost linear in logarithmic scale, between the neutron energy and the elapsed (slowing down) time after a short (ns) burst of D-T neutrons. A ns pulsed D-T neutron source of OKTAVIAN[7] and a set of small Li-glass detectors (Li-6 and Li-7) were used for this purpose.

The pulsed D-T neutrons were produced at the center of spherical assemblies. Either Li-6 or Li-7 glass scintillation detecor was inserted in the sphere along the 45 deg experimental channel as shown in Figs.1-3, so as to take foreground or background time spectrum as we show examples in Fig.4 a and b, where NE902 is the Li-6 detector and NE903 is the Li-7 detector. The Li-7 detector is sensitive to threshold reactions in itself by fast neutrons and also sensitive to gamma-rays. Except the short time interval near the D-T neutron burst, time-dependent background is very small compared with foreground of NE902 by the $^{6}Li(n,t)$ reactions. Therefore, the time-dependent experiment improves very much S/N ratio and we can obtain accurate time profile of TPR. When we changed detector positions along the 45 line, we filled up the removed volume with small disks of lithium metal canned with 1mm thick SS316 container in front and back of the detector so as to make the perturbation effect as small as possible. We measured time-profiles of TPRs pace-dependently, so that we can deduce either spatial distribution of TPR (time-integration), space-integrated time profile or TBR (overall tritium breeding ratio) as we like. For Li-glass scintillators, 1 mm thick 1.27 cm diam plates of NE902 and NE903 were adopted considering the self-shielding and flux perturbation calculations for detectors with various thicknesses.

For the calculational analyses with the JENDL-3 nuclear data, a time-dependent Sn code NITRAN-TD[8] was used. The NITRAN-TD code employs a data base of double differential cross sections, so that it is free from the generation of negative

scalor fluxes. By comparing the results with MCNP[9], it has been confirmed that the accuracy of NITRAN-TD calculation is very good upto very late time region where neutrons are almost thermalized. Together with the fact that we can apply one-dimensional analyses well for the experimental spherical assemblies, the results of time-dependent TPR calculations by NITRAN-TD with JENDL-3 can be compared effectively with the experimental TPR data to assess accuracies of nuclear data for Li, Be and Pb.

3. Results and Discussions

3.1 Lithium sphere

The outer shell (A-block in Fig.1) of natural lithium metal has 60 cm outer radius and 40 cm inner radius. Lithium metal is contained with a SS316 vessel which has 5 mm thick outer wall and 2 mm thick inner wall. The inner shell (C-block in Fig.1) was replaced with an inner shell of lithium metal having same dimensions and contained with a SS316 vessel of 2 mm thickness.

Space-dependent time-profiles of TPR were measured with 5 cm mesh width. Space-integrated time profile of TPR is shown in Fig.5, compared with the calculation by NITRAN-TD with JENDL-3. The lower figure in Fig.5 shows C/E values. Mean neutron energy coresponding to elapsed time is indicated upper. In the 30-700 ns time region which is equivalent to the 1 MeV to 12 keV energy region, the calculation with the JENDL-3 nuclear data reproduces the experimental TPR within 10 % discrepancies which are comparable to the experimental error band.

In our previous paper, we reported the results of TPR for the ^{6}Li(n,t) and ^{7}Li (n,n't) reactions which were measured with lithium carbonate pellets[1]. We obtained already good agreements in T-6 and T-7 between measured values and calculated values with the JENDL-3 preliminary data that are very close to the final JENDL-3 data. The present results for time-profiles reproduce similarly good agreement for T-6. We can therefore conclude that the JENDL-3 neutron data for Li-6 and Li-7 are accurate enough as far as tritium productions in blankets are concerned.

3.2 Pb-Li and Pb-Li-C spheres

The neutron multiplication by lead is a key issue for these experiments. Calculational results with different evaluated nuclear data files are shown in Table 1 for net neutron multiplications and leakage factors of 10 cm thick Pb shell. In parentheses, ratios to the case of JENDL-3 are given. We have about 10 % discrepancies in net multiplications among 4 data files, which should be resolved. Effects of these discrepancies on tritium breeding ratios (T-6 and T-7)

are shown in Table 2 and Table 3 respectively for the Pb-Li and the Pb-Li-C assembly: The largest discrepancy is about 10 % for T-6 with ENDF/B-4.

Space-integrated time-profiles of TPR in the Pb-Li assembly are shown in Fig.6, where C/E values are shown in the lower figure. Calculation with JENDL-3 underestimates the experiment by about 10 % in the 20-100 ns time region (equivalently 1.3 MeV to 0.2 MeV energy region), but agrees in later time region. Since we do not have problems in the lithium data of JENDL-3, this underestimation can be attributed to the insufficiency of Pb(n,2n) data in JENDL-3: The same result was mentioned in the previous paper[1] for leakage multiplication factors.

For the Pb-Li-C assembly, space-integrated time-profiles of TPR are shown in Fig.7, being compared with those of the Pb-Li assembly. We can see clearly that the effect of graphite reflector appears in the time region later than about 100 ns. Calculation with JENDL-3 underestimates the experiment in the 1-0.1 MeV region and overestimates, complementarily, the experiment in the 70-1 keV region. Time-integrated and space-dependent TPR distributions are shown in Fig.8, being compared with three calculations with different combinations of nuclear data. The calculation with JENDL-3 only gives the best overall agreement with the experiment, though we can point out overestimation in the 20-25 cm region and underestimation in the end of Li region.

Considering the difference in results between the Pb-Li and the Pb-Li-C assembly, we may point out that there would exist insufficiency of carbon neutron data of JENDL-3, or that the two experimental points near the reflector would contain large errors due to the strong flux depression and detector-self-shielding effects for well thewrmalized or low energy neutrons.

3.3 Be-Li-C assembly

Beryllium is the candidate material of neutron multiplier of solid breeder blanket for ITER[6]. To improve the predictability of neutron multiplication performance of beryllium, a joint benchmark experiment using beryllium shells from USA and China has been planned to undertake integral neutronics experiments at OKTAVIAN in Japan and SWINPC in China. In this paper, an iterim result of TPR time profiles which is one of items for measurement is mentioned[4].

As shown in Fig.3, an inner shell of beryllium metal with 11.65 cm thickness is set at the C-block position. Absolute source neutron yield of D-T reactions is monitored by a Nb cup which covers the tritium target assembly and is activated by the Nb(n,2n) reaction. Space-dependent time-profiles of TPR were measured in the 45 deg experimental channel. The results are shown in Figs.9-1 through 9-3, in comparison with calculated profiles with JENDL-3. Clearly, calculations overestimate

experiments in the region of second broad peak of profile, in the mean energy region less than about 200 keV, in positions up to 25 cm: At positions near the beryllium zone, underestimations are significant as is reported in the sandwiched Be-Li_2O slab experiment at JAERI[10]. On the contrary, very good agreements between calculation and experiment are seen in the 30-58 cm region.

Space-integrated (within Li zone) time-profiles of TPR are shown in Fig.10. Calculation with JENDL-3 (solid curve in the figure) reproduces very well the experimental results. The reason why we have had very good agreement for the overall TPR time-profiles, although we have significant disagreements in near distances, will be attributed to the fact that the weight of shell volume for the integration is proportional to r^2. Conclusively, we can say that calculations with the JENDL-3 Be data will provide accurate estimation of overall TBR (tritium breeding ratio) for fully covered blanket configurations as is the case of present spherical assembly, but will give underestimations for partially covered blankets. Partially covered blankets are of actual cases as seen in ITER designs[9], so that the discrepancy in the keV energy region should further be resolved.

Time-integrated and space-dependent TPR data are shown in Fig.11, in comparison with the calculated curve with JENDL-3. As already discussed, significant underestimations by the calculation with JENDL-3 are seen in the 20-30 cm region. In Table 4, summary is given for TBR values. The measured T-6 value of 1.209 is close to the calculated value with JENDL-3T, but a conclusive statement should be given after estimating the experimental error for T-6.

4. Conclusions

In order to assess the JENDL-3 neutron data for major blanket elements (Li, Be, Pb), measured data of TPR time-profiles in spherical and multiregional assemblies have been analyzed in comparisons with calculations using the JENDL-3 data.

To summarize the calculational predictabilities with JENDL-3 for tritium production rates in blankets, we can state the following;

a) nuclear data are sufficiently accurate for Li-6 and Li-7,
b) Pb(n,2n) cross sections should be rechecked,
c) and secondary neutron data of Be(n,2n), especially in low secondary energy region should be improved.

References

1)A. Takahashi: Integral Measurements and Analysis of Nuclear Data Pertaining to Fusion Reactors, Proc. Conf. Nucl. Data, Santa Fe, Vol.1, 59-79, Gorden and Breach Science Publ.,(1986)
2)K. Sugiyama, et al.: Neutronic Experiments in a Li-Pb Spherical Assembly, Proc. 14th SOFT, Avignon, Sept.8-12, 1986
3)J. Cetnar, et al.: Tritium Breeding Ratio in Li/Pb-Li/Pb-Li-C Spheres Measured with Li_2CO_3 Pellets and/or LiF TLDs, to be appeared in Proc. Conf. Nucl. Data, Juelich Germany, 1991
4)K. Sumita, et al.: Neutronic Integral Experiments for Evaluation on Tritium Breeding in a Fusion Blanket, Proc. IAEA AGM on Nuclear Data for Neutron Multiplication in Fusion Reactor First Wall and Blanket Materials, Chendu PRC, 1990
5)K. Shibata, et al.: Japanese Evaluated Nuclear Data Library, Version-3- JENDL-3-, JAERI-1319 (1990)
6) ITER Conceptual Design Report, ITER DOC. SER.18, IAEA, 1991
7)A. Takahashi, et al.: J. Nucl. Sci. Technol., 21, 577-598, (1984)
8)F. Maekawa: NITRAN Manual, OKTAVIAN Rep.A-90-01, (1990)
9) MCNP-A General Montecarlo Code for Neutron and Photon Transport, Version-3, LA-7396-M, Rev., LANL, (1983)
10)Y. Oyama, et al.: JAERI-M-89-215, -89-154, (1989)

Table 1 Comparison of calculational results by four nuclear data libraries in a Pb(10cm) assembly

	ΔM	Leakage
JENDL-3	0.513 (1.000)	1.510 (1.000)
JENDL-3T	0.470 (0.916)	1.467 (0.972)
ENDF/B-IV	0.563 (1.097)	1.559 (1.032)
EFF-1	0.486 (0.947)	1.484 (0.983)

Table 2 Comparison of calculational results by four nuclear data libraries in a Pb(10cm)+Li(40cm) assembly

	T 6	T 7	T t	ΔM	Leakage
JENDL-3	0.318 (1.000)	0.183 (1.000)	0.501 (1.000)	0.551 (1.000)	1.218 (1.000)
JENDL-3T	0.301 (0.947)	0.188 (1.027)	0.489 (0.976)	0.509 (0.924)	1.165 (0.956)
ENDF/B-IV	0.349 (1.097)	0.193 (1.055)	0.542 (1.082)	0.604 (1.096)	1.238 (1.016)
EFF-1	0.311 (0.978)	0.193 (1.055)	0.504 (1.006)	0.527 (0.956)	1.174 (0.964)

Table 3 Comparison of calculational results by four nuclear data libraries in a Pb(10cm)+Li(40cm)+C(20cm) assembly

	T 6	T 7	T t	ΔM	Leakage
JENDL-3	0.924 (1.000)	0.187 (1.000)	1.112 (1.000)	0.551 (1.000)	0.570 (1.000)
JENDL-3T	0.886 (0.956)	0.193 (1.032)	1.079 (0.970)	0.509 (0.924)	0.566 (0.993)
ENDF/B-IV	0.979 (1.060)	0.198 (1.059)	1.177 (1.058)	0.604 (1.096)	0.533 (0.935)
EFF-1	0.907 (0.982)	0.198 (1.059)	1.105 (0.994)	0.527 (0.956)	0.561 (0.984)

Table 4 Comparison of measured and calculated TBRs

	T_6	T_7	T_t
Present Experiment	1.209		
Cal. JENDL-3	1.174 (0.971)	0.250	1.424
JENDL-3T	1.209 (1.000)	0.224	1.433
ENDF/B-IV	1.232 (1.019)	0.237	1.469

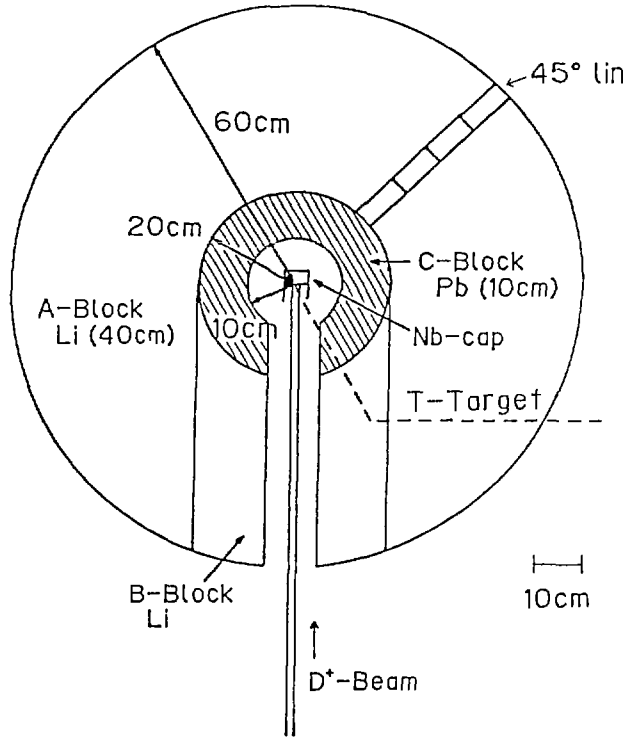

Fig.1 Pb-Li spherical assembly with D-T source target

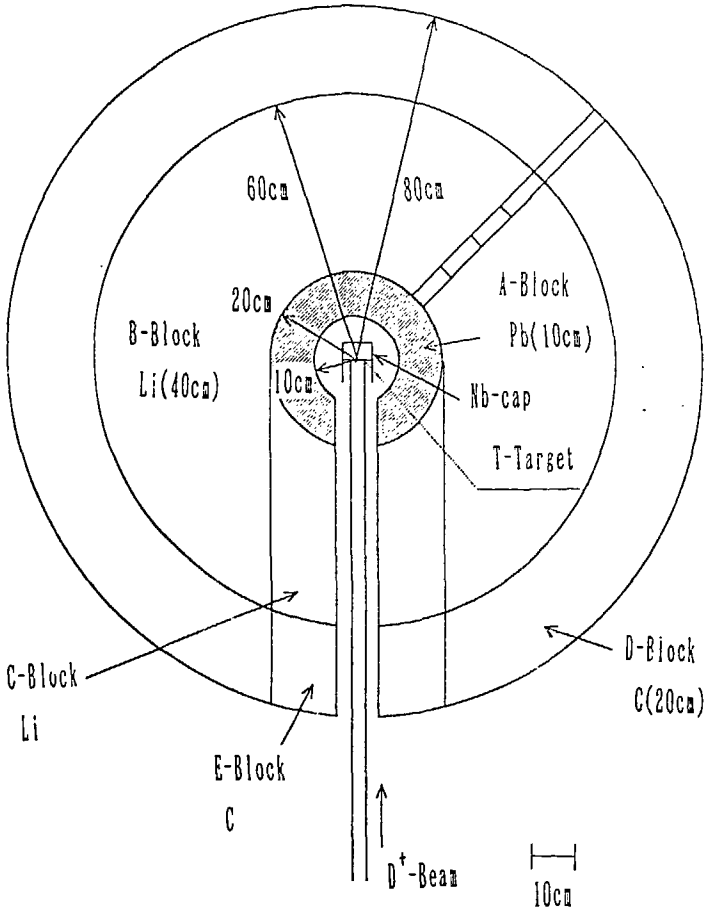

Fig.2 Pb-Li-C spherical assembly with D-T source target

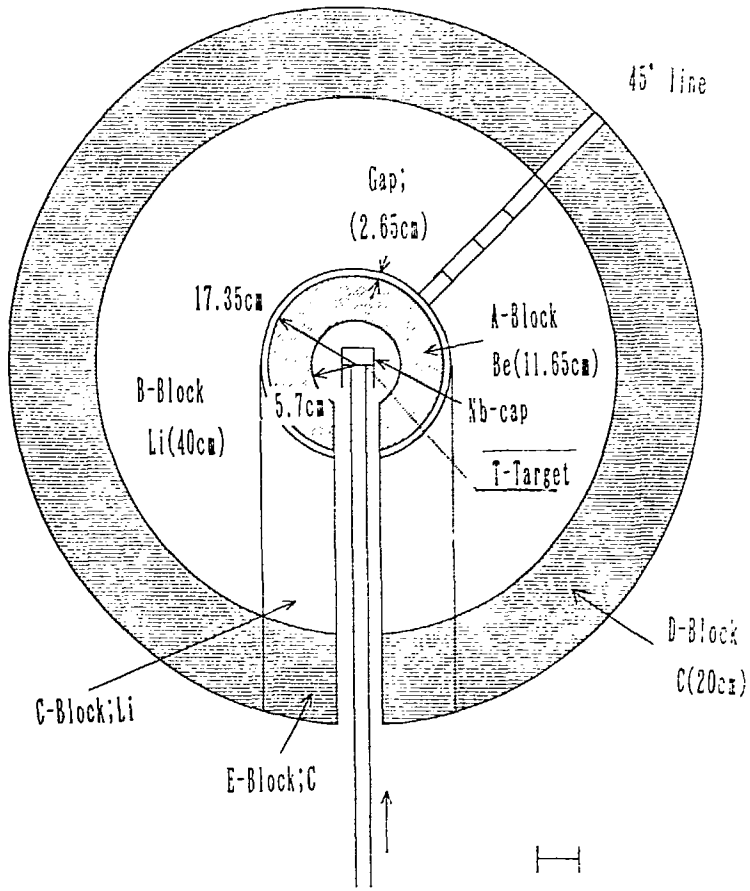

Fig.3 Be-Li-C spherical assembly with D-T source target

JAERI M 91 062

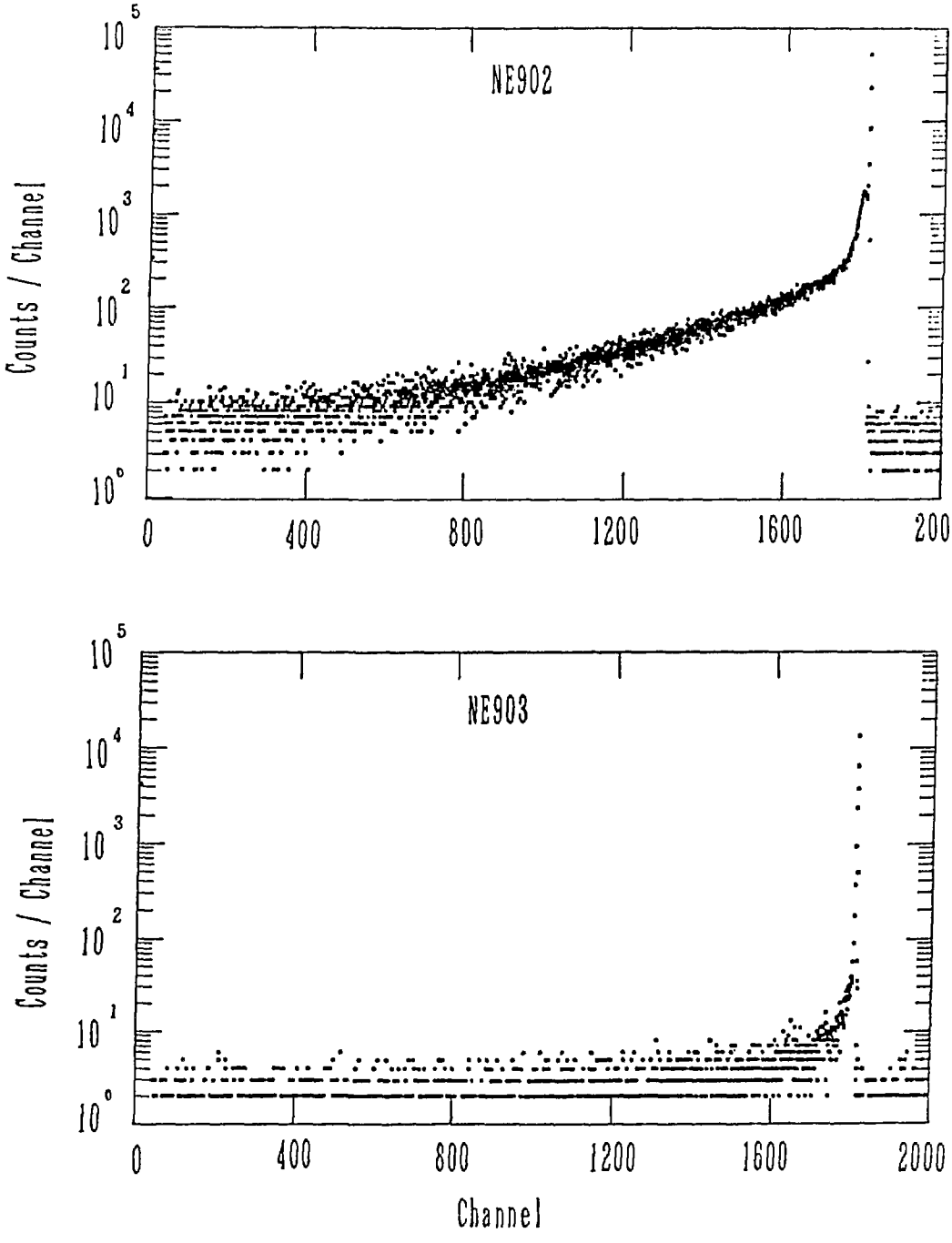

Fig.4 Time-dependent count rates measured with Li-glass detectors; a) by Li-6 glass scintillator NE902, b) Li-7 glass scintillator NE903
Time runs from right to left (5.2 ns/ch.).

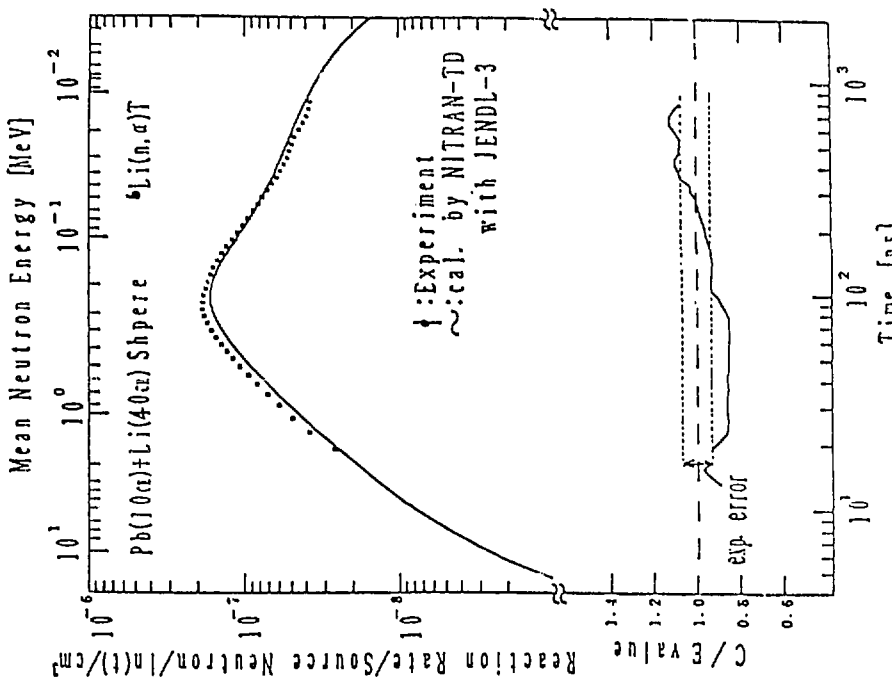

Fig.6 Time-dependent $^{6}Li(n,t)$ reaction rates in a Pb-Li spherical assembly

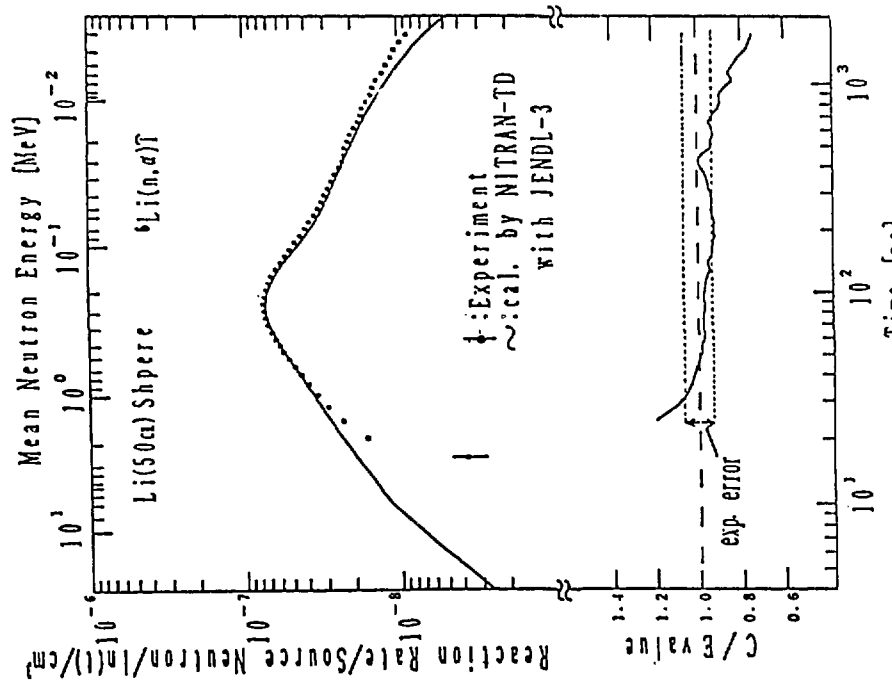

Fig.5 Time-dependent $^{6}Li(n,t)$ reaction rates in a Li spherical assembly

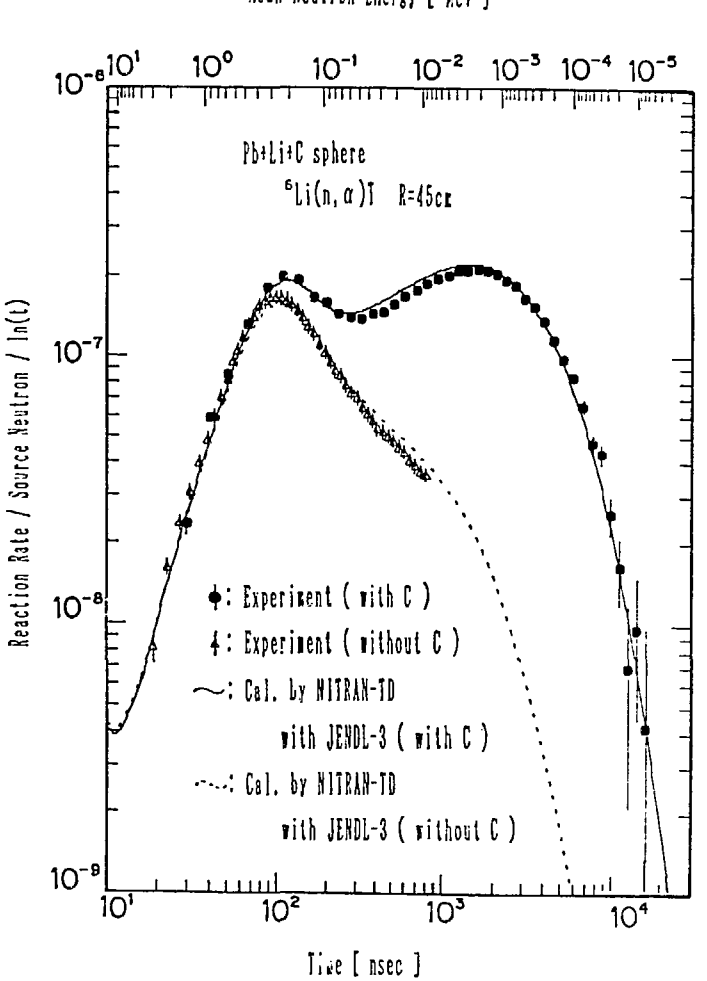

Fig.7 Time-dependent ^{6}Li(n,t) reaction rates in a Pb-Li-C spherical assembly, in comparison with those without C-reflector

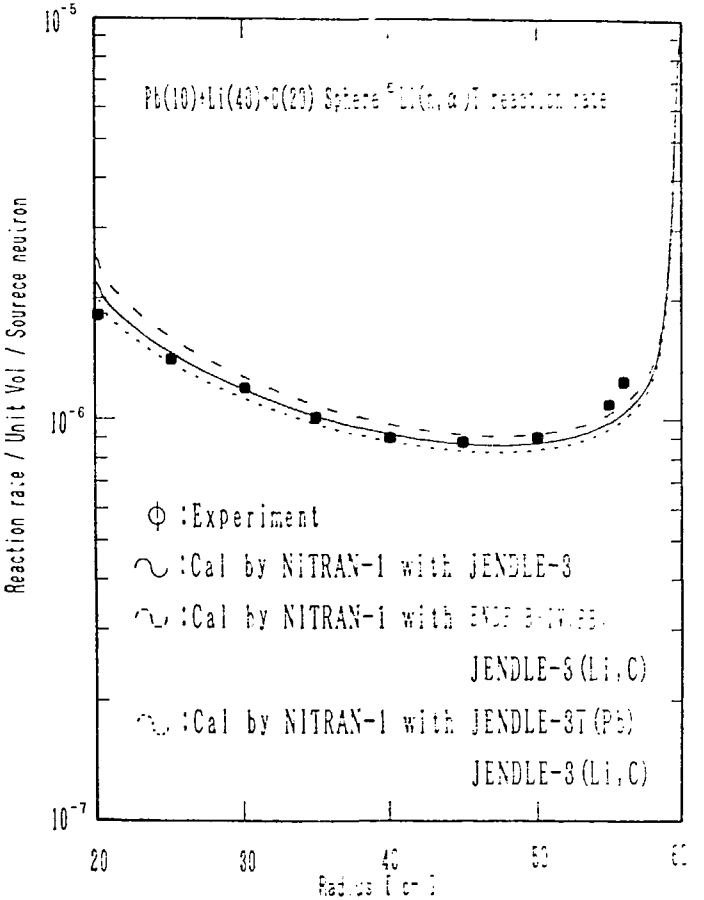

Fig.8 Spatial distribution of ^{6}Li(n,t) reaction rates in a Pb-Li-C assembly

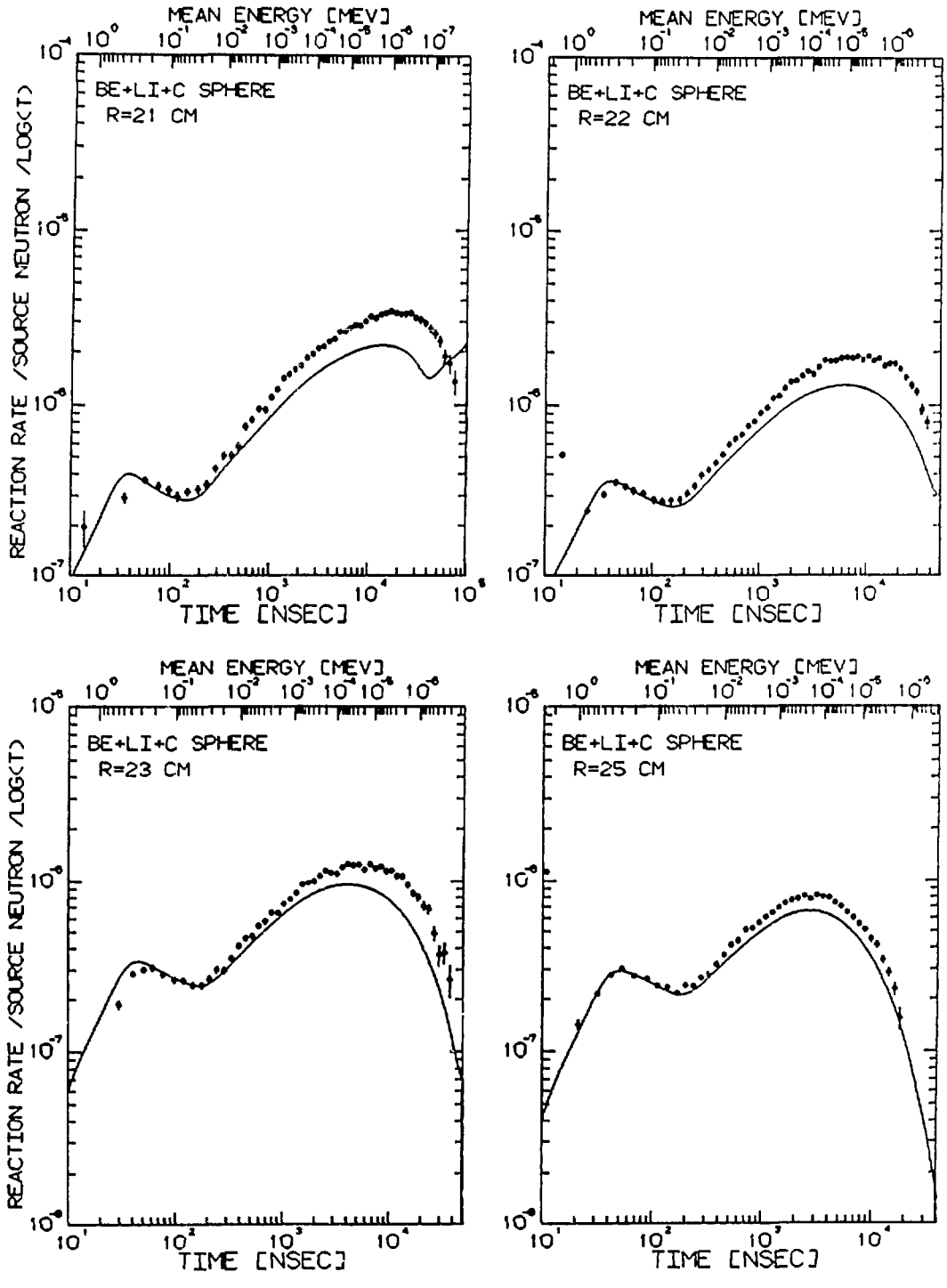

Figs.9-1 Time profiles of TPR at distances nearer to Be layer

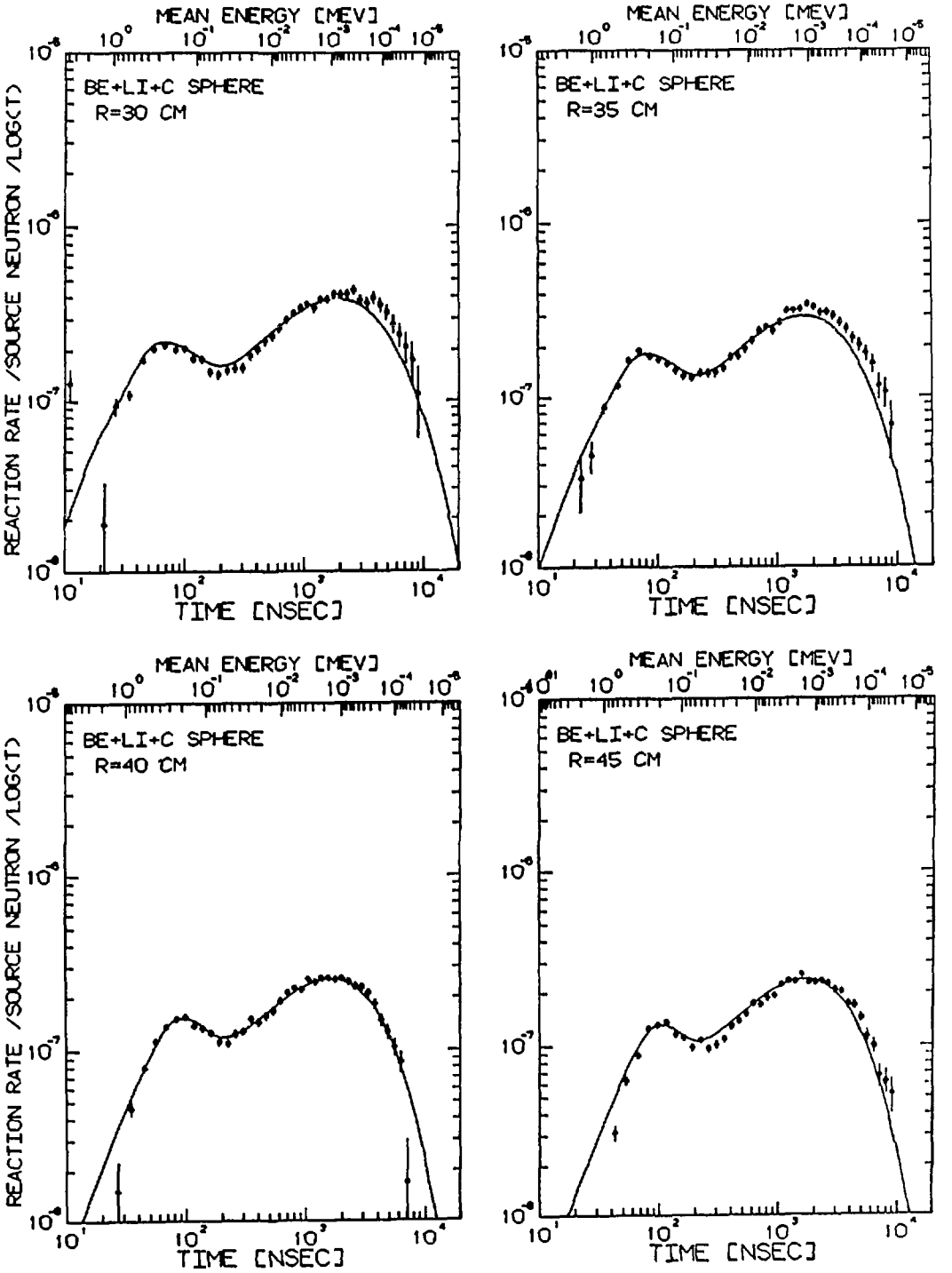

Figs.9-2 Time profiles of TPR at distances in mid region of Li layer

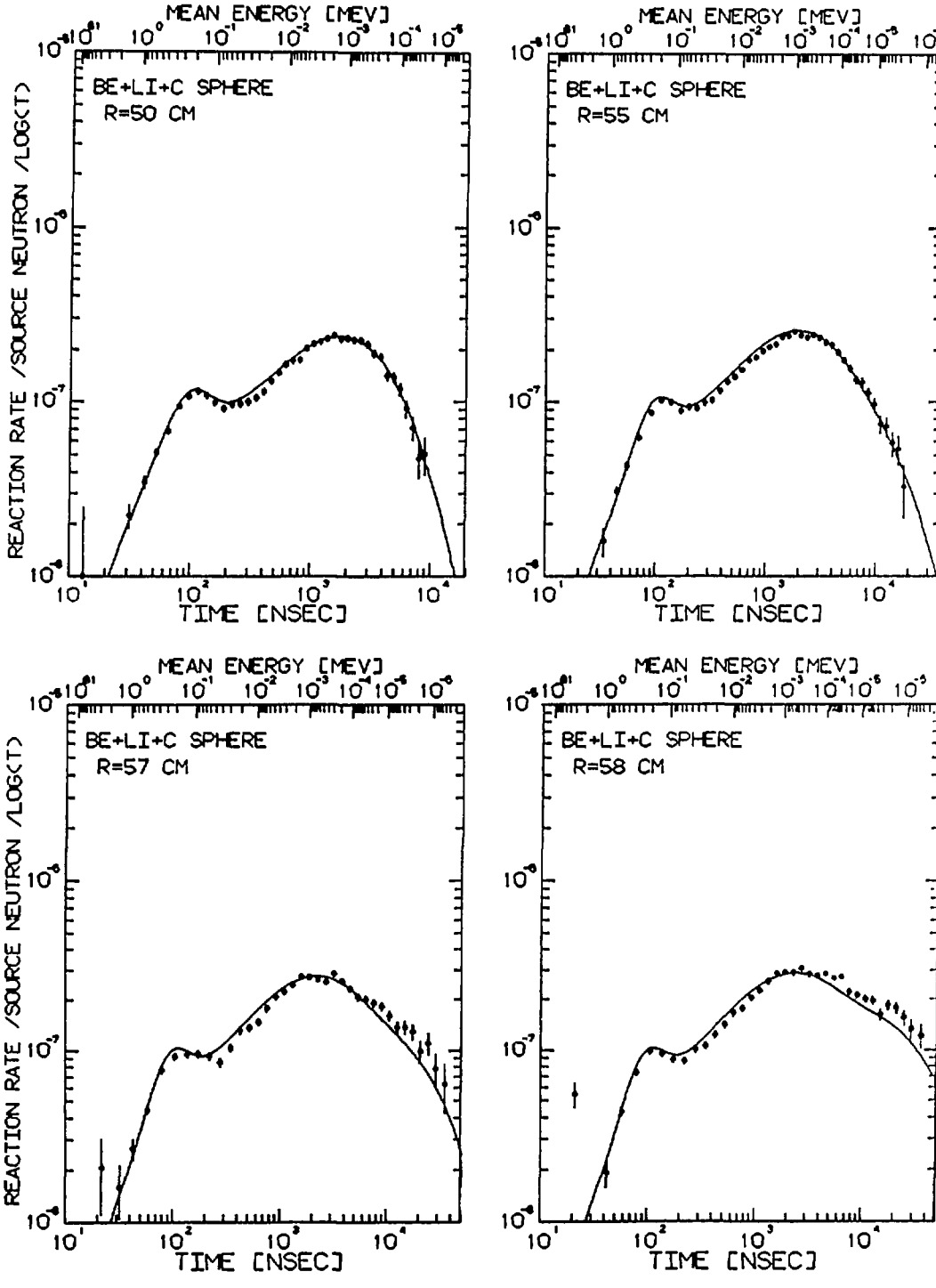

Figs.9-3 Time profiles of TPR at distances nearer to C-reflector

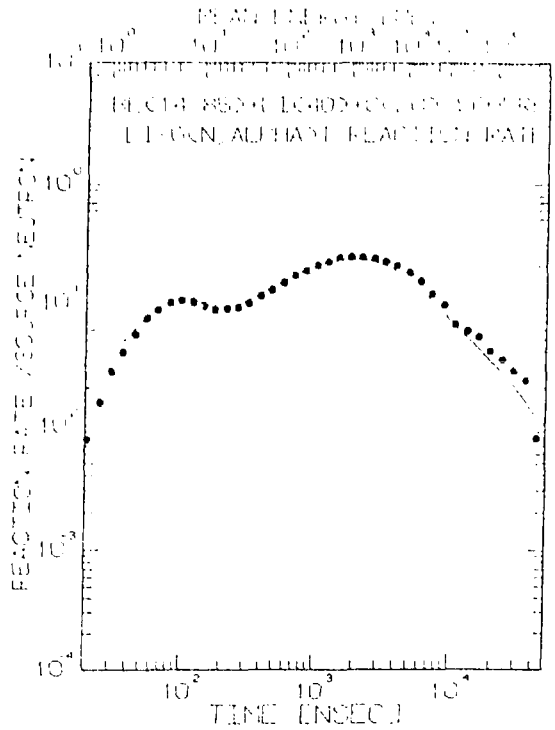

Fig.10 Space-integrated time profiles of TPR in a Be-Li-C assembly

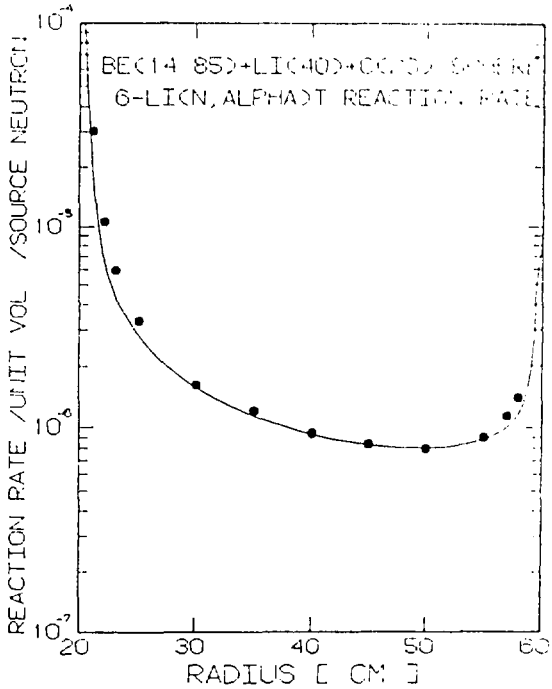

Fig.11 Spatial distribution of TPR in a Be-Li-C assembly

6. Nuclear Data Relevant to Gamma Rays

6.1 Review of Photon Production Data in JENDL-3

M. Igashira
Research Laboratory for Nuclear Reactors,
Tokyo Institute of Technology,
2-12-1 O-okayama, Meguro-ku, Tokyo 152, Japan

Photon production data in JENDL-3 were reviewed. Files used to represent the data and methods of evaluating the data were explained, and typical data were shown in comparison with experimental data.

1. Introduction

Neutron induced photon production data are indispensable for shielding design calculation, for radiation damage estimate, and for radiation heating calculation. However, the first and second versions of Japanese Evaluated Nuclear Data Library, JENDL-1 and 2, did not contain the data at all. Therefore, JENDL-3 was requested to contain the data from the beginning. Then, photon production data of 59 nuclides, about one third of nuclides in the general purpose file of JENDL-3, have been contained.[1]

In Sec. 2, files used to represent photon production data are explained. In Sec. 3, methods of evaluating the data are reviewed. Finally, typical data are shown in comparison with experimental data in Sec. 4.

2. Files for Photon Production Data[2]

Photon production data in JENDL-3 are divided into four distinct files, Files 12 through 15. With the exception of File 12, all the files are closely analogous to the corresponding neutron data files with same number (modulo 10). The purpose of File 12 is to provide additional methods for representing the energy dependence of photon production cross sections. The allowed reaction tape (MT) numbers are the same as those assigned for neutron reactions, Files 1 through 5.

File 12 can be used to represent the neutron energy dependence of photon production cross sections by means of either multiplicities or transition probability arrays. Both methods rely upon processing codes that use neutron cross sections from File 2 and/or File 3 to generate absolute photon cross sections.

Multiplicities can be used to represent the cross sections of discrete photons and/or the integrated cross sections of continuous photon spectra. The MT numbers in File 12 designate the particular neutron cross sections (File 2 and/or File 3) to which the multiplicities are referred. For most nuclides that have File 12 in JENDL-3, data are given as multiplicities.

For well-established level decay schemes, the use of transition probability arrays offers a concise method for presenting (n,xγ) information. With this method, the actual decay scheme of the residual nucleus for a particular reaction (defined by MT number) is entered in File 12. This information can then be used by a processing code together with discrete level excitation cross sections from File 3 to calculate discrete photon production cross sections. This option cannot be used to represent the integrals of continuous photon spectra. Only several nuclides have data as transition probability arrays in File 12 of JENDL-3.

The purpose of File 13 is the same as that of File 12; namely, it can be used to represent the neutron and photon energy dependence of photon production cross sections. In File 13, however, absolute cross sections in barns are tabulated, and there is no need to refer to the neutron files.

The purpose of File 14 is to provide a means for representing the angular distributions of secondary photons produced in neutron interactions. Angular distributions should be given for each discrete photon and photon continuum appearing in Files 12 and 13, even if the distributions are isotropic. For all nuclides that have photon data in JENDL-3, angular distributions are given to be isotropic in the laboratory or center-of-mass system.

File 15 provides a means for representing continuous energy distributions of secondary photons, expressed as normalized probability distributions. The energy distribution of each photon continuum occurring in Files 12 and 13 should be specified in File 15 over the same neutron energy range used in Files 12 and 13. Each section of File 15 gives the data for a particular reaction tape (MT number) and the sections are ordered by increasing MT number.

The energy distributions, $f(E_\gamma \leftarrow E)$, are in units of eV^{-1} and are normalized so that

$$\int_0^{E_\gamma^{max}} f(E_\gamma \leftarrow E)\, dE_\gamma = 1 \ , \qquad (1)$$

where E_γ^{max} is the maximum possible secondary photon energy and its value depends on the incoming neutron energy, E, as well as the particular nuclei involved.

3. Evaluation Methods

Experimental data are the basis of the evaluation of photon production data. If there are enough experimental data, the evaluation could be made based on experimental data only. Unfortunately, available experimental data for the evaluation were (n,γ) spectra in the thermal neutron region for most nuclides, (n,γ) spectra in the keV neutron region for several nuclides, (n,xγ) spectra in the MeV neutron region for about 20 nuclides, and (n,fγ) spectra in the thermal neutron region for only two nuclides. Therefore, the evaluation methods based on empirical formula and theoretical calculations became needed.

The empirical formula proposed by Howerton and Plechaty[3] are well known and an absolute secondary photon spectrum, $N(E_\gamma)$, is expressed by

$$N(E_\gamma) = A E_\gamma \exp[- R(E) E_\gamma] . \quad (2)$$

R (E) can be determined by the systematics of secondary photon spectra, and A also by R (E), some physical quantities, and neutron cross sections for reactions emitting secondary photons, but R(E) and A are essentially adjustable parameters. Here, it was noted[3] that Eq. (2) presented a secondary photon spectrum for neutron energies between 5 and 15 MeV for target nuclides with mass > 20 amu.

To evaluate secondary photons from individual reactions in wide neutron energy regions for all nuclides, theoretical calculations based on nuclear reaction models become needed. Therefore, computer codes, GNASH[4], TNG[5], CASTHY[6], and ECIS[7] were used to calculate secondary photon spectra. GNASH, TNG, and CASTHY are mainly based on the Hauser-Feshbach statistical model, and GNASH and TNG can calculate multi-step particle emission reactions. ECIS is based on the coupled-channel model, and was used to calculate inelastic cross sections for low-lying states of Al and Si nuclides. The validity of calculated results were, of course, checked by the comparison with available experimental data.

Table 1 shows evaluation methods of photon production data in JENDL-3[1]. It should be noted that there are two features in Table 1: all nuclides except for light 6 nuclides were evaluated mainly by theoretical calculations and many experimental (n,γ) spectra in the thermal neutron region were adopted.

Photon production data in Files 12 through 15 should consist with neutron data in Files 2 through 5. For example, the energy conservation should be guaranteed in the whole files. When both of neutron and photon data are simultaneously evaluated by theoretical calculations, the consistency is

automatically guaranteed. Therefore, it was recommended that theoretical calculation methods should be used as far as possible in the evaluation of data of JENDL-3. This is the reason why theoretical calculation methods were used for most nuclides in Table 1.

Characteristics of a certain resonance of individual nucleus is often strongly reflected in its thermal neutron capture cross section. In that case, the capture cross section and the secondary photon spectrum can not be calculated inevitably by statistical models that can treat only average quantities of nucleus. Therefore, experimental (n,γ) spectrum data in the thermal neutron region were adopted for many nuclides in Table 1. In resolved resonance regions, where no existing theory can reproduce any quantity due to an individual resonance, only average (n,γ) spectra were evaluated by calculations based on statistical models for lack of experimental data.

4. Typical Photon Production Data in JENDL-3

The 2.125 MeV inelastic photon production cross section of ^{11}B in JENDL-3 is compared with the experimental data of Dickens and Larson[8] in Fig. 1. The multiplicity of the 2.125 MeV photon was calculated by using GNASH in the neutron energy region below 7.8 MeV. Above 7.8 MeV, the photon production cross section of non-elastic scattering reaction was calculated, so that the evaluated result in Fig. 1 ends at 7.8 MeV. The evaluated values are a little larger than the experimental data in the region of 4 - 8 MeV. Here, it is noted that resonance structures in the corresponding neutron data are reflected in the photon production cross section.

The secondary photon spectra in MeV neutron regions from natural Si, ^{55}Mn, and natural Mo are compared with experimental data[9-11] in Figs. 2 through 4, respectively. The spectra of Si and ^{55}Mn were calculated by using GNASH and TNG, respectively, while the spectrum of Mo was calculated with the Howerton's method.[3] All the evaluated spectra are in good agreement with the experimental ones. Here, it is noted that intensities of inelastic photons in Fig. 2 were modified with the aid of ECIS.

Finally, Fig. 5 shows the evaluated (n,γ) spectrum in the thermal neutron region for natural Fe which was based on the photon intensity data contained in Evaluated Nuclear Structure Data File[12], ENSDF, together with the experimental data of Maerker.[13] The evaluated spectrum is consistent in the Maerker's data.

References

1) Shibata, K., Nakagawa, T., Asami, T., Fukahori, T., Narita, T., Chiba, S., Mizumoto, M., Hasegawa, A., Kikuchi, Y., Nakajima, Y. and Igarasi, S.: "Japanese Evaluated Nuclear Data Library, Version-3 JENDL-3", JAERI 1319, (1990).
2) Kinsey, R.: "Data Formats and Procedures for the Evaluated Nuclear Data File, ENDF", BNL-NCS-50496, 2nd ed. (1979).
3) Howerton, R.J. and Plechaty, E.F.: Nucl. Sci. Eng., 32, 178 (1968).
4) Young, P.G. and Arthur, E.D.: "GNASH: A Preequilibrium, Statistical Nuclear-Model Code for Calculation of Cross Sections and Emission Spectra", LA-6947, (1977).
5) Fu, C.Y.: A Consistent Nuclear Model for Compound and Precompound Reactions with Conservation of Angular Momentum", ORNL-TM-7042, (1980).
6) Igarasi, S.: J. Nucl. Sci. Technol., 12, 67 (1975).
7) Raynal, J.: "Optical Model and Coupled-Channel Calculations in Nuclear Physics", IAEA SMR-9/8, (1970).
8) Dickens, J.K. and Larson, D.C.:"^{10,11}B(n,xγ) Reactions for Incident Neutron Energies Between 0.1 and 25 MeV", Proc. Int. Conf. Nuclear Data for Science and Technology, Mito, 1988, p.213 (1988).
9) Dickens, J.K., Love, T.A. and Morgan, G.L.: "Gamma-Ray Production from neutron Interactions with Silicon for Incident Neutron Energies Between 1.0 and 20 MeV: Tabulated Differential Cross Sections", ORNL-TM-4389, (1973).
10) Morgan, G.L.: ORNL-TM-5531, (1976).
11) Morgan, G.L. and Newman, E.: "The Mo(n,xγ) Reaction Cross Section for Incident Neutron Energies Between 0.2 and 20.0 MeV", ORNL-TM-5097, ENDF-220, (1975).
12) Evaluated Nuclear Structure Data File, a computer file of evaluated experimental nuclear structure data maintained by the National Nuclear Data Center, Brookhaven National Laboratory. (File as of Aug., 1989).
13) Maerker, R.E.: "SB2. Experiment on Secondary Gamma-Ray Production Cross Section Arising from Thermal-Neutron Capture in Each of 14 Different Elements Plus a Stainless Steel", ORNL-TM-5203, (1976).
14) Fukahori, T.: "Evaluation of Neutron Nuclear Data of B-11", JAERI-M 89-046, (1989).
15) Mizumoto, M.: "Nuclear Data Evaluation for Medium and Heavy Nuclei", Proc. the 1987 Seminar on Nuclear Data, Tokai, 1987, JAERI-M 88-065, p.29 (1988).

Table 1 Evaluation methods of photon production data in JENDL-3

Nuclides	Evaluation methods	Nuclides	Evaluation methods
H-1	N	Cu	GNASH+Th.(n,γ)
Li-6	N+Th.(n,γ)	Cu-63	GNASH
Li-7	N+Level scheme	Cu-65	GNASH
Be-9	N+Th.(n,γ)	Zr	TNG+Th.(n,γ)
B-10	N+Level scheme+Ex.	Nb-93	GNASH
B-11	GNASH	Mo	CASTHY+Howerton+Ex.
C-12	N+Th.(n,γ)+Ex.	Ag	TNG
N-14	GNASH+Th.(n,γ)	Ag-107	TNG
N-15	GNASH	Ag-109	TNG
O-16	GNASH	Cd	GNASH
Na-23	GNASH+Th.(n,γ)	Eu	GNASH
Mg	GNASH+Th.(n,γ)	Hf	GNASH+Ex.
Al-27	GNASH+ECIS	Hf-174	GNASH+Ex.
Si	GNASH+ECIS	Hf-176	GNASH+Ex.
Si-28	GNASH+ECIS	Hf-177	GNASH+Ex.
Si-29	GNASH+ECIS	Hf-178	GNASH+Ex.
Si-30	GNASH+ECIS	Hf-179	GNASH+Ex.
Ca	GNASH	Hf-180	GNASH+Ex.
Ca-40	GNASH	Ta-181	GNASH
Ti	GNASH+Th.(n,γ)+Ex.	W	GNASH+Th.(n,γ)
Cr	GNASH+Th.(n,γ)+Ex.	Pb	GNASH
Mn-55	TNG+Th.(n,γ)	Pb-204	GNASH
Fe	GNASH+Th.(n,γ)+Ex.	Pb-206	GNASH
Fe-54	GNASH	Pb-207	GNASH
Fe-56	GNASH	Pb-208	GNASH
Fe-57	GNASH	Bi-209	GNASH
Fe-58	GNASH	U-235	GNASH+Ex.
Ni	GNASH+Th.(n,γ)+Ex.	U-238	GNASH+Ex.
Ni-58	GNASH	Pu-239	GNASH+Ex.
Ni-60	GNASH		

Th.(n,γ): Experimental (n,γ) spectra in the thermal neutron region.
Ex. : Experimental data except for Th.(n,γ).
N : Consideration of individual reactions emitting secondary photons. For example, one photon with the energy of (2.22+E/2) MeV is emitted from the ^{1}H(n,γ) reaction.

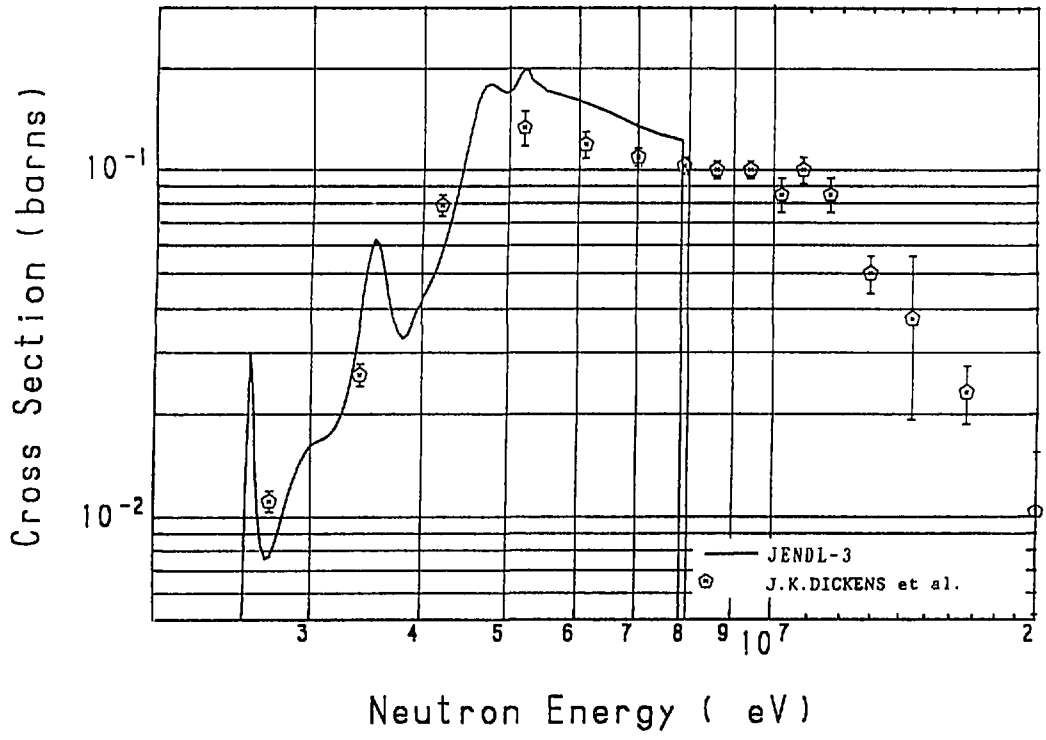

Fig. 1 The 2.125 MeV inelastic photon production cross sections of ^{11}B. The evaluation was made below 7.8 MeV. (Cited from ref. 14.)

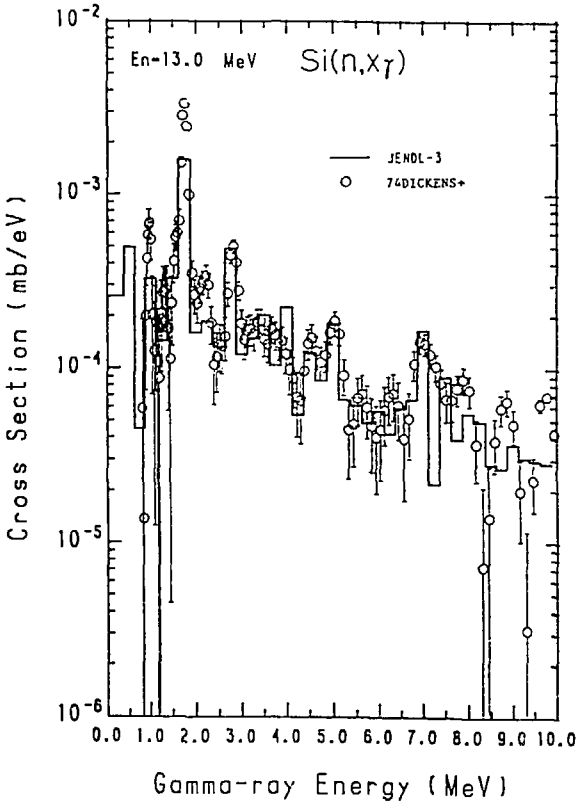

Fig. 2 Secondary photon spectra from natural Si. The evaluation was made by using GNASH. (Cited from ref. 1.)

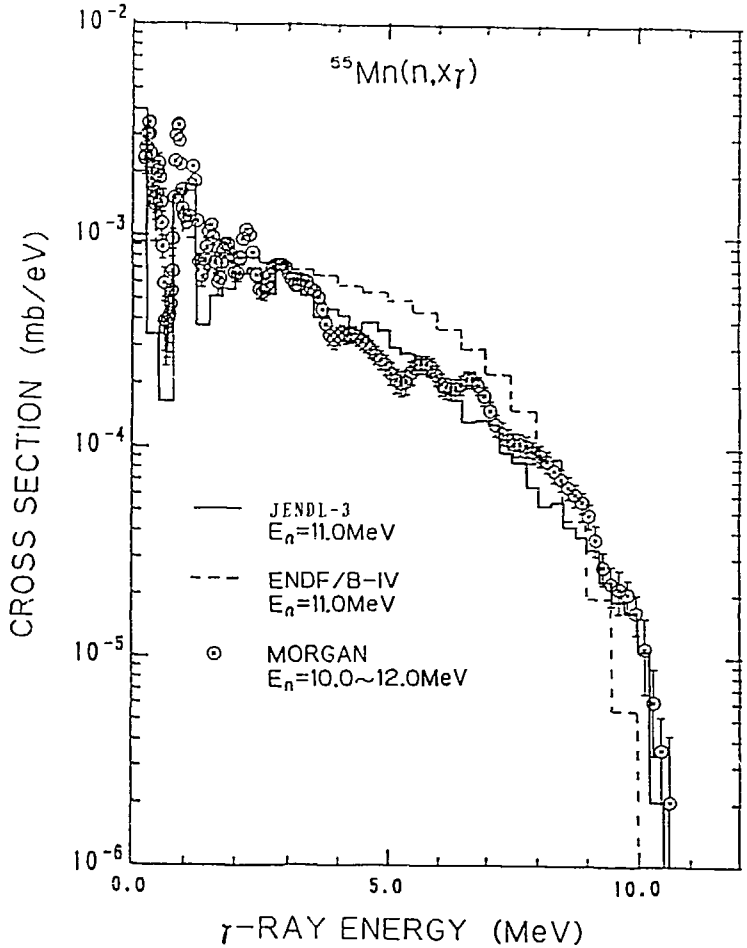

Fig. 3 Secondary photon spectra from ^{55}Mn. The evaluation was made by using TNG. (Cited from ref. 15.)

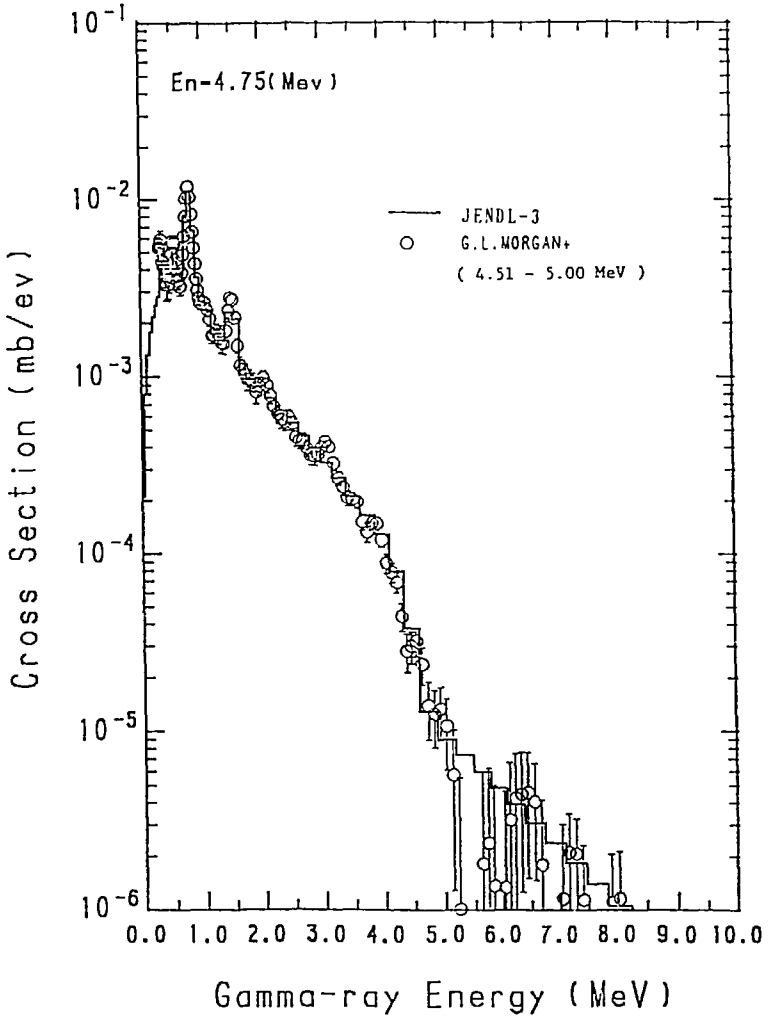

Fig. 4 Secondary photon spectra from natural Mo. The evaluation was made by the Howerton's method. (Cited from ref. 15.)

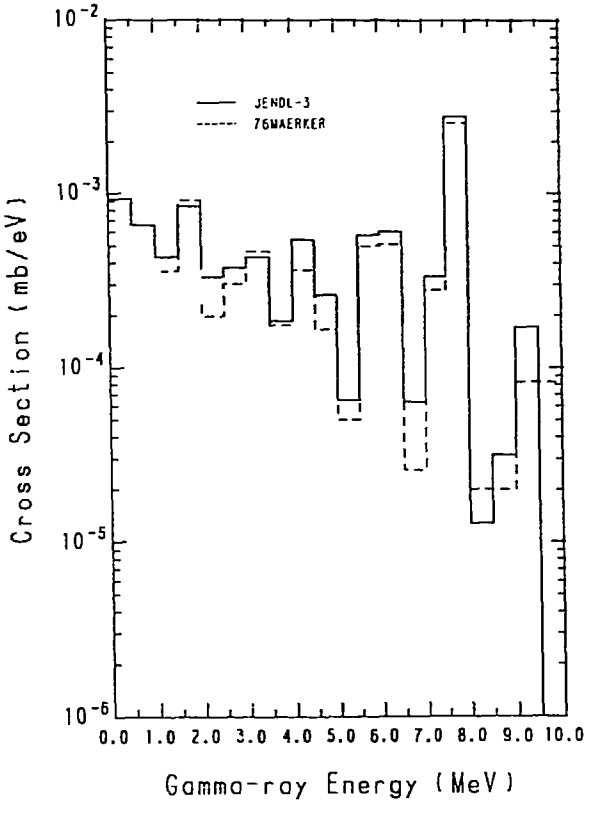

Fig. 5 (n,γ) spectra in the thermal neutron region for natural Fe. The evaluation was based on the photon intensity data in ENSDF. (Cited from ref. 1.)

6.2 Experiments of Nuclear Heating by Gamma-Rays at FNS

Yukio Oyama
Department of Reactor Engineering
Japan Atomic Energy Research Institute
Tokai-mura, Naka-gun, Ibaraki-ken, Japan

Experimental works of nuclear heating rate measurement on fusion reactor candidate material performed at the Fusion Neutronics Source facility (FNS) in JAERI is reviewed. The materials in which heating rates were measured are Be, C, Li_2O, Fe and W. The measurements were carried out using the interpolation method with a plural kinds of TLDs and the weighting function method with a small spherical NE213 liquid scintillation detector. The experiments were compared with the computed results by DOT3.5/FUSION-J3 code and nuclear data processed from JENDL-3.

1. Introduction

Nuclear heating rate is one of critical issues for the nuclear design of a fusion reactor. The data are concerned with many aspects of the design, e.g., mechanical cooling system, heat stress, power generation and so on. The heating rate by gamma-rays shared the total heat with the nuclear heat by neutron reaction. The fraction of the gamma-ray heat to total nuclear heat for fusion neutrons depends on the materials. The gamma-ray heat is larger than the neutron heat for heavy elements, while smaller for light element, as seen in Figs. 1 and 2 which show the calculated heating rate for slab materials bombarded with 14 MeV neutrons. Thus the gamma-ray heating is very important for the structure materials. e.g., iron and stainless steel, the shielding materials, e.g., as lead and tungsten, and copper for magnetic coil.

2. Experiment

Experimental arrangement is shown in Fig. 3. The test material is assembled in a shape of cylinder to keep a symmetry for two dimension calculation. The assembly is emplaced at the distance of 20 cm from the D-T target. The radius of the cylinder is 31.4 cm and thickness is 60 cm typically. The measurement is performed along the central axis of the cylinder using the drawer mechanism. Two types of independent measurement

methods are adopted. They are the interpolation method of heating rate in a plural kinds of thermoluminescence detectors (TLD)[1] and the weighting function method using a small spherical NE213 scintillation detector with the gamma-ray response matrix.[2]

Experimental system is highly integrated in a sense of integral experiment for nuclear data test. The final result is heating rate and the start is DT neutrons. Thus all uncertainties due to the neutron transport calculation, (n,gamma) production cross section, gamma-ray transport calculation and mass energy absorption coefficient are included in the results. This should be taken into account to discussed in the results for the present experiment.

3. Principles of Measurement

Interpolation method by TLDs

The interpolation method for gamma-ray heating measurement using TLDs was proposed by Tanaka et al.[3,4] We applied this method to neutron and gamma-ray mixed field. The neutron response on TLDs is calculated by assistance of the transport code and subtracted by total TL output to obtain gamma-ray component alone. After rejection of gamma-ray component, the relation in chamber theory between the absorbed dose in a medium and that in a TLD is written as follows:

$$D_M = f(\ M,\ TLD,\ E_\gamma\ )^{-1} D_{TLD},$$

where, D_M is the absorbed dose in a medium M; D_{TLD} the absorbed dose in a TLD; E_γ the gamma-ray energy; f the conversion factor as a function of them.

According to Tanaka, an absorbed dose in a TLD overestimates that in the surrounding medium with an atomic number smaller than that of the TLD, while it underestimates for the opposite case, and measured values of TLDs increase monotonically with the atomic number. Therefore, the absorbed dose in a medium can be obtained as an interpolated or extrapolated value at the atomic number of the medium of interest, when the measured values of TLDs are plotted versus the effective atomic number. The greatest advantage of this method is that it does not require any gamma-ray energy spectrum information.

The TLDs used here are BeO, ^{7}LiF, Mg_2SiO_4, Sr_2SiO_4 and Ba_2SiO_4, and their effective atomic numbers are 7.1, 8.2, 11.1, 32.5 and 49.9, respectively.

Weighting function method

The heating rate H in a medium is given by,

$$H = \int K(E_\gamma)\cdot\Phi(E_\gamma)\, dE_\gamma,$$

where, $K(E_\gamma)$:kerma factor of surrounding material, $\Phi(E_\gamma)$:photon flux with energy E_γ. The kerma factor can be expressed by the photon spectrum using mass energy absorption coefficient in the medium, and the photon spectrum is related to the recoil electron spectrum produced in the scintillator.

The gamma-ray response of the NE213 detector is calculated by the Monte Carlo code as Fig. 4. If we assume existence of the following relation between the response matrix and the KERMA factor by the weighting function.

$$K(E_\gamma) = \int R(E_\gamma, E_e)\cdot G(E_e)\, dE_e.$$

The first equation is rewritten as follows:

$$\begin{aligned} H &= \int K(E_\gamma)\cdot\Phi(E_\gamma)\, dE_\gamma \\ &= \int[\int R(E_\gamma,E_e)\cdot G(E_\gamma)\, dE_e]\cdot\Phi(E_\gamma)dE_\gamma. \end{aligned}$$

Exchanging a turn of integration,

$$\begin{aligned} H &= \int[\int R(E_\gamma,E_e)\cdot\Phi(E_\gamma)\, dE_\gamma]\cdot G(E_e)\, dE_e \\ &= \int C(E_e)\cdot G(E_e)\, dE_e. \end{aligned}$$

In the last equation, $C(E_e)$ is a electron energy spectrum measured by the NE213 scintillator The spectrum weighting function $G(E_e)$ is determined by both gamma-ray response matrices and kerma factor by iterative method.[5] Thus the gamma-ray heating rate is obtained directly from the measured electron spectrum of the detector.

The advantages of this method are that the detector can reject neutron contribution by electronically using pulse shape discrimination technique and directly correspond to gamma-ray spectrum in the medium.

4. Results and Discussions

The estimated experimental errors for the both methods are summarized in Table 1. The error of TLD method is slightly larger, especially for the case of extrapolation with effective atomic number axis. For the weighting function method, the uncertainty of solution for the weighting function and low energy electron cut-off are affective to heavy elements.

The results for five materials were compared with the results calculated by DOT3.5 neutron and gamma-ray transport code with GICX40[6] and FUSION-J3 cross section sets, which were retrieved from ENDF/B-IV for neutron and POPOP4 for gamma-ray, and JENDL-3 and DLC99[7], respectively. The results and observations are listed as follows.

Be

Figure 5 shows the results for the Be slab. Both calculated results are smaller than the experimental results by 30-80%. In the deep position, the calculation is improved by using the MCNP Monte Carlo code, but at the mid depth the calculation still underestimates the heating rates.

Graphite

Figure 6 shows the results for the graphite slab. The both calculations underestimate the heating by 20-30% at the deep positions. This tendency is similar to the previous results for the neutron induced reaction rate distributions. Thus this can be attributed to the part of neutron transport calculation.

Lithium Oxide

This case shows fairy good agreement with the experiment within 10-20% as shown in Fig. 7.

Iron

The measurement on iron was performed for the 100 cm-thick slab. In this case, there is a problem related to self-shielding correction for resonance region at the deep positions in the neutron transport calculation by DOT3.5 and FUSION-J3.[8] However, the results of heating rate show fairly good agreement even in deep positions as shown in Fig. 8. This should be re-calculated with self-shielding correction.

Tungsten

The comparison of the measured results with the calculations is shown in Fig. 9. The calculation by FUSION-J3 is larger than the experiments by a factor of 2-3. The GICX40 show very large underestimation, so there exists something wrong in the library.

5. Summary

The measurements of gamma-ray heating rate in the slab materials by using two independent techniques showed good agreement almost within the experimental errors. The results of comparisons with the calculations showed better agreements for the graphite, lithium oxide and iron, while large discrepancies are found for the beryllium and tungsten.

Acknowledgments

Most part of the TLD measurements were performed by Dr. S. Yamaguchi and the development of the weighting function technique for gamma-ray heating is due to Mr. K. Sekiyama. The author greatly thanks them for their contributions.

References

1) S. Yamaguchi, et al., Fusion Eng. Des., 10, 163 (1989)
2) Y. Oyama, et al., Nucl. Instrum. Meth., A2556, 333 (1987)
3) S. Tanaka, et al., Proc. 1st ASTM-EURATOM Symp. Reactor Dosimetry, Petten, 1 EUR 5667 e/f, Part 1, 599 (1975)
4) S. Tanaka and N Sasamoto, J. Nucl. Sci. Technol., 22, 109 (1985)
5) Y. Oyama and S. Tanaka, JAERI-M 9982 (1982)
6) Y. Seki and H. Iida, JAERI-M 8818 (1980)
7) R. W. Roussin, et al., ORNL/RSIC-46 (ENDF-335) (1983)
8) Y. Oyama, et al., Proc. 1990 Nuclear Data Seminar, to be published. (1990)

Table 1 Estimated experimental errors for both techniques

TLD

Instability of TL measurement	2-20 %
Calibration	3 %
Calculation of neutron response	20-30 %
Inter- and extra-polation	10-20 %
Neutron source intensity	3 %
Overall	20-40 %

Weighting function technique

Gamma-ray response matrix (20%)	
Calculated KERMA factor (10%) ==>	10 %
Determination of weighting function (5-50%) ==>	3-10 %
Counts statistics	< 1 %
Neutron source intensity	3 %
Overall	5-15 %

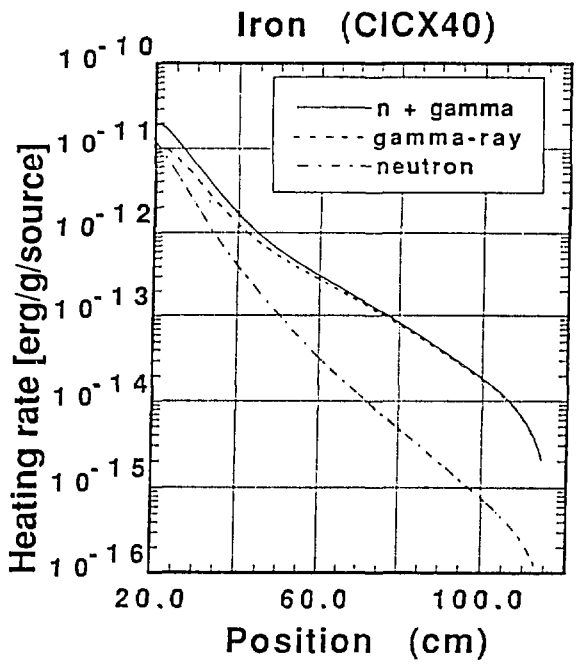

Fig. 1 Calculated nuclear heating rate in iron slab

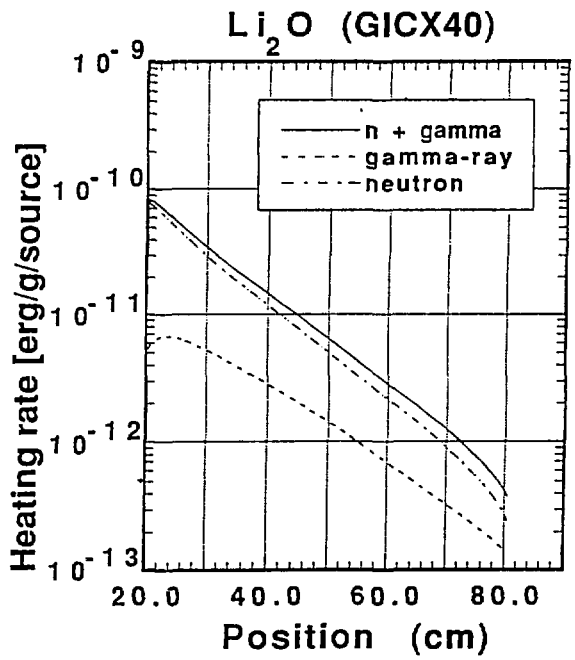

Fig. 2 Calculated nuclear heating rate in Li_2O slab

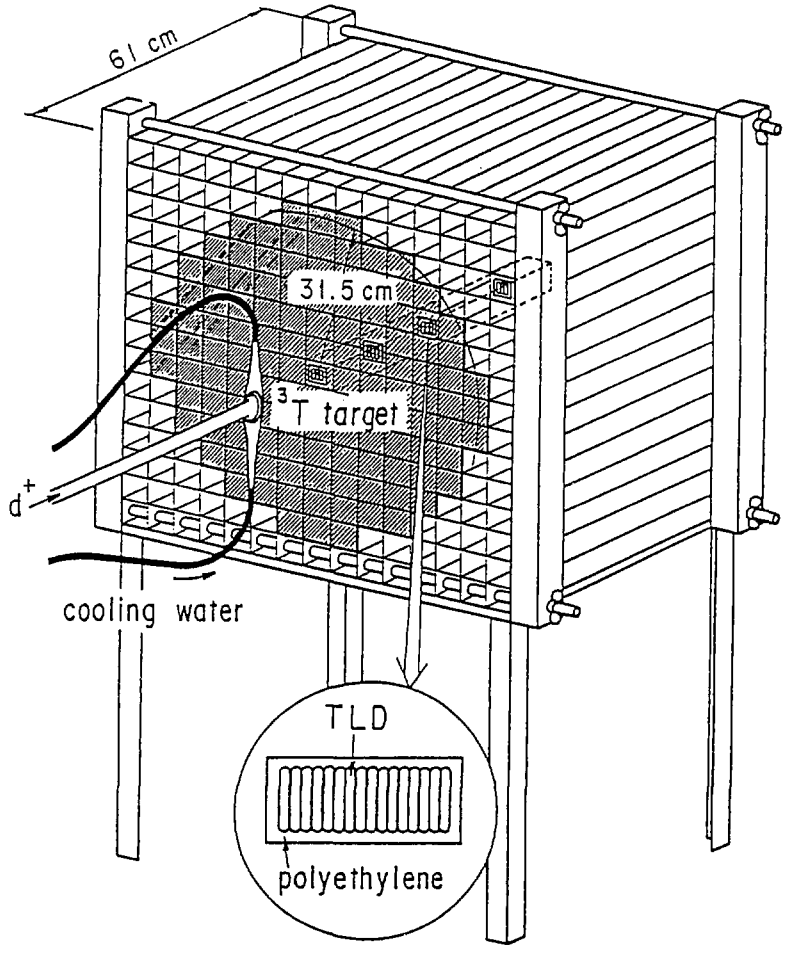

Fig. 3 Experimental arrangement

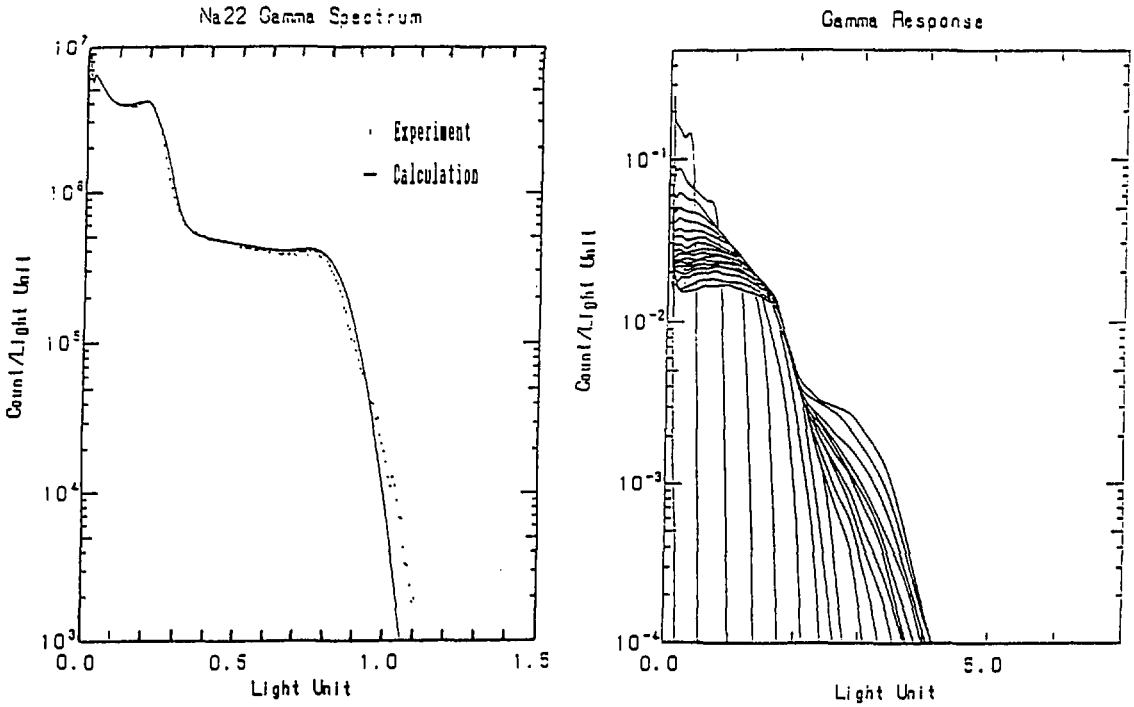

Fig. 4 Calculated and measured gamma-ray responses of ^{22}Na standard gamma-ray source (left) and all responses used in the matrix for the energy of 0.3 to 13 MeV (right) for 14 mm diameter spherical NE213 scintillation detector

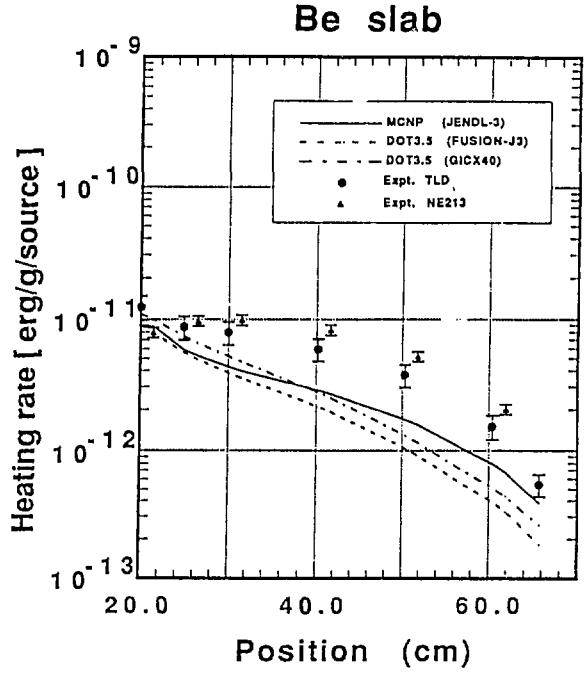

Fig. 5 The comparison of the experimental and calculated results for Be slab

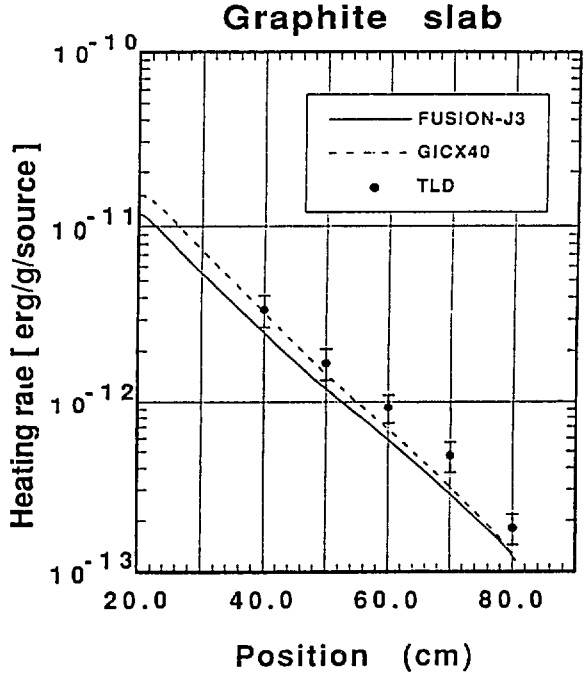

Fig. 6 The comparison of the experimental and calculated results for graphite slab

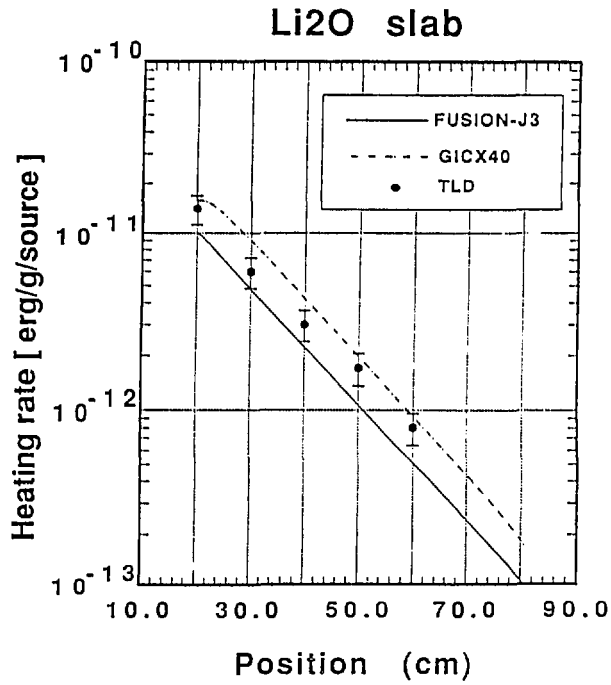

Fig. 7 The comparison of the experimental and calculated results for lithium oxide slab

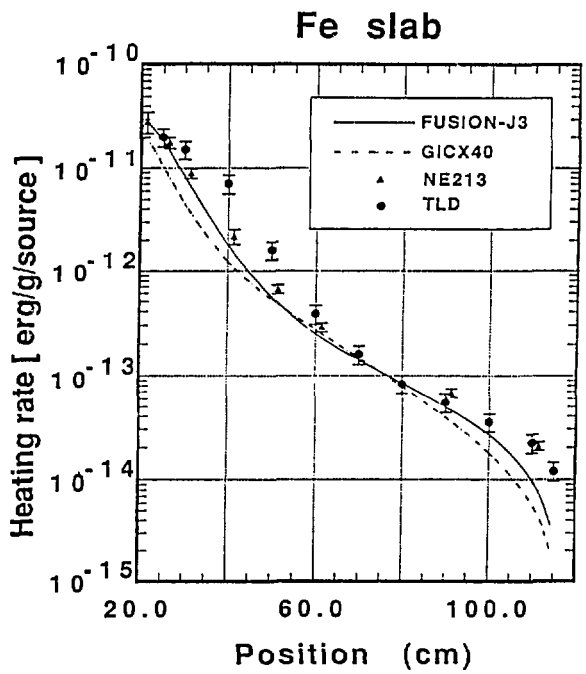

Fig. 8 The comparison of the experimental and calculated results for iron slab

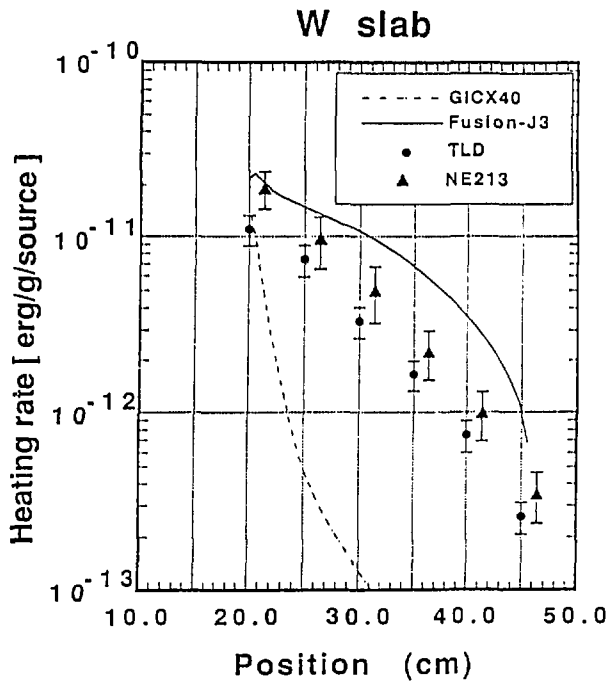

Fig. 9 The comparison of the experimental and calculated results for tungsten slab

6.3 Integral Experiment on Gamma-Ray Production at OKTAVIAN

Junji Yamamoto

Department of Nuclear Engineering, Osaka University
2-1 Yamada-oka, Suita, Osaka 565, Japan

The outline of the integral experiment with regard to γ-ray production is described. The results for the samples of Al, Si, Ti, Cr and Mo are presented in comparison with the transport calculations using the nuclear data in JENDL-3. The present status of the nuclear data of γ-ray production in JENDL-3 is briefly discussed.

1. Introduction

A series of measurements for neutron-induced γ-rays emitted from spheres was carried out using the 14 MeV neutron source OKTAVIAN of Osaka University. Main objective of the present work was to obtain the benchmark data for the assessment of the nuclear data with respect to the γ-ray productions newly compiled in JENDL-3[1]. The energy spectra of the neutron emission were also measured using the exactly same spheres and neutron source[2], so that the emission spectra of neutrons and γ-rays were useful to complement each other in the assessment of the evaluated nuclear data.

The detail of the work was given elsewhere[3]. In addition to the summary of the paper, current results of aluminum, silicon and titanium are presented.

2. Measurements and calculations

Samples in use were LiF, Al, Si, Ti, Cr, Mn, Co, Cu, Nb, Mo, W and Pb. The sample materials were contained in respective shells of stainless steel because of either powdered or granular samples except the lead sphere. The diameters of the spheres were 60 cm for LiF, Mn, Cu and Mo, 40 cm for Al, Si, Ti, Cr, Co, W and Pb, respectively. Only the

niobium sphere was 28 cm in diameter. Fourteen MeV neutrons were generated at the center of the sphere and the γ-rays were produced from neutron-induced reactions in the sphere. A γ-ray detector was a cylindrical NaI crystal of 7.62 cm in diameter by 7.62 cm in length. The well-shielded detector was located at 5.6 m from the neutron source and at 55° with respect to the D^+ beam line of OKTAVIAN. In order to discriminate the desired prompt γ-rays from the neutron background, time spectrum was measured by means of a TOF technique simultaneously with pulse-height spectrum(PHS). Figures 1 and 2 show a TOF spectrum from the Mn sphere and a PHS from the Pb sphere, respectively. A radioactive method by using niobium foils was applicable to the monitor for the fluence of 14 MeV neutrons in every run. After irradiation the fluence was determined from radioactivity induced by $^{92}Nb(n,2n)$ reaction. The PHS was unfolded using the FERDOR code [4] to convert that into energy spectrum. The γ-ray fluxes of the emission spectrum was obtained as total leakage current per a source neutron. The γ-ray energy covered the range from 500 keV to 10 MeV.

Transport calculations were done with the MCNP Monte Carlo code[5]. The NJOY processing code[6] generated from either JENDL-3 or ENDF/B-IV [7] the pointwise cross section set that was supplied for the MCNP code. The Sn transport calculations were also done using the first version of FUSIONJ3[8] that was newly produced from JENDL-3. The preliminary results, however, were poor due to the incorrect group constants for the γ-ray transport.

3. Results

The thickness of outer wall of the shell was 4.5 mm for the 60 cm-diam. sphere and 2 mm for the 40 cm-diam. one, respectively. The emission γ-rays from the samples were shielded by the outer wall and the unnecessary γ-rays were produced by the interaction of neutrons with the wall of stainless steel. The influence of the shell on the emission spectrum was analyzed. In the case of the copper sphere, the γ-ray fluxes decreased by 10 % between 1 and 6 MeV. The magnitude of the decrement was constant. This is because the γ-ray production by (n,n') reaction and the γ-ray shield by the 4.5 mm-thick wall compensated each of the other. The considerable increment was found in the γ-ray energy around 7 MeV, because of $^{56}Fe(n,\gamma)$ reaction induced by the slowing down

neutrons. As for the γ-ray production at the neutron source, the contamination of the emission spectra with the source γ-rays was quite small. The period to measure the prompt γ-rays from the sphere in the present experiment was about 70 ns after the source neutrons generating, so that it was necessary to estimate neutron slowing down times in the spheres. Steady state transport calculations could be applied by a simple method, in which the neutron-mean-emission times from the sphere were investigated as a function of neutron energies.

Figures 3 to 5 show the γ-ray emission spectra from the spheres of aluminum, silicon and titanium, respectively. The JENDL-3 calculations of aluminum and silicon agree fairly well with the respective measurements and the agreement is poor for titanium. The energy-resolution of the NaI spectrometer was good enough to analyze the prominent discrete γ-rays: in the silicon spectrum 0.97 MeV γ-rays from ^{28}Si(n,p) reaction and two peaks at 1.8 and 2.8 MeV from ^{28}Si(n,n') reaction.

In the molybdenum spectra shown in Fig.6, the JENDL-3T evaluation was better than the B-IV one in the energy range below 2 MeV. The present status of the γ-ray production data would be fairly good for molybdenum in JENDL-3, considering firstly that the reaction channels for producing the γ-rays are complex in natural molybdenum due to many isotopes and secondly that the (n,n') reactions are in competition with the (n,2n) reactions that have the large cross section values.

Both energy spectra of neutrons and γ-rays are shown in Fig.7. As for the γ-ray emission spectra, the ENDF/B-IV calculation considerably overestimates the measured spectrum in the energy range below 4 MeV. The overestimation of the calculation can be also observed in the neutron emission spectrum shown in Fig.7(a). It was therefore notable that the discrepancy in the γ-ray spectrum resulted from the insufficient evaluation of inelastic scattering cross sections since the emissions of 1.4 MeV γ-rays are the transitions from 2.676 to 1.434 MeV excited level and 1.434 to the ground state of ^{52}Cr induced by the (n,n') reaction.

4. Summary

Systematic data were obtained for the emission spectra of γ-rays from the spheres bombarded with 14 MeV neutrons. The neutron emission spectra, which were measured under the same condition as that of the γ

-ray spectra, took a significant role in the assessment of the nuclear data for γ -ray production in JENDL-3. Most of the production data in JENDL-3 are more accurate than those of ENDF/B-Ⅳ in the emission spectra for low energy γ -rays, since in many elements in JENDL-3 the emission spectra of secondary neutrons from discrete inelastic scattering are well analyzed.

Acknowledgment

Some spheres were supplied from the Research Reactor Institute of Kyoto University. The author would like to thank Mr. C. Ichihara and Dr. S. Hayashi of the institute and Prof. I. Kimura of Kyoto University for their cooperation.

References

1)Shibata,K. et al.:"Japanese Evaluated Nuclear Data Library, Version 3", JAERI 1319(1990).

2)Ichihara,C. et al.:"Measurement of Leakage Neutron Spectra from Various Sphere Piles with 14 MeV Neutrons", JAERI-M 88-065, 263(1987).

3)Yamamoto,J. et al.:"Gamma-Ray Emission Spectra from Spheres with 14 MeV Neutron Source", JAERI-M 89-026, 232(1989).

4)Harris,L. et al.:"An Introduction to the Principles and Use of the FERDOR Unfolding Code", GA-9882, Gulf Radiation Technology(1970).

5)Los Alamos Radiation Transport Group(X-6):"MCNP-A General Monte Carlo Code for Neutron and Photon Transport", LA-7396-M, Rev.(1981).

6)MacFarlane,R.E. et al.:"The NJOY Nuclear Data Processing System, Volume 1: User's Manual", LA-9303-M, vol.1(ENDF-324)(1982).

7)ENDF/B Summary Documentation, BNL-NCS-17541(ENDF-201), 2nd Edition (1975).

8)Kosako,K.:private communication(1990).

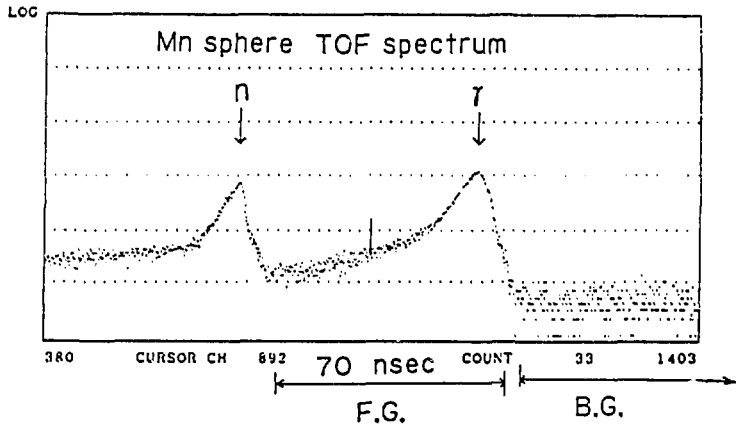

Fig.1 TOF spectrum from the Mn sphere.

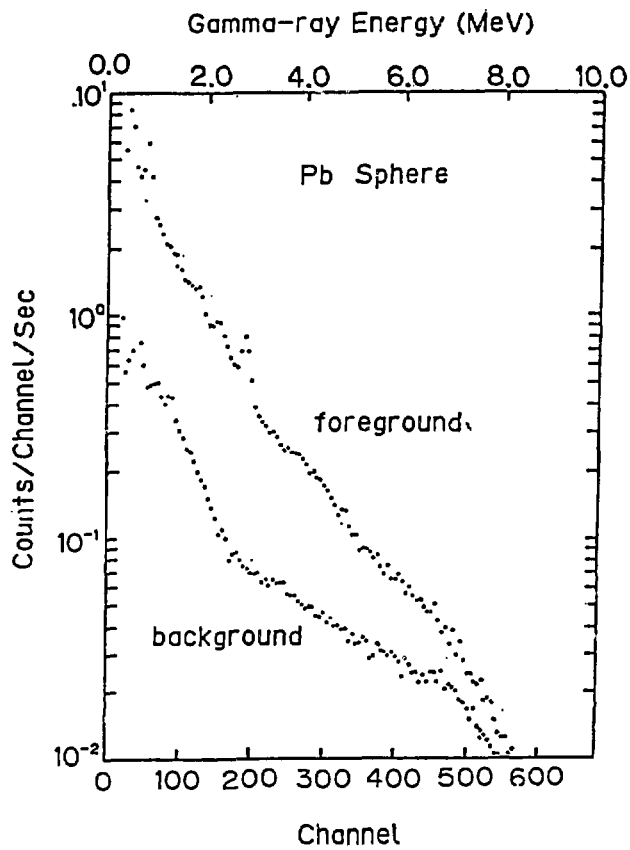

Fig.2 Pulse-height spectrum from the Pb sphere.

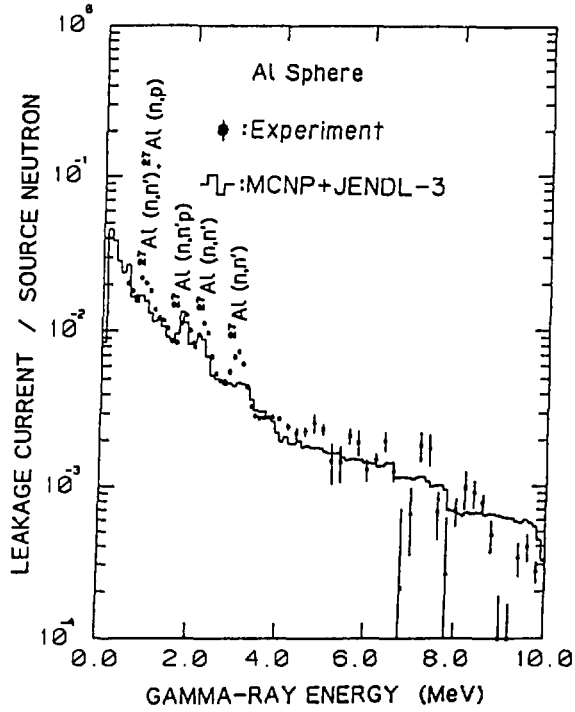

Fig.3 Gamma-ray emission spectra from the Al sphere in comparison with the calculations.

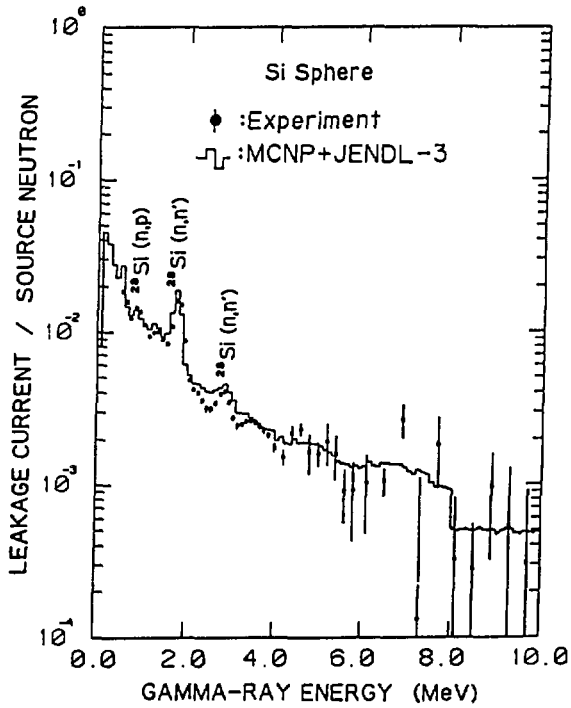

Fig.4 Gamma-ray emission spectra from the Si sphere.

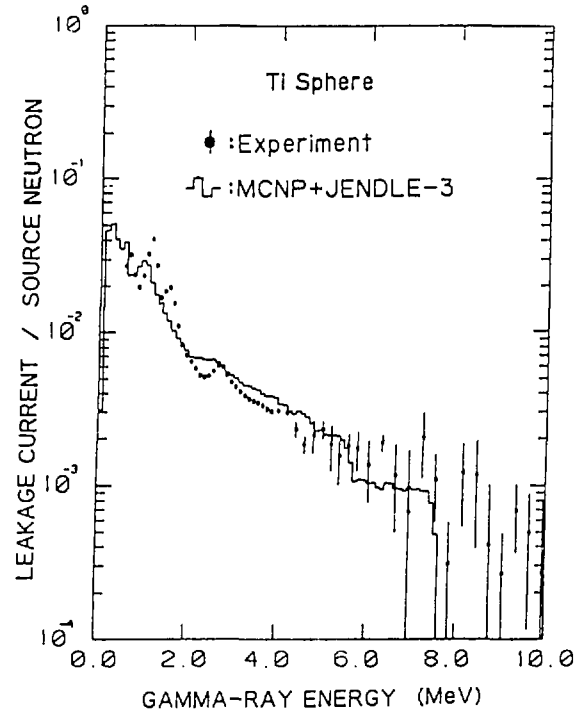

Fig.5 Gamma-ray emission spectra from the Ti sphere.

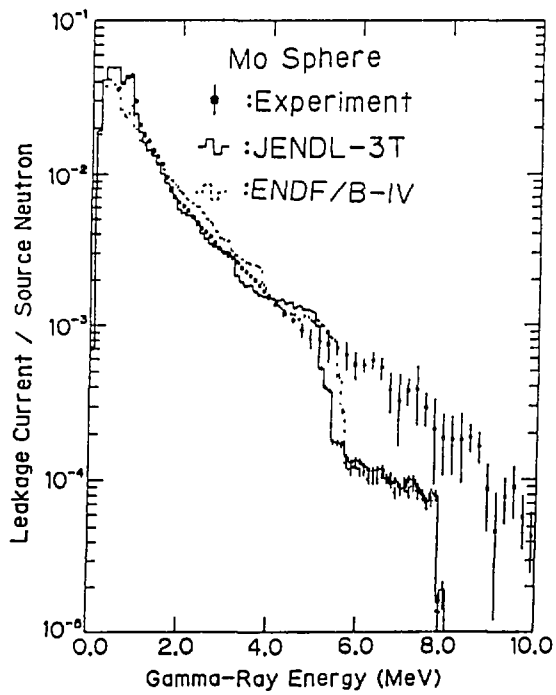

Fig.6 Gamma-ray emission spectra from the Mo sphere.

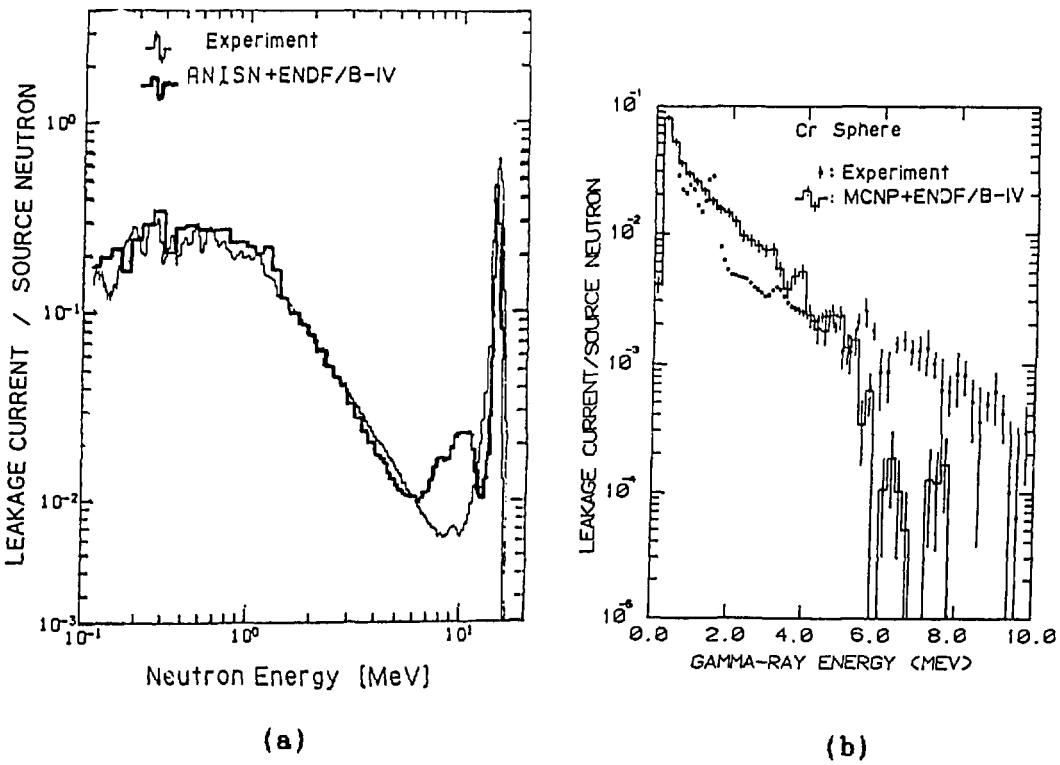

Fig.7 The energy spectra of neutrons (a) and γ-rays (b) emitted from the Cr sphere.

6.4 Analysis of ORNL 14 MeV SUS304 Benchmark Experiment

K. Sakurai and K. Ueki*
Japan Atomic Energy Research Institute
Tokai-mura, Naka-gun, Ibaraki-ken

An experimental configuration No. 3 of ORNL 14 MeV SUS304 benchmark experiment was analyzed by MCNP code with ENDF/B-4 and JENDL-3 cross section libraries. The point wise cross sections were compiled by NJOY-83 and MACROS code system. The C/E of the total gamma-ray flux above 1 MeV is about 0.8 for ENDF/B-4, and about 0.9 for JENDL-3.

1. Introduction

ORNL 14 MeV SUS304 benchmark experiment[1] is a typical benchmark problem to evaluate not only a calculational method of fast neutrons but also neutron cross sections and secondary gamma-ray production cross sections, as well. The overall experimental configuration is shown in Fig. 1[1]. The experimental configuratio No. 3 (only SUS304 with 30.48 cm) was analyzed by the Monte Calro code MCNP[2] with the ENDF/B-4[3] and the JENDL-3[4] cross section libraries. The point wise cross sections were compiled by the NJOY-83 and MACROS code system[5]. The Monte Calro results of the secondary gamma-ray energy spectra penetrated through the SUS304 are shown, and the reliability of cross section libralies are discussed with the results in this study.

2. Calculational Method and Results

The composition of materials used in the calculation is shown in Table 1[1]. In the analysis with the JENDL-3, the nuclides in the materials except the SUS304 were obtained from the ENDF/B-4 library. The calculations were performed by the MCNP code with the region and the energy dependent weight values. The energy bin is 0.5 MeV

* Ship Research Institute

for the neutron and the gamma-ray energy spectra. The calculated energy spectra were processed by the resolution of the NE-213 detector[4]. The gamma-ray energy spectra (200000 histories, point estimator) are shown in Fig. 2. In this calculation, the thickness of one cell for SUS304 is 30.48/5 cm. The SFD is about 3~7 % for the energy spectrum and about 2~3 % for the total flux. The C/E of the total gamma-ray flux above 1 MeV is about 0.8 for the ENDF/B-4, and about 0.9 for the JENDL-3. The sensitivity analysis was carried out on the conditions of ①number density 1/10 for iron can, ②for concrete, ③for thermal neutron shield plate, ④for concrete shield plate. The total gamma-ray flux above 10 keV is good agreement within the SFD 2~3 %. The gamma-rays from other materials except SUS304 are negligible small. The ratio of total gamma-ray flux is about 1/1.3 on the condition of the neutron cutoff energy from 0.5 eV to zero.

3. Discussions

The calculated secondary gamma-ray energy spectrum agreedd well with the measured values and the result of JENDL-3 is slightly better than that of ENDF/B-4. The secondary gamma-ray production data of JENdL-3 are improved in the energy region above 2 MeV better than those of ENDF/-4. The photon production number values of the JENDL-3 are larger than those of the ENDF/B-4 as much as a factor of 2~3, in the neutron energy region of 0.3~0.9 MeV. The magnitude of the secondary gamma-ray production number for neutrons between 0.3 and 0.9 MeV is less than that of energy above 1 MeV by a factor of 10. Accordingly, the secondary gamma-rays produced by neu trons between 0.3 and 0.9 MeV energy region would be a less contribution in the secondary gamma-ray energy spectrum. The iron cross sections in the ENDF/B-4 are not taken into account the inelastic scattering cross sections of Fe-57; on the other hand, the cross sections in the JENDL-3 are deliberated on the inelastic cross sections of it. The SUS304 cross sections in the JENDL-3 have better reliability than those of the ENDF/B-4 .

References

1) R. T. Santro, et. al., Nucl. Sci. Eng., 78, 259 (1981)
2) MCNP: Monte Calro Neutron and Photon Transport Code, CCC-200 (1983)
3) D. Garber ed., ENDF/B Summary Documentation, BNLNCS-17541 (1975)
4) JENDL COmpilation Group, JAERI-1391 (1990)
5) K. Kosako, et. al., JAERI-M 88-076 (1988)

Table 1 Composition materials used in the calculation[1].

Element	Composition (at./cm·b)					
	Concrete	Air	Iron Can	Type 304 Stainless Steel	BP	Hevimet
Hydrogen	7.86×10^{-3}				7.13×10^{-3}	
^{10}B					4.87×10^{-4}	
^{11}B					1.97×10^{-3}	
Carbon					3.41×10^{-2}	
Nitrogen		3.64×10^{-5}				
Oxygen	4.39×10^{-2}	9.74×10^{-6}			3.64×10^{-3}	
Sodium	1.05×10^{-3}					
Magnesium	1.40×10^{-4}					
Aluminum	2.39×10^{-3}					
Silicon	1.58×10^{-2}					
Potassium	6.90×10^{-4}					
Calcium	2.92×10^{-3}					
Chromium				1.77×10^{-2}		
Manganese				1.77×10^{-3}		
Iron	3.10×10^{-4}		8.48×10^{-2}	6.02×10^{-2}		
Nickel				7.83×10^{-3}		1.05×10^{-2}
Copper						6.45×10^{-3}
^{182}W						1.32×10^{-3}
^{183}W						7.21×10^{-3}
^{184}W						1.54×10^{-2}
^{186}W						1.43×10^{-2}

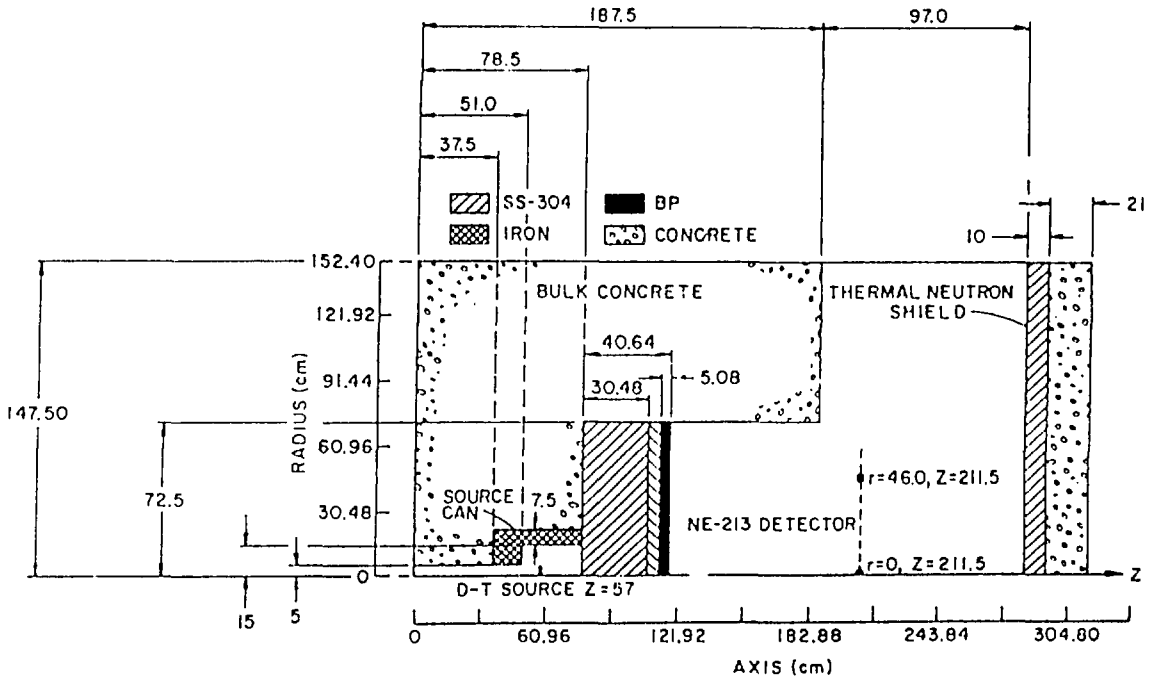

Fig. 1 Calculational model of experimental configuration[1]

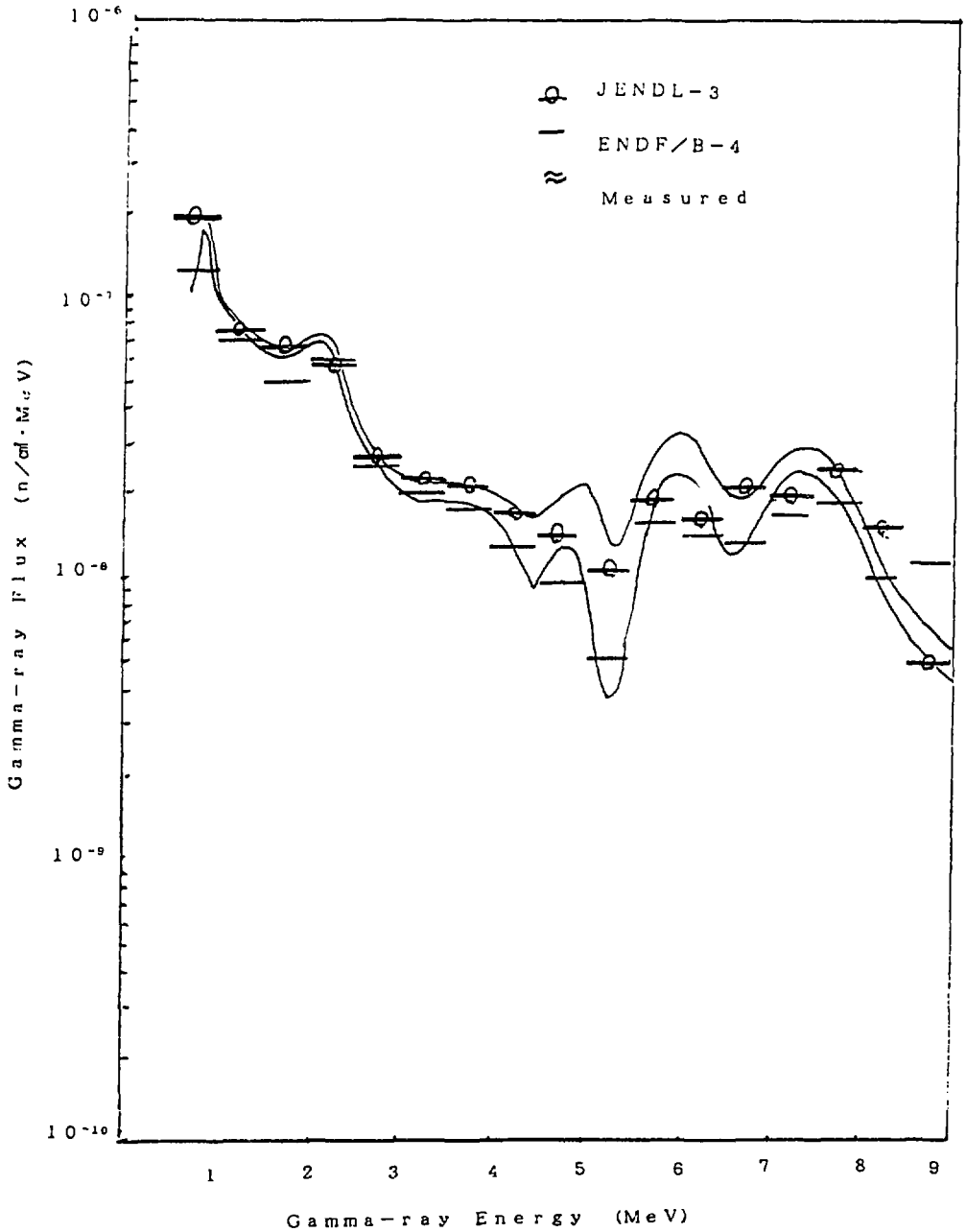

Fig. 2 Comparison of calculated and measured gamma-ray spectra

7. Activation Cross Sections

7.1 A Nuclear Model Calculation for JENDL Activation Cross Sections

N. Yamamuro
Data Engineering, Inc.
Midori-ku Yokohama-shi Kanagawa-ken

JENDL Activation Cross Section File includes the cross section data of the activations with half-life of longer than one-day for 59 elements. JENDL-3 general purpose file is used to determine the total activation cross sections for about 40 elements. But for other elements, a nuclear model calculation has been carried out to evaluate the ground and isomeric states production cross sections. The consistent nuclear model calculation shows the reasonable results in the activation cross sections over the wide range of nuclear mass and the predictive ability for the cross sections of long-lived nuclides.

1. Introduction

JENDL Activation Cross Section File is being prepared as one of the special purpose files. Materials are classified in three groups according to the priority determined from fission and fusion energy applications. The activation file includes all reaction cross sections which produce the activity with half-life of more than one-day for 37 elements of priority 1 and 22 elements of priority of 2.

There are two ways for the data evaluation.

(1) Total reaction cross sections are cited from the file 3 of JENDL-3 general purpose file and isomeric ratios are calculated with the code GNASH.

(2) The activation cross sections are essentially the production cross sections. In medium and heavy nuclei, many isomeric states are produced whose cross sections are important for the estimation of residual activity. In addition, some of JENDL-3 data are not sufficient compared with newly evaluated and experimental data. For about 20 elements, hence, the activation cross sections are calculated with a nuclear model code system, SINCROS-II[1].

In section 2, SINCROS-II is briefly described and examples of calculated results are depicted with the respective experimental data in section 3. Discussion and summary are shown in sections 4.

2. A Nuclear Model Calculation System

To calculate the nuclide product cross sections in the nuclear reactions, a simplified input nuclear calculation system (SINCROS-II) has been developed. The detail of SINCROS-II has been mentioned in ref. 1[1], so the brief description is given in the present paper. One of aims of SINCROS-II is that the consistent cross section calculations are performed over the wide range of nuclear-mass from 20 to 200.

The parameters used in the cross section calculation were predetermined if possible. The global optical-model potential parameters were built-in the code and the level density parameters "a" of Fermi-gas model were programmed as the data initialization statements. The isomeric state production cross sections are calculated as well as the ground state production cross sections. To quickly examine the results of the calculation, the list of the total production of particles and gamma-rays, and the ground and isomeric states production cross sections is printed out. The out-put data can be stored into computer diskette and converted to the ENDF/B format with a personal computer.

3. Examples of the Calculated Result on the Activation Cross Sections

At present, the cross section calculation for 30 elements, 109 isotopes from ^{27}Al to ^{209}Bi has been made. Some of the results are not final and the revised estimations will be carried out. Within them the cross sections for about 20 elements are enrolled in the JENDL Activation File. In this section, five examples of the calculated results are shown in order to present the feasibility and the predictive ability of the calculation system.

3.1 ^{60}Ni(n,p)^{60}Co reaction cross section

Fig. 1 shows the calculated result of ^{60}Ni(n,p)^{60}Co cross sections with the experimental data. The calculation referred the experimental data of Graham et al.[2] and Ikeda et al.[3] for the total production and Katoh et al.[4] for the isomer production. This figure was used in the ANL activation cross section meeting, September 1989. At the meeting, Vonach [5] presented their new measurement, hence we plotted the experimental data

on the figure. As shown in Fig. 1, the agreement between the calculation and the new data is good. Thus, Paulsen's[6] data was excluded, which was usually used in the old cross section evaluation.

3.2 $^{92}Mo(n,2n)^{91}Mo$ reaction cross section

Molybdenum has 7 isotopes, in which ^{92}Mo is the most poor neutron number nucleus. The experimental data for the total production of ^{91}Mo from the $^{92}Mo(n,2n)^{91}Mo$ reaction are divided into two groups as shown in Fig. 2. Brolley et al.[7] and Bormann et al.[8] show higher yield and ,on the other hand, Abboud et al.'s data[9] shows low cross section. The present calculation of total production cross section agrees well with Abboud et al. as well as the ground and isomeric states production cross sections agree with the experimental data[3,4,10]. If high total (n,2n) cross sections are accepted, as in the JENDL-III, the proton production cross section becomes very low value. The present calculational value is 905 mb at 15 MeV, which agrees with the experimental cross section of 967$\pm$ 110 mb.

3.3 $^{109}Ag(n,2n)^{108m}Ag$ reaction cross section

The isomeric state of ^{108}Ag has the half-life of 127 years, thus its production cross section is one of important ones for the safety and environmental assessment of nuclear energy applications. Several experimental data, however, give only the short-lived ground state production cross sections. Fig. 3 shows the result of the calculation for the ground and isomeric states production cross sections and their sum. The calculated ground state production cross section agrees fairly well with the experiments except for the Augustyniak's[11] some low energy data. New data for the isomeric production cross section at 15 Mev presented by Lu[12] in the ANL meeting is about 230 mb. It is very low value compared to the calculation. Hence, it is seems that the half-life of the isomeric state of ^{108}Ag is very longer than 127 years.

3.4 $^{197}An(n,\gamma)^{198}Au$ reaction cross section

As an example of the calculation of radiative capture cross sections, the result of $^{197}Au(n,\gamma)^{198}Au$ reaction cross section is shown in Fig. 4. The code CASTHY[13] is used in this calculation with the same parameters as those in the calculation of the threshold reactions for ^{197}Au. The absolute value is normalized to 325 mb at 100 keV. The agreement between

the calculation and the experiments is very good except for above 4 MeV. Gold is classified in the priority 3, but this evaluated result is included in the JENDL Activation and Dosimetry Files.

3.5 Long-lived ^{94}Nb production cross sections

A long-lived ^{94}Nb(half-life of 20 kiro-years) is produced via the reactions ^{94}Mo(n,p), ^{95}Mo(n,np) and ^{93}Nb(n,γ). If sequential reactions are considered, the (n,2n) reaction of ^{95}Nb(half-life of 35 days) also contributes the production of ^{94}Nb. Fig. 5 show the calculated results of the production cross sections of ^{94}Nb via ^{95}Nb(n,2n), ^{94}Mo(n,p) and ^{95}Mo(n,np) reactions. The measurements by Greenwood[14,15], which are experimental data only exist at present, agree with the calculation. We have no data for ^{95}Nb(n,2n)^{94}Nb reaction, but the calculated result seems to be reasonable because the (n,2n) cross section at 15 MeV agrees fairly well with the systematic trend of the cross sections as a function of the asymmetry parameter (N-Z)/A.

4. Discussion and Summary

We show the results of calculation with SINCROS-II together with the respective experimental data. Examples involved the wide range of nuclear mass, the ground and isomeric states production, the production of long-lived isotopes and the reaction for radio-active target. In all cases, the general agreement between the calculation and the experiments is very good.

As mentioned in sec. 2, in the present calculation the consistency of the calculational method is respected and the parameters used are cross-checked by the experimental data available. Hence, the predictive ability for the cross sections is expected to be great which is the leading aim of the SINCROS-II. The productions of all isotopes, whatever the ground and isomeric states exist or the half-life is shorter or longer, are calculated at the same time for the nuclear reactions except for the reactions where the fission process is included. When the cross sections are calculated with SINCROS-II, the activation cross sections with shorter half-life will be stored in the JENDL Activation File.

Some of the calculated activation cross sections have been submitted to the FENDL meeting held at IAEA June 1990, and many of them are recommended to the FENDL-1 activation file.

Recently, the code is revised at two points. (1) Ignatyuk's level density formula[16] and (2) a modification of alpha-particle optical-model potential parameter[17] are taken into account and the cross sections are being recalculated for the structural materials. The extension of incident energy up to 50 MeV for neutron and proton induced reactions is tried and the preliminary calculations are put into practice.

References

1) Yamamuro, N. : "A Nuclear Cross Section Calculation System with Simpliefied Input-Format Version-II (SINCROS-II)", JAERI-M 90-006 (1990).

2) Graham, S.L., Ahmad, M., Grimes, S.M., Satyanarayana, H., Saraf, S.K.: Nucl. Sce. Eng., 95, 60 (1987).

3) Ikeda, Y., Konno, C., Oishi, K., Nakamura, T., Miyade, H., Kawade, K., Yamamoto, H., Katoh, T. : "Activation Cross Section Measurements for Fusion Reactor Structural Materials at Neutron Energy from 13.3 to 15.0 MeV Using FNS Facility", JAERI 1312 (1988).

4) Katoh, T., Kawade, K., Yamamoto, H. : "Measurement of Activation Cross Sections", JAERI-M 89-083 (1989) (in Japanese).

5) Vonach, H., Wagner, M., Haight, R.C. :"Neutron Acivation Cross Sections of ^{58}Ni and ^{60}Ni for 8-12 MeV Neutrons" NEANDC-259 "U" p.165 (1990).

6) Paulsen, A., : Nukleonik, 10, 91 (1967).

7) Brolley,Jr., J.E., Fowler, J.L., Schlacks, L.K. : Phs. Rev., 88, 618 (1952).

8) Bormann, M., Feddersen, H.K., Hoelscher, H.H., Scobel, W., Wagner, H. : Z. Phys., A277, 203 (1976).

9) Abboud, A., Decowski, P., Grochulski, W., Marcinkowski, A., Piotrowski, J., Siwek, K., Wilhelmi, Z. : Nucl. Phys., A139, 42 (1969).

10)Marcinkowski, A., Stankiewicz, K., Garuska, U., Herman, M. : Z. Phys., A323, 91 (1986).

11)Augustyniak, W., Herman, M., Marcinkowski, A. : Nucl. Phys., A247, 231 (1975).

12)Lu, H., Yu, W., Zhao, W., Zaho, Y. : "Reseach of Activation Cross Sections for Long-Lived Radionuclides on Elements of Cu, Mo, Ag, Eu, and Tb", INDC(NDC)-232/L p.33 (1990).

13)Igarashi, S. : J. Nucl. Sci. Technol., 12, 67 (1975).

14)Greenwood, L.R., Doran, D.G., Heinisch, H.L. : Phys. Rev., C35, 76 (1987).

15)Greenwood, L.R., Bowers, D.L. J. Nucl. Materials, 155-157, 585 (1988).

16)Ignatyuk, A.V., Smirenkin, G.N., Tishin, A.S. : Sov. J. Nucl. Phys., 21, 255 (1975).

17)Bychikov, V.M., Pashchenko, A.B., Grudzevich, O.T., Zelenetsky, A.V., Plyaskin, L.I. : "Absorption Cross-Secton of Charged Particle by Nuclei in the Ground and Excited State", Proc. Int. Conf. Nuclear Data for Science and Technology, Mito Japan, p.1221 (1988).

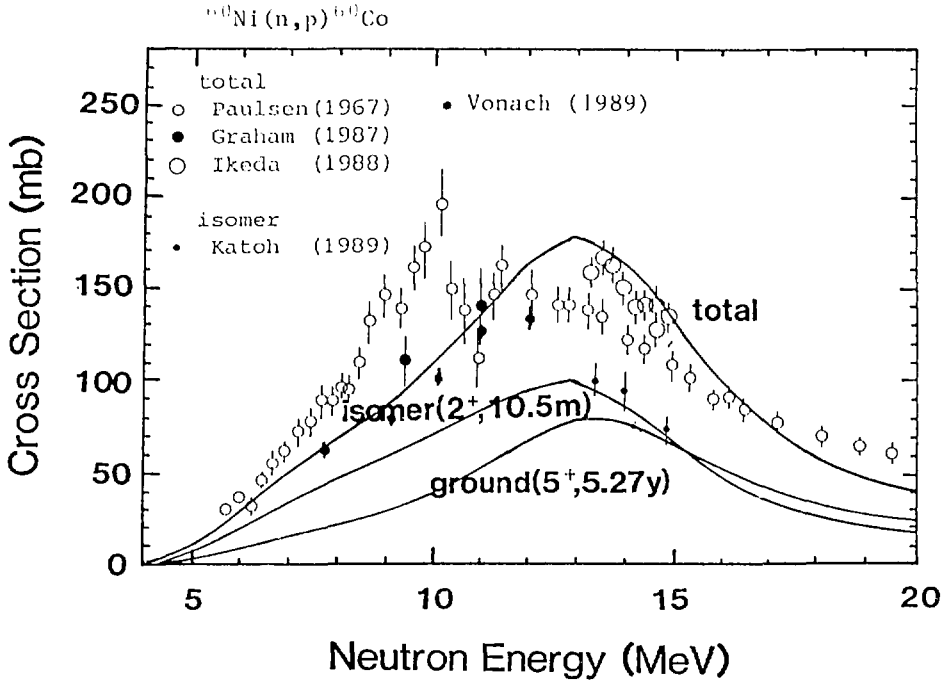

Fig. 1 Calculated ground and isomeric states production cross sections and their sum of ^{60}Co via ^{60}Ni(n,p)^{60}Co reaction compared with experimental data

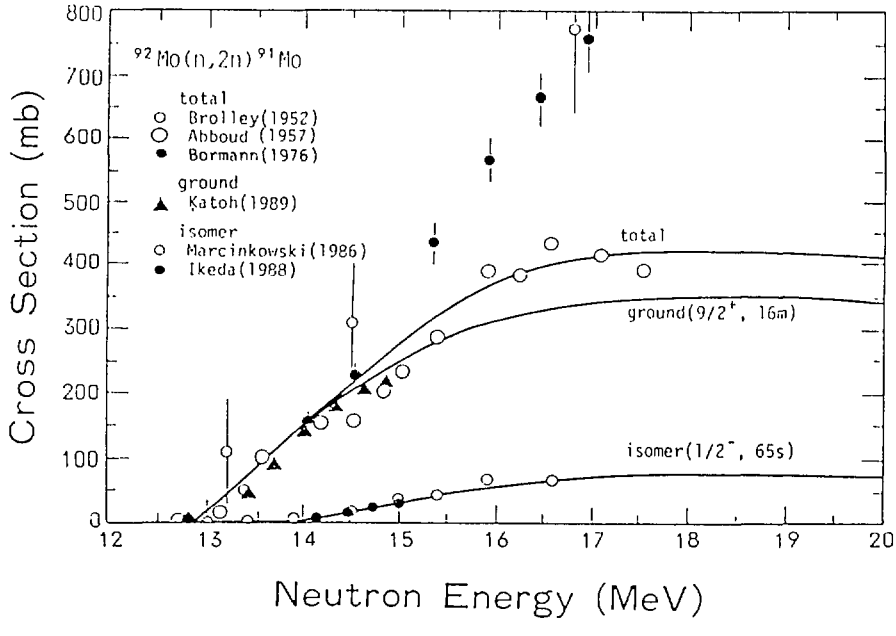

Fig. 2 Calculated ground and isomeric states production cross sections and their sum of ^{91}Mo via ^{92}Mo(n,2n)^{91}Mo reaction compared with experimental data

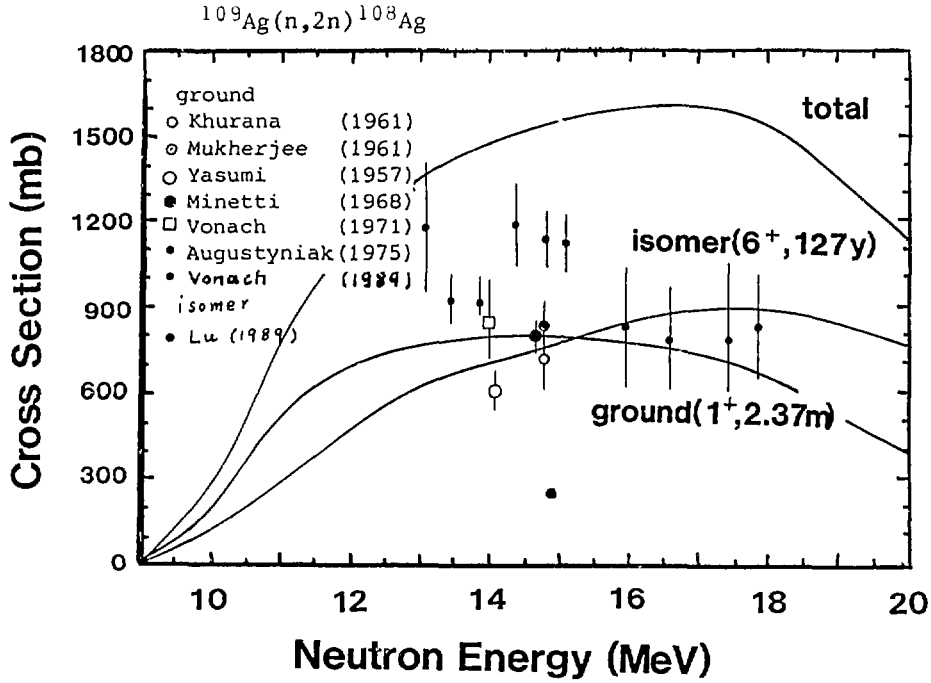

Fig. 3 Calculated ground and isomeric states production cross sections and their sum of ^{108}Ag via $^{109}Ag(n,2n)^{108}Ag$ reaction compared with experimental data

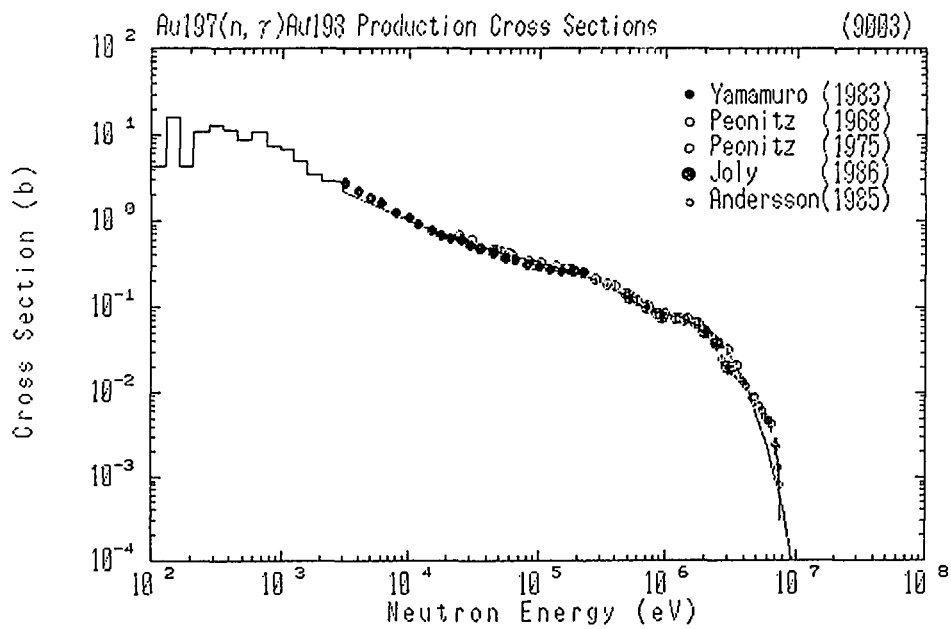

Fig. 4 Calculated radiative capture cross section of ^{197}Au compared with experimental data

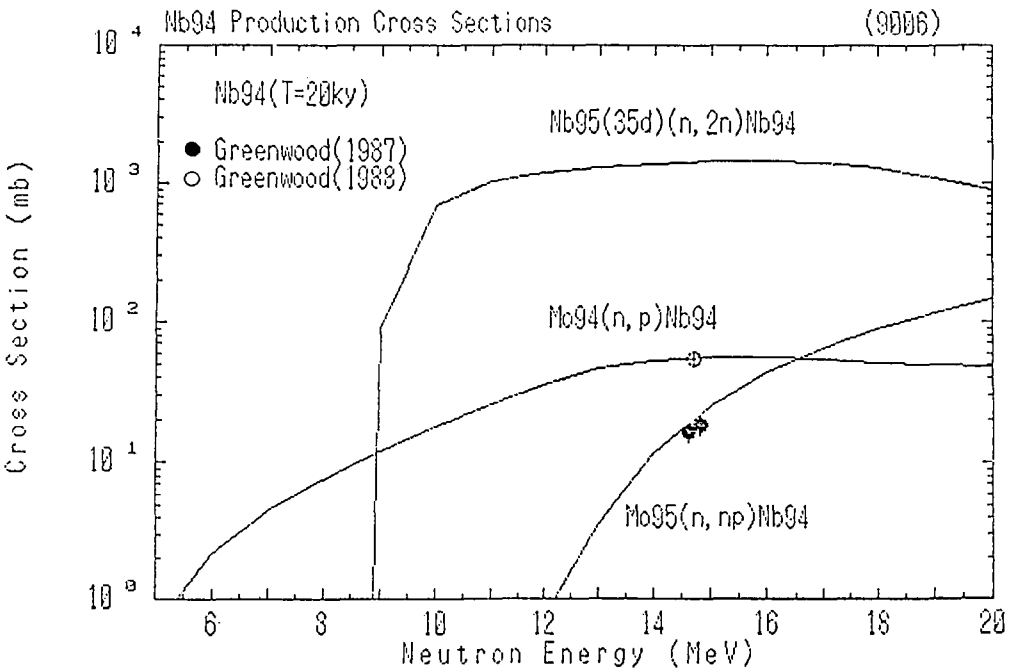

Fig. 5 Calculated production cross sections of long-lived ^{94}Nb from ^{95}Nb(n,2n), ^{94}Mo(n,p) and ^{95}Mo(n,np) reactions compared with Greenwood's data

7.2 Activation Cross Sections for Fusion Structural Materials

Y. Ikeda

Department of Reactor Engineering
Japan Atomic Energy Research Institute
Tokai-mura, Ibaraki-ken 319-11

Abstract: Present status of the induced activity calculation code systems, THIDA-2, REAC-2 and DKR-ICF, has been reviewed in terms of prediction accuracy through a benchmark test using irradiation experiments under typical D-T neutron environments. It was pointed out that the main uncertainty arose in inadequacy of the activation cross section data associated with respective libraries. An importance of integral experiments was emphasized to validate the code system. In order to meet the data requirement, extensive experimental programs have been conducted at JAERI/FNS and TANDEM facilities. This paper reviews the ongoing programs

1. Introduction

Activation cross section data for fusion structural materials are of improtance in terms of induced radioactivity, decay-heat, dose rate, and radioactive waste estimation. Extensive efforts have been addressed concerning the compilation of the cross section data and calculation code development. In order to arrive at the target accuracy in such parameters, several experiments subjecting many structural materials have been conducted in the framework of fusion neutronics studies.[1-5] They have investigated the adequacy of the cross section data as well as the calculation codes to predict induced activities production in the simulated D-T neutron environment so far as rather short time ranges from 10 min to several days after irradiations. As the result, it was pointed out that [1] there were sever discrepancies among results obtained by different code systems, THIDA-2[6], REAC-2[7] and DKR-ICF[8], which are currently available ones and [2] large deviations up to orders of magnitude were observed in the comparison between the experiment and calculations. It was concluded that the main source of the uncertainty in the calculation arose in the activation cross section inadequacy. This fact gave a significant requirement to improving accuracy in activation cross section data,in particular, for satisfying the prediction accuracy from a view point of the safety consideration of the next fusion reactor design.

To provide substantial data base meeting the requirement from the fusion applications, a program on the systematic measurement of neutron activation cross sections around 14 MeV[9]

has been underway at FNS facility[10] . The scope of program was extended to measure the cross section around 2.5 MeV region by using D-D neutron source. Another cross section measurement utilizing $^{1}H(^{11}B,n)^{11}C$ monoenergetic neutron source has been initiated to provide data at the energy region from 10 to 13 MeV.[11]

This report review the present status of these ongoing experimental programs as well as the integral experiment concerning the verification of the activation cross section libraries.

2. Integral Experiments and analysis

Up to now, there have been much progress in the design and broad choice of the materials in the next generation fusion testing devices have been proposed. Thus, it is urgent requirement to establish more systematic data base pertinent to the induced radioactivity and decayheat assessment.

An integral experiment was conducted at the FNS facility[10] in the framework of JAERI/USDOE collaborative program on fusion neutronics during Phase-IIC[12]. The objectives of the experiment were to provide data for verifying radioactivity calculation codes, and to investigating the suitability of different materials in meeting the selection criteria based on low activation and decayheat considerations. The major independent variables considered in this study are materials, neutron spectrum, the operation time and the time after shutdown. The experimental analysis has been carried out by using codes of THIDA-2, REAC2 and DKR-ICF. Aiming at making a systematic experimental data base, materials considered in the present study includes sixteen different materials, not only substantial structural materials of Iron, Nickel, Chromium, but the other potential materials of Aluminum, Silicon, Titanium, Molybdenum, etc..

The system consisted of Li_2O breeder blanket with a first wall enclosed by 200 mm Li_2CO_3 with 50 mm polyethylene. The DT neutron source was located in the cavity of the enclosure, at 780 mm distance from the first wall of the Li_2O region. The cross sectional view of the system is shown in Fig. 1 along with two irradiation positions. As the first position(**A**) was close to the DT neutron source, it is expected that the neutron spectrum simulates a typical one at first wall region. The second position(**B**) provided simulation of typical spectrum inside tritium breeder blanket,Li_2O. The spectrum inside the cavity includes neutron components reflected by the surrounding materials so that the field was expected reasonably to simulate the fusion radiation environment.

One of parameters to be investigated here is a dependence of radioactivity on the time(the operation and cooling after shutdown). It is of importance because of inherent time dependent nature of the radioactivity. Two irradiation times for 30 m and about 10 h were taken to respectively emphasize shorter and longer half-live products. After irradiation, sample were extracted from the system and γ-ray spectra were measured with four Ge detectors at cooling times ranging 10 m to 5 h for the short irradiation and 1 h to 7 days for the long irradiation.

The experimental analysis has been carried out by the code systems, THIDA-2, REAC-2 and DKR-ICF, which have been available and considered to be most potential ones. The comparison was made in terms of γ-ray energy spectrum emitted from the irradiation samples, which implied the decay γ-ray sources induced by the neutrons at the respective positions. In Fig. 2, the comparison of γ-ray spectrum for the case of Molybdenum at position **A** and short irradiation between calculation of THIDA-2 and experiment, for example. Figure 3 gives the C/Es for all cases corresponding to all measurements (after short and long irradiations and at position **A** and **B**). It was clearly shown that there were large discrepancies among results for several materials calculated by different codes. It was concluded that the main source for this sever discrepancies was in the difference in the activation cross section data libraries because it was reasonably expected that the calculation procedures for activation products are identical. Through the experimental analysis for the integral experiment, improvement of the accuracy in the cross section data for the D-T fusion neutron has been strongly addressed.

3. Review of programs for activation cross sections measurement at JAERI

3.1 Cross sections around 14 MeV using FNS

Cross sections at energy from 13.3 to 15.0 MeV for two hundred reactions have been measured so far systematically using FNS facility[10]. A large body of data on the same experimental basis enabled us to extract a more precise systematic trend for specific reactions such as (n,p), (n,np), (n,α) and (n,2n) as a function of the asymmetry parameter, (N-Z)/A. In Figs. 4 and 5, data for (n,p) and (n,2n) reactions are plotted as a function of the asymmetry parameter. For the (n,p) reaction, it is observed that existence of certain fine structures in the systematic trend depending on the proton number and a degree of neutron excess. It is worthwhile to investigate more in detail this semi-empirical rule with a fine structure in order to establish a systematic trend for the cross section for getting more accurate prediction of unknown reaction cross section being difficult to be measured. It is in the same sense, evident that the present data for (n,2n) reaction so far accumulated give a good quality in the figure of the systematic trend. It seems better than previously reported by many authors. The same better condition are found in the (n,α) and (n,np) reaction cross sections.

3.2 Cross sections around 2.5 MeV using FNS

In addition to the 14 MeV cross section measurements, we started a series of measurements at an energy range from 2.0 to 3.1 MeV using the FNS facility. This program was primarily related to the application of the foil activation technique into the D-D plasma diagnostics. Also it is important to supplement the cross section data at 14 MeV.

The reactions with threshold energies below 1 MeV measured so far were

$^{47}Ti(n,p)^{47}Sc$, $^{54}Fe(n,p)^{54}Mn$, $^{58}Ni(n,p)^{58}Co$, $^{64}Zn(n,p)^{64}Cu$, $^{111}Cd(n,n')^{111m}Cd$, $^{113}In(n,n')^{113\mu}In$, $^{117}Sn(n,n')^{117m}Sn$ and $^{136}Ba(n,n')^{137m}Ba$. In Fig. 6 and 7, the cross sections for reactions of $^{47}Ti(n,p)^{47}Sc$ and $^{58}Ni(n,p)^{58}Co$ are shown together with data in the currently available evaluations as well as data in the literature.

3.3 Cross sections from 10 to 13 MeV using TANDEM

The deficiency in experimental data of neutron cross sections at the energy region between 10 MeV and 13 MeV has been often stressed. This shortage in the experiments has been mainly due to the lack of the appropriate monoenergetic neutron sources. Recently, use of $^{1}H(^{11}B,n)^{11}C$ reaction to generate monoenergetic neutrons from 10 to 13 MeV has been investigated in JAERI by using the TANDEM heavy ion accelerator.[11] Utilizing this particular neutron source, we have carried out activation cross section measurements to provide data at energies of 11.0, 12.0 and 13.2 MeV for several important reactions in the dosimetry application.

The reactions investigated in the present experiment are selected from a view point of the importance in the dosimetry. The reaction of $^{27}Al(n,\alpha)^{24}Na$ is used as a standard for the cross section determination experiments. The reactions of $^{90}Zr(n,2n)^{89}Zr$ and $^{93}Nb(n,2n)^{92m}Nb$ are the most promising monitor reaction for the 14 MeV neutron flux. The reactions of $^{47}Ti(n,p)^{47}Sc$, $^{64}Zn(n,p)^{64}Cu$ and $^{115}In(n,n')^{115m}In$ are the spectral indices for the first neutrons with relatively low threshold energies.

The monoenergetic neutrons were generated by bombarding the hydrogen gas target with ^{11}B beam energy of which were from 50 to 68 MeV by using the TANDEM accelerator at JAERI. Three different irradiations were conducted changing the energy of the incident ^{11}B beam. After irradiation, reaction rates of interest were deduced by the conventional foil activation technique. Cross sections were obtained relative to the that of $^{197}Au(n,2n)^{196}Au$, which were taken from JENDL-3 dosimetry file. In Fig. 8, the measured cross sections for $^{93}Nb(n,2n)^{92m}Nb$ are plotted along with the data in the literature as well as data in the evaluations.

Though there are considerably large numbers of data in the energy region from 13.5 to 15 MeV, data below 13 MeV were very limited. The present data supplemented significantly the data needed in this particular energy region. In summary, it is demonstrated that the monoenergetic neutron source via. $^{1}H(^{11}B,n)^{11}C$ is very powerful to provide experimental data in the deficient region, even the activation technique is applied. Further measurements on the other important reactions are planed to be done in the future.

3.4 Topics for the long-lived activation and sequential cross section measurements

An endeavor to arrive at sufficient accuracy in the nuclear data for long-lived activation cross section have been initiated a few years ago as the IAEA-CRP[13] to satiety the nuclear data needs from radioactivity waste disposal assessment. One experiment for this purpose has been proposed in the framework of the JAERI/US collaborative program on fusion neutronics.[12] The other experimental program was an inter-laboratory collaboration[14] was proposed by Dr. D. L. Smith at ANL under a support by the IAEA-CRP, which included different neutron sources, d-Be at ANL[15], T-p at LANL[16] and D-t at FNS.[10] In this collaboration, it was expected that cross sections of concerned cover the neutron energy range from several MeV to 14 MeV. The measurement of cross sections at 14 MeV was carried out at FNS as a part of this collaboration The long-lived radioactivities with half-lives from 10 to 10^6 years were concerned in this experiments. Samples for both programs of JAERI/USDOE collaboration and ANL/LANL/FNS inter-laboratory collaboration were irradiated simultaneously with 14 MeV neutrons for 4 days (8 hours irradiation per a day). It resulted in 1.7 x 10^{17} neutrons of total neutron yield at the DT target. Neutron flux at each sample was monitored with the $^{93}Nb(n,2n)^{92m}Nb$ reaction. The neutron fluences at the samples were estimated to range 1 - 2 x $10^{15}/cm^2$ and about 2 x 10^{14} n/cm^2 for JAERI/USDOE collaboration and the inter-laboratory collaboration, respectively.

From summary peak counts, reaction rates of concern were derived with necessary corrections, e. g. decay constant, cooling time, collection time, detector efficiency, natural abundance of the target material, γ-ray branching ratio, sample weight, self-absorption of γ-ray, neutron flux fluctuation during irradiation, and so forth.

The cross sections were obtained from the reaction rates divided by neutron flux determined by $^{93}Nb(n,2n)^{92m}Nb$ reaction rate. So far the preliminary cross section data for six reactions of $^{27}Al(n,2n)^{26}Al$, $^{151}Eu(n,2n)^{150m}Eu$, $^{153}Eu(n,2n)^{152m}Eu$, $^{159}Tb(n,2n)^{158m+g}Tb$, $^{179}Hf(n,2n)^{178m2}Hf$ and $^{107}Ag(n,2n)^{108m}Ag$ has been obtained. The counting of activities are still underway to arrive at sufficient statistics.
Recently, an importance of the sequential reaction which lead to the long lived activity production have been reported.

Recently, an importance of the sequential reactions has been recognized for the long-live activation production in the fusion materials. This type of reaction is induced by the charged particles which is emitted by the primary neutron induced reactions. To estimate the product, not only the (n,z) reaction cross sections, but also the (z,n)

reaction cross sections are needed. One approach to calculate the induced activity including the sequential process has been proposed.[17] It is, in generally, difficult to detect the product because of low cross section value and strong interfering activities.

To provide experimental data for verifying the calculation code, production cross sections at 14 .9 MeV for the sequential reaction of (a) Fe(n,p)+^{56}Fe(p,n) ^{56}Co and (b) Cu(n,p)+^{65}Cu(p,n)^{65}Zn have been measured. The γ-ray spectrum of Iron measured by a Ge detector after irradiation of D-T neutrons is shown in Fig. 9. The γ-lines from the ^{56}Co are clearly observed. Production cross sections of 0.2 mb and 0.05 mb were derived As preliminary results for reaction (a) and (b), respectively.

4. Summary

The results of integral experiment and analysis for induced radioactivity and decayheat indicated inadequacy for considerable large numbers of the activation cross section data in the currently available libraries so far as the short time range was concerned. To improve the consistency and accuracy of the cross sections at 14 MeV for threshold type reactions in the fusion reactor materials, systematic experimental data are affordable in the framework of the ongoing experimental program at FNS using intense D-T and D-D neutron sources. As for the cross section data at the energy range from 10 to 13 MeV, the data production is not so extensive because of a restriction from the less availability of the machine time for the irradiation at TANDEM facility. Since importance of radioactivities in the impurity and decayheat consideration will strongly increase in the future, much experimental effort will be addressed on cross sections for the exotic reaction, β-emitter production.

One of serious problems associated with (n,γ) reactions concerning the radioactivity production, however, is still left to be verified. As long as the integral experiment referred in this paper is concerned, further examinations of cross section data are needed through the various well defined neutron field with considerable amounts of low energy neutrons.

References

1. Y. Ikeda et al.,"An Experimental Study of Induced Activity in Type 316 Stainless Steel by Irradiation in D-T Neutron Fields," JAERI-M 83-177 (1983).
2. Y. Ikeda, et al.,"Measurements of Induced Activity in Type 316 Stainless Steel by Irradiation in D-T Neutron Fields," Fusion Technology., 8, 1466 (1985).
3. K. Oishi, et al.,"Experiment and Analysis of Induced Activities in Concrete Irradiated by 14 MeV Neutrons," Fusion Technology., 10, 579 (1986).
4. K. Oishi, et al.,"Measurement and Analysis of Induced Activities in Concrete Components Irradiated by 14 MeV Neutrons," to be published in Fusion Technology.
5. A. Kumar, et al.,"Analysis of Induced Activities Measurements Related to Decayheat

in Phase-IIC Experimental Assembly: JAERI/USDOE Collaborative Program," Proc. of 9th Topical Meeting on Technology of Fusion Energy, Oct. 7 - 11, 1990, Chicago, U.S.A., to be published.

6. Y. Seki, et al., "THIDA-2: An Advanced Code System for Calculation of Transmutation, Activation, Decay Heat and Dose Rate", JAERI-1301 (1985).
7. F. M. Mann, " REAC2: Status of Codes and Libraries", Technology of Fusion Energy, 8th Topical Meeting, October 1988, Salt Lake City, Fusion Technology, March 1989.
8. D. L. Henderson and O. Yasar,"DKR-ICF: A Radioactivity and Dose Rate Calculation Code Package," Vol. 1 and 2, UWFDM-714 (1986).
9. Y. Ikeda, et al.,"Activation Cross Section Measurement for Fusion Reactor Structural Materials at Neutron Energy from 13.3 to 15.0 MeV Using FNS Facility," JAERI-1312 (1988).
10. T. Nakamura, et al. ;" Present Status of the Fusion Neutron Source(FNS)," Proc. 4th Symp. on Accelerator Sci. Technol., RIKEN, Saitama, 24 - 26 November 1982, pp 155- 156.
11. S. Chiba, et al.,"The $^{1}H(^{11}B,n)^{11}C$ Reaction as a Practical Low Background Monoenergetic Neutron Source in the 10 MeV Region," Nucl. Instr. & Methods, A281 581 (1989).
12. Y. Oyama, et al.,"Measured Characteristics of Be Multi-Layered and Coolant Channel Blankets: Phase-IIC Experiments of the JAERI/USDOE Collaborative on Fusion Neutronis," Proc. of 9th Topical Meeting on Technology of Fusion Energy, Oct. 7 - 11, 1990, Chicago, U.S.A., to be published.
13. INDC(NDS)-232/L, "Activation Cross Sections for the Generation of Long-Lived Radionuclides of Importance in Fusion Reactor Technology", Proc. of an IAEA Consultants' Meeting, Argonne National Laboratory, 11th - 12th. Sept 1989
14. J. W. Meadows, et. al. "A Search for Activation Produced by Fast-Neutron Irradiations of Copper, Silver, Europium, Terbium and Hafnium", Proc. of an IAEA Consultants' Meeting, Argonne National Laboratory, 11th - 12th. Sept 1989.
15. D. L. Smith and J. W. Meadows; ANL/NDM-95, Argonne National Laboratory (1986).
16. R. C. Haight "Activation with an Intense Source of Monoenergetic Neutrons in the Range 8-14 MeV", Proc. of a Specialists' Meeting on "Neutron Activation Cross Section for Fission and Fusion Energy Applications", Argonne National Lab., USA, 13th-15th sept. 1989 pp95-97.
17. S. Cierjacks and Y. Hino,"The Role of Sequential (x,n) Reactions on Element Activation of Fusion Reactor Materials and Related Nuclear Data Needs," ibid., pp 19 - 28.

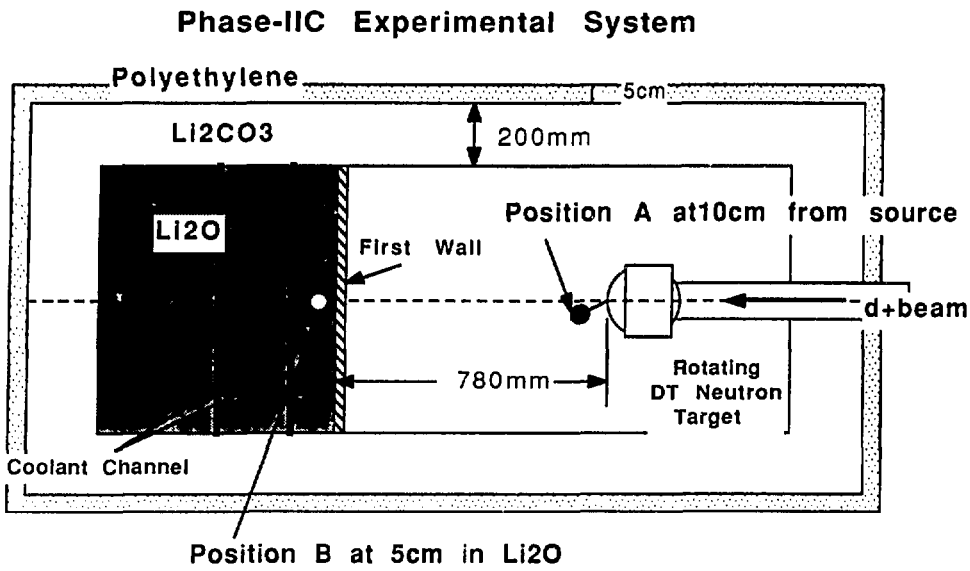

Fig. 1 Cross sectional view of the system configuration for the Phase-IIC experiment with water cooling channels.

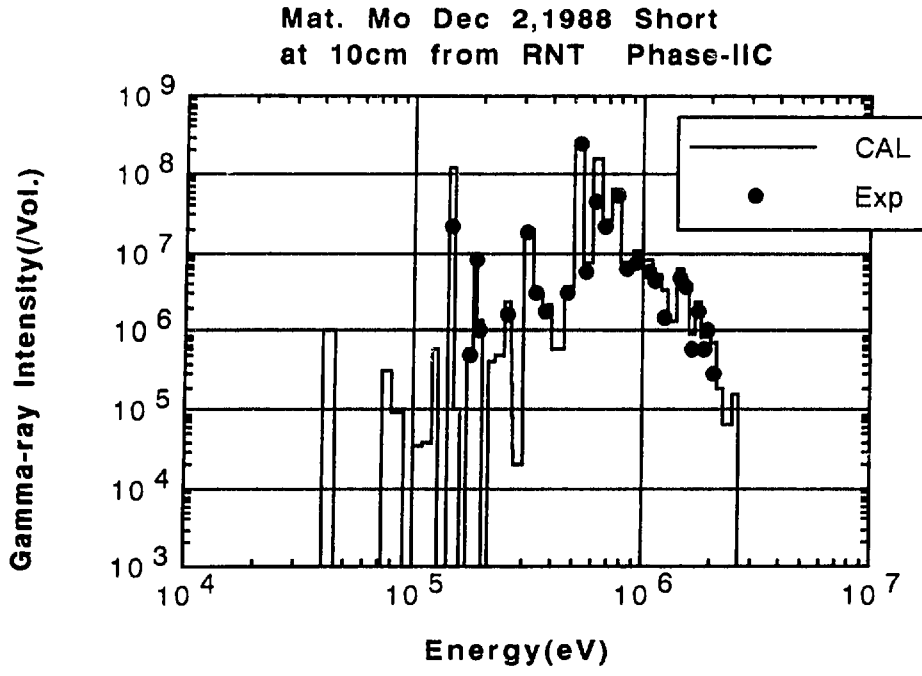

Fig. 2 Comparison of γ-ray spectrum for Mo between measurement and calculation by THIDA-2.

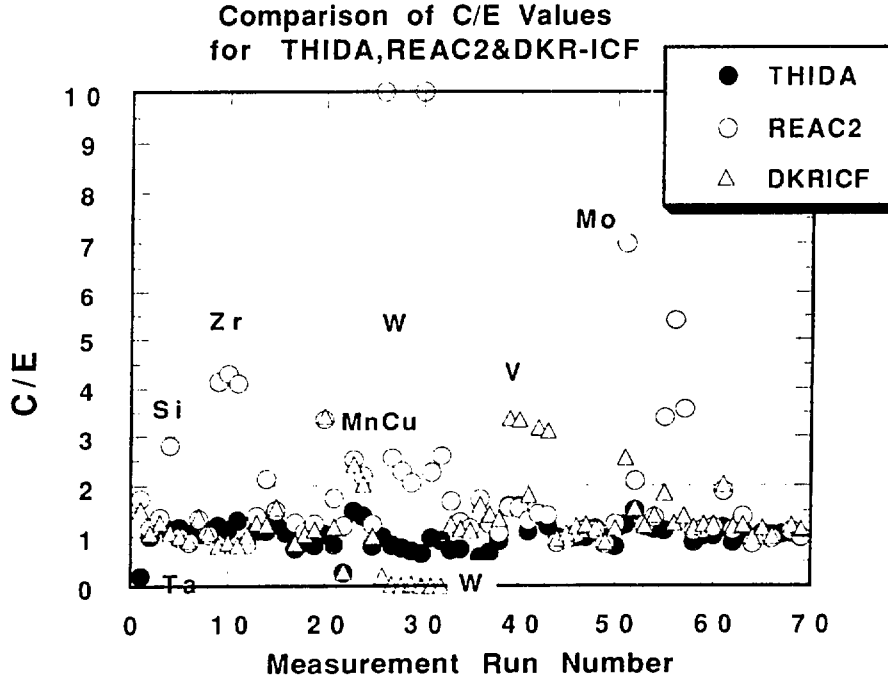

Fig. 3 C/E values of all measurement cases corresponding.

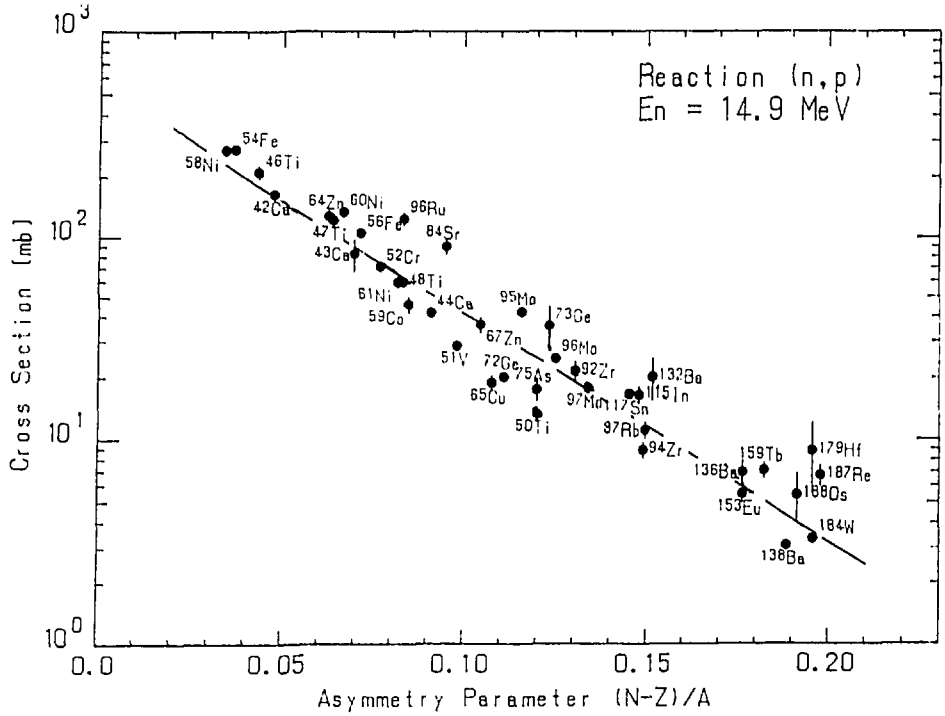

Fig. 4 Systematic trend of cross sections for (n,p) reaction as a function of (N-Z)/A.

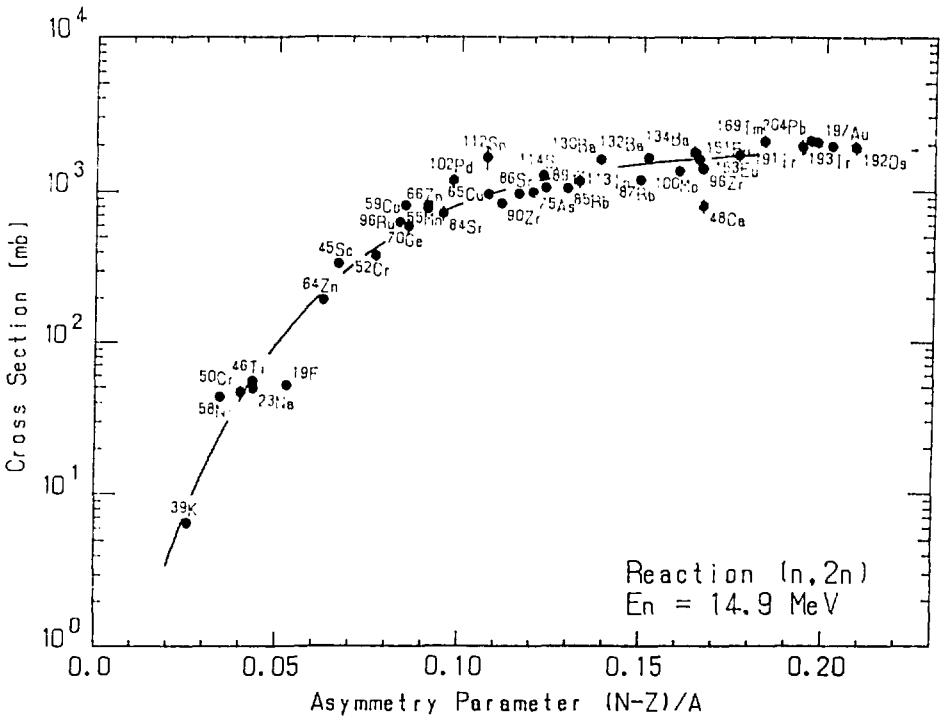

Fig. 5 Systematic trend of cross sections for (n,2n) reaction as a function of (N-Z)/A.

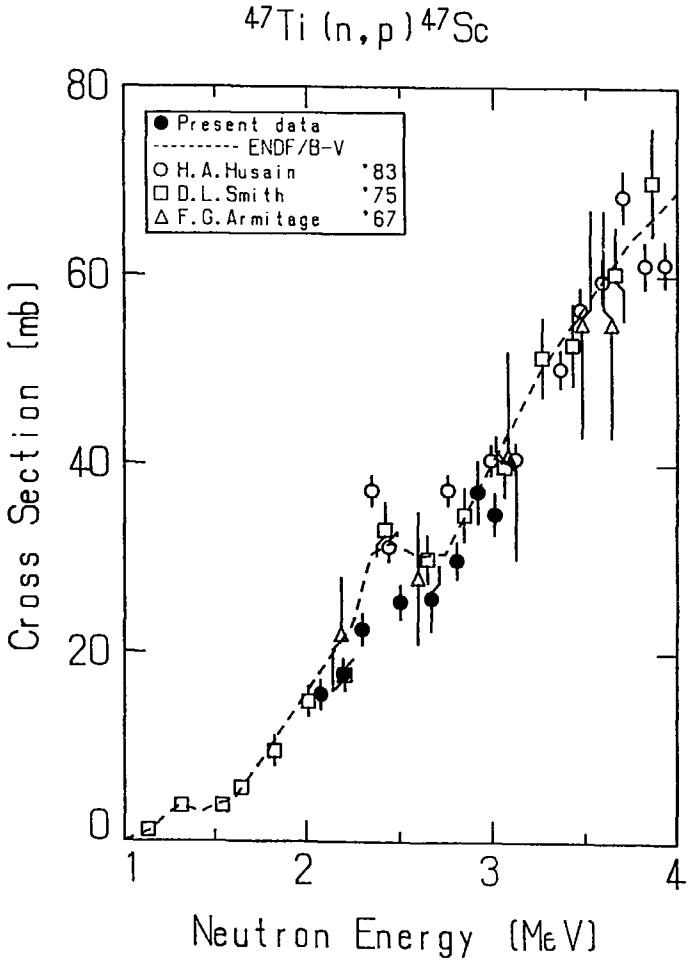

Fig. 6 Cross sections of $^{47}Ti(n,p)^{47}Sc$ at the energy range from 1 to 4 MeV.

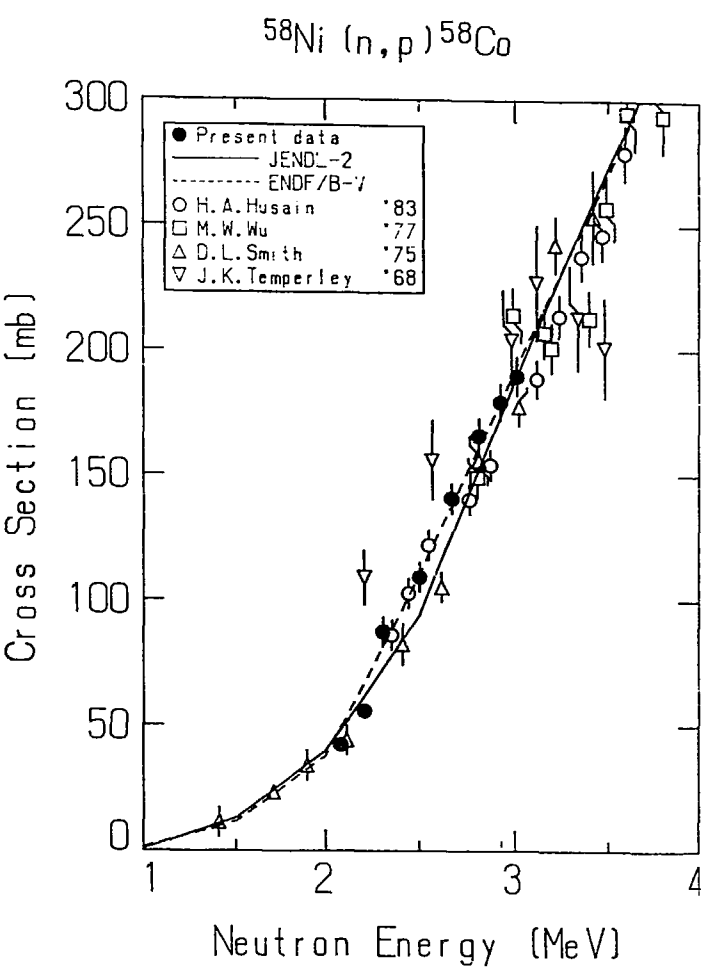

Fig. 7 Cross sections of $^{58}Ni(n,p)^{58}Co$ at the energy range from 1 to 4 MeV.

JAERI-M 91-062

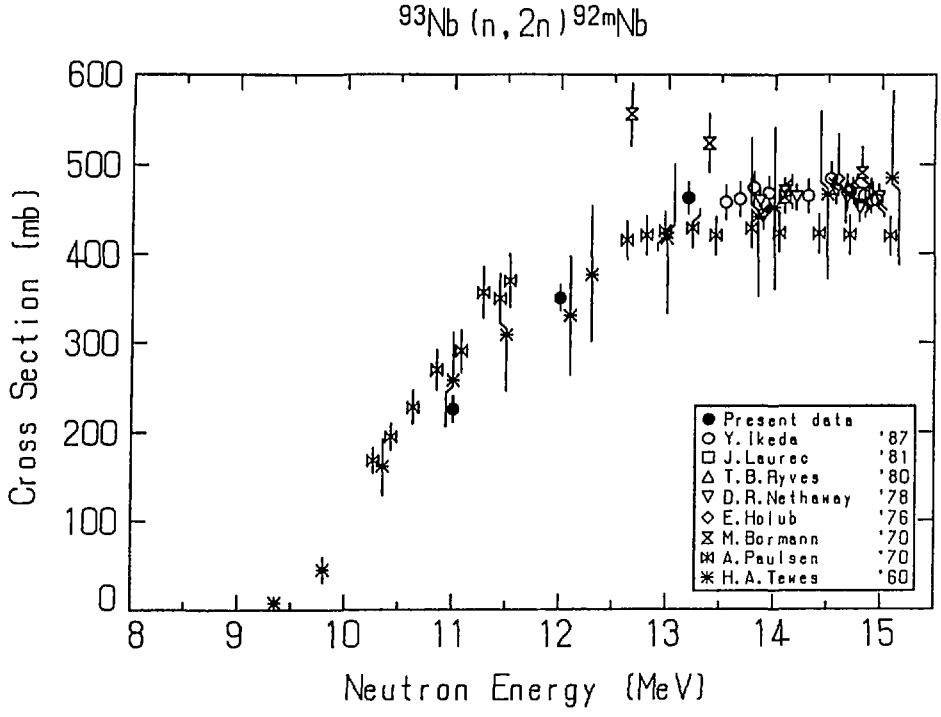

Fig. 8 Cross sections of $^{93}Nb(n,2n)^{92m}Nb$ reaction at the energy range from threshold to 15 MeV.

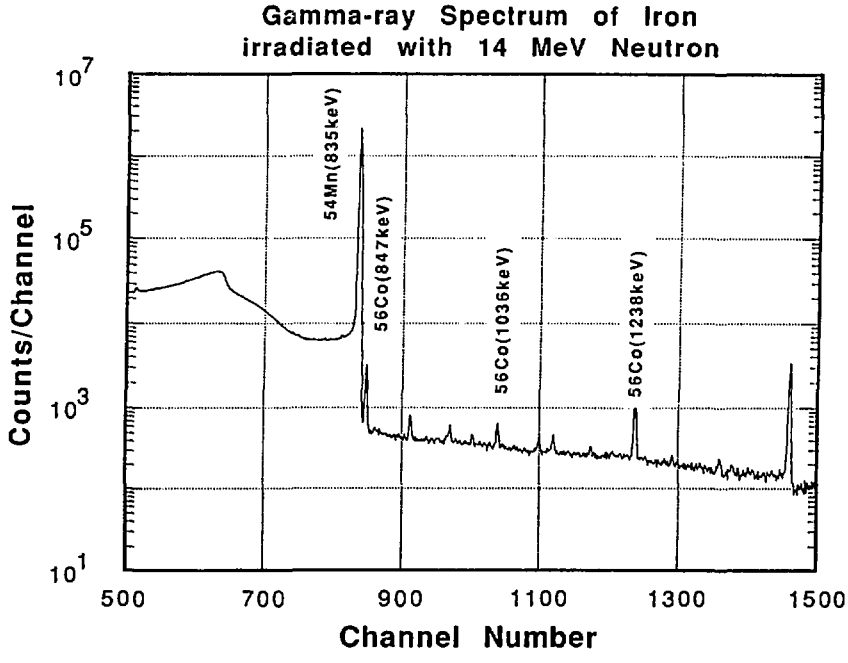

Fig. 9 Gamma-ray spectrum of Iron sample measure after heavy irradiation by D-T neutrons.

8. PKA, KERMA and DPA Files

8.1 Evaluation and File Making of PKA, KERMA and DPA Data

Masayoshi KAWAI and Shungo IIJIMA

Nuclear Engineering Laboratory, Toshiba Corporation
4-1 Ukishima-cho, Kawasaki-ku, Kawasaki, 210

Abstract

The formulas to calculate PKA spectrum, KERMA factor and DPA cross section are summarized as well as modeling effect on PKA spectrum. Enhancement of the higher energy neutron emission due to pre-equilibrium process hardens the spectrum of PKA recoiled by neutron but inversely the anisotropy of secondary neutron makes it softer. As a whole, pre-equilibrium process affects on softening the PKA spectrum and increases by a few ten percent DPA cross section due to inelastic scattering. For (n, 2n) reaction, significance of two particle emission is shown in case of the iron PKA spectrum. A scope of PKA and KERMA related data file is also presented.

1. Introduction

There is an increasing demand for the data of PKA (primary knock-on atom) spectra, DPA (displacement per atom) cross sections and KERMA (kinetic energy release in matter) factors from radiation damage study, fusion neutronics, and medical and biological applications. It has been rather customary in calculation of these PKA/KERMA data to use rather crude approximations for particle emission spectra. Results were often affected significantly by a slight violation of energy balance or by the crudeness of the reaction model. Recently, the authors[1] proposed an improved and yet a simplified method of calculation of KERMA data. In the method, the evaluated neutron data file of ENDF/B-5 format is fully utilized, being supplemented by the average energy values of

emitted charged particles from cross section calculation code. An approximate compact expression is given for the KERMA factor and the DPA cross section, in which the multi-particle emissions are properly taken into account. The reliability of the method was confirmed by comparing the calculated results with those by the RADHEAT code[2] which performs the exact numerical integration to obtain DPA cross sections. Remainder interest is about calculation method of PKA spectra and file-making of PKA/KERMA related data.

In the present report, modeling effect on the PKA spectrum and the scope of the data file is described.

2. Fundamental Formulas

The formulas are described in Ref. 1 and the main formulas are written in the following. The PKA spectrum is obtained by converting the cross section given in the center-of-mass (c.m) system to the laboratory frame. Let m_{01} and m_{02} be the masses of the incident neutron and target atom at rest, and m_1 and m_2 be those of the emitted particle and recoil atom, respectively. From the reaction kinematics sketched in Fig. 1, the double differential and the angle-integrated PKA spectra from the first stage reaction are expressed by

$$\sigma(E_n,E_p,\theta_p) = (M/m_1)^{3/2}(E_p/\varepsilon_c)^{1/2}\,\sigma(E_r,\varepsilon_c,\theta_c) \qquad (1)$$

$$\sigma(E_n,E_p) = \pi M(m_1m_2)^{-1/2}\int_{\varepsilon_c^{(1)}}^{\varepsilon_c^{(2)}} d\varepsilon_c\,(\varepsilon_c E_G)^{-1/2}\,\sigma(E_r,\varepsilon_c,\theta_c) \qquad (2)$$

where,

E_n and E_r: the laboratory and relative incident neutron energies,
$E_G=MV^2/2=(m_{01}/M)E_N$: the kinetic energy of the compound nucleus
$M = m_{01} + m_{02} = m_1 + m_2$,
(E_p, θ_p) and $(\varepsilon_c, \theta_c)$: the energies and the angles of recoil atom in laboratory system and of emitted particle in c.m system,
$\sigma(E_r,\varepsilon_c,\theta_c)$: the double differential cross section in c.m system; suffix c stands for the quantities in c.m system.

Kinematics relation gives

$$E_p = \frac{m_2}{M} E_G + \frac{m_1}{M} \varepsilon_c - 2(m_1 m_2/M^2 \cdot E_G \varepsilon_c)^{1/2} \mu_c, \quad (3)$$

$$\mu_p = (1-\eta_c \mu_c)/(1+\eta_c^2 - 2\eta_c \mu_c)^{1/2}, \quad (4)$$

where,

$$\eta_c \equiv (m_1 \varepsilon_c / m_2 E_G)^{1/2}. \quad (5)$$

The integration range in Eq.(2) is determined from the reaction Q-value and Eq.(3).

In case of the second stage reaction, the PKA spectrum is given by applying the Jacobians twice in Eqs.(1) and (2). The spectra of both the 1st and the 2nd particles in c.m system are needed in this calculation.

For emission of more particles, the analytical calculation becomes very cumbersome but we may calculate the PKA spectrum from Eq. (1) by using composite spectra for the emitted particles with an approximation of single particle emission model as follows:

$$\sigma_x(E_n, E_p, \theta_p) \cong \frac{1}{4\pi} \left(\frac{M}{m_1}\right)^{3/2} \left(\frac{Ep}{\varepsilon_c}\right) \sigma_{x\text{-prod}}(E_r, \varepsilon_c) \frac{\sigma_{cont}(E_n)}{\sum_x \sigma_{x\text{-prod}}(E_n)} \quad (6)$$

Here, $\sigma_{x\text{-prod}}(E_r, \varepsilon_c)$ and $\sigma_{x\text{-prod}}(E_n)$ are the x-particle spectrum and production cross section; $\sigma_{cont}(E_n)$ is the continuum spectrum particle emission cross section i.e. the difference between nonelastic and discrete inelastic scattering cross sections. Eq. (6) satisfies the following normalization condition:

$$\sum_x \iint dE_p d\theta_p \, \sigma_x(E_n, E_p, \theta_p) = \sum_x \int dE_p \, \sigma_x(E_n, E_p) = \sigma_{cont}(E_n). \quad (7)$$

Kerma factor (per atom) is written as

$$KF(E_n) = \sum_x (\bar{E}_p + \bar{E}_k)\, \sigma_{n,x}(E_n) \qquad (8)$$

Here, $\bar{E}_p$ and $\bar{E}_k$ are the average values of E_p and E_k over the double differential particle spectrum in the c.m system. Suffix k stands for the charged particle emission. Kerma factors due to the elastic and the discrete inelastic scattering are calculated exactly from the data in an evaluated data file. For other reactions involving multi-particle emission, the calculation of reaction-wise kerma factor is quite complicated. However, by taking the sum over reactions using the above expressions of average energies of recoil atom and particles, we obtain an approximate but a compact formula :

$$KF(En) \cong \frac{m_2}{M} E_G \sigma_R + \frac{m_1^{(n)}}{M} \bar{\varepsilon}_n \sigma_{n\text{-prod}} + \sum_x^{p,d,a} \bar{\varepsilon}_x \sigma_{x\text{-prod}}$$
$$-2(m_1^{(n)} m_2 M^{-2} \cdot E_G \bar{\varepsilon}_n^{(1)})^{1/2} \bar{\mu}_n^{(1)(1)} \sigma_{n,nx}. \qquad (9)$$

Here, superfix (1) denotes the quantities of the 1st stage reactions. In Eq. (9), σ_R is the reaction cross section, $\sigma_{x\text{-prod}}$ the particle production cross section, and $\bar{\varepsilon}_x$ the average energy of emitted particle in c.m system. In deriving Eq.(9) it was assumed that the mass of the compound nucleus is much greater than that of the emitted particle, and that the second (and more) particles are emitted isotropically.

DPA cross section is expressed in standard NRT[3] model. For the elastic and the discrete inelastic scattering DPA cross sections are calculated exactly from PKA spectra. For other reactions involving multi-particle emissions the calculation of PKA spectra is very complicated as stated earlier. However, again summing over all the reactions and making use that the Lindhard correction factor is a slowly varying function of PKA energy, DPA cross section is expressed approximately in terms of the average PKA energy as

$$\sigma_{DPA}(E_n) = \frac{0.8}{2E_d} \frac{1}{1+kg(\bar{E}_p)} \sum_x \bar{E}_p \, \sigma_{n,x}(E_n) \ , \tag{10}$$

$$\bar{E}_p = \frac{m_2}{M} E_G + \sum_x^{n,p,d,a} \frac{m_1}{M} \bar{\varepsilon}_x^{(x)} \, \sigma_{x\text{-prod}} / \sigma_R \ . \tag{11}$$

Here, $kg(E_p)$ is the correction factor for electronic energy loss by Lindhard and Robinson[4]; E_d is the threshold energy of displacement from a lattice.

3. Model Effect

(1) Effect of improvement of secondary particle spectrum

In an available evaluated nuclear data file such as JENDL-3 and ENDF/B-VI, there are little data of charged particle spectrum. Moreover, neutron spectrum is sometimes evaluated without considering the preequilibrium process which enhances the high energy neutron emission. This high energy neutron also shows anisotropy in angular distributions. The effect of approximated spectrum is discussed in the following.

First, the neutron cross sections are calculated with the multistep evaporation model code, PEGASUS[5]. Three case calculations were made as follows:

(a) equilibrium and pre-equilibrium process calculation, considering anisotropy of secondary neutrons,

(b) the same as (a), except for isotropic distributions,

(c) calculation with only equilibrium process (isotropic distributions).

In all cases, the reaction cross sections take the same value.

Figure 2 shows the double differential cross sections of the neutron and the proton emission calculated with the most exact model (Case (a)) of the PEGASUS code. The calculated results agree with the experimental data. A similar agreement between the calculations and the measurements was obtained for alpha particle.

Figure 3 compares the PKA spectra calculated at 15 MeV incidence on Ni-58 with different models. For (n,nx) reaction, the contribution of the preequilibrium process was 56%. It is seen by comparing the results in Cases (b) and (c) that high energy neutrons due to the pre-equilibrium make a PKA spectrum harder. On the other hand, Case (a) gives the softest spectrum, in despite of model including the preequilibrium process. This result means that anisotropy of the inelastically scattered neutron plays an important role in the PKA spectrum of high energy incidence of neutron. If we treat correctly only the energy distribution of secondary neutron and neglect its anisotropy, the results will be misleading as described above.

For (n, xp) reaction, the pre-equilibrium process contributes by 20% to the proton emission cross section. The effect of the preequilibrium process on the PKA spectrum for proton emission reactions are not so large as shown in Fig. 3. Table 1 compares the damage cross sections of the three cases. The value in parenthesis is a ratio to Case (a) and its discrepancy from unity is small, 29% at largest.

(2) Effect of second stage neutrons on PKA spectrum of (n,2n)

PKA spectrum of the (n, 2n) reaction is usually calculated with an approximated model of equivalent single particle emission. However, the neutron spectrum of the second stage is quite different from that of the first stage attributed to (n, 2n) reaction, as shown in Fig. 4 where the secondary neutron spectrum for iron is given. In general, the spectrum of the second stage is remarkably softer than that of the first stage. We studied the effect of this on the PKA spectrum.

Figure 5 shows the PKA spectrum formed in each stage of (n, 2n) reaction as well as that of the inelastic scattering. The spectrum broadening by the second stage neutrons is not so large. This is because the low energy second neutrons cannot recoil the atom so strongly. Accordingly, we may apply the single particle emission model, whenever we will not need a rigorous treatment of the upper energy bound of the PKA spectrum.

4. Scope of PKA/DPA Related Data File

Data file of PKA, KERMA and DPA cross sections is required from

various fields as described in Chapter 1. Accordingly, the nuclides/elements to be contained in the file are numerous as follows:

H-1, D-2, Li-6*, Li-7*, Be-9, B-10, B-11, C-12**, N-14*, O-16*, F-19, Na-23**, Mg***, Al-27*, Si*, P, S, Cl, K***, Ca**, Ti***, V-49***, Cr*, Mn-55***, Fe*, Co-59, Ni*, Cu*, Ge, Ga, As-75, Y-89, Zr, Nb-93, Mo***, Ag, Cd, Sn, Sb, Ba, Eu, Gd, Hf, Ta, W, Au-197**, Pb, Bi.

Here, number of asterisk denotes to the priority of the ESNIT project[6] of JAERI for material irradiation facility by using a high energy neutron source from Li(p, n) reaction.

In the data file, the numerical data will be stored in ENDF-6 format, because this format can treat any kinds of particles; neutron, proton, deutron, triton, alpha particle, photon, and additionally recoil atom (PKA). Fig. 6 shows the ENDF/B hierarchy. The data of each material are stored in order of file(MF), section(MT), subsection, and so on. The PKA/KERMA data file structure is given in Table 2. In the table, the quantities related to the PKA/KERMA file are:

MF=1: general information,
2: resonance parameters,
3: reaction cross sections and KERMA factors (energy release parameters),
4: angular distribution of the elastic and the discrete inelastic scattering,
6: energy-angle distributions for the PKA and the charged particles
63: DPA cross sections,
66: damage energy spectra.

For convenience of compact storage of data, we will make two kinds of data files: the primary and the secondary files. The primary file contains the raw data necessary for generating the integrated/processed data such as the KERMA factors and the DPA cross sections. The integrated/processed data are stored in the secondary file. Table 3 gives the structure of the PKA/KERMA data file.

Since the amount of the cross section data is quite large, the data

storage format of the file should be designed so as to save the memory capacity. Incident neutron energy dependence of the PKA spectrum is much weaker than that of the neutron cross section. Accordingly, we may treat the normalized energy-angle distributions of PKA at some representative incident energies with the proper interpolation scheme. Thus, we adopt the ENDF-6 format, which provides an area, MF=6, to store the energy-and-angle-dependent double differential cross sections of charged particles and PKA. In the primary file, the data of PKA spectra for the elastic and the discrete inelastic scattering are given with only the data flag to calculate it according to the reaction kinematics, since energy and angle of the PKA and secondary neutron by these reactions are uniquely determined by the kinematics and their distributions can be hardly provided in the tabular form. For the other reactions, spectra of secondary particles and PKA are given in the tabular form of MF=6 (option LAW=7). The detail of the data format is described in Ref. 7. In this format, partial contributions are separately stored with the particle identifying index LIP. So, we define the number for identifying reaction channel as follows: LIP=0 for PKA, 1 for (n,n'), 2 for (n,gamma), 3 for (n, p), 11 for (n, 2n), 13 for (n, np) and so on. In the present study, MF=66 is newly defined to store the damage energy spectra. Its data format is similar to that of MF=6.

In the secondary file, KERMA factor is given in MF=3 as an energy release parameter with the section number which is sum of the general section number (MT) and 300. Its partial contributions are given in MF=6. MF=63 is also defined so as to store the DPA cross sections. Its data format is similar to the one of MF=3, except for the displacement energy, Ed, is given in MF=63. For general application, we had better give normalized data separated from neutron cross sections which shows the complicated incident neutron energy dependence.

Figure 7 shows the flow of data processing from the evaluated nuclear data file to the PKA/KERMA file. The data for the primary PKA/KERMA file are calculated by the PKAR code. The KERMA factor and DPA cross sections are calculated by Eqs. (9) through (11) using composite particle production cross section and particle mean energies.

5. Concluding Remarks

PKA/KERMA file is required from many fields of science and technology. In the present work, the methodology to calculate the PKA spectrum is studied. For inelastic scattering at high energy, the anisotropy of secondary neutron due to preequilibrium process turned out to be as important as its energy distribution. On the other hand, the spectrum broadening by the second stage neutrons of (n, 2n) reaction is not so large, and the single particle emission model may be applicable. For the data format of the file, ENDF-6 is considered to be convenient for the present work, with adding new data files (MF=63, 66) for DPA cross sections and damage energy spectra. Future scope of the data file is to contain the data for about 50 materials in the energy range up to 50 MeV.

The development of PKA processing code is the most important task and is now in progress. Authors are thankful to the members of PKA/Kerma Data working group of Japanese Nuclear Data Committee for discussions.

References

(1) Iijima, S., Kawai, M.: J. Nucl. Sci. Tech., 27, 375, (1990).
Iijima, S., Kawai, M.: Development of the JENDL Special Purpose Data File for PKA Spectra, DPA Cross Sections and Kerma Factors, JAERI-M 90-025, p. 329 (1990).

(2) Yamano, N.,Koyama, K.,Minami, K.: A Code System to Generate Multi-group Constants and Analyze Radiation Transport for Shielding Safety, JAERI-1316 (1989).

(3) Robinson, M.T., Torrens, I.M.: Recommendation for Displacement Calculation for Reactor/Accelerator Studies in Austenitic Steels, Nucl. Eng. & Design, 33, 91 (1975)

(4) Lindhard, J. et al. : Kgl. Danske Vidensk Selsk. mat-fys. Medd., 33 (1963) Np.10
Robinson, M.T. : Proc. B.N.E.S. Conf. on Nuclear Fission Reactors, Culham 1969 (BNES, London), p.364

(5) Iijima, S., Sugi, T., Nakagawa, T., Nishigori, T.: Program PEGASUS, A Precompound and Multistep Evaporation Theory Code for Neutron Threshold Cross Section Calculation, JAERI-M 87-025, p. 337 (1987).

(6) Kondo, T., Ohno, H., Mizumoto, M., Odera, M.: J. Fusion Energy, 8, 229 (1989).

(7) Rose, P.F. et al. (ed.): Data Formats and Procedures for the Evaluated Nuclear Data File ENDF-6, BNL-NCS-44945 (ENDF-102) (1990).

Table 1 Comparison of damage cross sections calculated with different models.

Reaction	Case (a) Preeq.+Eq. Anisotropic	Case (b) Preeq.+Eq. Isotropic	Case (c) Eq. Isotropic
(n, nx)	108 (1.00)	139 (1.29)	129 (1.19)
(n, px)	197 (1.00)	217 (1.10)	212 (1.08)
(n, ax)	59.6 (1.00)	62.8 (1.05)	61.8 (1.04)

Table 2 File (MF) Structure of ENDF/B

MF	Description
1	General Information
2*	Resonance parameter data
3*	Reaction cross sections
4*	Angular distributions for emitted particles
5	Energy distributions for emitted particles
6*	Energy-angle distributions for emitted particles
7	Thermal neutron scattering law data
8	Radioactivity and fission product data
9	Multilicities for radioactivive nuclide production
10	Cross sections for radioactivive nuclide production
12	Multiplicities for photon production
13	Cross sections for photon production
14	Angular distributions for photon production
15	Energy distributions for photon production
17	Discrete delayed gamma rays
18	Continuous spectra of delayed-photon emission
23	Photo-atomic interaction cross sections
27	Atomic form factors for photo-atomic interactions
31	Data covariances for nubar
32	Data covarinces for resonance parameters
33	Data covariances for reaction cross sections
34	Data covariances for angular distributiuons
35	Data covariances for energy distributions
39	Data covariances for radionuclide production yields
40	Data covariances for radionuclide production cross sections
63*	DPA cross sections (secondary file of PKA/KERMA file)
66*	Damage energy spectra (primary file of PKA/KERMA file)

N.B. *) Contained in PKA/KERMA file that was defined in the present work.

Table 3 PKA/KERMA File Structure

File	Quantities	MF	MT
Primary File	Resonance parameters	2	151
	Reaction Cross Sections	3	1～116
	PKA & Charged Particle Spectra	6 (LAW=7)	1～116
	Damage energy spectra	66 (LAW=7)	1～116
Secondary file	Kerma Factors (KF) (Energy Release Parameter)	3	321～416
	Partial Contributions of KF	6 (LAW=0)	301～416
	DPA Cross Sections	63 (LAW=0)	101～116

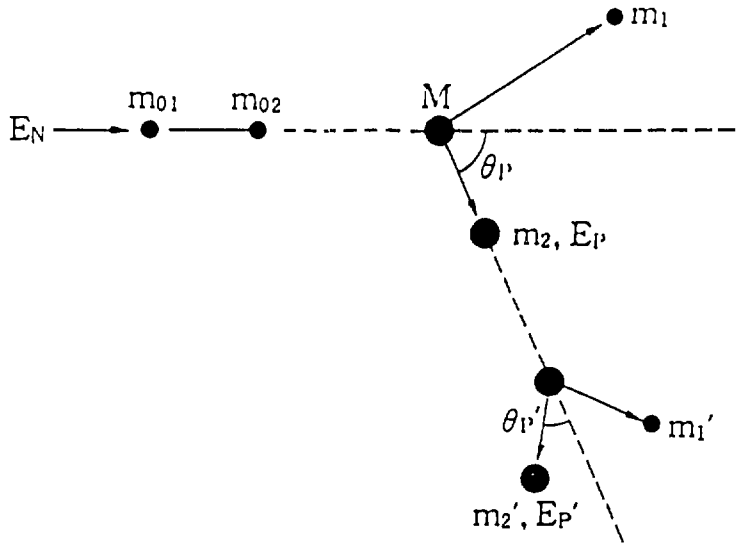

Fig. 1 Kinematics of nuclear reaction

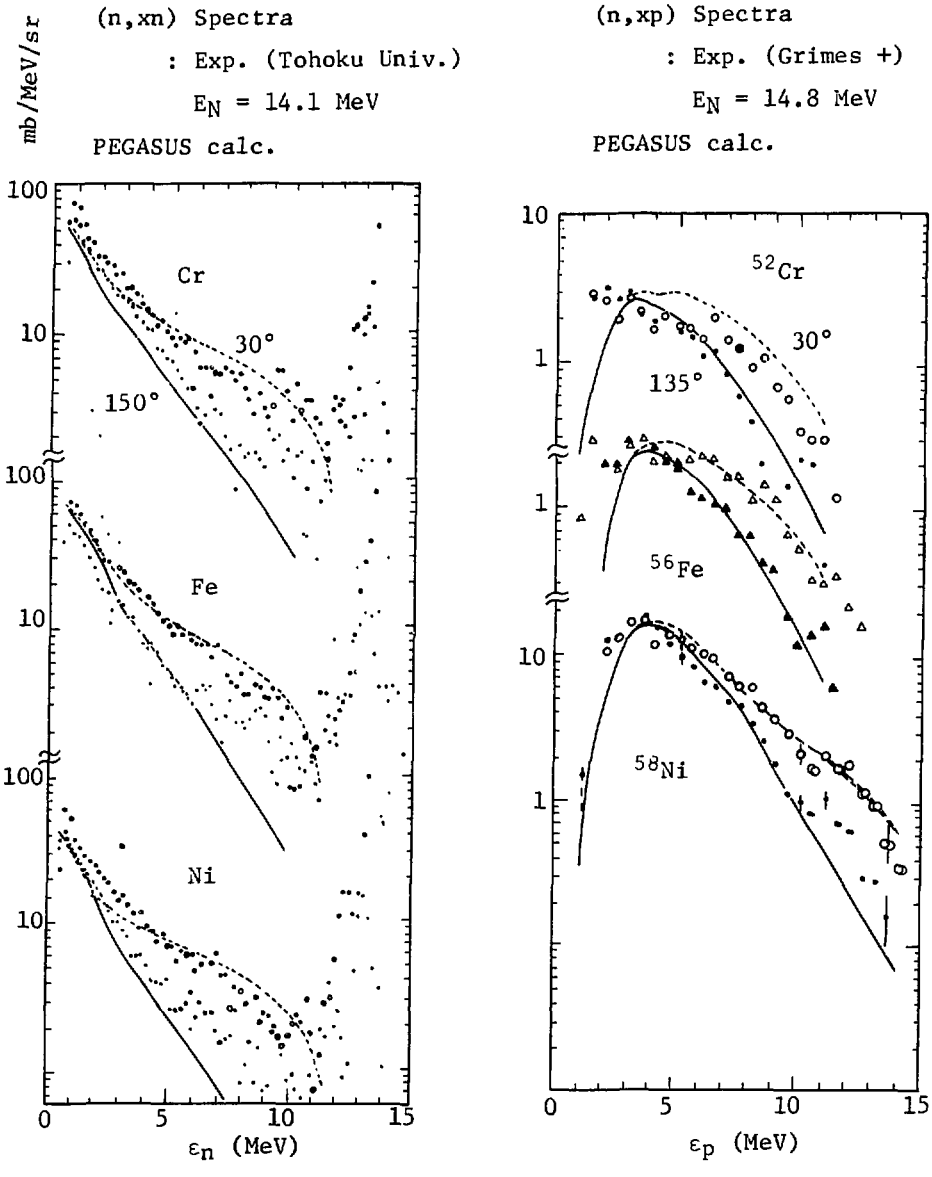

Fig. 2 Double differential cross sections of neutron and proton emission for Cr, Fe and Ni.

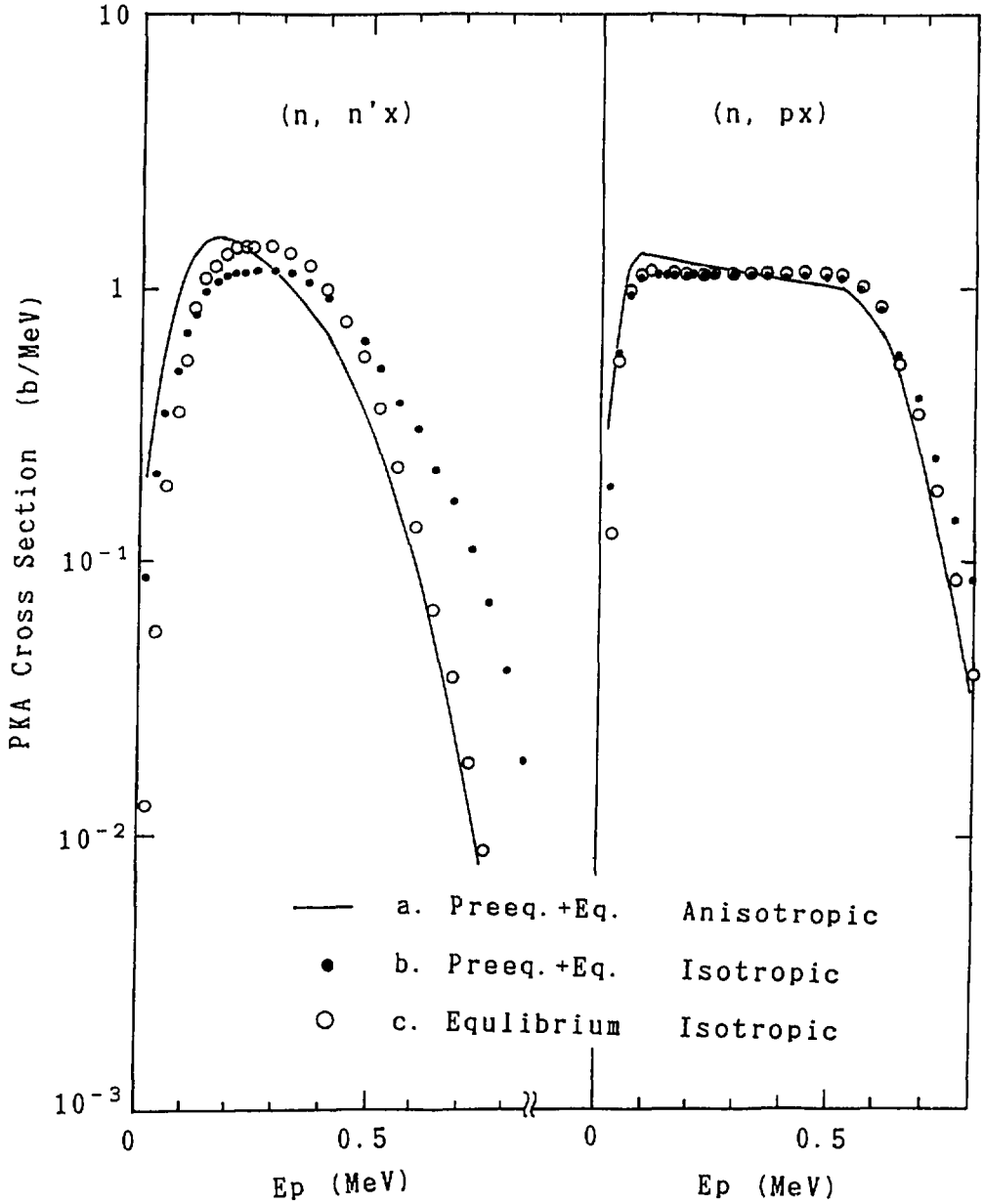

Fig. 3 PKA spectra for neutron and proton emission of 15.8 MeV neutron incidence on Ni-58.

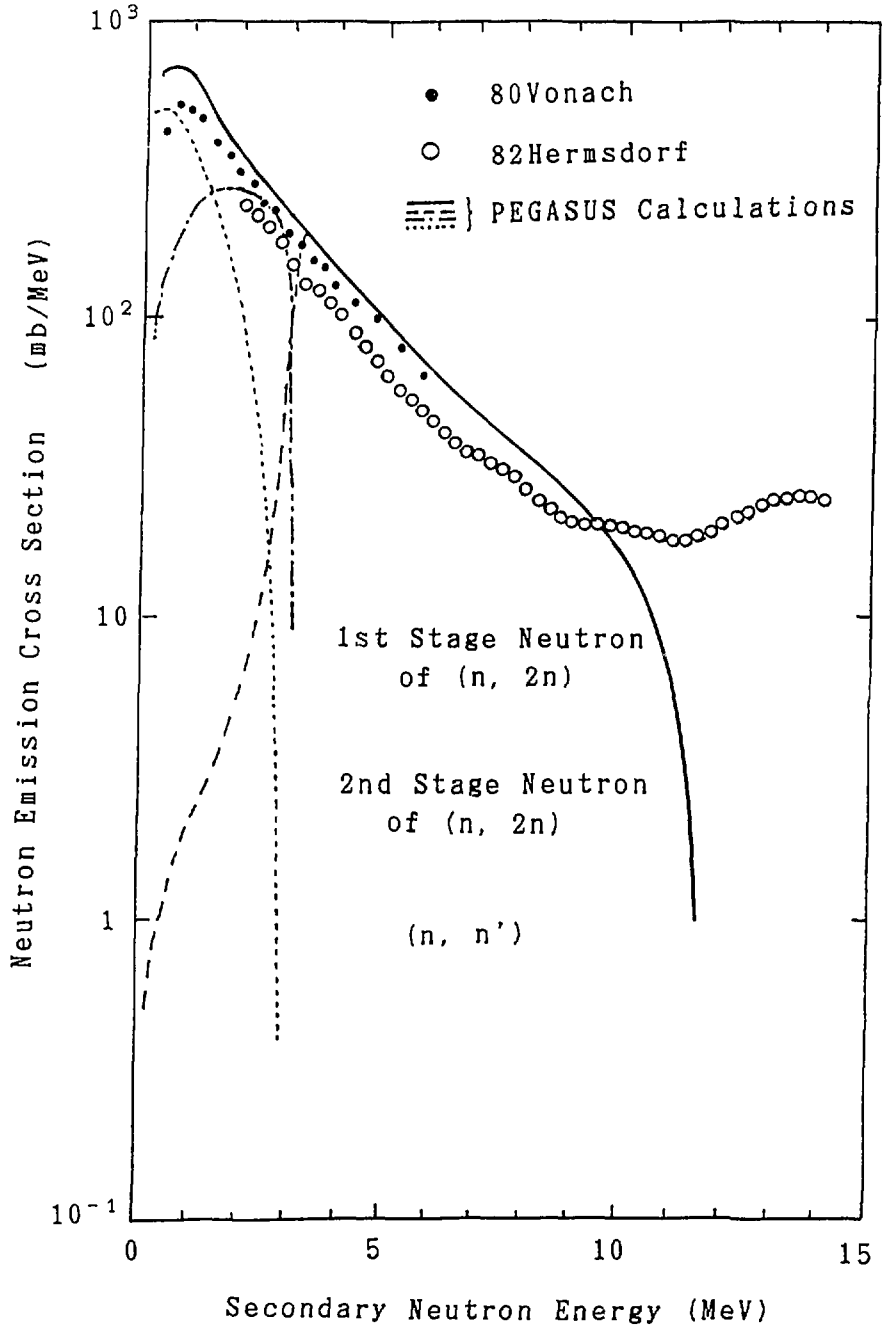

Fig. 4 Neutron Spectra from inelastic scattering and (n, 2n) reaction of iron with 14 MeV neutron.

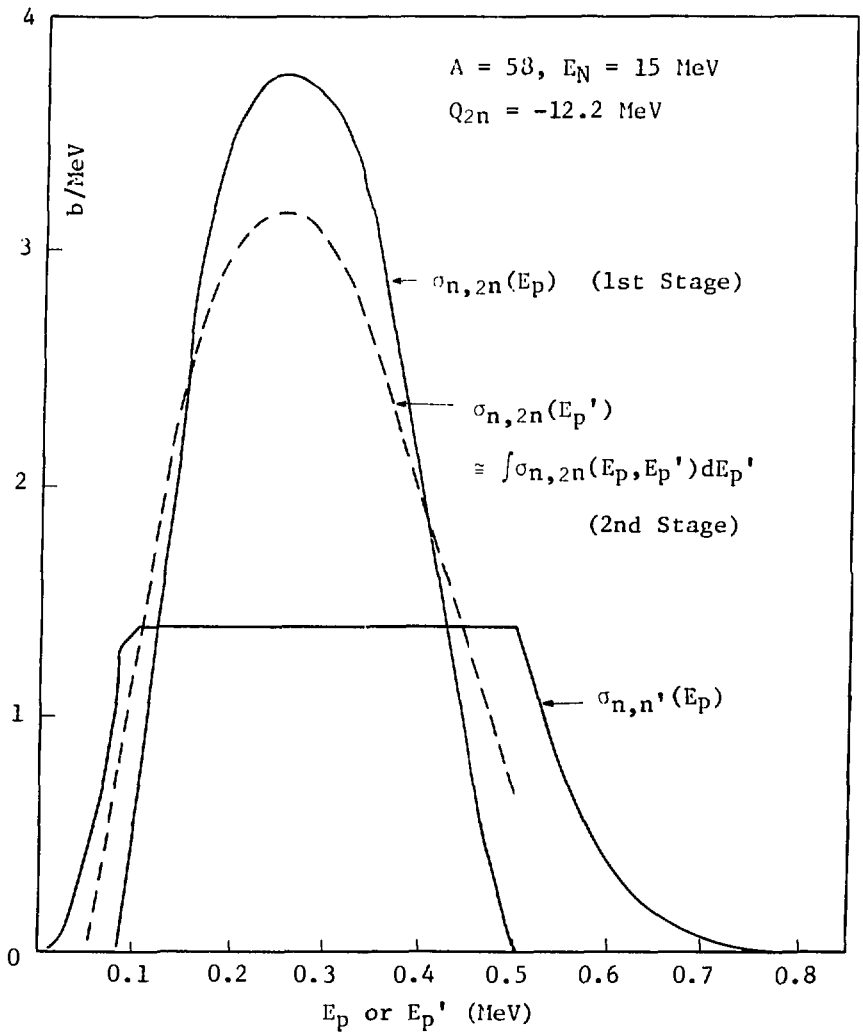

Fig. 5 PKA spectra due to inelastic scattering and (n, 2n) reaction of Ni-58 with 15 MeV neutron.

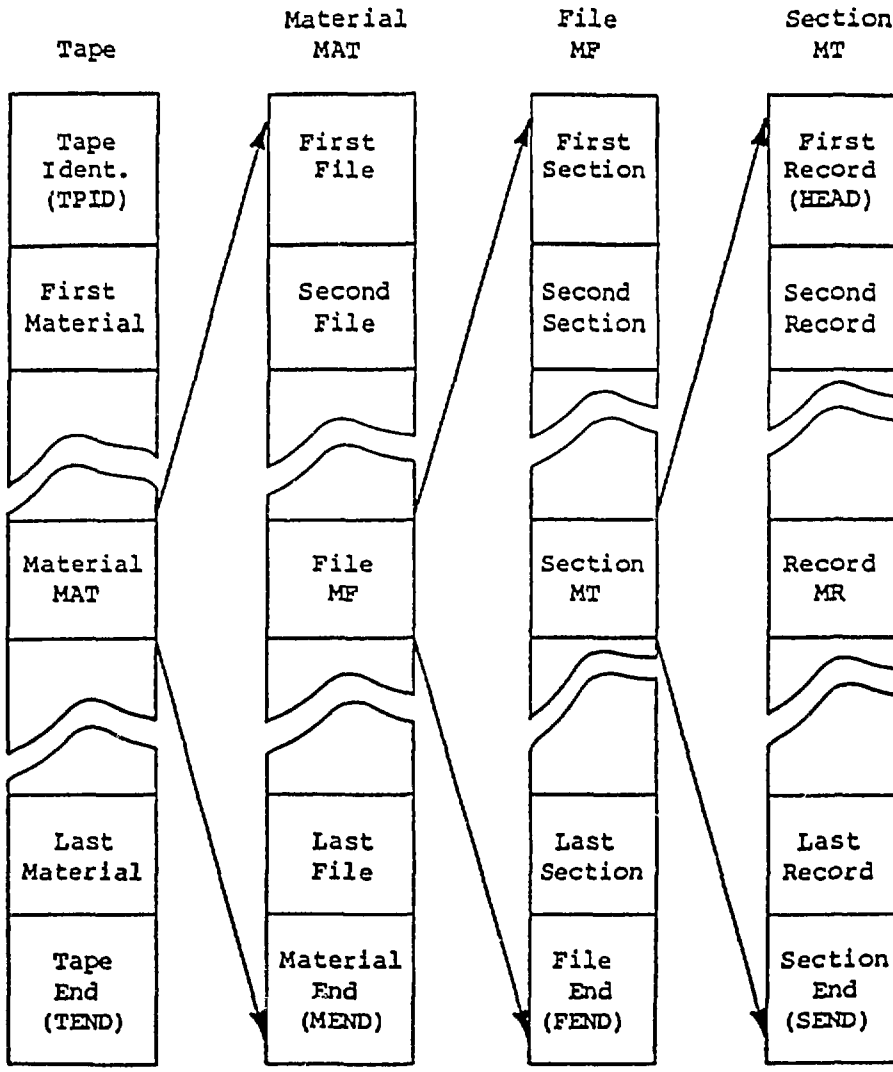

Fig. 6 ENDF/B Hierarchy.

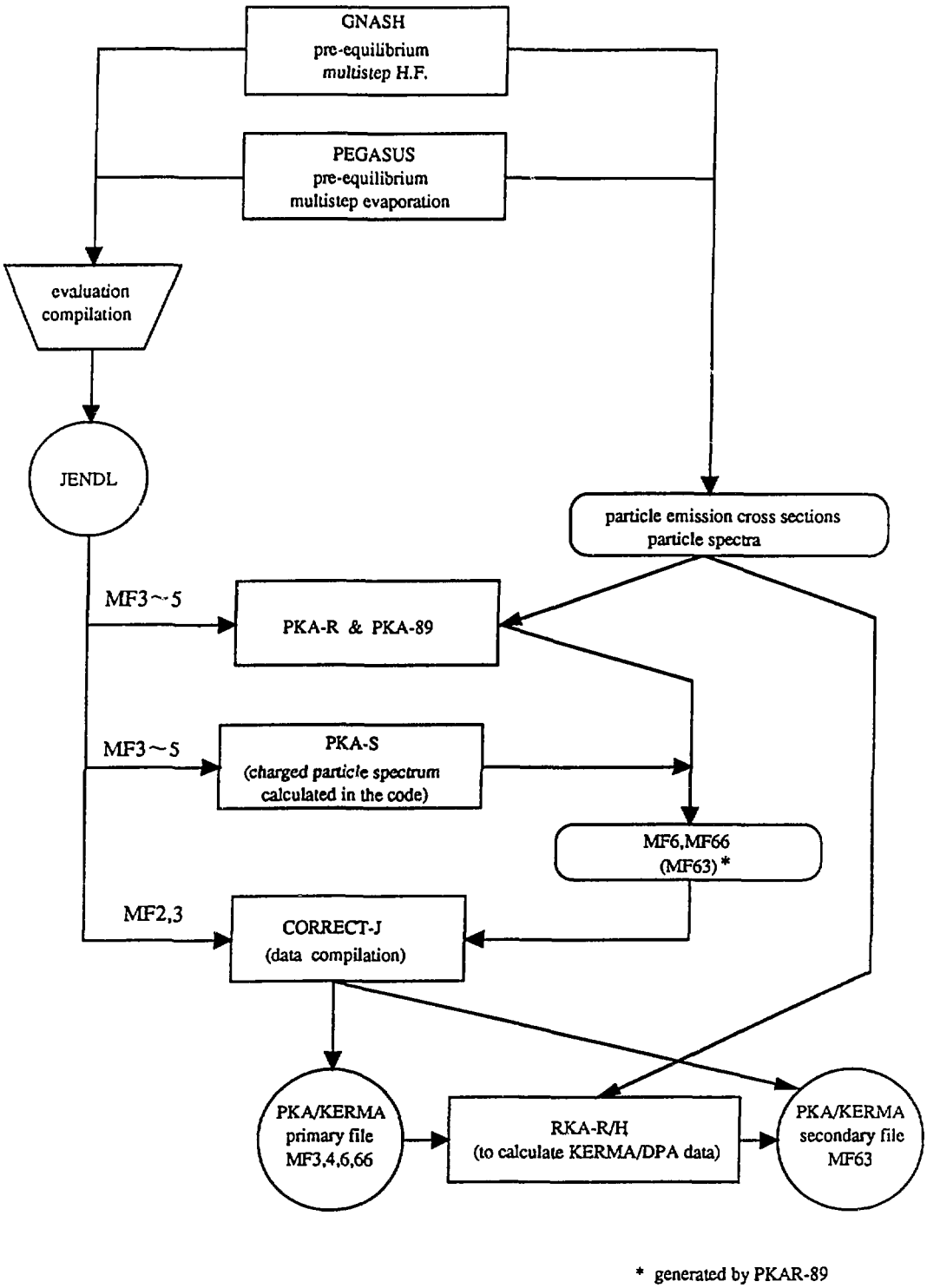

Fig. 7 Flow chart of PKA/KERMA data file generation.

9. Requirements and Comments from Fusion Reactor Design

9.1 Nuclear Data Needs from Fusion Reactor Safety Analysis

Yasushi Seki

Naka Fusion Research Establishment
Japan Atomic Energy Research Institute
Naka-machi, Naka-gun, Ibaraki-ken, JAPAN

In this review, at first a basic consideration of fusion reactor safety approach is described. The problems caused by activation of materials are described and the low activation considerations for FER and the fusion power reactors are given. The result of a comparison of the activation of 6 candidate structural materials for a fusion reactor is introduced. Finally the nuclear data needs for fusion reactor safety analysis are briefly shown.

1. Introduction

There are many reviews on the nuclear data needs for a fusion reactor[1]-[4]. This review describes about the nuclear data needs for fusion reactor safety analysis, especially on activation problems

2. Safety approach in a fusion reactor

A fusion reactor is much safer than a fission reactor because of the following inherent features:

1) It does not have a criticality accident.
2) Reaction products from the D-T fusion reaction are neutron and helium so that fission products or actinides are not present in a fusion reactor.
3) Decay heat density is lower than in case of fission core so that its removal is relatively easy.

A safety approach in a fusion reactor is proposed considering the above inherent features.

As shown in Fig.1, the major concern in fusion reactor safety comes from the 14 MeV neutrons generated as a result of the D-T fusion reaction, the tritium used as the fuel, and the activation products from the neutron interaction with materials constituting the reactor components.

Radiation doses to the general public outside the reactor site boundary and personnel of the reactor plant should be minimized based on the ALARA principle. The doses by the 14 MeV neutrons and gamma rays during operation and abnormal states will be minimized by the proper radiation shielding technique. Special attention should be paid to take account of the numerous penetrations and ducts existing in the shielding structures of a fusion reactor.

Tritium inventory should be reduced as much as possible and the components with large amount of tritium are made to possess multiple barriers for tritium containment. Usually this is accomplished by the device boundary, glove box or some similar secondary containment and the room or building installing the component. For the secondary containment and the room or building with components with large tritium inventory, inert gas/atmospheric detritiation systems are provided to deal with tritium leakage. Leak tight joints and valves are employed for the tritium loops with special permeation reducing measures, as required, as in the case of high temperature components. In view of the fact that tritium is flamable, proper measures are taken to avoid the tritium combustion condition and explosion protection is provided. In case of off-normal events such as earthquakes or power loss, the components are made to achieve tritium containment mostly by isolation, passively as much as possible.

As for the activation products produced by the neutrons, the quantity is large but the most will be contained forever within the metals and a process for their full mobilization is inconceivable. However, a partial mobilization could occur by the following processes:

1)Activated corrosion products in the coolant of the primary cooling system, which will come from cooling tube material/coolant interaction in the first wall and blanket and divertor.

2)Activated dust in the plasma chamber produced by the erosion and sputtering of the plasma facing components.

3)In case of highly unlikely, extreme condition of air ingress into the vacuum vessel and contacting with very high temperature plasma facing material, the volatilization of the metals could be considered.

It has been found that the volatilization of tungsten divertor plate is the most serious cause of accidental dose to the public in the ITER safety analysis[5].

In addition to activated solids, there are some activation products in form of liquid and gases. They are;

1)Activation of the coolant itself.

2)Inert gas surrounding penetration ducts.

3)High voltage insulating gas for the neutral beam injector.

The normal effluent dose from these sources have been evaluated for ITER and found to be sufficiently small[5].

On the other hand, by selecting the low activation materials these activation products could be reduced. The problems and countermeasures related to activation products are described in the next two section.

3. Activation products

The major design problems caused by the activation products are described:

The gamma-ray dose after shutdown of a fusion reactor restricts accessibility of workers and limits the lifetime of sensors or TV camera to be used in the remote operations for repair and maintenance to be conducted after shutdown.

The decay heat becomes the main heat source in the event of LOCA and LOFA after plasma shutdown. Removal of decay heat during the replacement of components accompanying the detachment of cooling system is necessary. Decay heat removal for radwaste is also required.

Risk of activation products release during normal operation, during maintenance operations, and at accidents must be minimized.

Finally the activation produces long term radwaste, the quantities and the level of which differs significantly with the material choice.

4. Low activation materials

For FER[6], the use low activation materials are recommended as much as practicable, for example the use of nitrogen gas instead of SF_6 for cover gas to enhance electrical resistivity, and the use of water in place of metal shielding material are recommended. It is also recommended to fabricate components in a manner to allow easy separation of radwaste according to classifications. The use of low activation structural materials are proposed for components where selection is practical, for example, the shielding materials and support structures where the stress conditions are not so restricted.

For a fusion power reactor[7], the use of low activation ferritic steel has been selected as the main structural material to reduce long lifetime radwaste. The possibility of using very low activation materials such as ceramics and composites for the main structural material will be investigated. In view of the large quantities of radwaste expected, the recycling of the materials will be seriously considered.

The effect of impurities on the activation characteristics of six candidate materials in Table 1 has been investigated[8]. In case of the Type 316 stainless steel (316 SS), the nickel and molybdenum contents are 16% and 2.4%, respectively. Table 2 shows that in the case of 316 SS

the long term activation problem will be dominated by ^{63}Ni at 100 years after irradiation and by ^{59}Ni and ^{94}Nb at 1000 years after irradiation. ^{63}Ni and ^{59}Ni are mostly produced from Ni and ^{94}Nb from Mo. The effect of the activation of Ni and Mo is relatively large for the steel with large content of these elements compared with that of impurities such as Co, Nb and Ag.

In case of Low activation materials with controlled amount of Ni and Mo, as in the F82H steel or the high manganese steel proposed by JAERI, a significant difference in the long term activation has been observed between the case with Co and Nb impurities and the case without those impurities. As shown in Fig. 2, the introduction of the Co and Nb impurities resulted in the increase of the gamma ray dose from the reduced activation steels by about an order of magnitude at 100 years after shutdown. As a result, the contact dose at the first wall became greater than the .025 mSv/h limit by an order of magnitude.

5. Nuclear data needs

For the evaluation of long term radwaste, the major activation reactions to produce long half-life nuclides which are shown in Table 2 are important.

A sensitivity analysis of elements has been conducted[9] for the gamma-ray dose rate at one day after shutdown after a one year continuous operation of a fusion reactor with the neutron wall load of 1 MW/m^2. The dose rate sensitivity of an element is defined as the increment in shutdown dose rate caused by a small amount of increase in the element nuclide density. The dose rate sensitivity is dependent on the neutron energy spectrum at the location and on the time after irradiation time. It is therefore dependent on the location and the compositions of the materials of the reactor model. The dose rate sensitivities for 1 day after shutdown following 2 years irradiation time for a fusion reactor with 316 SS structural material have been calculated.

The composition of all the 316 SS in the reference model is changed by increasing the nuclear density of Cr, Mn, Fe, Co, Ni, Cu, Mo and Nb in the stainless steel by 0.08 g/cm^3. The increase in the dose rate brought on by the element density increase is calculated at five locations of the reactor model. The dose rate sensitivities of the eight elements at the five locations are plotted in in Fig. 3. The figure shows that the dose rate sensitivity of the Co is exceptionally large compared to those of other elements. The dose rate sensitivity of Co is more than one order of magnitude larger than any other elements. This large value is mainly due to the exceedingly large cross section of the $^{59}Co(n,\gamma)^{60}Co$ reaction and the two high energy gamma rays emitted by the decay of of ^{60}Co.

The sensitivity of Co, Cu and Mo shown with dashed lines generally increase with the distance from the plasma axis. This trend is caused by the softening of the neutron energy spectrum with the distance, which results in the increased (n,γ) reactions, i.e., $^{59}Co(n,\gamma)^{60}Co$, $^{63}Cu(n,\gamma)^{64}Cu$ and $^{92}Mo(n,\gamma)^{93}Mo$. The product nuclides ^{60}Co, ^{64}Cu and ^{93}Mo of the (n,γ)

reactions emit gamma rays to increase the dose rate. The sensitivities of other five elements show an overall decrease with the distance in Fig. 3. This is because threshold reactions are the main source of gamma ray emitting nuclides for these elements. Threshold reactions decrease with the reduction of high energy neutrons with the distance.

Similar sensitivity analyses should be conducted to precisely evaluate the requirements of nuclear data for the safety analysis of a fusion reactor.

References

(1) Nuclear data for Fusion Reactor Technology, IAEA-TECDOC-223, IAEA (1979)
(2) E. T. Cheng et al., Magnetic Fusion Energy Program Nuclear Data Needs, GA-A18152, UC-20 (1985)
(3) V. Goulo, edited., Fusion Evaluated Nuclear Data Library (FENDL), INDC(NDS)-223/GF (1989)
(4) K. Maki, this conference
(5) J. Raeder et al., ITER Safety, ITER Documentation Series, No.36, IAEA (1991)
(6) S. Matsuda et al., Conceptual Design of the Fusion Experimental Reactor (FER), Proc. 13-th International Conference on Plasma Physics and Controlled Nuclear Fusion Research, Washington, DC (1990) IAEA-CN/G-2-2
(7) Y. Seki et al., The Steady State Tokamak Reactor (SSTR), ibid. IAEA-CN/G-1-2
(8) Y. Seki and Y. Takeyasu, Long-Term Radioactive Waste for the Fusion Experimental Reactor (FER), Proc. IAEA TCM on Fusion Reactor Safety, Jackson Hole (1989)
(9) Y. Seki et al., Radioactivation of Structural Material of the Superconducting Magnet for a Fusion Reactor, J. Fusion Energy Vol. 3, No. 4 (1983) 241

Table 1 Detailed Composition of the Candidate Steels (Wt.%)

Composition elements	Steel Type(Acronym) A(F82)	B(F82H)	C(HT-9)	D(High Mn)	E(304)	F(316)
B	0.0035	0.0034	-	-	0.0008	0.0038
C	0.100	0.093	0.188	0.249	0.021	0.060
N	0.0018	0.0019	0.0022	0.0234	0.0013	0.0019
Al	0.01	0.01	0.02	0.01	0.01	0.01
Si	0.17	0.09	0.22	0.20	0.51	0.53
P	0.003	0.005	0.018	tr.	0.016	0.028
S	0.002	0.001	0.001	0.004	0.001	0.001
Ti	0.005	0.005	0.005	0.15	0.27	0.23
V	0.19	0.18	0.29	-	-	-
Cr	7.52	7.65	12.01	13.57	18.08	14.93
Mn	0.49	0.49	0.48	25.71	1.48	1.78
Fe	89.25	89.43	84.66	60.06	61.97	63.91
Ni	0.05	0.01	0.59	tr.	17.63	16.14
Co	0.005	0.005	0.005	0.003	0.010	0.010
Nb	0.00007	0.00007	0.00007	0.00005	0.00005	0.00005
Mo	tr.	tr.	1.01	-	tr.	2.38
Ta	-	0.038	-	-	-	-
W	2.19	1.98	0.51	-	-	-

In the table, tr. represents trace amount for which 0.01Wt.% is assigned.

The values have been supplied by Dr. A. Hishinuma of JAERI. The Co and Nb content values for steels other than F82H steel are estimated values based on the measured values for F82H steel.

Table 2 Nuclides Contributing to Long-Term Activation of Candidate Steels

Nuclide	Half-life in years	Major radiation generated with the decay	Induced activity per unit fusion power(Ci/MWt) at 100 years(and 1000 years) after operation				Major activation reaction to produce the nuclide
			Reduced activity Steel:B	HT-9 C	High Mn D	SS 316 steel F	
^{14}C	5740	β^-	0.037 (0.033)	0.043 (0.038)	0.459 (0.411)	0.038 (0.034)	$^{14}N(n,p)^{14}C$ $^{13}C(n,\gamma)^{14}C$
^{53}Mn	3.7×10^6	X	0.006 (0.006)	0.005 (0.005)	0.004 (0.004)	0.004 (0.004)	$^{54}Fe(n,np)$
^{59}Ni	7.5×10^4	X		0.335 (0.328)		9.45 (9.25)	$^{60}Ni(n,2n)$
^{60}Co	5.27	β^-,γ				0.007	$^{60}Ni(n,p)$
			0.030	**0.030**	**0.018**	0.068	$^{59}Co(n,\gamma)$
^{63}Ni	100	β^-	0.124	7.15 (0.014)	0.128	202 (0.396)	$^{62}Ni(n,\gamma)$
^{93m}Nb	13.6	γ	0.005 (0.004)	0.463 (0.390)		1.14 (0.962)	β^-decay of ^{93}Mo
^{93}Mo	3500	X	0.005 (0.004)	0.515 (0.431)		1.27 (1.06)	$^{92}Mo(n,\gamma)$
^{94}Nb	20300	β^-,γ		0.005 (0.005)		0.012 (0.012)	$^{94}Mo(n,p)$
			0.060 (0.059)	**0.065 (0.064)**	**0.043 (0.043)**	**0.055 (0.054)**	$^{93}Nb(n,\gamma)$
^{99}Tc	2.1×10^6	β^-,γ	0.002 (0.002)	0.206 (0.205)		0.508 (0.506)	$^{100}Mo(n,2n)$ ^{99}Mo:β^-decay
TOTAL without Co & Nb			0.178 (0.049)	8.72 (1.42)	0.591 (0.416)	214 (12.2)	
TOTAL with Co & Nb impurities			**0.268 (0.108)**	**8.82 (1.48)**	**0.616 (0.458)**	**214 (12.3)**	

Values lower than 0.001 Ci/MWt is omitted from the table. Values in parenthesis are the induced activity 1000 years after the operation. Values shown with bold letters are the ones affected by the consideration of Co and Nb impurities.

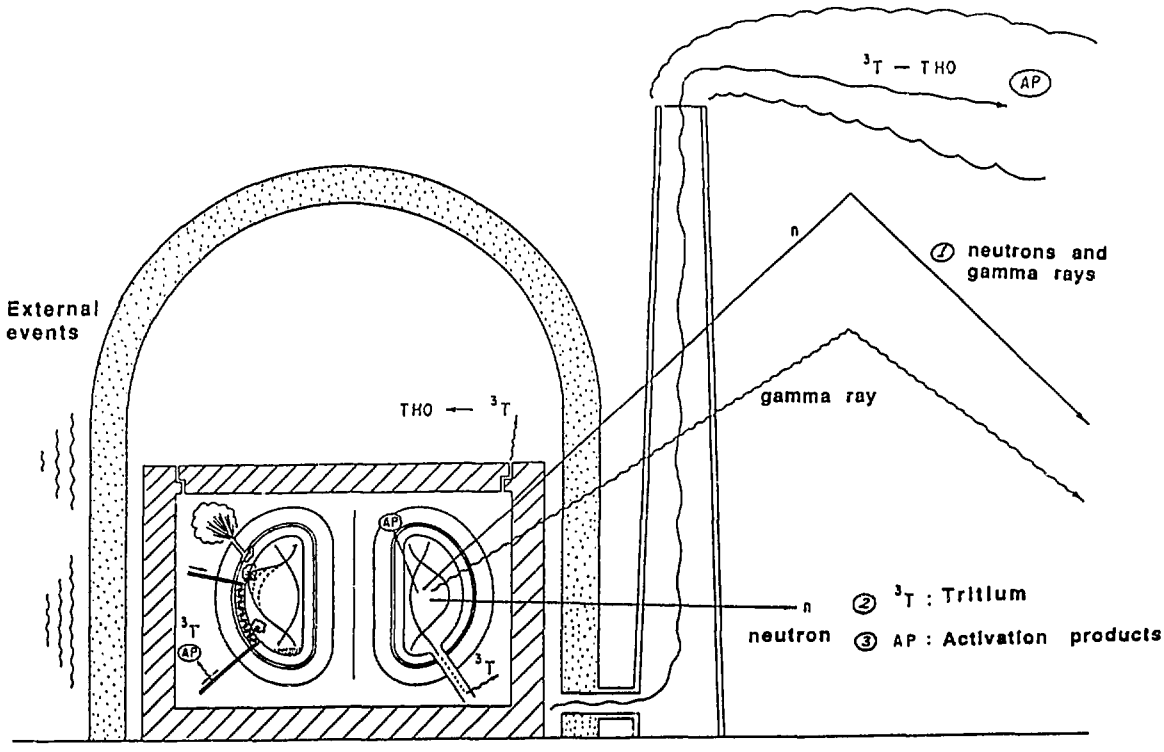

Fig. 1 Safety concerns for a fusion reactor

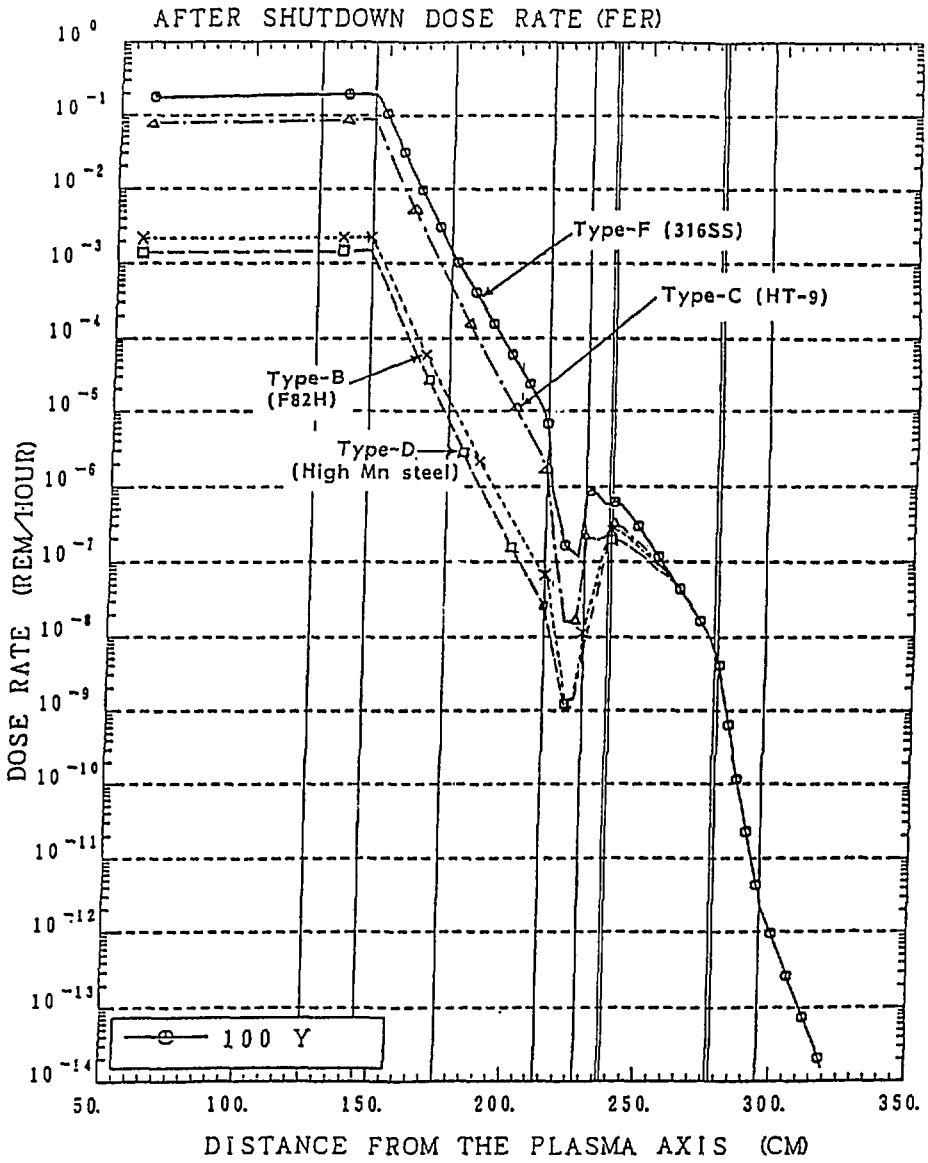

Fig. 2 Radial distribution of dose rate for the four steels without Co and Nb impurities in the FER inboard shield and superconducting magnets at 100 years after shutdown following 1-year operation at 1 MW/m^2

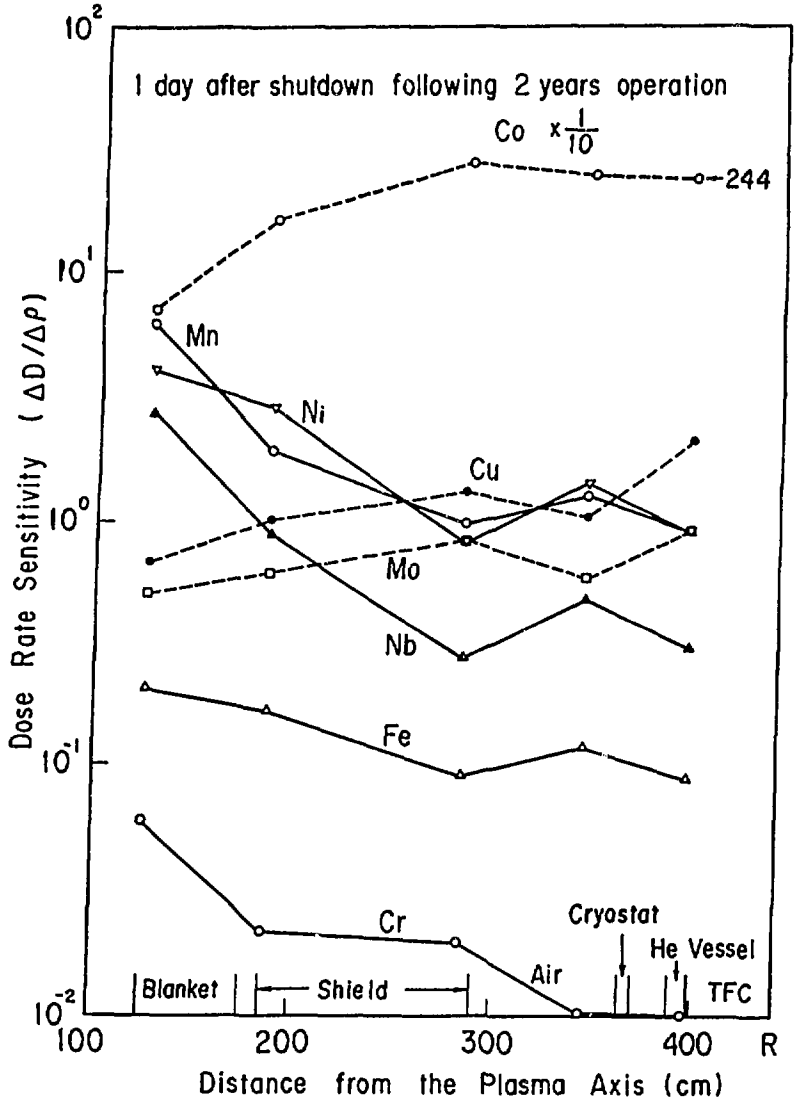

Fig. 3 Dose rate sensitivities of nine elements in the reference model at 1 day after shutdown following 2 years of operation at 1 MW/m^2

9.2 Requirements for Nuclear Data from ITER/FER Nuclear Design

Koichi MAKI*

Fusion Experimental Reactor Team
Naka Fusion Research Establishment
Japan Atomic Energy Research Institute

801-1 Mukohyama Naka-machi Naka-gun Ibaraki-ken, Japan

ABSTRACT

Considering ITER and FER activities and future programme of fusion reactor developments, the present situations in fusion neutronics were explained up to now from the previous fusion nuclear data specialist meeting. Vicissitude of development of FUSION-J3 was also explained. From these discussions we clarifyed the required accuracies in nuclear data, their time limits and their priorities of nuclides to be improved for fusion reactor developments.

1. INTRODUCTION

The previous specialist meeting was held on July 23 to 25 in 1985. In that period, conceptual design of INTOR (International Tokamak Reactor)[1] had been being performed until 1987. At an interval of one year from closing INTOR, CDA (Conceptual Design Activity) of ITER (International Thermonuclear Experimental Reactor)[2] had been progressed since 1988. It was closed at the end of December 1990. In the country, various design of FER (Fusion Experimental Reactor)[3] were being performed every a few years in the INTOR period. Following that period, new FER[4] design has been investigated since 1988 in parallel with ITER.

On the other hand, we had only nuclear group constant set GICX40[5] for fusion neutronic calculation in the INTOR period. We had only JENDL-2[6] as the evaluated nuclear data file in the country. Following that period, preliminary evaluated nuclear data file JENDL-

---

* On leave from Hitachi Ltd.

3PR1 and -PR2 were compiled in order to analyze experimental data, both differential and integral data. Since JENDL-3[7] became tentatively available in April 1989, the nuclear group constant set FUSION-J3[8] was immediately made for fusion neutronic calculation on the basis of the JENDL-3. Tentative JENDL-3 was, however, found to have a few defects in gamma-production cross sections by comparing ITER benchmark calculation results used tentative FUSION-J3 with those used ENDF/B-IV, etc. Correcting those defects, JENDL-3[7] was published at last in December 1989. Then the group constant set FUSION-J3 was revised. In spite of revision, gamma-ray spectra by the FUSION-J3 had under estimated values in comparison with those by VITAMIN-C[9] based on ENDF/BIV. From the following investigation, gamma ray transport cross section processing code used at first was found to be not appropriate to higher gamma ray energy than several MeV of fusion neutronics. Therefore, gamma ray group constants in FUSION-J3 were revised again by the other processing code. At the same time, KERMA library[10] for FUSION-J3 was estimated by direct method considering kinematics.

The present situations in fusion reactor neutronic calculation are expressed from the experiences in ITER shielding neutronic design in the present paper. Shielding properties for superconducting magnets are explained on the basis of the results of ITER shielding investigations from the view point of nuclear heating, insulator dose, copper radiation damage and fast neutron fluences in the magnets. Design safety factors discussed in ITER shielding specialist meeting are expressed and their problems are discussed. From the benchmark calculation results in ITER, differences among nuclear properties by various group constant sets based on different evaluated nuclear data files are represented and the level of FUSION-J3 is discussed. Fusion reactor construction programme are explained and structural, blanket, and thermal and electric insulator materials are listed up for fusion reactors, experimental and demonstration reactors. From the construction plans and listed up materials, required accuracies and their limits for nuclides and their quantities are discussed for fusion reactor developments.

2. SITUATIONS AND ISSUES IN NEUTRONIC CALCULATION

2.1 ITER Neutronic Design Situations

Shielding design limits for superconducting magnet and biological shield are shown as in Table 2.1. The limit of total nuclear heating depends on the capacity of refrigerator, that is, it is trade-off for total cost of the facility. The limit of nuclear heating rate is determined with dependent on the critical values against quenching coils, that is, violation of superconducting state. This limit depends on the structure of winding pack. The limit of absorbing dose is determined with dependent on the reduced strength of insulator material by radiation damage.

The value of copper dpa (displacement per atom) is dependent of enhancing resistivity of copper by radiation damage. The limit of fast neutron fluence in winding pack is determined with dependent on radiation damage in windings. On the other hand, the limit of dose rate in reactor room after reactor shutdown is determined with that in personal exposure of workers. No person can undoubtedly enter into the reactor room during operation.

Table 2.1 Radiation limits and safety factors.

Toroidal Field Coils	Limits	Safety Factors 1D Analysis*)	3D Analysis
Total nuclear heating	55 kW	2	1.4
Peak nuclear heating in winding pack	5 mW/cm^3	3	1.5
Peak dose to electrical insulator	5.10^9 rad	3	1.5
Peak fast neutron fluence (E>0.1 MeV) to Nb_3Sn superconductor	1.10^{19} n/cm^2	3	1.5
Peak displacement damage in Cu stabilizer	6.10^{-3} dpa	3	1.5
Biological dose rate	0.5 mrem/h	10	10

*) The safety factors 2 and 3 are valid for all locations except the outboard side, where they should be higher

Table 2.2 Recommended correction and safety factors for ITER shielding analysis.

Responses	1D Analysis Local	1D Analysis Integral	3D Analysis Local	3D Analysis Integral
Correction factors for:				
Assembly gaps	1.7	1.2	--*	--*
Modeling	1.3	1.3	1.1	1.1
Uncertainties in Xn data	1.4	1.3	1.4	1.3
Safety factors for inboard and divertor regions	3	2	1.5	1.4
Safety factors for outboard regions	>3#	>2#		
Safety factors for Biological shield	10	10		

* Gaps included in 3-D models
# Outboard blanket/shield design dependent

Uncertainties of design or calculated values are caused by uncertainties included in calculational methods, modeling and nuclear data. Considering these uncertainties, design safety factors should be estimated with including design margin. However, design safety factors were remarked in ITER shielding specialist meeting without discussion on these uncertainties in detail except as shown in Table 2.2. Design safety factors for 1-dimensional and 3-dimensional analyses, given in the ITER specialist meeting, are also shown in Table 2.1. Further more experimental analyses and sensitivity analyses are indispensable to obtain these uncertainties. Nevertheless, we have scarcely error files of group constant sets and sensitivity coefficients for sensitivity analysis.

Poloidal cross section of ITER is represented as shown in Fig.2.1. The major radius is 6 m, minor radius 2.15 m and the elongation 2.0. There are two areas having large effects on the superconducting magnet

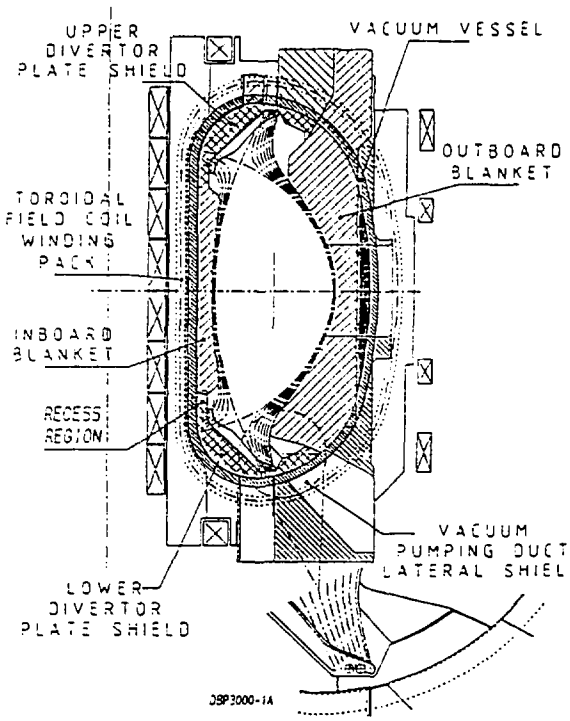

Fig.2.1 Poloidal cross section of ITER.

shielding properties. The one is inboard mid-plane area, whose thickness is 84 cm including 5 cm thick extra shield, 10.5 cm thick blanket, and 2 cm wide gaps and slits. And the other is divertor area, whose thickness of thinnest area in divertor region is approximately 60 cm. The average first wall loading in physics phase is different from that in technology phase, as 1.01 and 0.74 MW/m^2, respectively. And the average first wall fluences in physics and technology phases are 0.02 and 3 MWa $/m^2$, respectively. In physics phase, shielding properties dependent on operation time need not, therefore, to be considered. They are insulator dose, copper radiation damage dpa and fast neutron fluence. Shielding properties in two weakened area are expressed as shown in Table 2.3. These values are including safety factors. In this table, shielding properties have various width by following reason. Because inboard shields have different type and thickness of blankets, and different type of extra shields, etc.

From Table 2.3, most of nuclear heating rates in winding pack satisfy the design limit except a few types of shields. Insulator doses in most types of shields do not satisfy the limit, especially those in divertor region. Copper radiation damages in inboard shield barely satisfy the limit, but those in divertor region do not scarcely satisfy. Fast neutron fluences in winding pack in a few types of shields of inboard and divertor regions do not satisfy the limit.

Dose rates in reactor room in a day after reactor shutdown are not in excess of the biological shield design limit within considering only outboard shield.

Table 2.3 Shielding performance parameters in ITER (safety factors are included)

	Design limit	Safety factor	Region	Calculated value	
				Physics phase	Technology phase
Shielding for SCM					
Total nuclear heating (kW)	55	2		44-75	35-59
Peak values					
Nuclear heating rate in winding pack(mW/cm^3)	5	3	Inboard leg	1.4-3.3	1.1-2.6
			Divertor region	4.8-5.1	1.8-6.0
Insulator dose(10^9rad)	5	3	Inboard leg	—	3.9-7.5
			Divertor region	—	7.5-13.8
Copper radiation damage (10^{-3}dpa)	6	3	Inboard leg	—	2.1-5.1
			Divertor region	—	5.4-7.5
Fast neutron fluence in winding pack ($10^{19}n/cm^2$)	1	3	Inboard leg	—	0.45-2.0
			Divertor region	—	0.51-1.62
Biological shield					
Dose rate in reactor room (mrem/h)	0.5	10	outboard region	0.5	0.5

2.2 Benchmark Calculation

In ITER shielding neutronic specialist meeting and joint work, benchmark calculations were performed in order to clarify differences among nuclear properties by various nuclear group constant sets.

The benchmark calculation of problem 1a, the inboard shield composed of 80% SS and 20% H_2O is the most basic case for inboard shield configuration of the other benchmark calculation problems proposed in 1989 winter specialist meeting of ITER. Therefore, it is considered sufficient to perform the problem 1a in order to obtain informations about effects of different nuclear constant sets on shielding properties.

One dimensional transport code 'ANISN[11]' is adopted to shielding calculations with P5-S8. A torus model as shown Fig.2.2, one dimensional cylinder model, is applied to ITER mid-plane with neutron first wall loading of $1MW/m^2$. Shielding properties in inboard shield are surveyed for various shielding configurations, problems 1a to 1d. Representing Fig.2.2, the problem 1a is composed of SS (stainless steel) and water, the problem 1b of SS and borated water, the problem 1c of SS-water and lead, and the problem 1d of SS-water and B_4C. Purpose of problems 1b, 1c and 1d are to understand differences between calculated shielding property improvement with borated water, lead and B_4C zones, respectively, by applying FUSION-J3[8] and those by VITAMIN-C[9]. The material number densities

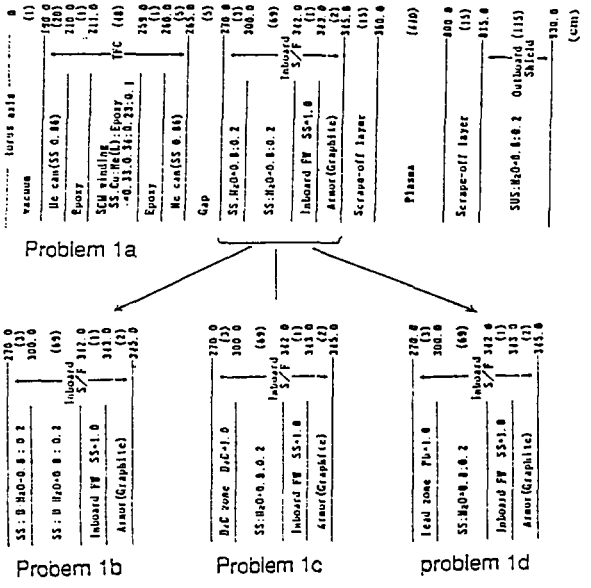

Fig.2.2 One-dimensional torus model in mid-plane.

Table 2.4 Material number densities for benchmark calculations.

No	Material	Element	Number Density
1	Plasma	^1H	1.0×10^{-14}
2	Carbon	C	9.023×10^{-2}
3	SS	Fe Cr Ni Mn	5.599×10^{-2} (Mo .) 1.556×10^{-2} 1.664×10^{-2} 1.464×10^{-2}
4	H_2O	H O	6.700×10^{-2} 3.350×10^{-2}
5	Pb	Pb	3.348×10^{-2}
6	$B.H_2O$	^{10}B ^{11}B H O	5.592×10^{-3} 2.237×10^{-2} 6.700×10^{-2} 3.350×10^{-2}
7	B_4C	^{10}B ^{11}B C	2.197×10^{-2} 8.787×10^{-2} 2.746×10^{-2}
8	Cu	Cu	8.493×10^{-2}
9	Insulater	H C O N Si Al Ca	2.033×10^{-2} 1.792×10^{-2} 2.551×10^{-2} 1.350×10^{-3} 6.884×10^{-3} 2.158×10^{-3} 2.300×10^{-3}
10	Liq.He	^4He	1.837×10^{-2}
11	Inb/outb.Shield	SS H_2O	0.8 0.2
12	SCM	SS Cu Insulater Liq.He	0.5(Nb_3Sn) 0.4 0.05 0.05
13	b.Shield	SS $B-H_2O$	0.8 0.2

used in the preset calculation are listed in Table 2.4. The nuclear group constant set FUSION-J3 is the coupled constant set composed of neutron 125 groups and gamma ray 40 groups. Gamma ray group constants in FUSION-J3 were revised again by the other processing code. We call the old version of FUSION-J3 as "old FUSION-J3" and revised version as "revised FUSION-J3". Difference between them is explained as follows.

In revised FUSION-J3, gamma-ray transport cross sections were processed by the gamma-ray processing code "NJOY[12]" and gamma-ray DLC-99. While the cross sections in old version FUSION-J3 had been done by "RADHEAT-V4[13]" and DLC-15. Difference between those processing codes is procedure of pair creation cross sections, that is,

NJOY;

Total cross section: $\sigma_t = \sigma_{incoh} + \sigma_{coh} + \sigma_{pp} + \sigma_{pe}$,

Absorption cross section: $\sigma_a = \sigma_{pe}$,

Scattering cross section: $\sigma_s = \sigma_{incoh} + \sigma_{coh} + \sigma_{pp} \times 2$.

RADHEAT-V4;

Total cross section: $\sigma_t = \sigma_{incoh} + \sigma_{coh} + \sigma_{pp} + \sigma_{pe}$,

Absorption cross section: $\sigma_a = \sigma_{pp} + \sigma_{pe}$,

Scattering cross section: $\sigma_s = \sigma_{incoh} + \sigma_{coh}$.

Therefore, total gamma ray fluxes by revised FUSION-J3 become slightly larger than those by VITAMIN-C in all regions as shown in Table 2.6. Consequently, gamma ray heating by the FUSION-J3 is slightly larger than those by VITAMIN-C in all regions as also shown in Table 2.5. Gamma ray spectra by the FUSION-J3 and those by VITAMIN-C approximately agree with each other as shown in Fig.2.3. Gamma ray heating rates calculated with 2-dimensional slab model with both group constant sets. Revised FUSION-J3, old version FUSION-J3 and VITAMIN-C are represented in Fig.2.4 together with the experimental values by FNS. From this figure, the values with revised FUSION-J3 and VITAMIN-C are approximately in agreement with the experimental ones in almost region except farther than 70cm from the surface. From these results, the revised FUSION-J3 is adoptable to nuclear calculations for shieldings.

Comparing typical nuclear shielding properties by revised and old FUSION-J3's, ENDF/B-V and -IV, it can be seen that the values by revised FUSION-J3 agree approximately with those by ENDF/B-V as shown in Table 2.6.

Table 2.5 Neutron and gamma ray fluxes, and nuclear heating rates estimated by FUSION-J3, VITAMIN-C and GICX40 in ITER benchmark Problem 1a.

Items & Positions \ Transport x'sec Data base / Reaction x'sec	FUSION-J3 JENDL-3 JENDL-3	FUSION-J3+ JENDL-3 JENDL-3	VITAMIN-C ENDF/B-IV MACKLIB-IV	GICX40 ENDF/B -III, IV GICX40
Neutron & γ flux (/cm^2・s)				
First wall (R:815-816cm)				
fast neutron (E_n>0.1MeV)	**2.477E+14**	2.477E+14	2.485E+14	2.377E+14
total neutron (E_n<14.1MeV)	**3.923E+14**	3.923E+14	3.851E+14	3.822E+14
gamma ray flux (total)	**3.239E+14**	2.468E+14	2.615E+14	1.572E+14
Carbon tile (R:344-345cm)				
fast neutron (E_n>0.1MeV)	**2.062E+14**	2.062E+14	2.063E+14	1.959E+14
total neutron (E_n<14.1MeV)	**3.451E+14**	3.451E+14	3.377E+14	3.364E+14
gamma ray flux (total)	**2.752E+14**	2.119E+14	2.264E+14	1.364E+14
Winding pack (R:257-259cm)				
fast neutron (E_n>0.1MeV)	**1.237E+10**	1.237E+10	1.083E+10	8.320E+09
total neutron (E_n<14.1MeV)	**3.207E+10**	3.207E+10	2.545E+10	2.014E+10
gamma ray flux (total)	**1.332E+10**	6.947E+09	1.099E+10	4.0162+09
Nuclear heating rates(w/cm^3)				
First wall (R:815-816cm) n	**8.105E+0**	8.105E+0	6.482E+0	5.976E+0
γ	**1.162E+1**	9.320E+0	9.918E+0	7.246E+0
total	**1.972E+1**	1.742E+1	1.640E+1	1.322E+1
Carbon tile(R:344-345cm) n	**3.137E+0**	3.137E+0	4.975E+0	3.688E+0
γ	**1.993E+0**	1.533E+0	1.687E+0	1.253E+0
total	**5.131E+0**	4.671E+0	6.662E+0	4.941E+0
Coil case (R:264-265cm) n	**1.124E-4**	1.124E-4	7.163E-5	5.310E-5
γ	**1.678E-3**	1.095E-3	1.443E-3	5.946E-4
total	**1.790E-3**	1.208E-3	1.514E-3	6.477E-4
Winding pack(R:257-259cm) n	**5.552E-5**	5.537E-5	4.373E-5	2.800E-5
γ	**6.322E-4**	4.165E-4	5.924E-4	2.868E-4
total	**6.877E-4**	4.719E-4	6.361E-4	3.148E-4

FUSION-J3 :"Recommended group constant set for Fusion neutronic calculation" Gamma-ray transport cross-sections are proceeded by NJOY SYSTEM.
FUSION-J3+:Gamma-ray transport cross-sections are proceeded by RADHEAT-V4 SYSTEM.

Table 2.6 Differences among nuclear properties by various nuclear group constant sets in ITER inboard shielding.

	FUSION-J3	FUSION-J3+	ENDF/B-V	ENDF/B-IV
Sperconducting magnet winding pack				
Neutron flux	1.0	1.0	1.0	0.75～0.8
Nuclear heating rate	0.87	0.59	1.0	0.75～0.8
First wall carbon tile				
Nuclear heating rate	1.04	0.97	1.0	1.35～1.4

FUSION-J3 :"Recommended group constant set for Fusion neutronic calculation" Gamma-ray transport cross-sections are proceeded by NJOY SYSTEM.

FUSION-J3+:Gamma-ray transport cross-sections are proceeded by RADHEAT-V4 system.

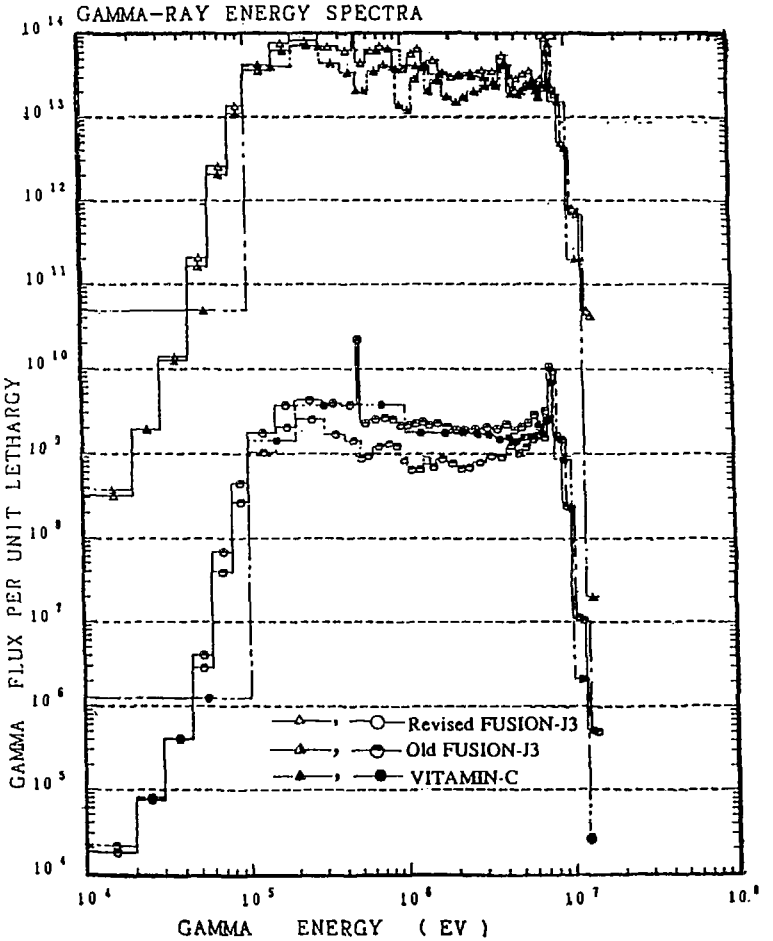

Fig.2.3 Comparison of gamma-ray spectra in the first wall and in the winding pack by revised FUSION-J3 and old FUSION-J3 (based on JENDL-3), with those by VITAMIN-C (based on ENDF/B-IV) (problem.1a).

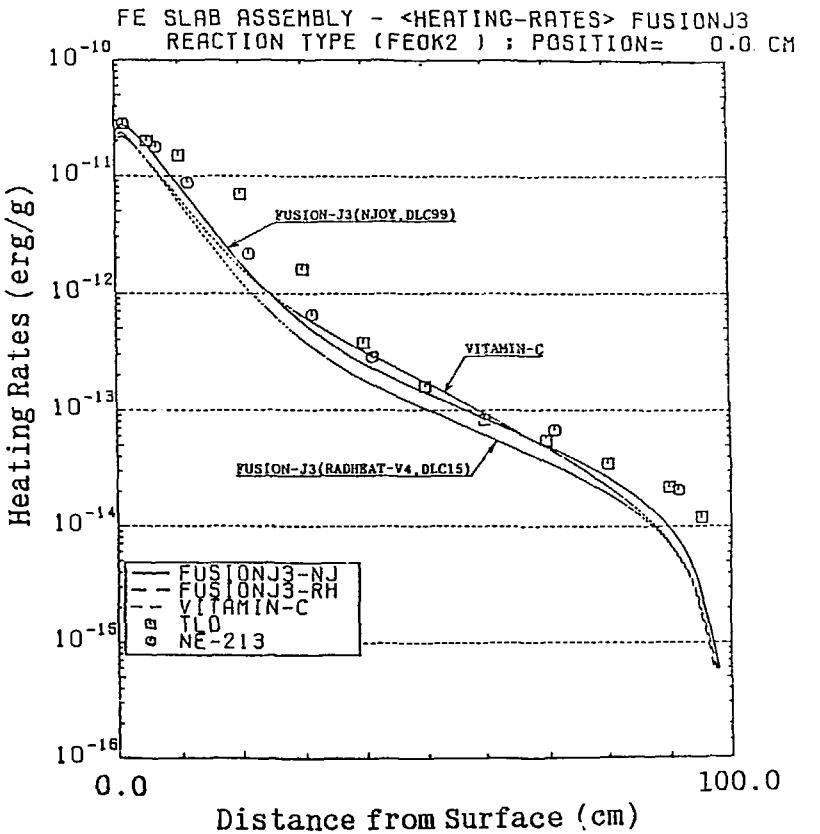

Fig.2.4 Comparison of calculated gamma-ray heating rates by various nuclear group constant sets with experimental values.

JAERI M 91 092

3. REQUIREMENTS FOR NUCLEAR DATA

3.1 Proposed Materials and Their Nuclear Data Priorities

The construction of the fusion reactors, FER or ITER, and demonstration fusion reactors are being programmed. According to this program, the experimental reactors will be designed and constructed from 1997 to 2005. Demonstration reactor following them are considered to be designed from ~2005 and to be started constructing from 2015.

Materials possibility to be used in fusion experimental reactors and demonstration fusion reactors are listed up in Table 3.1. Reactor components are categorized into structure, blanket, plasma facing, electric insulator and other materials as shown in far left column. In the next column adjacent it, materials composing these components are proposed. In the third column from the left side, nuclides consisting of the materials are presented. In the five columns following them, ranks of necessities for reaction type of the nuclides are evaluated. Considering material priorities and whether they are possible to be used in fusion experimental reactors or demonstration reactors, priorities of proposal for these nuclide's nuclear data are synthetically judged in the last column.

Proposed materials and their nuclear data priorities are summarized as follows.

1) Stainless steel type 316 is the first priority for structural materials in high weight load components.
2) Alumina dispersion strengthened copper (DS-Cu) and molybdenum rhenium alloy are the first priority for the divertor structural materials.
3) Lithium oxide, lithium aluminate, lithium silicate and lithium zirconate are the first priority for the breeding materials.
4) Beryllium is the first priority for neutron multiplier.
5) Carbon and tungsten are the first priority for the first wall and divertor armor materials, where silicon and boron are listed for the reason why they include as impurities.
6) Aluminium oxide and magnesium aluminium oxide are the first priority for electric insulator.
7) Coolant, concrete, air and material for window are also the first priority.

3.2 Required Accuracies and Time Limits for Nuclear Data

Proposed materials, nuclides composing them and their reaction types of quantities were previously explained for design of fusion experimental reactors. Their future programme were also presented. According to those discussions, nuclear data uncertainties of the nuclides composing structural and blanket materials are required to be reduced by the time at starting

Table 3.1 Materials, nuclides and their quantities listed up in FER/ITER design

	Materials	Nuclides	Neutron transport cross section	γ-ray trasport cross section	Activation cross section	Charged particle reaction cross section	Photo reaction cross section	Priority of proposal (note:1)
Structural materials (Shielding materials)	316 S S	Cr, Mn, Fe, Co, Ni, Mo	◎	◎	◎	△	×	A
	D S − C u	Al, Cu, O						A
	T Z M (Ti, Zr, Mo)	Ti, Zr, Mo						B
	Mo − Re	Mo, Re						A
	Nb − Zr	Zr, Nb						B
	V − alloy	V						C
	SiC	Si, C						C
Blanket materials	Li_2O	Li, O	◎	◎	◎	△	×	A
	$LiAlO_2$	Li, Al, O						A
	Li_4SiO_4	Li, Si, O						A
	Li_2ZrO_3	Li, Zr, O						B
	Beryllium	Be						A
	Lead	Pb						B
	Lithium-Lead	Li, Pb						B
Plasma facing materials	Carbon (with Si, B)	C, Si, B	◎	◎	◎	○	△	A
	Beryllium	Be						B
	Tungsten	W						A
	Gallium	Ga						B or C
Electric insulator	Al_2O_3	Al, O	○	○	◎	△	△	A
	$MgAl_2O_4$	Mg, Al, O						A
	BeO	Be, O						B
	AlON	Al, O, N						B
	Si_3N_4	Si, N						B
	Diamond	C						B
Other materials	Coolant (H_2O, He)	H, O, He	◎	◎	◎	×	×	A
	Concrete	H, O, Si, Na, K, Ca, Fe, C	◎	◎	◎	×	×	A
	Air	N, O, Ar	○	○	◎	×	×	A
	Window materials (Al_2O_3)	Al, O	×	×	◎	○	△	A

(note) ◎:Most necessary, ○:Necessary, △:Preferably, ×:Not necessary.

(note:1) A : The first priority proposal for the next facility.

B : Proposal for the next facility,

C : Proposal for demonstration reactors.

For neutron transport cross section : Secondary neutron angular disribution and Energy spectra.

For γ-ray transport cross section : γ-ray production cross section, Secondary γ-ray angular distribution and γ-ray energy spectra.

point of experimental reactor design for construction, that is, by 1997. However, they are considered to be required for shielding experiments and their analyses to reduce design uncertainty. These experimental and their analyses are going to be probably started from the midpoint of ITER EDA (Engineering Design Activity) phase. Consequently, these accurate nuclear data ranking with the first priority are expected to be required by 1993-1995.

According to Table 2.2, uncertainty in shielding property by modeling is predicted approximately 10 % and that caused by nuclear data uncertainties 40 to 50 %. In order to reduce the uncertainties caused by nuclear data to the same values as those by modeling, that is, 10%, it should be estimated how many per cent uncertainties in nuclear data must be decreased. Sensitivity analysis is necessary to estimate them. While, we have no sensitivity coefficient and scarcely covariance matrixes for nuclear group constant errors. Then we cannot perform sensitivity analysis.

In the present report, we assume the calculational uncertainties $\Delta x/x$ in shielding properties given by transport cross section uncertainties $\Delta\sigma_i / \sigma_i$ and slowing down scattering times N_S as follows.

$$(\Delta x / x)^2 = \sum_{i}^{N_S} (\Delta\sigma_i / \sigma_i)^2 .$$

From this equation, the uncertainties in transport cross sections should be improved as 5 - 10 %, that is, $\Delta\sigma_i / \sigma_i = 5\text{-}10$ % , in order to reduce uncertainties in shielding property calculation to ~10 %, where scattering times is assumed as 10 times in 70 - 80 cm thick shield. Performing these estimations, we can obtain the required accuracies in various nuclear data in every components.

Considering above discussions, we can summarize the required accuracies and time limits for nuclear data improvement as shown in Fig. 3.1.

1) Required accuracies in transport cross sections of major nuclides including in the first priority structural and blanket materials must be reduced ~5 % by ~1993. Nuclides of Fe, Ni, Cr, H, O, Li, Be and Pb belong to this group.

2) Required accuracies in transport cross sections of minor nuclides including in the first priority structural and blanket materials must be reduced ~10 % by ~1993. Nuclides of Mn, Mo, Al and Cu belong to this group.

3) Required accuracies in transport cross sections of nuclides including in the first priority plasma facing component and concrete materials must be reduced ~10 % by ~1993. Nuclides of C, Si, B and W belong to this group.

4) Required accuracies in activation cross sections of nuclides including in the first priority shielding, blanket, plasma facing and concrete materials must be reduced ~20 % by ~1993. Nuclides of Cr, Mn, Fe, Ni, W, Co, Mo, Al, Cu, Pb, C, Si, B, Ca and Ar belong to this group.

5) Required accuracies in activation cross sections of nuclides including in the first priority

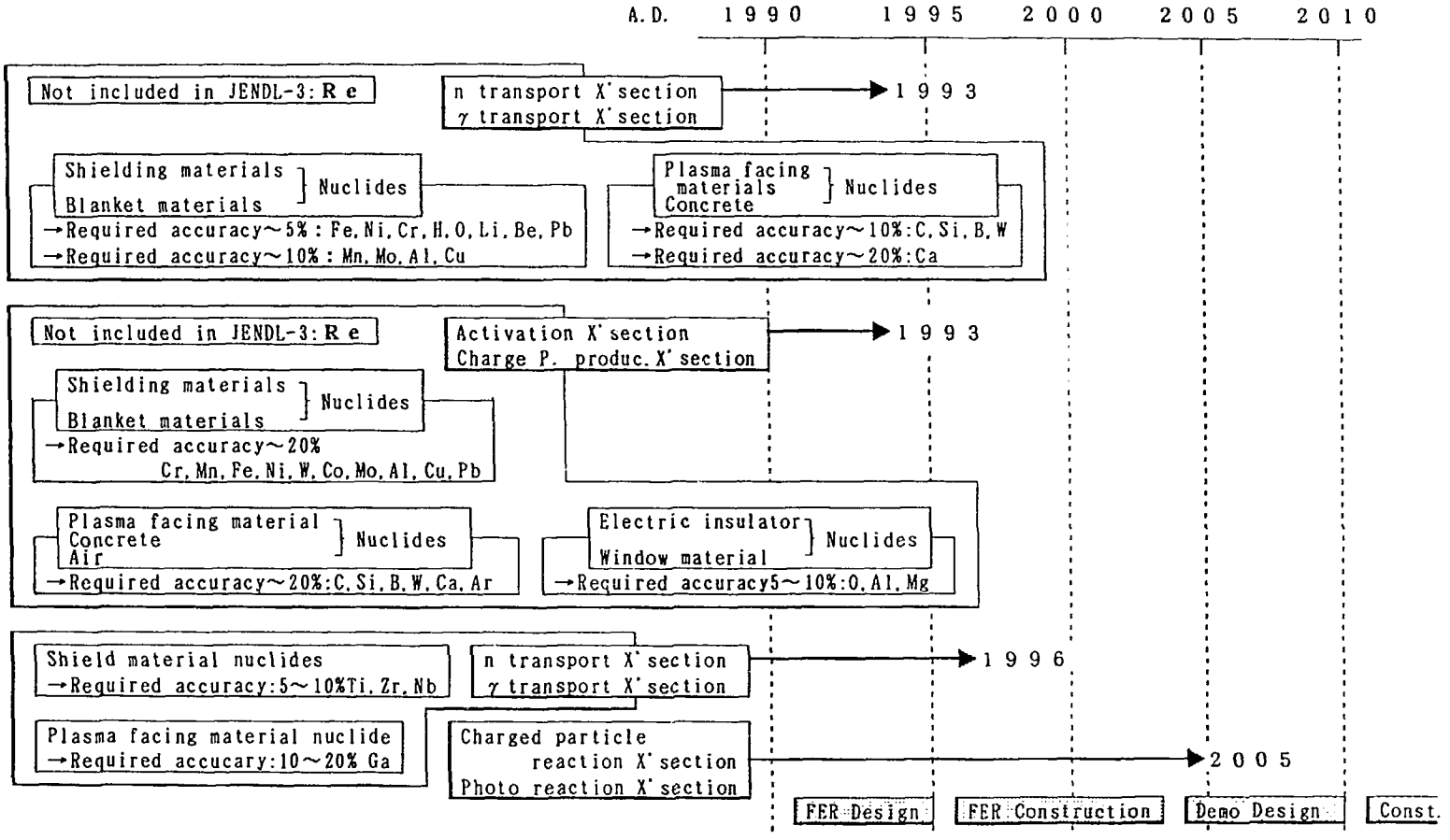

Fig. 3.1 Required accuracies and performing time limits for Nuclear data to develope fusion reactors

$$\text{Nuclear property Accuracy}: \Delta X/X = \pm \sqrt{\sum_{i}^{N_s} (\Delta \sigma_i/\sigma_i)^2}$$

($\Delta \sigma_i/\sigma_i$: Nuclear data accuracy, N_s: scattered times)
Assuming $\Delta X/X = 0.1$ for neutron flux accuracy

electric insulator and window materials must be reduced ~10 % by ~1993. Nuclides of O, Al and Mg belong to this group.
6) Required accuracies in transport cross sections of major nuclides including in the second priority structural and blanket materials must be reduced 5 - 10 % by ~1996. Nuclides of Ti, Zr and Nb belong to this group.
7) Required accuracies in transport cross sections of nuclide including in the second priority plasma facing component material must be reduced 10 - 20 % by ~1996. Nuclide of Ga belongs to this group and does not include in JENDL-3.
8) Uncertainties in charged particle reaction and photo reaction cross sections are considered necessary to be improved by 2005 when demonstration reactors will be designed for construction.

Reflecting the status of integral experimental analysis of JENDL-3, present nuclear data accuracies can be seen to satisfy considerably these required accuracies.

4. CONCLUSION

Considering ITER and FER activities, the present situations in fusion neutronics were explained up to now from the previous fusion nuclear data specialist meeting. Vicissitude of fusion nuclear group constant sets was also explained and especially FUSION-J3 was developed and improved. Moreover, future programme of fusion reactor developments were introduced and priorities of proposed materials for fusion reactor constructions were represented. From these discussions we required the accuracies in nuclear data for fusion reactor developments as follows.
1) Required accuracies in transport cross sections of major and minor nuclides including in the first priority structural and blanket materials must be reduced respectively ~5 and ~10 % by ~1993.
2) Required accuracies in transport cross sections of nuclides including in the first priority shielding, blanket, plasma facing component and concrete materials must be reduced 10 - 20 % by ~1993.
3) Required accuracies in activation cross sections of nuclides including in the first priority electric insulator and window materials must be reduced ~10 % by ~1993.
4) Required accuracies in transport cross sections of nuclide Ga including in the second priority plasma facing component material must be reduced 10 - 20 % by ~1996.
5) Uncertainties in charged particle reaction and photo reaction cross sections are considered necessary to be improved by 2005.

ACKNOWLEDGMENTS

Author would particularly like to thank to Y.SEKI and H.Maekawa for valuable and useful discussions, and K.Kosako for helpful supporting. He would also like to thank those who participated the Specialist Meeting on Fusion Nuclear data.

REFERENCES

1) IAEA, "International Tokamak Reactor Phase Two A part I," International Atomic Energy Agency (1983).
2) IAEA, "ITER Conceptual Design : Interim Report," ITER Documenting Series, No.7, International Atomic Energy Agency, Vienna, 1990.
3) Department of Large Tokamak Research,"Conceptual Design Study of Fusion Experimental Reactor (FER)," JAERI-M86-134 (Nov.1986).
4) Fusion Experimental Reactor Team, "Overview of FER (Fusion Experimental Reactor) - Design Report, "Japan Atomic Energy Institute JAERI-M90-090 (1990).
5) Y.Seki, H.Iida, "Coupled 42-Group Neutron and 21-Group Gamma Ray Cross Section Set for Fusion Reactor Calculation," JAERI-M8818, (1980).
6) T.Asami edited, "Evaluated Neutron Cross Sections in JENDL-2," Japan Atomic Energy Research Institute, JAERI-M84-052 (March, 1984).
7) K.Shibata, et al., JENDL Compilation Group (Nuclear Data Center, JAERI), "Japanese Evaluated Nuclear Data Library, Version-3 - JENDL-3 - ,"Japan Atomic Energy Research Institute, JAERI-1319 (June 1990)
8) K.Maki, et al., :"Fusion Nuclear Group Constant Set FUSION-J3 and Shielding Properties for Fusion Experimental Reactor by FUSION-J3," 1990 Annual Meeting of the Atomic Energy Society of Japan F8 (April 1990).
9) Y.Gohar, M.A.Abdou, DLC-60, Oak Ridge National Laboratory (1978).
10) K.Maki, "KERMA Liburary for FUSION-J3," JAERI-M report to be published.
11) W.W. Engle, "A User's Manual for ANISN, A One-Dimensional Discrete Ordinate Transport Code with Anisotropic Scattering," K--1693, Union Carbide Corporation, Computing Technology Center (1976).
12) R.E.Macfarlane, et al., Trans. American Nuclear Society, vol.23, 22(1979).
13) N.Yamano, K.Minami, K.Koyama, Y.Naito, "RADHEAT-V4, A Code System to Generate Multi group Constant and Analyze Radiation Transport for Shielding Safety Evaluation," JAERI-1316, (1989).

10. Discussion

10.1 Summary of Discussions

Summarized by Hiroshi MAEKAWA
Department of Reactor Engineering
Japan Atomic Energy Research Institute
Tokai-mura, Naka-gun, Ibaraki-ken, 319-11 Japan

1. Introduction

As the last session of this Specialists' Meeting, a free discussion was moderated by A. Takahashi. First, H. Maekawa summarized the presentations briefly. From the results of data tests and their discussions at this meeting, he evaluated the status of JENDL-3 nuclear data relevant to fusion neutronics as "85 points" for neutron data and "80 points" for gamma-ray data. Then the chairman proposed the order of discussion, i.e., the first discussion was concentrated to evaluating the status of nuclear data nuclide by nuclide. Next discussion was addressed in the items how and what to make a next step towards the improvement of JENDL and the progress of fusion neutronics study.

2. Status of JENDL-3 Nuclear Data Relevant to Fusion Reactors

Table 1 summarizes the status of JENDL-3 nuclear data based on the present discussions. The discussion was proceeded nuclide by nuclide according to the data tests presented in this meeting. The accuracy requested is not the same for all nuclei. Some nuclei such as ^{7}Li, ^{9}Be and Fe are major elements for fusion reactor and the high accuracy is requested for the data of these nuclei. The status of data for these nuclei in the table was judged critically.

Contributors to summarize this report :
Y. Nakajima, A. Hasegawa, T. Nakagawa, S. Chiba, K. Maki, Y. Oyama, K. Kosako, T. Narita, A. Takahashi and H. Maekawa.

It was pointed out for Be that the problems existed in the lower energy part of secondary neutron spectrum and in (n,γ) cross section. In the case of ^{10}B and ^{11}B, no integral test was presented here. The data of ^{10}B and ^{11}B seem to be not so bad from the comparison between measured and evaluated DDX data. The revised data of ^{14}N seems to be fine.

From the analyses of time-of-flight experiments at FNS, a few percents of minor changes are recommended for total and elastic cross sections of ^{9}Be, ^{12}C and so on. A small modification is also recommended for their (n,2n) cross sections including energy-angle distributions. Evaluators expressed that the status of ^{7}Li and Be data became to the limit of the accuracy in the evaluation. It is not so easy to improve the nuclear data of not only light elements but heavy elements, especially Be data. Some discrepancies exist near the region boundary such as Li_2O-Be. Further examinations are required for the transport calculations including modeling and positioning error.

Japanese Nuclear Data Center understood the problem of Mo data. The data of not only Mo but Nb, Zr, W and so on are under way. It was pointed out that Re data should be included in JENDL library from te standpoint of activation analysis.

3. Issues for Post JENDL-3

(1) Publication of benchmark problems for data testing

There are many experimental data produced in Japan. The publication of benchmark problems is a good task force for the activity of Sub-Committee on Fusion Reactor in the Research Committee on Reactor Physics.

(2) A simple method for improvement of nuclear data in JENDL-3

T. Asami proposed a simple method to improve the nuclear data in JENDL-3. Most of angular distributions for inelastic continuum were adopted from the result calculated by CATHY code. This made an overestimation of back-scattering. Therefore, in the region where the direct process is dominant, we had better adopt an isotropic scattering in the center-of-mass system. S. Chiba pointed out the usage of a systematics for the direct and pre-compound processes. There are systematics of Kalbach, Kalbach-Mann, Kuroda and so on.

(3) File-6 and processing code

At the first Specialists' Meeting on Nuclear Data for Fusion Neutronics in July 1985, the necessity of file-6 was strongly recommended. A processing code for the file-6 is being prepared. Since there is no result using the data energy-angle correlation, we can not refer the usefulness of the file-6. After the file-6 of around 8 nuclei (similar to JENDL-3PR1) is prepared, we should judge the usefulness of the file-6.

(4) Sensitivity and uncertainty analysis

The activity of sensitivity and uncertainty analysis is very low in Japan relevant to fusion neutronics. We should stimulate this activity.

(5) Fusion file

It is the best way to provide "Fusion File" as a special purpose file of JENDL-3. This file includes the file-6 of selected nuclei.

(6) Requests for post JENDL-3 activity

The material research group has requested the evaluated nuclear data up to 50 MeV for selected nuclei such as Li, O, Al and Fe, in order to examine an intense D-Li neutron source project ESNIT Energy Selective Neutron Irradiation Test Facility). There is, however, little request for the nuclear data needs from the fusion community (plasma physicists and reactor designers ?). We should pay our best efforts to improve the circumstances.

4. Concluding remarks

Most participants felt JENDL-3 seems to be good enough for applying to the fusion reactors, but there are many minor problems left. Minor changes are desirable for many nuclei in JENDL-3 to improve their accuracy. The range of these minor changes, especially in the cases of total and elastic cross sections, are now within the uncertainty of data evaluation and the error of differential experiments. Namely, the

accuracy for a large part of nuclear data in JENDL-3 becomes close to the limit of errors of both differential and integral experiments. This fact suggests that we should be careful to examine and discuss the status of evaluated nuclear data considering the accuracy and/or uncertainty of data evaluations and experiments.

This meeting was the first time to discuss the status of gamma-ray data in JENDL-3. Unfortunately, the integral experiments related to the gamma-ray data are very few. It is necessary to accumulate the benchmark experiments for the integral test of the gamma-ray data.

Table 1 Status of Nuclear Data in JENDL-3

Nuclide	Priority	Status		Comment
		neutron	gamma	
Li-6	High	△	○	There is a problem in DDX.
Li-7	High	○	○	There is no large problem.
Be-9	High	△	×	If the accuracy of TBR is requested to be less than 5%, the status is unsatistactory. Additional examination is requied especially for (n,2n) and DDX. (n,γ) seems to be not good.
C -12	High	□	○	Re-evaluation is desirable for total and elastic cross section. Information of spectrum in (n,n' 3α) is not enough and is important for calculation of DPA. Data for nuclear heating is good.
N -14	Medium	× (J-3) ○ (J-3M)		JENDL-3 is not good but newly evaluated JENDL-3M is good.
O -16	High	○		JENDL-3 seems to be enough.
F -19	Low	×	×	Data is not good but priority is low.
Al	High	□	○	
Si	High	○	○	Evaluation is fine.
Ti	Medium	×	△	
Cr	High	□	△	There are some problems.
Mn	High	□		
Fe	High	□		

JAERI M 91 092

Table 1 (Continued)

Nuclide	Priority	Status		Comment
		neutron	gamma	
Ni	High	□		
Co	Medium	×		
Cu	High	○	○	There is a problem on ^{63}Cu(n,2n) for dosimetory.
Zr	Medium	×		
Nb	High	△		
Mo	High	×		Evaluators understand the status.
W	High	×		
Pb	High	△		Addition of more inelastic levels is required. Re-evaluation is desirable for total, elastic and inelastic cross sections.

* Above status is judged considering the importance and priority of each nuclide.

○ : good, □ : almost good, △ : fairly good, × : not good.

11. Analyses of Benchmark Experiments

11.1 Evaluation of Beryllium, Carbon and Iron Neutron Cross Sections in the JENDL-3 by Monte Carlo Analysis of Benchmark Experiments

K. Ueki

Ship Research Institute
6-38-1 Shinkawa, Mitaka, Tokyo, 181

M. Kawai

Toshiba Co.
Nuclear Engineering Laboratory
4-1 Ukishima-cho, Kawasaki-ku Kawasaki, 210

Beryllium, carbon, and iron neutron cross sections in the JENDL-3 library were evaluated by the Monte Carlo analysis of the JAERI-FNS and the LLNL-Sphere D-T neutron benchmark experiments. Those experiments offer detailed angular fluxes with respect to several slab thicknesses as well as measuring angles.

The Monte Carlo analysis with the continuous energy code MCNP was carried out by using pointwise cross sections from the JENDL-3 and the ENDF/B-IV as a comparison. In order to take into account the experimental configuration faithfully as much as possible in the MCNP calculation, the particle scoring routine TALLYD was steeply modified to each configuration. The intensively narrow collimator was considered just as it is for the JAERI-FNS experiment and the NESX estimator was employed for the LLNL-Sphere experiment.

The reliability of the cross sections in the JENDL-3 were evaluated through comparison and investigation of the calculated results with the experiment in detail.

1. Introduction

Recently, the evaluated nuclear date library JENDL-3[1)]

was compiled and the library was published from the Nuclear Date Center of the JAERI. Taking this situation, evaluation work of cross sections in the JENDL-3 was started from a user's point of view at some organizations.

In this study, beryllium, carbon, and iron cross sections in the JENDL-3 were evaluated by calculations with the continuous energy Monte Carlo code MCNP[3], especially for D-T neutrons. The calculations with the ENDF/B-IV [2] were also carried out to compare the results with the JENDL-3.

In the first place, the JAERI-FNS angular-neutron-flux benchmark experiments[4,5,6] in which detailed angular fluxes were measured with respect to several slab thicknesses as well as measuring angles were selected to evaluate beryllium and carbon cross sections. The experimental configuration had the intensively narrow collimator between the slab and the NE-213 detector. Accordingly, the particle scoring routine TALLYD of the MCNP code was revised so as to take into account the collimator geometry in the calculations. Due do being the collimator, the point detector estimator was to be employed in the JAERI-FNS analysis. Next, the LLNL-Sphere benchmark experiments[7] were analyzed to evaluate iron cross sections. In order to reduce the statistical error in the Monte Carlo calculations, the NESX (next event surface crossing) estimator was employed in the revised TALLYD for the LLNL-Sphere calculations.

The computer was HITAC-680 of the Tokyo University.

2. Analysis

The particle scoring routine TALLYD in the MCNP code was steeply modified to take into account the experimental configuration of the JAERI-FNS neutron angular flux benchmark experiments, as shown in Fig.1. Due to the modification of the TALLYD routine, neutrons of which passed through the narrow collimator could be scored at the point on the detector surface. Accordingly, the experimental configuration of the JAERI-FNS benchmark experiments was faithfully reproduced in the MCNP Monte Carlo calculations. The values of solid angles, effective measured areas, and flight paths were employed from Ref.(6).

On the other hand, the NESX estimator as shown in Fig.2 was employed in the TALLYD routine for the LLNL-Sphere neutron angular flux benchmark experiments and neutrons of which entered into measuring angle ±5 deg. were scored by the TALLYD with the NESX estimator.

3. Summary and Discussions

3.1 On Beryllium

The C/E values of beryllium integrated fluxes and comparisons of angular fluxes between measured and MCNP calculations for 15.24-cm-thick are summarized in Fig.3 and Figs.4(a) ~4(e), respectively.

On the whole, the C/E values integrated over 10 MeV with the JENDL-3 are distributed around 1.0 except for 41.8 deg.. At 41.8 deg., the C/E is 0.86. However, the C/E values integrated over 10 MeV with the ENDF/B-Ⅳ decrease as the measuring angle increase; 0.95 at 0.0 deg., 0.84 at 24.9 deg., and 0.72 at 66.8 deg.. The C/E values integrated over 0.01 MeV are between 0.98~1.09 with the JENDL-3 and 0.91~0.96 with the ENDF/B-Ⅳ.

There are no essential differences between the measured angular fluxes and the MCNP calculations with the JENDL-3 over the whole energy region. However, at 41.8 deg., the once elastic-collision peak at 14.5 MeV is less than the measurement, significantly.

3.2 On Graphite

The C/E values of graphite integrated fluxes and comparison of angular fluxes between measured and MCNP calculations for 20.24-cm-thick are summarized in Fig.5 and Fig.6(a)~ 6(e), respectively.

On the whole, the C/E values integrated over 0.5 MeV, 1.0 MeV, and 10 MeV with the JENDL-3 and the ENDF/B-Ⅳ are within 1.0 ±0.1. However, the C/E values with the JENDL-3 show a tendency of >1.0 ; on the contrary, a tendency of <1.0 with the ENDF/B-Ⅳ. There are no essential differences between the JAERI-FNS measured angular fluxes and the MCNP results over the

whole energy regions. However, some differences are recognized at minor peaks and troughs.

3.3 On Iron

The comparison of angular fluxes between measured and MCNP results for 0.9, 2.9, and 4.8 mfp thicknesses of iron-spheres are shown in Figs. 7, 8, and 9, respectively.

For the three different iron-spheres, there are no significant differences between the measured angular fluxes and the calculations with the JENDL-3. However, a little bit underestimation is observed between 7~13 MeV for all the calculations. The cause of the underestimation between 7~10 MeV is due to that the discrete levels for inelastic scattering of ^{56}Fe are taken below 4.5 MeV, and also between 11~13 MeV is due to the underestimation of inelastic scattering cross sections for the low lying levels in the JENDL-3.

To sum up, the cross sections taken in the present study, that is beryllium, carbon, and iron in the JENDL-3, have enough reliability and bring consistent calculated results to benchmark experiments with respect to D-T neutrons.

The modified TALLYD routine in which the configuration of narrow collimator was taken into account the MCNP calculation just as it is contributed very much to simulate the JAERI-FNS benchmark experiment, so that the peaks and troughs in the angular fluxes were fairly exactly represented by the analysis.

References

1) K.Shibata, et al., "Japanese Evaluated Nuclear Date Library, Version-3 —JENDL-3—," JAERI 1319, Japan Atomic Energy Research Institute (1990).

2) ENDF/B, Summary Documentation, BNL-NCS-17541 (ENDF-201), 2nd edition compiled by D.Garber (1975).

3) MCNP-A General Purpose Monte Carlo Code for Neutron and Photon Transport, LA-7396-M (Rev.) Version 2B, Los Alamos Monte Carlo Group, Los Alamos National Laboratory (1981).

4) Y. Oyama and H. Maekawa, Nucl. Sci. Eng., 97, 220 (1987).

5) Y. Oyama, S. Yamaguchi, and H. Maekawa, J. Nucl. Sci. Technol., 25, 419 (1988).

6) Y. Oyama, S. Yamaguchi, and H. Maekawa, "Experimental Results of Angular Neutron Flux Spectra Leaking from Slabs of Fusion Reactor Candidate Materials(I)," JAERI-M 90-092, Japan Atomic Energy Institute, (1990).

7) L.F. Hansen, et al., "Updated Summary of Measurements and Calculations of Neutron and Gamma-Ray Emission Spectra from Spheres Pulsed with 14-MeV Neutrons," UCID-19604 (Rev.1), LLNL, (1989).

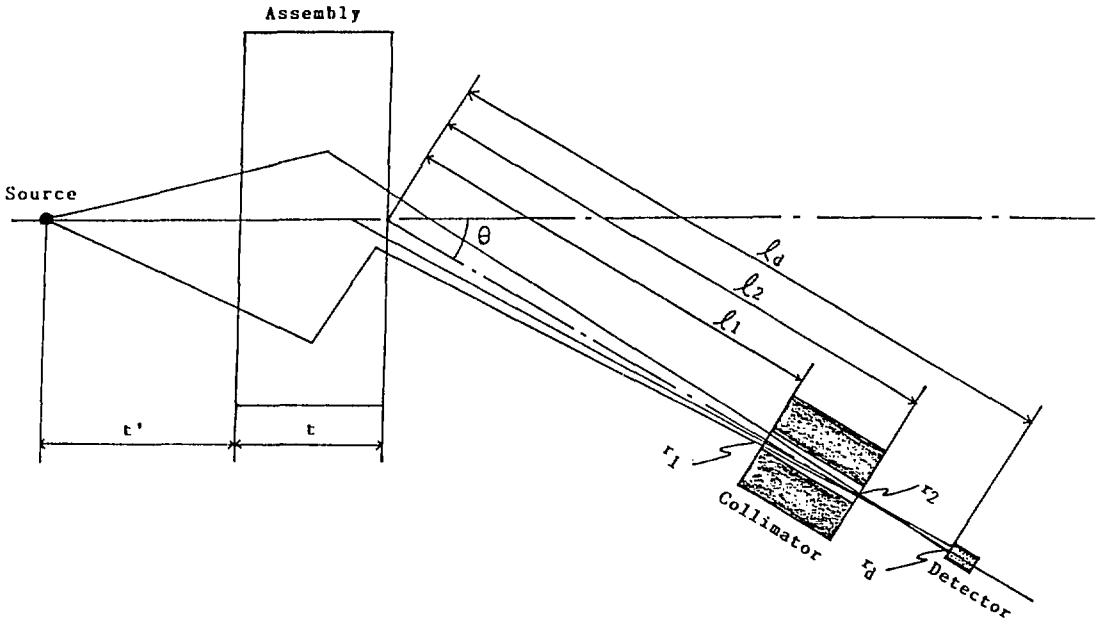

Fig.1 Calculational model of the FNS experiment by using modified subroutine TALLYD in the MCNP code.

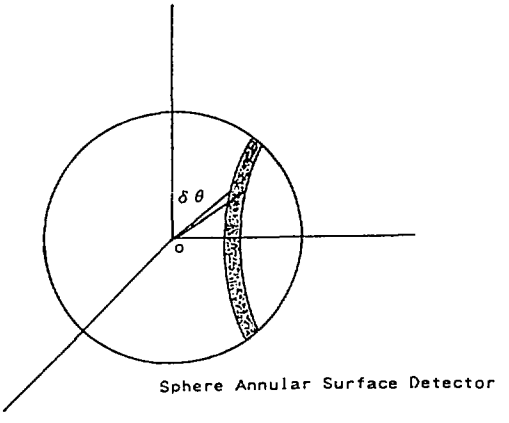

Fig.2 Concept of the Nest Event Sphere Annular Surface Crossing Estimator

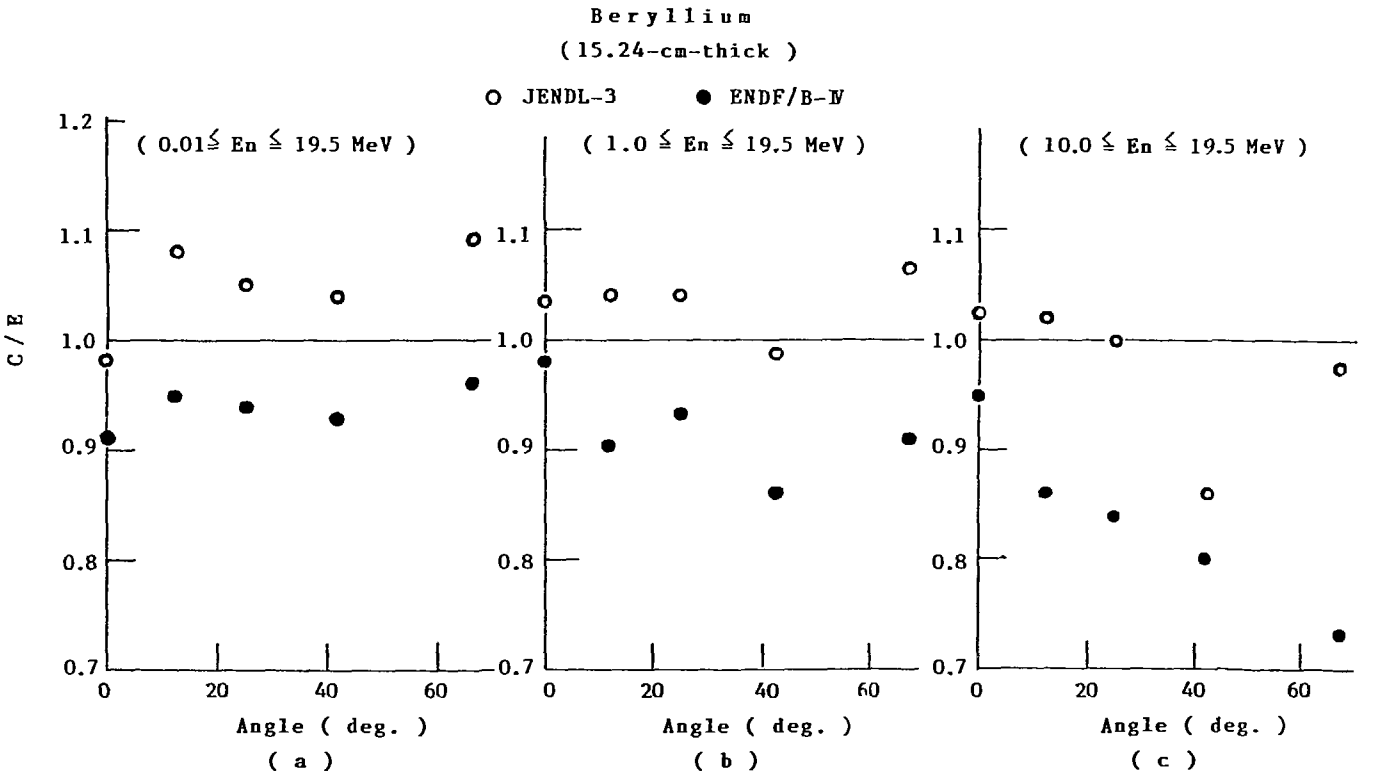

Fig. 3 The MCNP Calculation/ Experiment(C/E) ratio of fluxes integrated over three energy regions for the 15.24-cm-thick assembly; (a) above 0.01 MeV, (b) above 1.0 MeV, and (c) above 10.0 MeV.

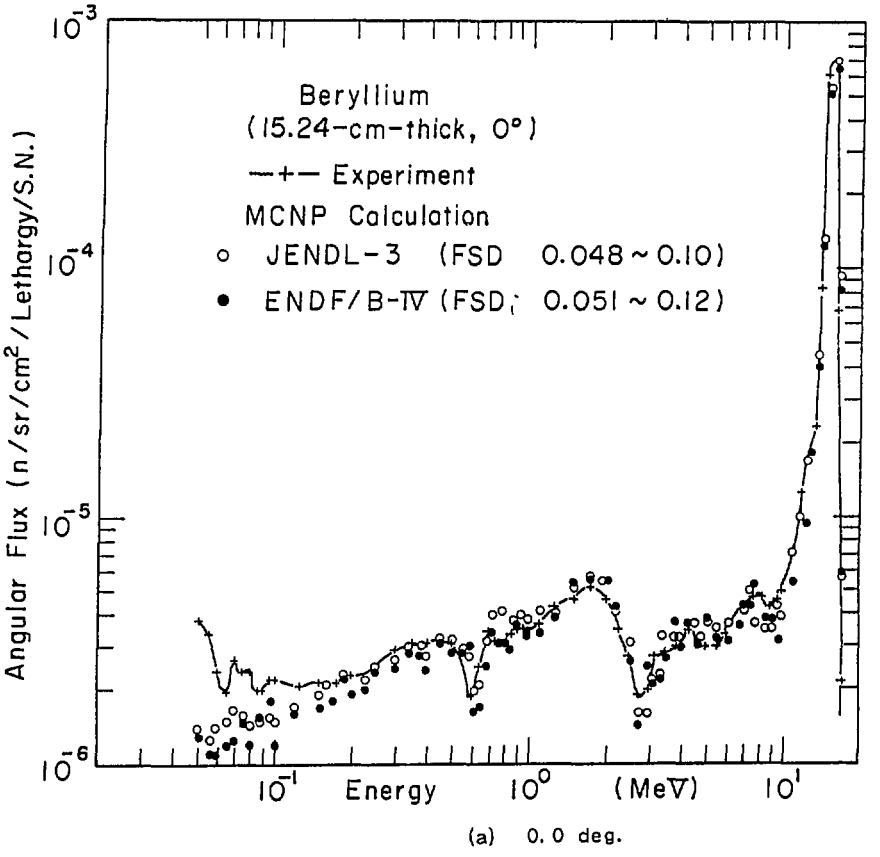

Fig. 4 Comparison of beryllium angular fluxes between FNS experiments and MCNP calculations with JENDL-3 and ENDF/B-Ⅳ for 15.24-cm-thick.

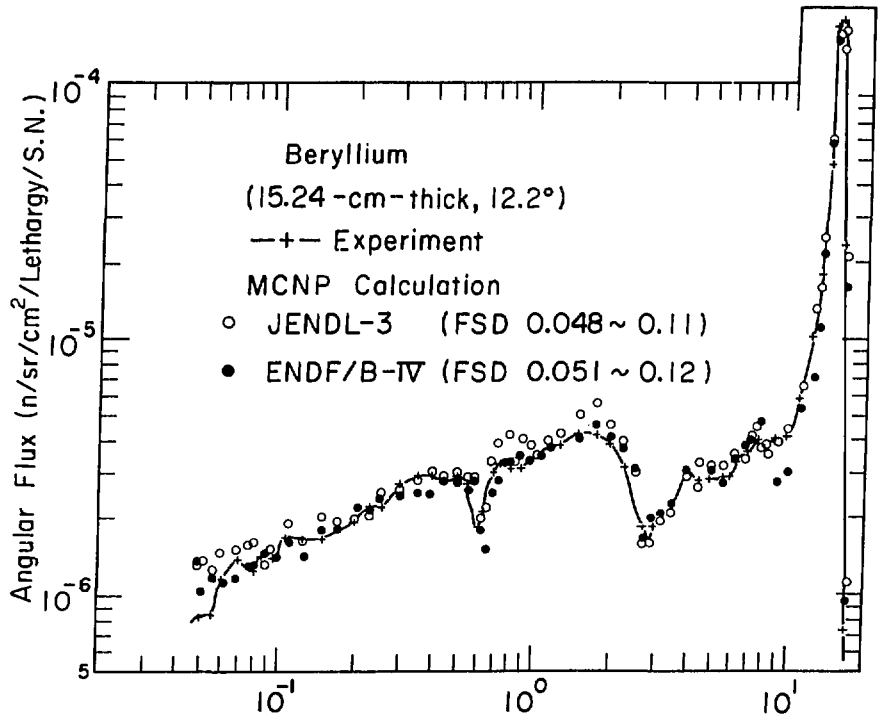

(b) 12.2 deg.

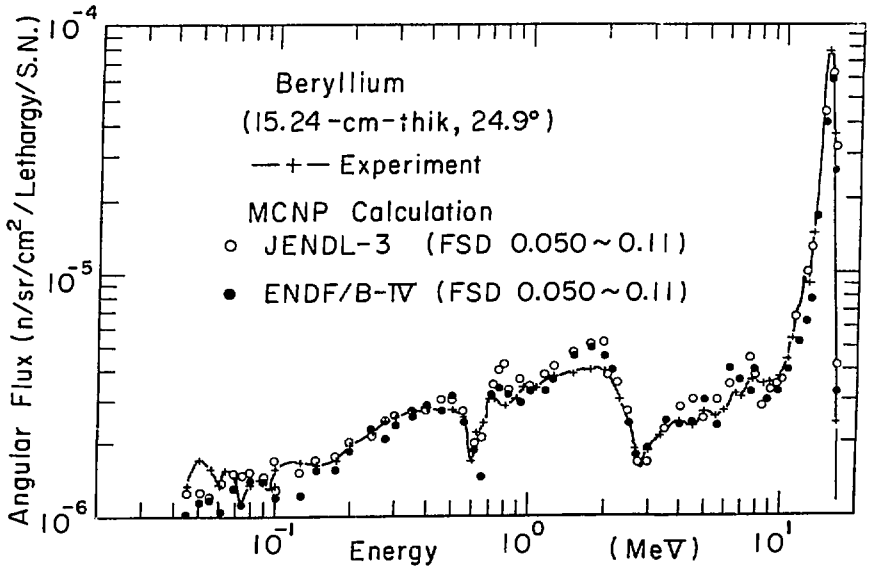

(c) 24.9 deg.

Fig. 4 (Continued)

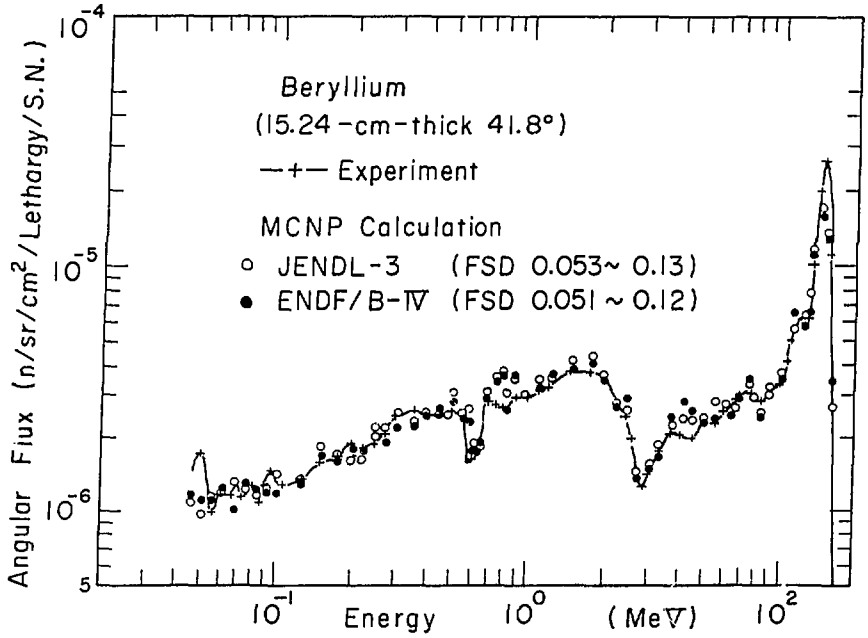

(d) 41.8 deg.

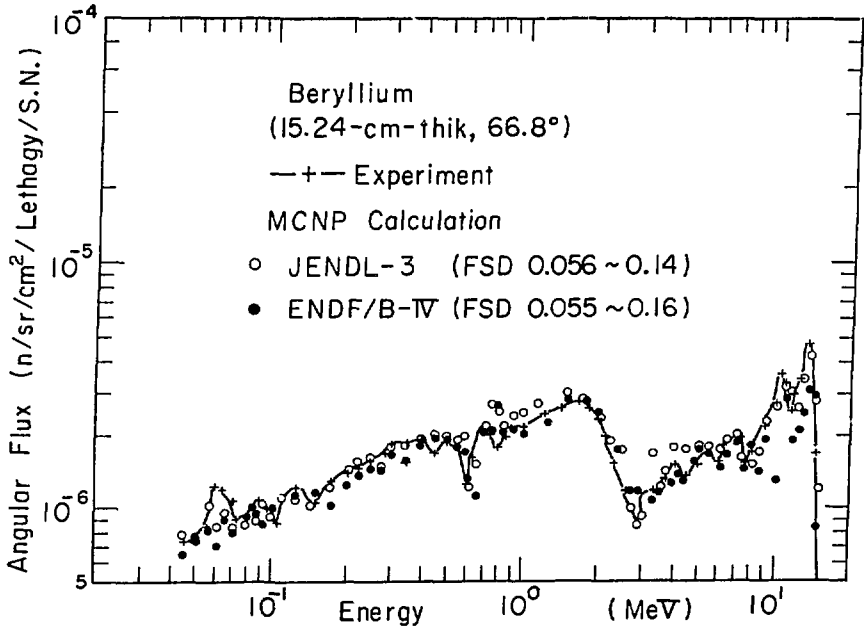

(e) 66.8 deg.

Fig. 4 (Continued)

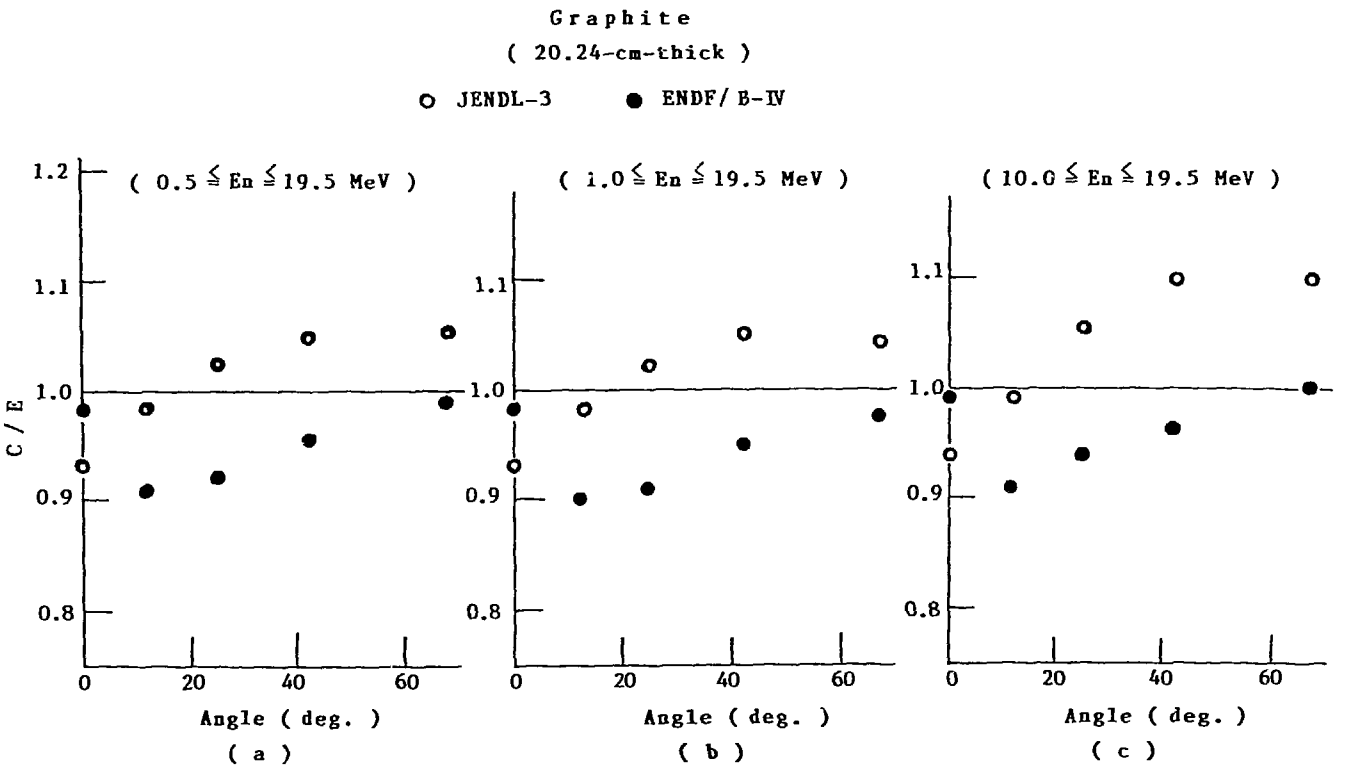

Fig. 5 The MCNP Calculation/Experiment(C/E) ratio of fluxes integrated over three energy regions for the 20.24-cm-thick assembly; (a) above 0.5 MeV, (b) above 1.0 MeV, and (c) above 10.0 MeV.

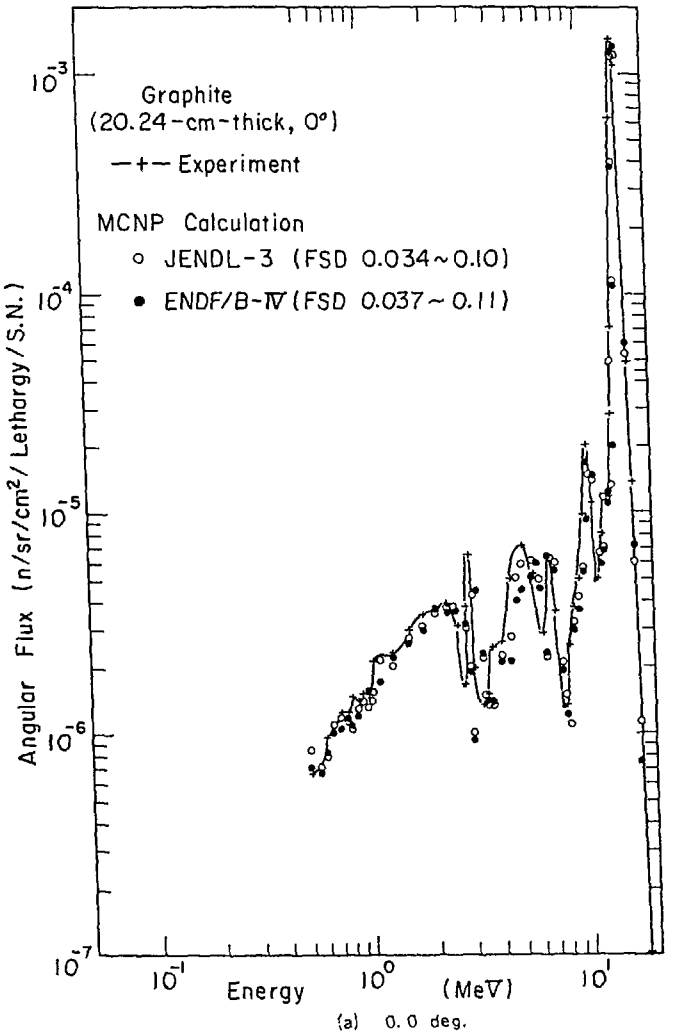

(a) 0.0 deg.

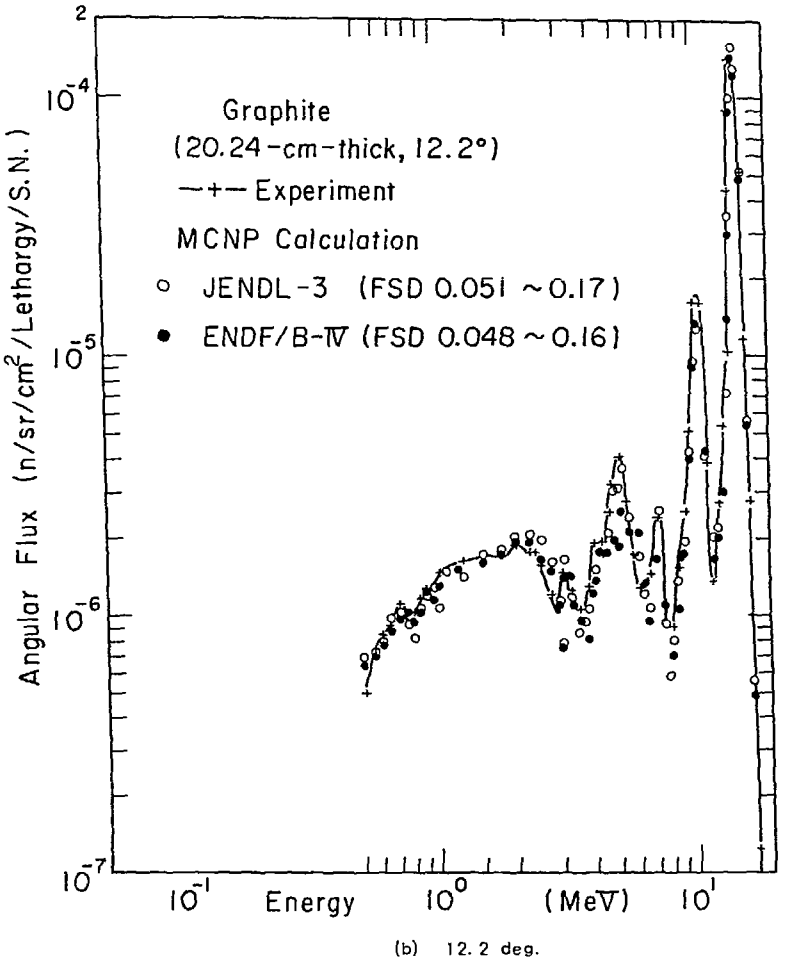

(b) 12.2 deg.

Fig. 6 Comparison of graphite angular fluxes between FNS experiments and MCNP calculations with JENDL-3 and ENDF/B-Ⅳ for 20.24-cm-thick.

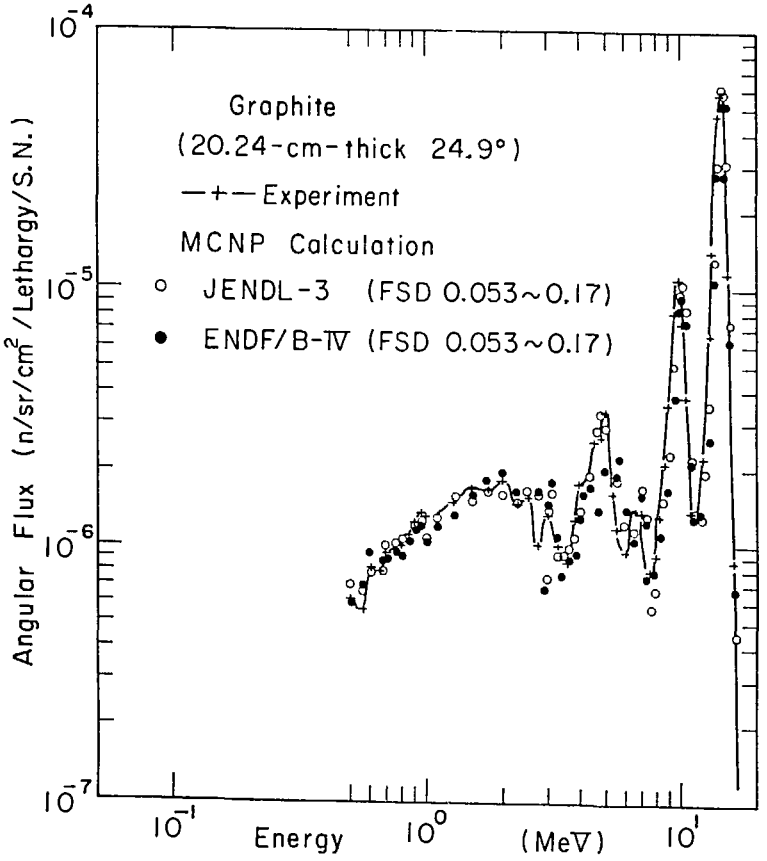

(c) 24.9 deg.

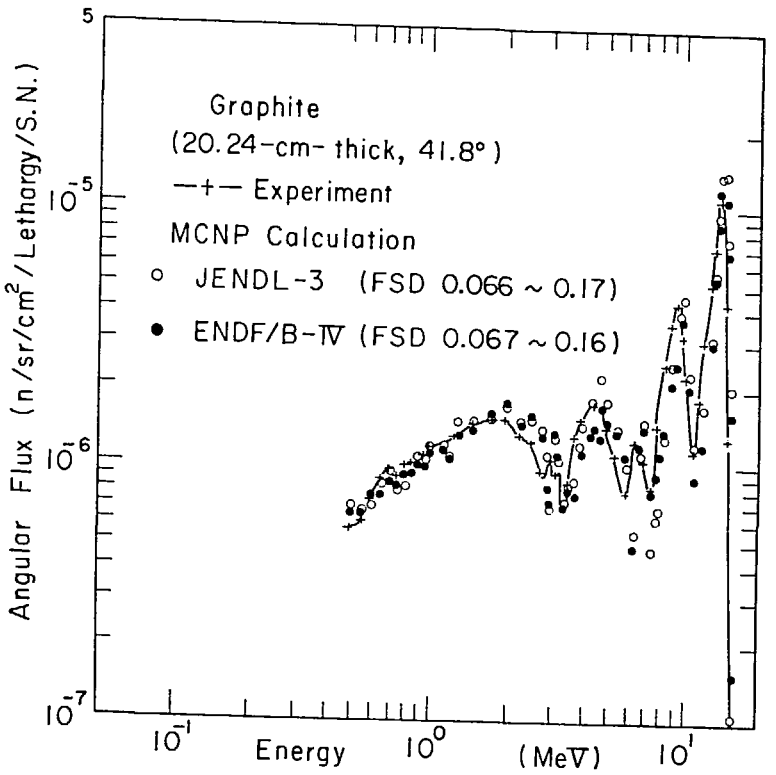

(d) 41.8 deg.

Fig. 6 (Continued)

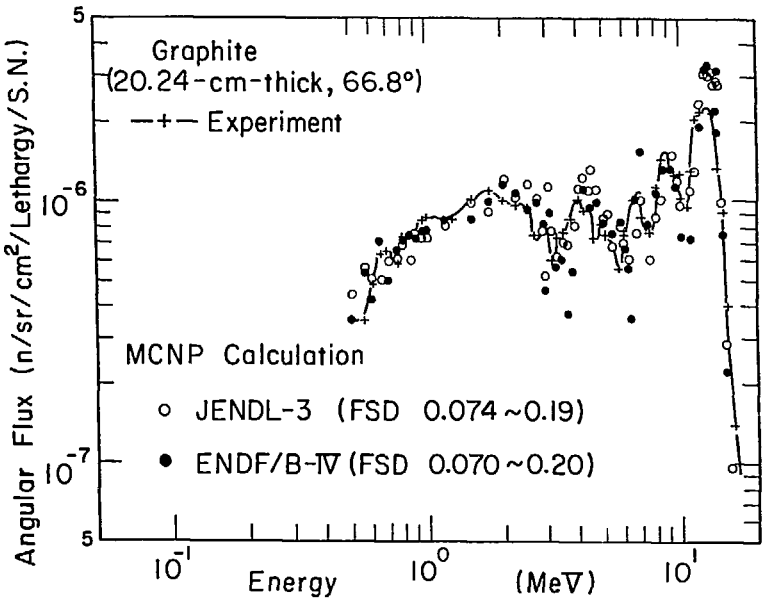

(e) 66.8 deg.

Fig. 6 (Continued)

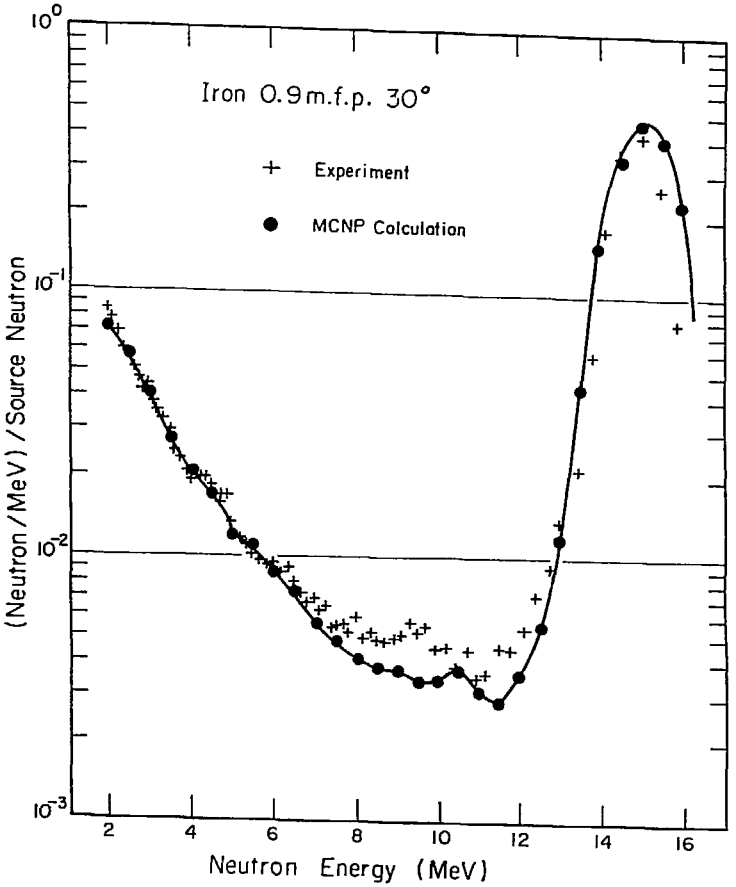

Fig. 7 Comparison of energy spectrum between LLNL experiments and MCNP calculations with JENDL-3 for 0.9 mfp of iron at 30°

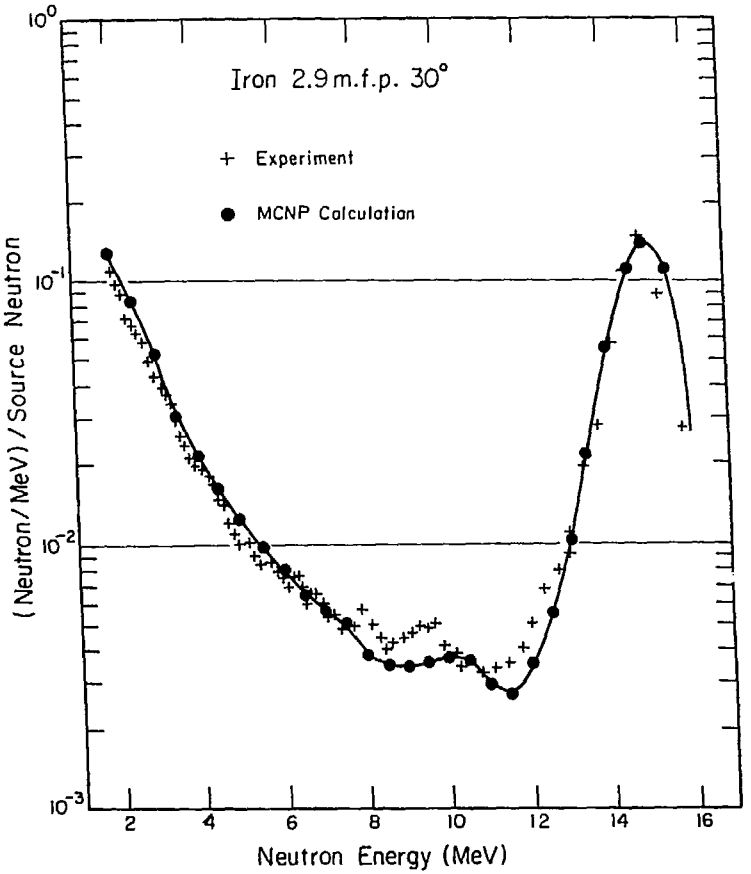

Fig. 8 Comparison of energy spectrum between LLNL experiments and MCNP calculations with JENDL-3 for 2.9 mfp of iron at 30°

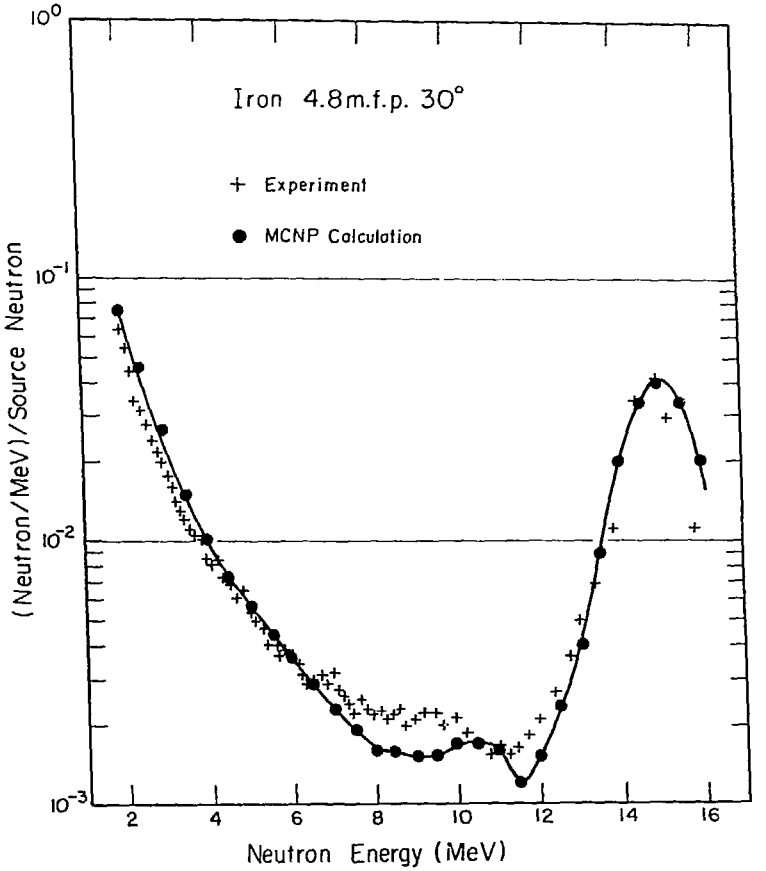

Fig. 9 Comparison of energy spectrum between LLNL experiments and MCNP calculations with JENDL-3 for 4.8 mfp of iron at 30°

11.2 Benchmark Test Through Analysis of Leakage Neutron Spectrum from Spherical Piles

M. Nakagawa
Japan Atomic Energy Research Institute
Tokai-mura, Naka-gun, Ibaraki-ken

A benchmark test of neutron cross sections of some materials has been performed by comparing the calculated and the measured leakage neutron spectra from spherical piles. Materials tested include ^{6}Li, ^{7}Li, Be, C, O and lead. In addition to JENDL-3, the results by JENDL-3/PR1 and JENDL-3T are also shown. JENDL-3 generally shows better agreement with the measurements compared with the other files.

1. Introduction

Leakage neutron angular spectrum from spherical piles composed of various materials have been measured in LLNL using a 14 MeV neutron source.[1] Since their geometries and configurations of piles are simple, those are quite useful for benchmark test of nuclear data related to fusion neutronics. Benchmark calculations for these problems have already been performed using ENDF/B-IV and JENDL-3/PR1 and the results are described in Ref(2). For a benchmark test of JENDL-3, a new 125 group double differential form cross section library has been produced and used in the present test.[3] In addition, the results obtained by JENDL-3T(a preliminary version of JENDL-3) are also shown in this article.

The radii of piles range from 0.5 to 1.4 mean free path. The energy and angular distribution of source neutrons are given in the reports by Hansen et al.[1]. All the calculations have been made by a Monte Carlo code MORSE-DD.[4]

2. Discussion

The conclusions derived from the comparison among the calculations and the measurements are described below for each material.

1) Lithium 6

The material used in this measurement is 95% enriched

lithium 6. The neutron spectrum at 30 degree are shown in Fig.1 where `●` shows the measured values and the calculated values by three files are presented together with the statistical uncertainties. The spectra by JENDL-3 and -3T agree within the statistical errors. Those overestimate the spectrum in the energy region 12 - 8 MeV and below 3 MeV. A better agreement is observed in 8 - 3 MeV in comparison with JENDL-3/PR1, so the nuclear data would be improved in those files. However, further revision is necessary to predict accurately the spectrum from ^{6}Li.

2) Lithium 7

As well known, ^{7}Li is an important material as a tritium breeder in a fusion reactor blanket. Therefore, a high accuracy is required in the neutron cross sections. The calculated spectra at 30 degree are compared with the measurement in Fig.2. The discrepancy above 12 MeV would be attributed to the treatment of the resolution in the measurement. JENDL-3 shows the best agreement in 10 - 8 MeV. A prediction accuracy of JENDL-3 seems to be satisfactory though a slight discrepancy is observed below 3 MeV.

3) Beryllium

Since beryllium is often used as a neutron multiplier, a high accuracy is required for the (n,2n) cross section and its energy and angular distribution of secondary neutron. The comparison of spectra is shown in Fig.3. The results by JENDL-3 agree very well with the measurement in 10 - 6 MeV, on the other hand slightly overestimate it in 6 - 4 MeV and at around 12 MeV. More detailed benchmark test is required in a lower energy part in order to evaluate an accuracy of the (n,2n) cross sections and the secondary energy spectrum.

4) Carbon

The spectra at 30 degree are compared in Fig.4. Three files can predict fairly well the measurement. JENDL-3T rather shows a better agreement than JENDL-3. Angular distribution at the forward direction of the inelastic scattering will be still inaccurate. The integrated spectra in E>10 MeV, 10>E>5 MeV and 5>E>2 MeV are compared in Table 1.a. JENDL-3 shows a good agreement with the measurement except for the energy region 10>E>5 MeV. The nuclear data of carbon satisfies a required accuracy at the present stage.

5) Oxygen

The spectrum was measured in the pile with liquid oxygen. The comparison is shown in Fig.5. The discrepancy observed in the elastic peak would be attributed to an inadequate conversion from the time spectrum to the energy spectrum. The energy of elastic peak can be accurately calculated based on the kinematics of the (d,t) reaction. All the calculations give larger values for the depressions at 6 MeV and around 4 MeV. Such a trend is observed in the integrated spectra as given in Table 1.b. The discrepancy observed in the results by JENDL-3/PR1 is significantly reduced in the other files. The integrated value of the elastic peak agree within ±2% between the measurement and the result by JENDL-3.

6) Lead

The angular spectra for lead are compared in Fig.6. The calculated spectra show large differences in 13 - 4 MeV. The discrepancy observed below 6 MeV in the case of JENDL-3T is reduced in JENDL-3, however it shows considerable underestimation in 6 - 10 MeV and overestimation in 12 - 10 MeV. The data, especially for discrete level inelastic scattering should be revised. It can be said that the (n,2n) cross section is improved in JENDL-3.

References

1) Hansen L.F. et al.: Nucl.Sci.Eng. 35, 227(1969), 40, 262(1970) and 60, 27(1976) see also Wong C. et al.: UCRL-51144(Rev.1 and 2)(1971)

2) Nakagawa M., Mori T. and Ishiguro Y.: "Benchmark Test of MORSE-DD Code Using Double-Differential Form Cross Section," JAERI-M 85-009(1985)

3) Nakagawa M., Mori T. and Kaneko K.: "Production of Multigroup Double-Differential Form Cross Section Library Using JENDL-3 and Benchmark Test of Fusion Neutronics Problems," JAERI-M 90-097 (1990)

4) Mori.T, Nakagawa M. and Sasaki M.: "One-, Two-, and Three-Dimensional Transport Code Using Multigroup Double-Differential Form Cross Sections," JAERI-1314(1988)

Table 1 Comparison of integrated neutron angular spectra

a) Carbon 2.9 m. f. p.

		Integrated flux (/str.) E>10MeV	10>E>5MeV	5>E>2MeV	TOTAL
30 degree	Expt.*	2.335−2	0.872−2	0.867−2	4.074−2
	J3/PR1**	2.184−2	0.912−2	0.912−2	4.008−2
		(0.94)	(1.05)	(1.05)	(0.98)
	J3/T**	2.290−2	0.928−2	0.907−2	4.125−2
		(0.98)	(1.06)	(1.05)	(1.01)
	JENDL−3**	2.325−2	0.945−2	0.847−2	4.117−2
		(1.00)	(1.08)	(0.98)	(1.01)

b) Oxygen 0.8 m. f. p.

		Integrated flux (/str.) E>10MeV	10>E>5MeV	5>E>2MeV	TOTAL
30 degree	Expt.*	5.703−2	0.447−2	0.810−2	6.960−2
	J3/PR1**	5.525−2	0.584−2	0.642−2	6.750−2
		(0.97)	(1.31)	(0.79)	(0.97)
	J3/T**	5.585−2	0.446−2	0.677−2	6.706−2
		(0.98)	(1.00)	(0.84)	(0.96)
	JENDL−3**	5.597−2	0.447−2	0.670−2	6.714−2
		(0.98)	(1.00)	(0.83)	(0.96)

* Ref. L.H. Hansen et al., NUcl. Sci. Eng. 60, 27 (1976)

** MORSE−DD, Source intensity = 0.936

( ) = Ratio of calculation to experiment

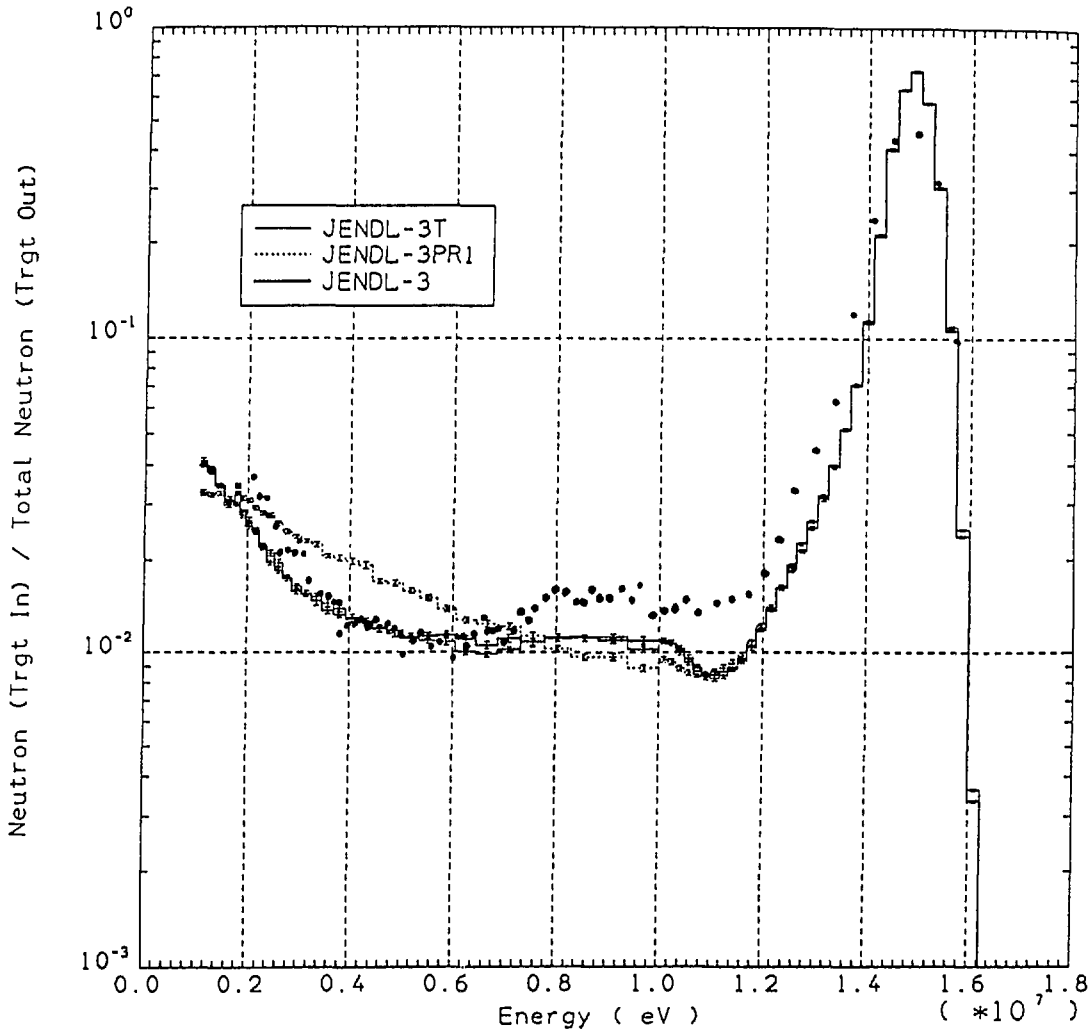

Fig.1 Leakage spectra from lithium 6 at 30 degree
`•` shows measured values.

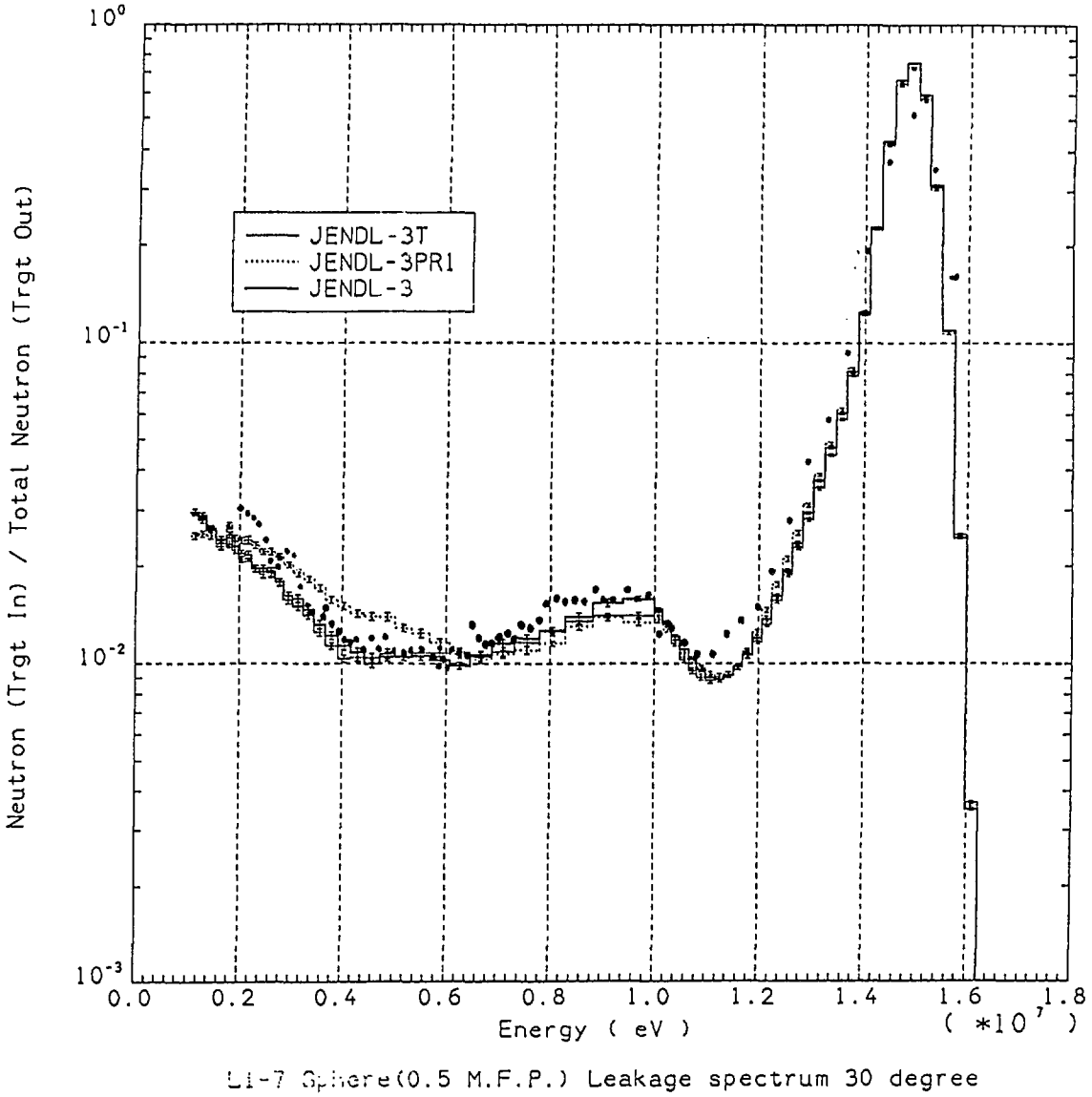

Fig.2 Leakage spectra from lithium 7 at 30 degree

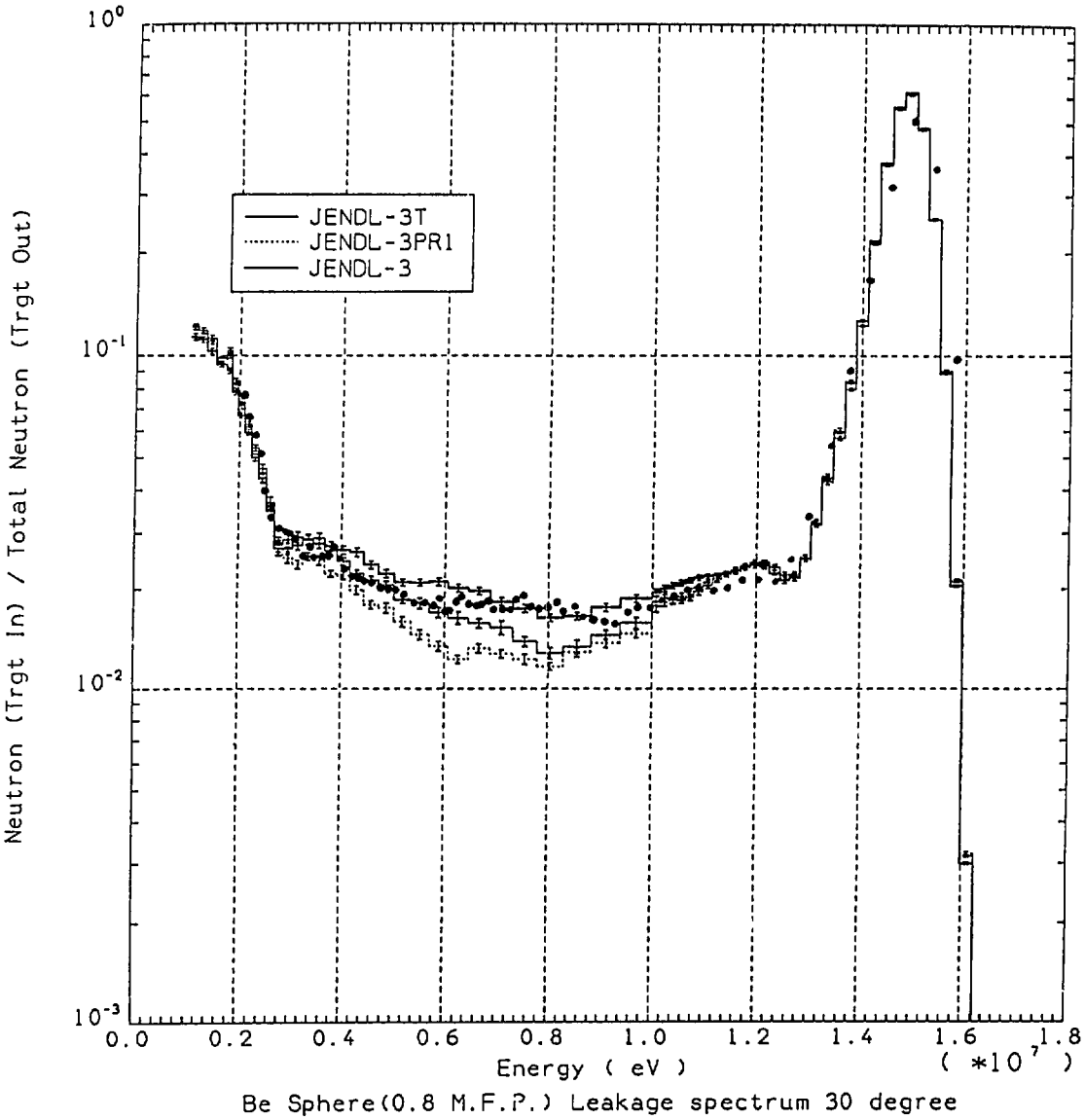

Fig.3 Leakage spectra from beryllium at 30 degree

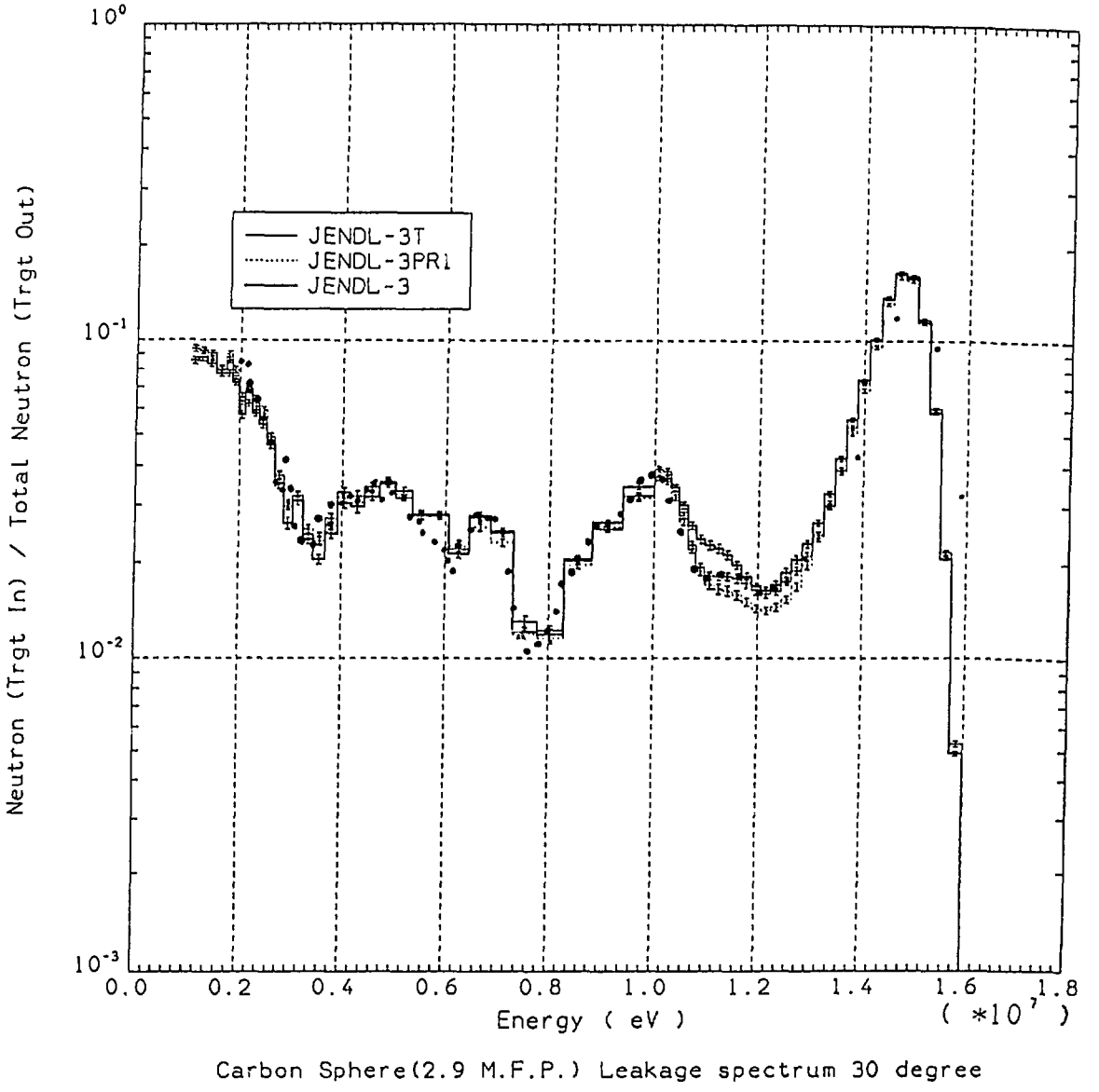

Fig.4 Leakage spectra from carbon at 30 degree

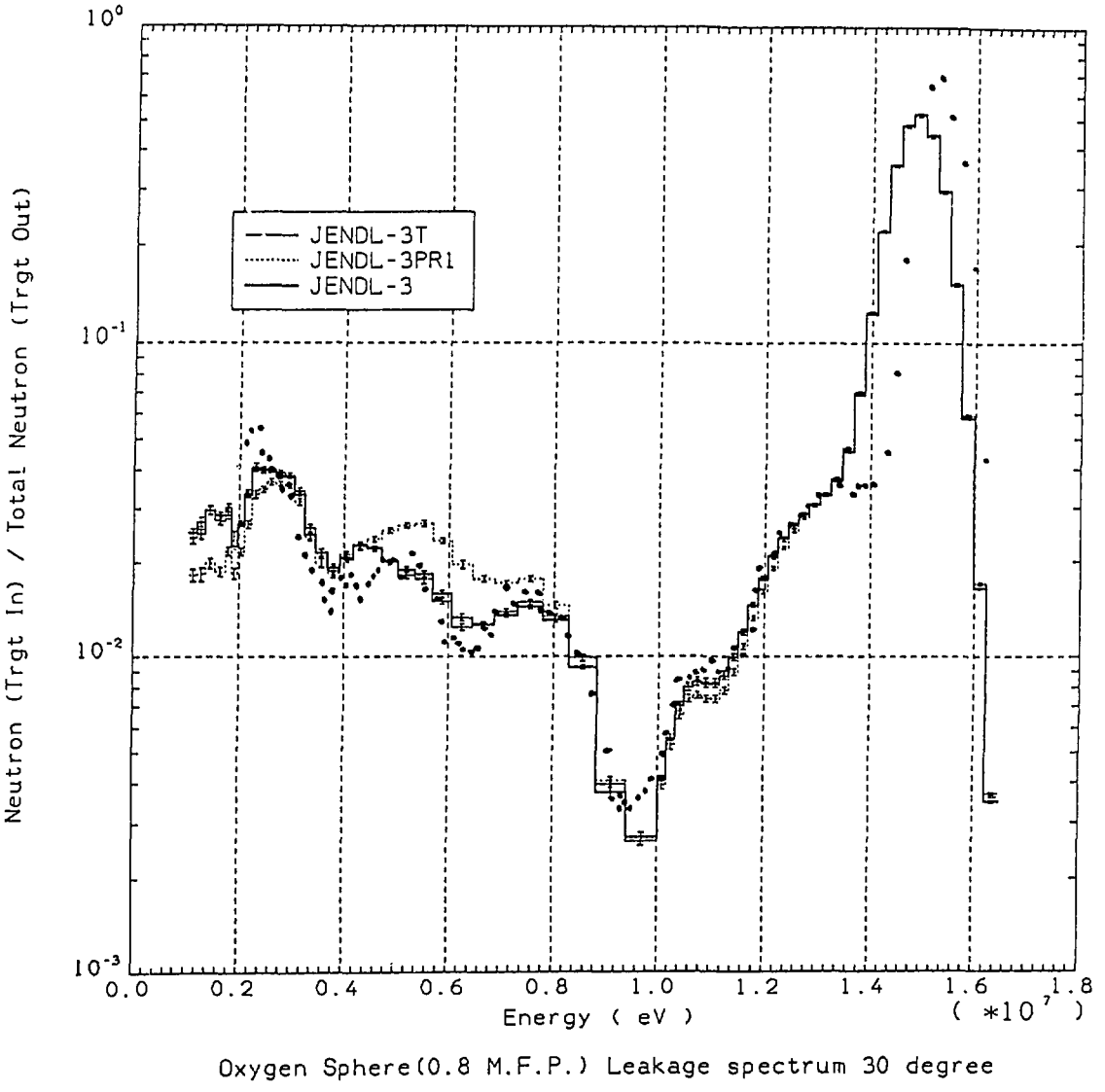

Fig.5 Leakage spectra from oxygen at 30 degree

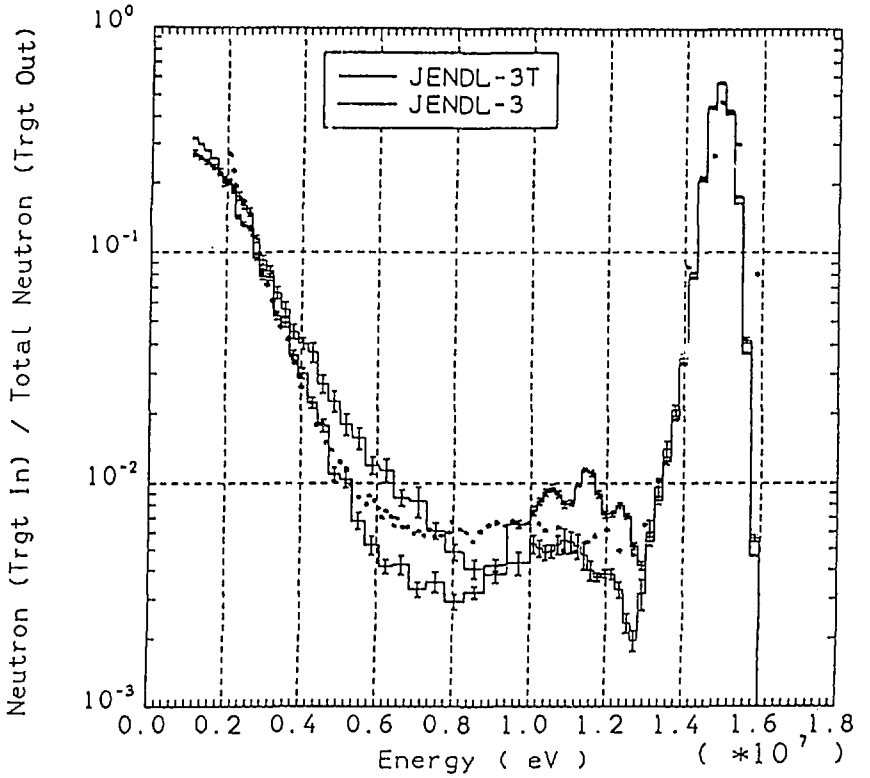

Fig.6 Leakage spectra from lead at 30 degree

11.3 Nuclear Data Test of JENDL-3 Using TOF Experiments at FNS

Yukio OYAMA and Hiroshi MAEKAWA
Department of Reactor Engineering
Japan Atomic Energy Research Institute
Tokai-mura, Naka-gun, Ibaraki-ken, 319-11 Japan

Angular neutron flux spectra leaking from slab assemblies of Be, C, Li_2O, Fe, Pb, liquid nitrogen and liquid oxygen have been analyzed by using the MCNP code to test the nuclear data in JENDL-3 through comparison with the experimental results. The comparisons are performed in the calculated to the measured value ratio with energy range and slab thickness as a function of leaking angle.

1. Introduction

To provide high quality benchmark data for the integral test of evaluated nuclear data such as JENDL-3, angular flux spectra were measured on fusion blanket materials, i.e., Be, C, Li_2O, iron, lead, liquid nitrogen and liquid oxygen for DT neutrons using the time-of-flight method.[1-5] The measurements were performed systematically with neutron leaking angle and transmission length. In the present paper, the status of nuclear data in JENDL-3 is discussed comparing the measured spectra with those calculated by the Monte Carlo code MCNP[6]. The comparison are summarized in the chart of the calculated to experimental values (C/E) for appropriate energy regions with thickness and angle.

2. Experiment and Calculation

The measured angles are 0, 12.2, 24.9, 41.8 and 66.8 degrees, and the slab thicknesses are 50, 200 and 400 mm except iron and liquid gases. Especially for iron, the slab of 600 mm in thick is added. A vacuum-insulated container was prepared for the experiments of liquid nitrogen and oxygen. Its inner size is 600 mm in diameter and 200 mm in thickness. The neutron spectra are obtained in the energy range of 0.05

to 15 MeV. The experimental method in detail is shown in the reference 1.

The measured data are reduced to the angular flux Φ by the following equation as illustrated by Fig. 1.

$$\Phi(\Omega,E_n)=\frac{C(E_n)}{\varepsilon(E_n)\cdot\Delta\Omega\cdot A_e\cdot S_n\cdot T(E_n)}$$

[n/sr/m^2/unit lethargy/source neutron],

where $\Phi(\Omega,E_n)$: neutrons with energy E_n per unit lethargy and emitting angle Ω per unit area and per unit source neutrons at the rear surface center of the assembly,

$C(E_n)$: counts per unit lethargy for neutrons of energy E_n,

$\varepsilon(E_n)$: efficiency of neutron detector at energy E_n,

$\Delta\Omega$: solid angle subtended by the detector to the point on the surface center of the assembly, i.e., $\Delta\Omega = A_d/L^2$, where

A_d: counting area of the detector,

L : distance from the rear surface to the detector,

A_e : effective measured area defined by the detector collimator system on the plane perpendicular to the axis at the assembly surface,

S_n : total source neutrons obtained by the associated alpha particle monitor,

$T(E_n)$: attenuation due to air in neutron flight path [=exp $\{-\Sigma_{air}(E_n)\cdot L\}$, Σ_{air}:macroscopic total cross section of air].

The MCNP calculations were performed with FSXLIB[7] library which includes the nuclear data processed by the NJOY code from JENDL-3. The calculation model is the same as the previous studies[2-3] which uses the point estimator and the no-importance region to simulate the collimator.

3. Results and Discussions

Lithium-Oxide

The calculated spectra seems to be perfect in comparison as shown in Fig. 2. The C/E trends also showed good agreements even in angle dependence shown in Fig. 3. The agreements are within 10% for all energy regions and angles.

Beryllium

Figure 4 shows the measured and the calculated spectra at 24.9 degree for 50.8 mm thick slab. It is clear that the JENDL-3 is improved much at the energy range of 2 to 10 MeV compared to the JENDL-3T. Figure 5 summarizes the C/E trends with energy, angle and thickness. The JENDL-3 improved for the range above 2 MeV, while the C/Es below 2 MeV is the same trends as the LANL but worse than the JENDL-3T.

Carbon

The calculated spectra are very good for three thicknesses of the slab as shown in Fig. 6. However, the C/E trends of high energy flux above 11 MeV at the 0 degree, shown in Fig. 7, diverge from each other with the slab thickness. This suggests that the elastic or the total cross sections is unbalanced compared to those of the JENDL-3PR2.

Nitrogen

It was pointed out in the previous test that there was the problem of nitrogen nuclear data in JENDL-3.[8] Recently, the data are re-evaluated. Figures 8 and 9 show the calculated spectra based on JENDL-3M (new evaluation) along with those based on ENDF/B-IV and the experiment. Good agreements are observed for all energy regions and the newly evaluated nuclear data of nitrogen seems to be fine.

Oxygen

It is clearly seen from Fig. 10 that the spectrum calculated with JENDL-3 follows all peaks and dips observed in the measured spectrum. The agreement between calculated spectra based on JENDL-3 are better than those based on ENDF/B-IV on the whole. Figure 11 shows the C/E

trends for the energy-integrated angular flux. Some of C/E values, especially, the flux above 10 MeV deviate from 1.0 over ±20%. This fact shows that the accuracy is insufficient in the nuclear data of angular-energy distributions.

Iron

The calculated spectra show fairly good agreement even in the resonance regions as shown in Fig. 12. However, Fig. 13 shows that there are large discrepancies in the flux at large angle above 10 MeV. Also in the low energy region below 100 keV, the large C/E change with increase of slab thickness is seen for the JENDL-3, in contrast to the ENDF/B-IV. Especially the difference below 100 kEv shows the deficiency of cross section around 100 keV.

Lead

Figure 14 shows a sample of measured and calculated angular spectra. The spectra calculated with JENDL-3 agree well with the measured ones except the region between 5 and 11 MeV. The C/E trends of integrated flux over energy for are shown in Fig 15. The under-estimation is clearly seen for the energy region of 5-10 MeV. This is caused by a lack of some inelastic levels. A good agreement should be expected when the number of inelastic level increases more than present limit in JENDL-3 or bunched levels are used.

4. Summary

Angular neutron flux spectra leaking from slab assemblies of lithium oxide, beryllium, graphite, liquid nitrogen, liquid oxygen, iron and lead have been analyzed by the MCNP code to test the nuclear data in JENDL-3. It is found from the comparisons that the Li_2O, Be, liquid nitrogen and liquid oxygen results show good agreements, but the graphite result is worse than that based on JENDL-3PR2 except for second level scattering, and for the iron the discrepancies are greatly changed with the thickness above 1 MeV and below 0.1 MeV regions. In the case of Pb, the calculation underestimates the experiment between 5 and 11 MeV, and good agreements are observed in the other energy region.

To improve the agreement more, some minor changes are required in

total, elastic scattering, (n,2n) and so on including secondary neutron energy and angular distributions for these nuclei. The range of such change is now close to the errors in both differential and integral experiments. At the present stage, the accuracy of neutron data of Li, Be, C, N, O, Fe and Pb in JENDL-3 seems to be good enough for the fusion neutronics application.

References

1) Oyama Y. and Maekawa H., Nucl. Instrum. Meth., A245, 173 (1986).
2) idem., Nucl. Sci. Eng., 97, 220 (1987).
3) Oyama Y., et al., J. Nucl. Sci. Technol., 25 [5],419 (1988).
4) Oyama Y., et al., "Measurements and Analyses of Angular Neutron Flux Spectra on Liquid Oxygen, Nitrogen and Iron Slabs," Int'l Conf. on Nuclear Data for Sci. & Technol., 13-17 May, 1991, Jülich, FRG.
5) Maekawa H. and Oyama Y., "Experiment on Angular Neutron Flux Spectra from Lead Slabs Bombarded by D-T Neutrons," Int'l Symp. on Fusion Nucl. Technol., 2-7 June, 1991, Karlsruhe, FRG.
6) Oyama Y., et al., Abstracts of Annual Meeting of J. At. Energy Soc., Tokyo, (1990).
7) Kosako K., et al., JAERI-M 88-076 (1988) (In Japanese).
8) Maekawa H., "Benchmark Test of JENDL-3," JAERI-M 90-025, pp69-87 (1990).

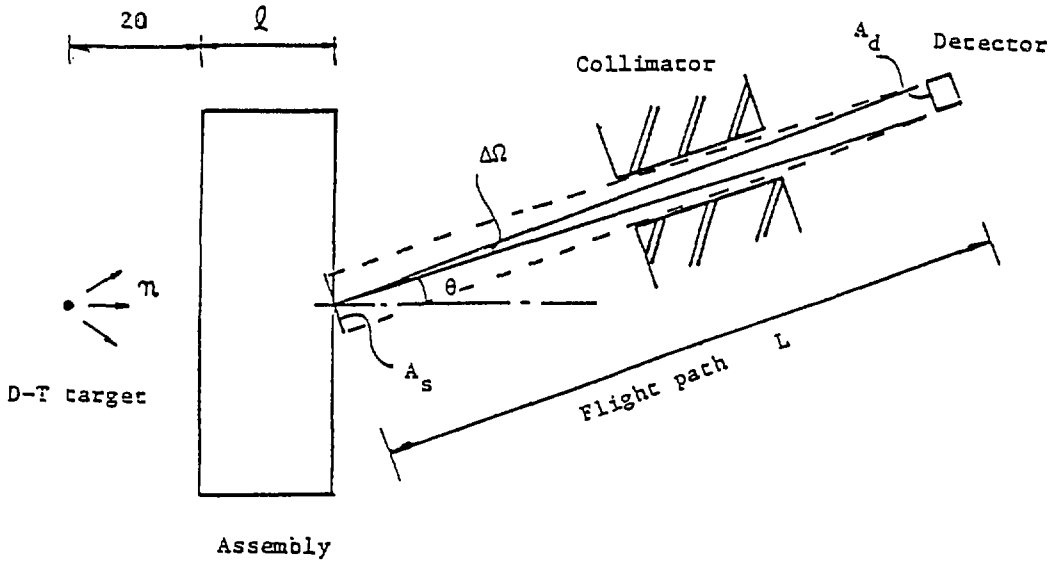

$$\Phi(r=0, z=20+t, \theta, E_n) = \frac{C(E_n)}{\epsilon(E_n)\cdot\Delta\Omega\cdot A_s\cdot S_n\cdot T(E)}$$

[n/sr/cm^2/unit lethargy/source neutron]

$C(E_n)$: counts per unit lethargy for neutrons of energy E_n

$\epsilon(E_n)$: detector efficiency for neutrons of energy E_n

$\Delta\Omega_n$: solid angle subtended by the detector at a point on surface of assembly ($\equiv A_d/L^2$)

A_s : area defined by the collimator on the vertical plane to the central axis at the surface of assembly

S_n : neutron yield

$T(E)$: attenuation by air

Fig. 1 Experimental arrangement.

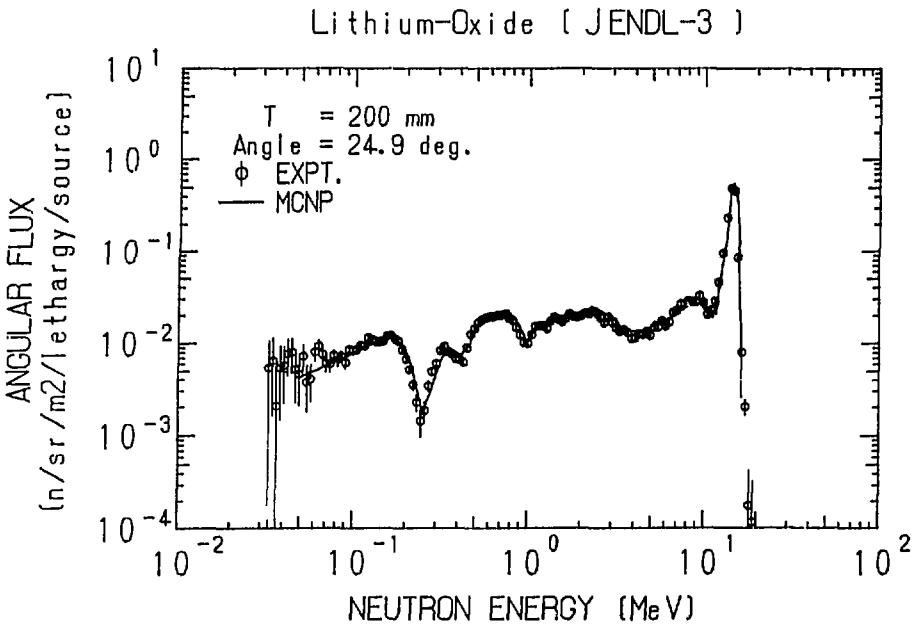

Fig. 2 Calculated and measured spectra on the Li_2O slab of 200 mm in thick at 24.9 degrees.

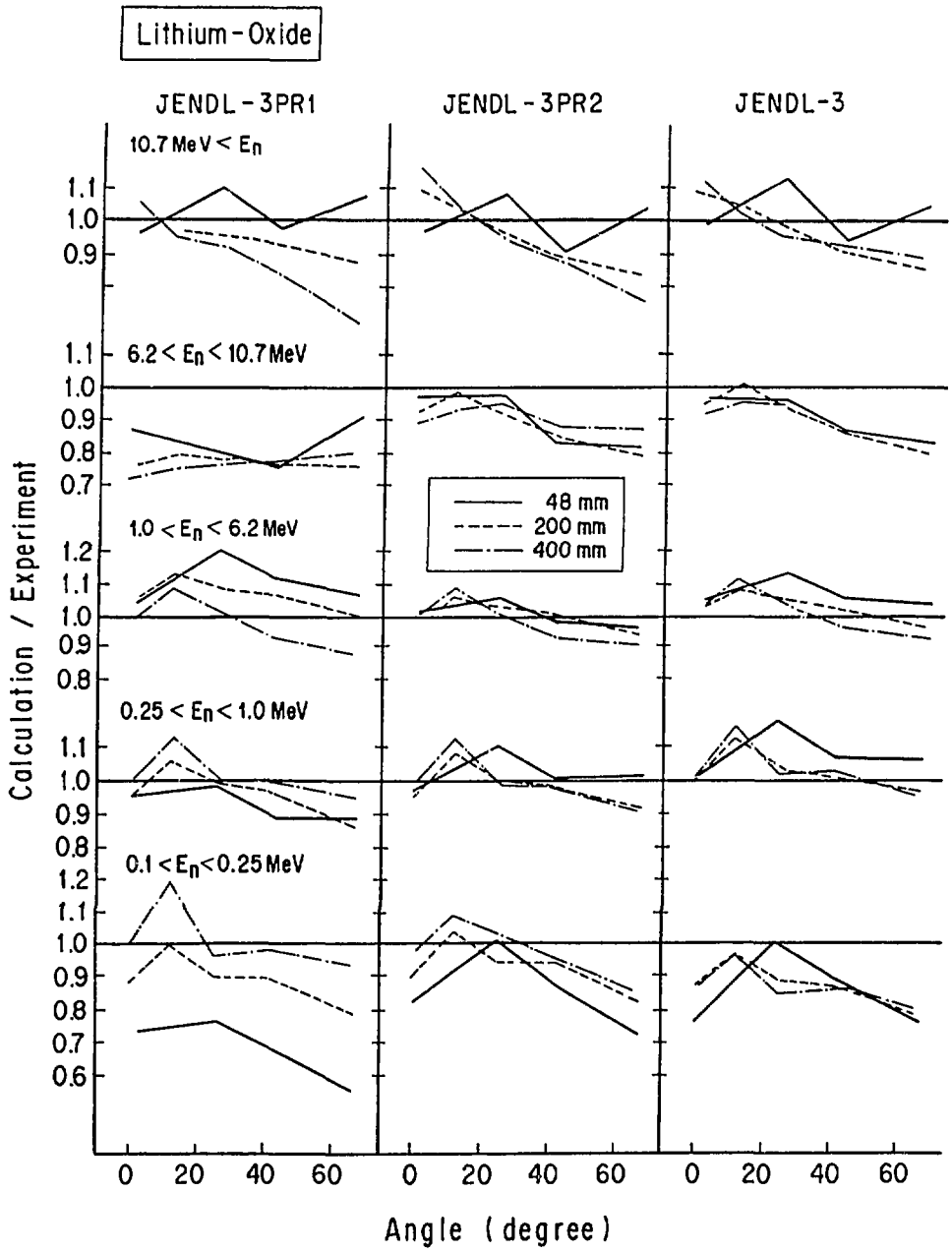

Fig. 3 Chart of the calculated and measured value ratios (C/E) of the Li_2O experiment with slab thickness and energy range as a function of leaking angle.

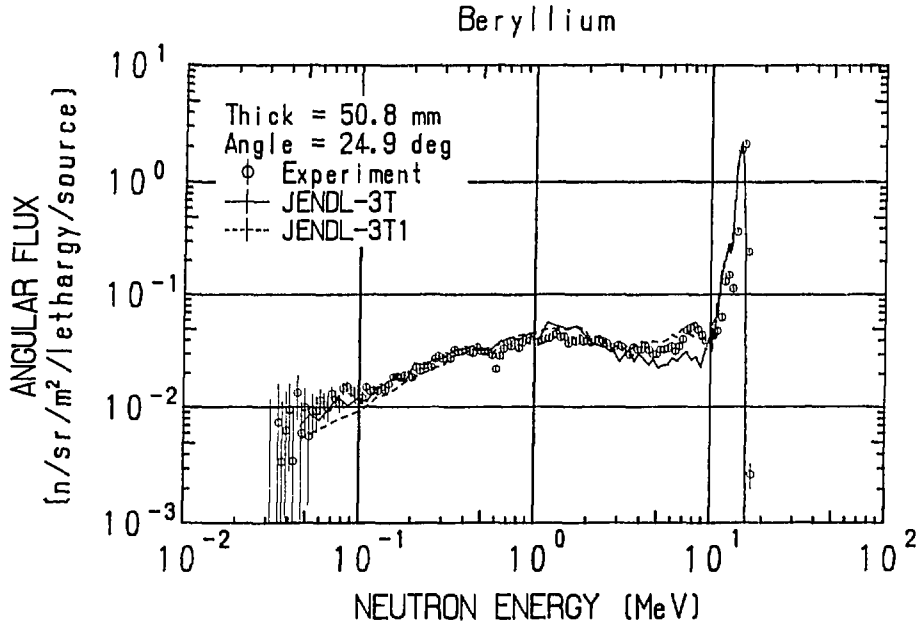

Fig. 4 Calculated and measured spectra on the Be slab of 50.8 mm in thick at 24.9 degrees.

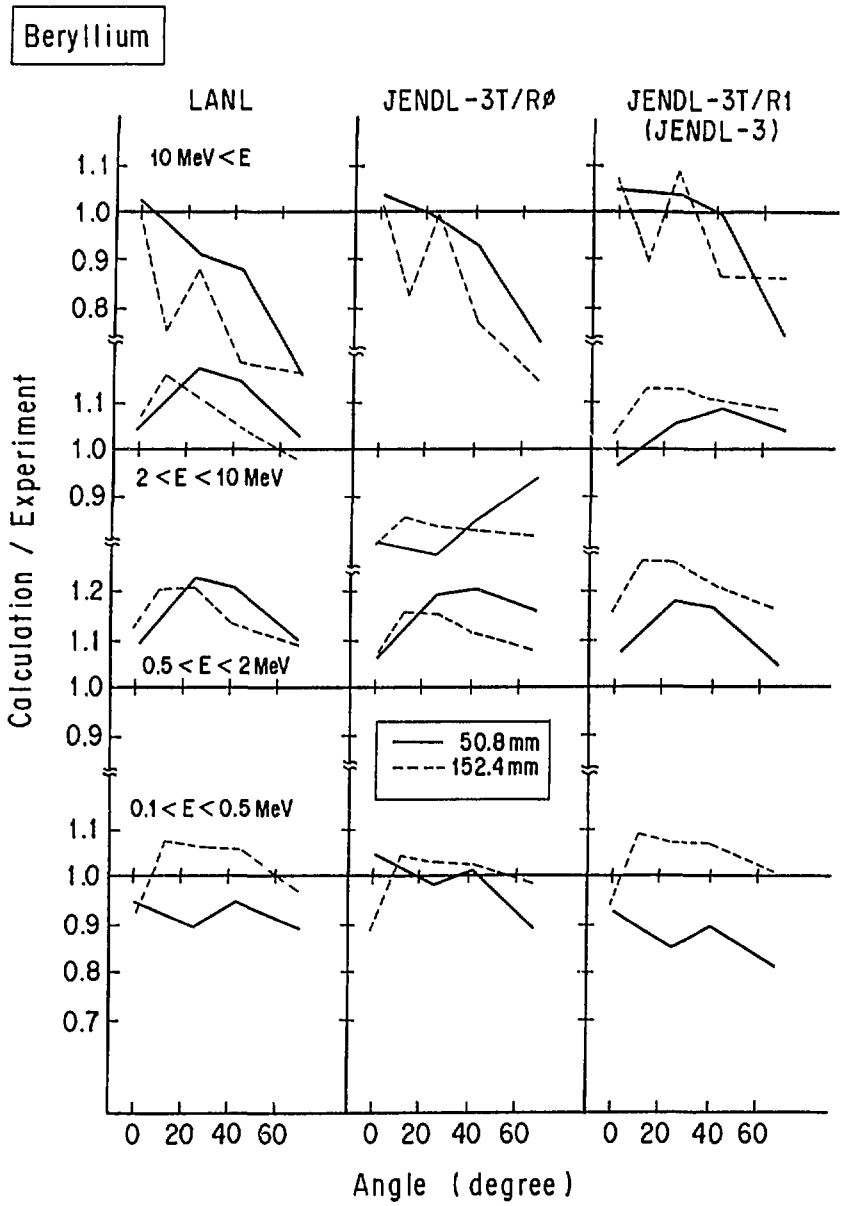

Fig. 5 Chart of the calculated and measured value ratios (C/E) of the Be experiment with slab thickness and energy range as a function of leaking angle.

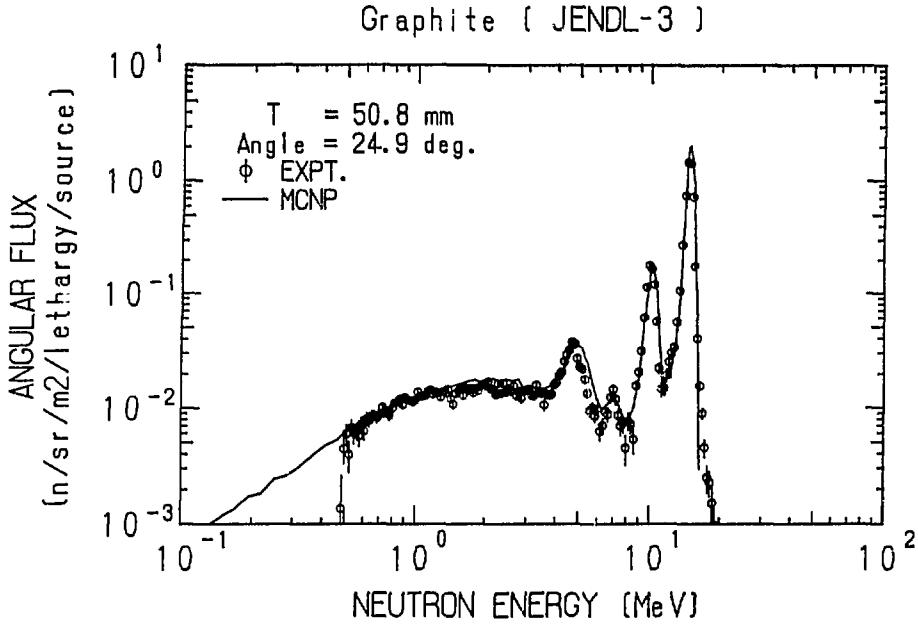

Fig. 6 Calculated and measured spectra on the graphite slab of 50.8 mm in thick at 24.9 degrees.

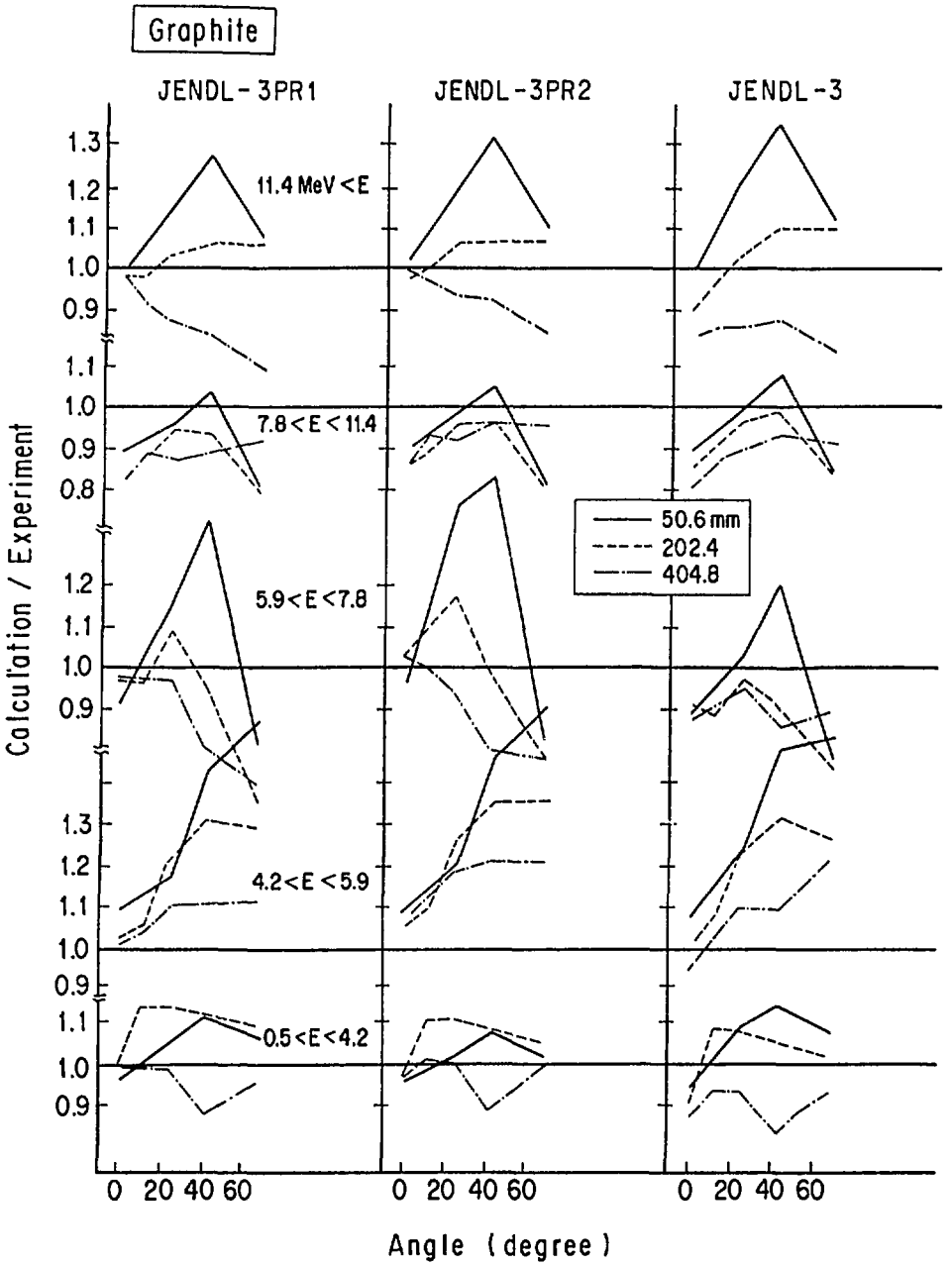

Fig. 7 Chart of the calculated and measured value ratios (C/E) of the graphite experiment with slab thickness and energy range as a function of leaking angle.

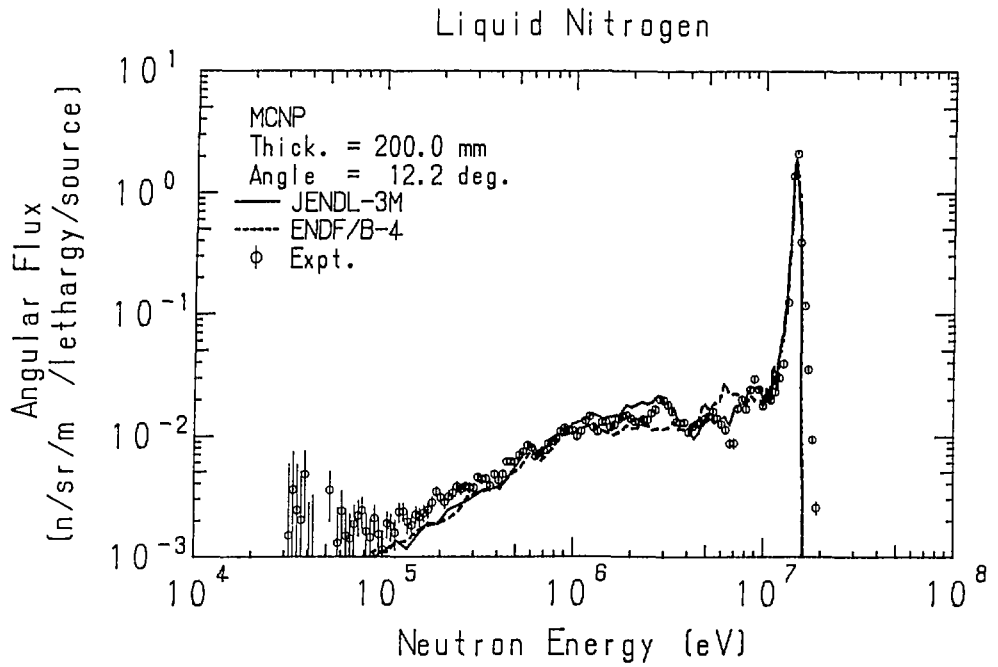

Fig. 8 Calculated and measured spectra on the liquid nitrogen slab at 12.2 degrees.

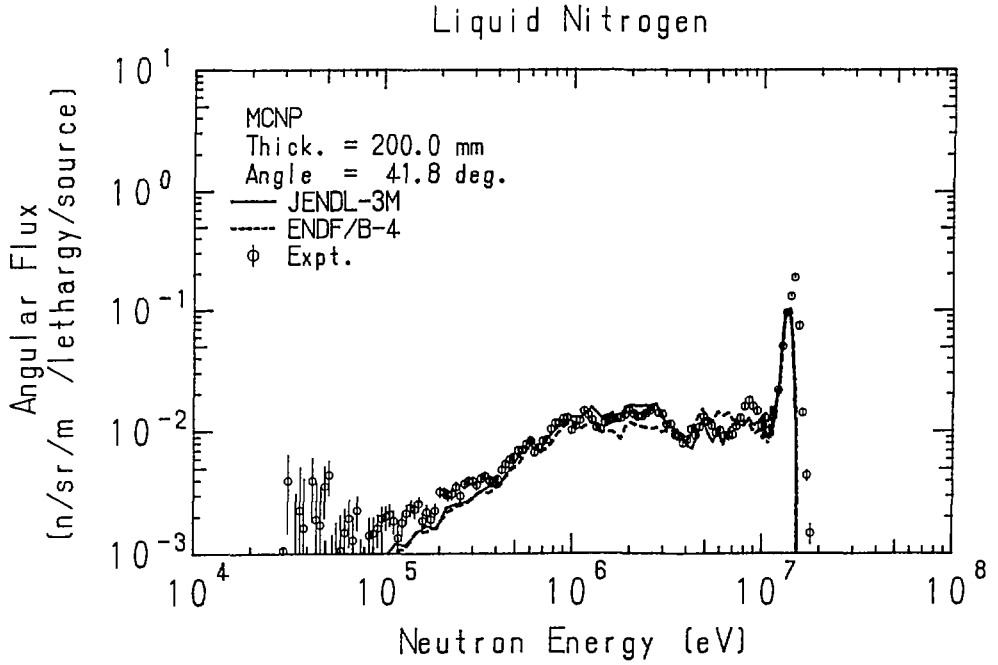

Fig. 9 Calculated and measured spectra on the liquid nitrogen slab at 41.8 degrees.

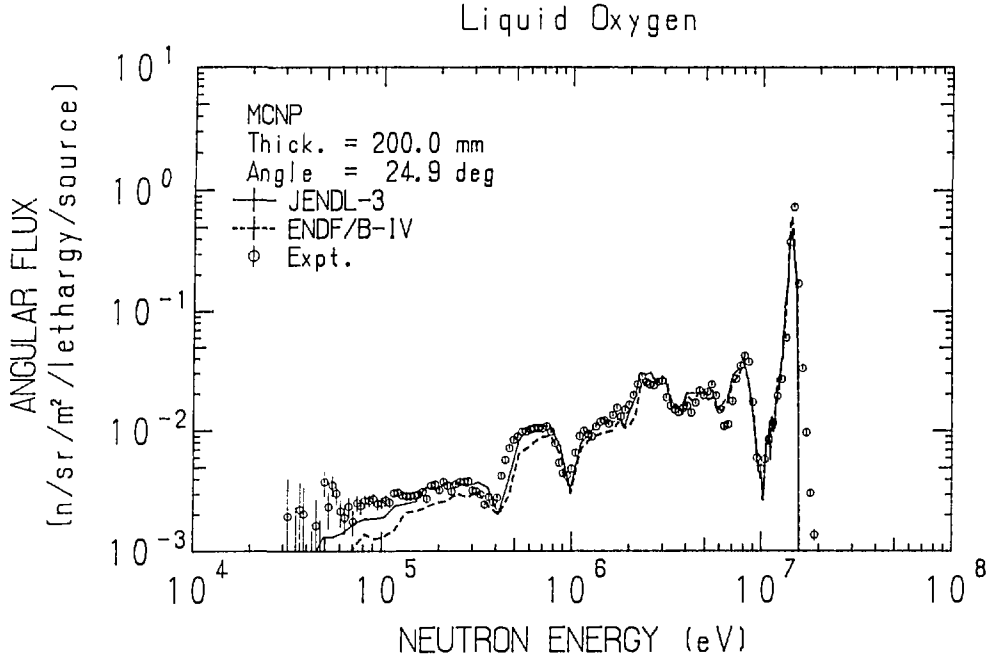

Fig. 10 Calculated and measured spectra on the liquid oxygen slab at 24.9 degrees.

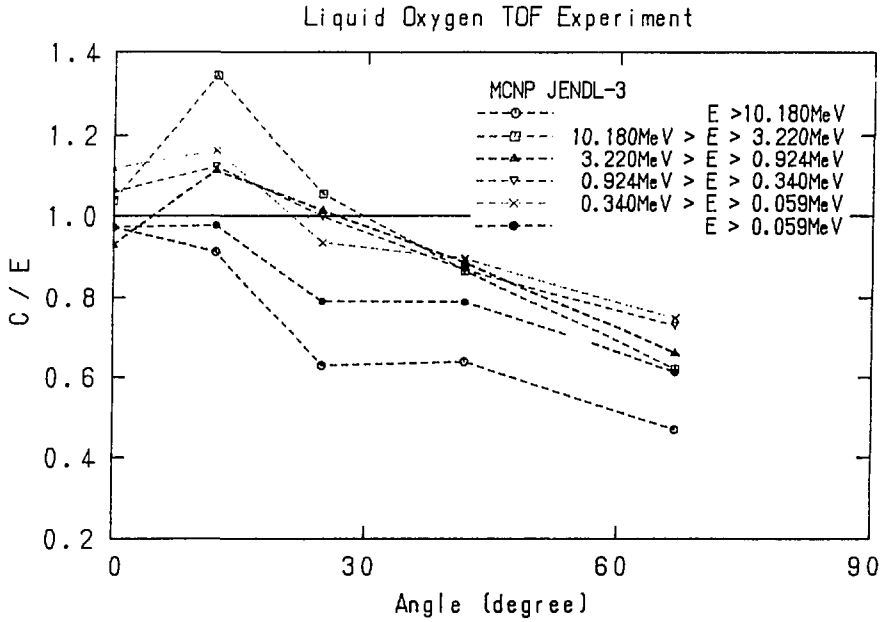

Fig. 11 Chart of the calculated and measured value ratios (C/E) of the liquid oxygen experiment with energy range as a function of leaking angle.

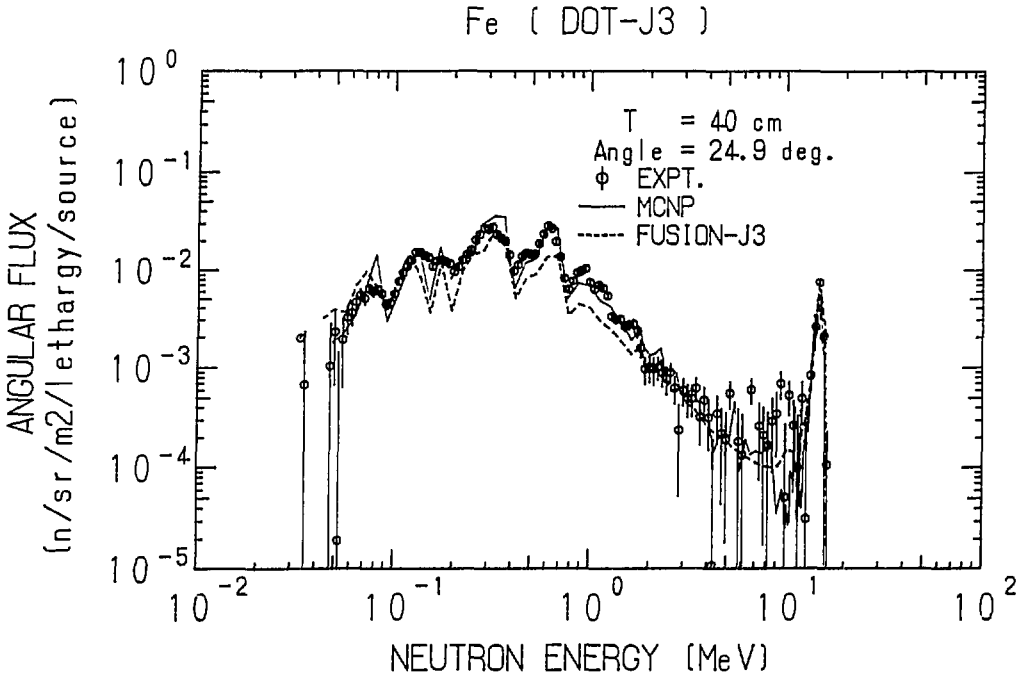

Fig. 12 Calculated and measured spectra on the iron slab of 400 mm in thick at 24.9 degree along with DOT3.5 calculation.

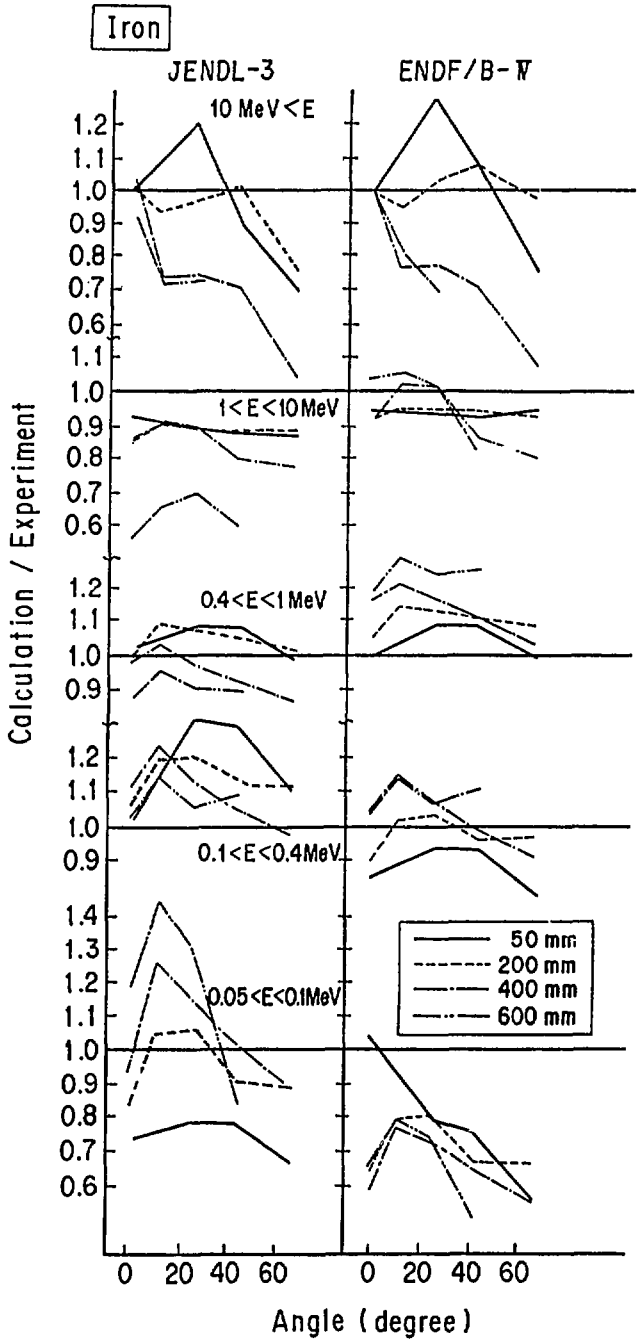

Fig. 13 Chart of the calculated and measured value ratios (C/E) of the iron experiment with slab thickness and energy range as a function of leaking angle

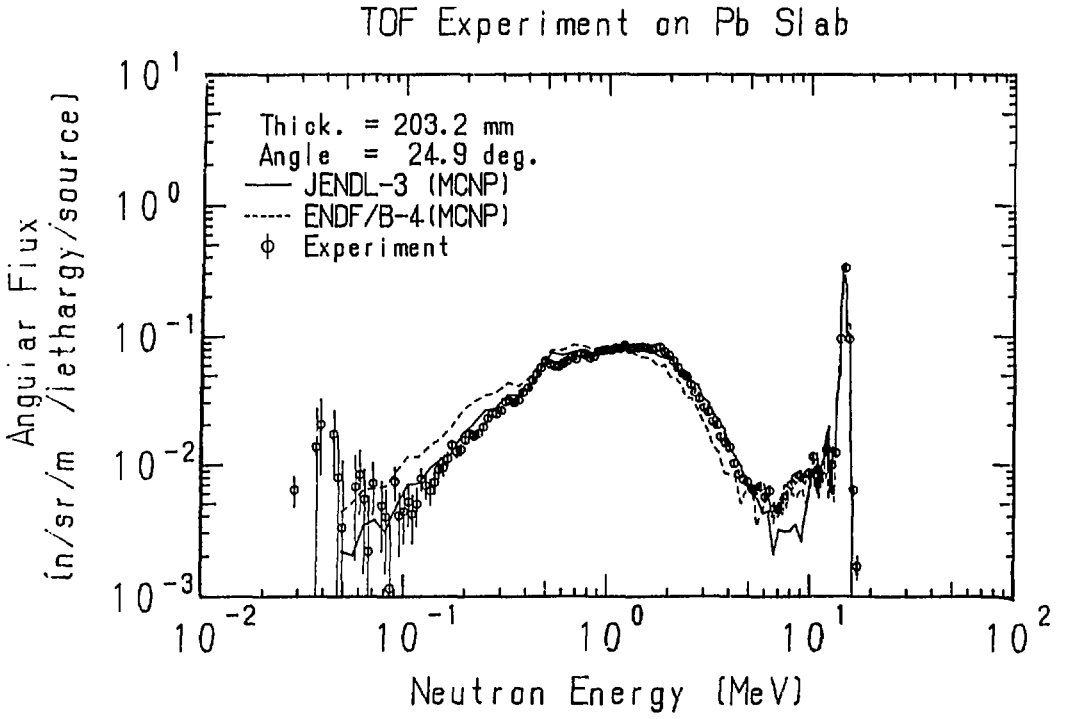

Fig. 14 Calculated and measured spectra on the lead slab of 203.2 mm in thick at 24.9 degrees.

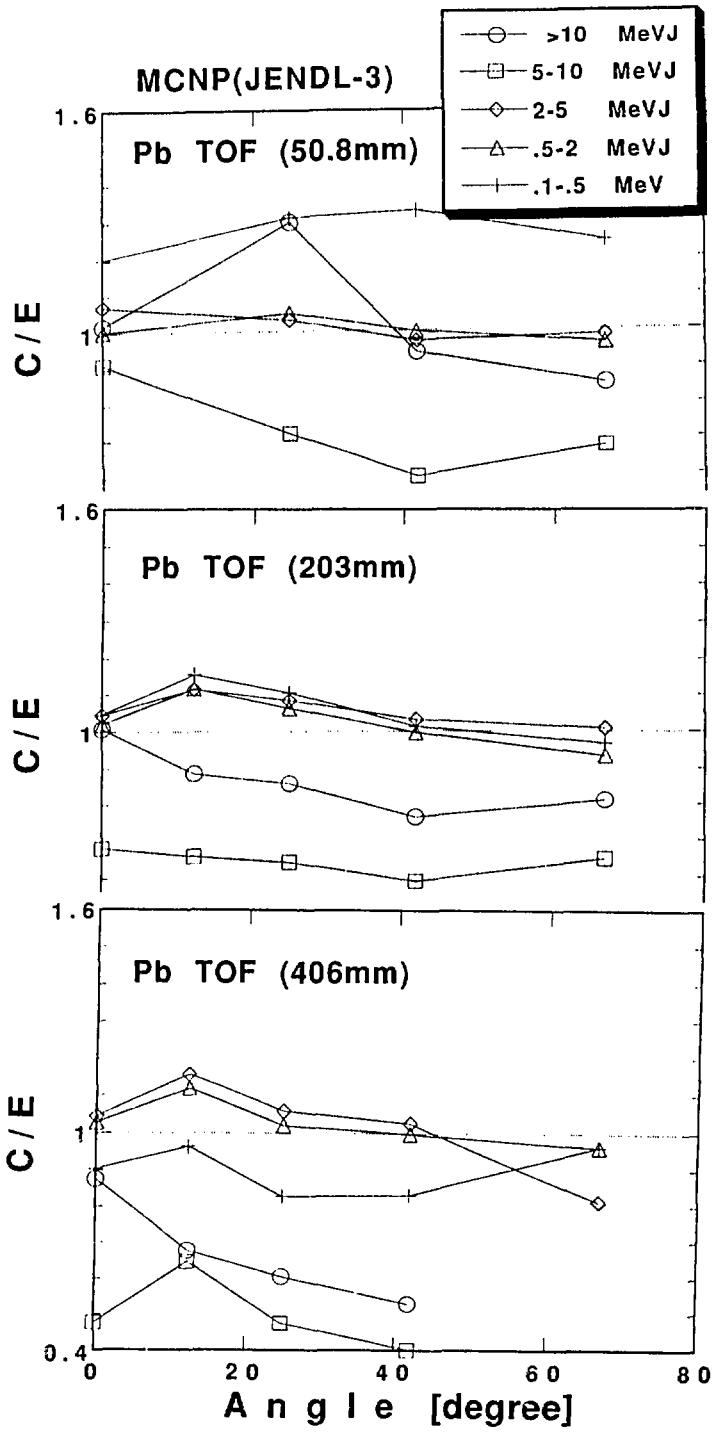

Fig. 15 Chart of the calculated and measured value ratios (C/E) of the lead experiment with slab thickness and energy range as a function of leaking angle.

11.4 Nuclear Data Test of JENDL-3 Using Integral Experiments at FNS

Hiroshi MAEKAWA and Chikara KONNO
Department of Reactor Engineering
Japan Atomic Energy Research Institute
Tokai-mura, Naka-gun, Ibaraki-ken, 319-11 Japan

A data test of JENDL-3 has been performed through the analyses of integral benchmark experiments at FNS. The experiments were carried out to measure various reaction rates such as $^{6}Li(n,\alpha)^{3}T$ and $^{27}Al(n,\alpha)^{24}Na$, and in-system neutron spectrum. Transport codes used in the analyses were SN code DOT3.5 and Monte Carlo code MCNP. The present data test suggests that the accuracy of neutron nuclear data for ^{7}Li, ^{9}Be, ^{12}C and Fe in JENDL-3 seems to be enough for the fusion neutronics application.

1. Introduction

Experimental examinations are required to verify the accuracy of both calculational methods and nuclear data which are used in the nuclear design and analysis of fusion reactors. For this purpose, the most suitable experiments are clean benchmark experiments on a simple geometry with simple material composition. A series of integral benchmark experiments have been carried out at FNS using materials of lithium-oxide, beryllium, graphite and iron.[1-4] Some of data test results for the preliminary versions of JENDL-3 were reported at the meetings and conferences.[5-7] A preliminary result of data test for JENDL-3 was presented at the 1989 Seminar on Nuclear Data.[8] This paper discusses the status of neutron data for ^{7}Li, ^{9}Be, ^{12}C and Fe in JENDL-3.

2. Integral Benchmark Experiments

The integral experiments discussed here have been carried out on the following four assemblies:

(1) 60cm-thick Li_2O cylindrical slab assembly (Li_2O assembly)
(2) 60cm-thick graphite cylindrical slab assembly (C assembly)
(3) 45cm-thick beryllium cylindrical slab assembly (Be assembly)
(4) 95cm-thick iron cylindrical slab assembly (Fe assembly)

The assemblies except Fe were prepared by stacking rectangular blocks in a framework consisting of thin-walled aluminum square tubes. The diameter for the three assembly was 630mm in area equivalent. In the case of Fe, the assembly was formed by 50 and 100mm-thick disks of 1m in diameter. The distance between the surface and D-T source target was 200mm. The quantities measured were tritium production rates of ^{6}Li and ^{7}Li, fission rates of ^{235}U, ^{238}U, ^{237}Np and ^{232}Th, reaction rates of $^{27}Al(n,\alpha)^{24}Na$, $^{58}Ni(n,p)^{58}Co$, $^{58}Ni(n,2n)^{57}Ni$, $^{93}Nb(n,2n)^{92m}Nb$, $^{115}In(n,n')^{115m}In$ and so on, and in-system neutron spectra. In the case of Fe, The experiment was concentrated to measure the neutron spectrum below 1 MeV. Because the neutrons of this energy region is important for the evaluation of nuclear heating in stainless steel shielding and super-conductive magnet. These quantities were measured along the central axis. The experiments were described in detail in the references[1-4].

3. Analyses

The present analyses were performed by the Monte Carlo code MCNP as well as the SN code DOT3.5. The cross section library for MCNP, named FSXLIB[9], was prepared using the NJOY system. The FUSION-J3 library[9] for DOT3.5 has 125 groups for neutron and 40 groups for gamma-ray. The calculational procedure was the same as that used in the previous data tests[5-8].

4. Discussions

Li_2O assembly

Figures 1 and 2 show the C/E (ratio of calculational to experimental values) distributions for $^{6}Li(n,\alpha)^{3}T$ and $^{27}Al(n,\alpha)^{24}Na$, respectively. The calculation was done by DOT3.5. As the data of ^{7}Li in JENDL-3 were modified a little from JENDL-3T based on previous benchmark test, the C/E distributions based on JENDL-3 are similar to those based on JENDL-3T. The tendency for the other reaction rates are almost the same as above two reactions. Most of the reaction rates calculated are in good agreement with measured ones within 10%. This fact suggests that integral values such as the tritium production rate can be predicted in the accuracy of at least 10%.

Be assembly

Figure 3 shows measured neutron spectrum at 327mm from the target along with that calculated by MCNP. Good agreements are observed between the measurement and calculation based on JENDL-3 for the spectrum above 10 MeV and 50 ~ 500 MeV. While there is a systematic deviation between them in energy range of 2 ~ 10 MeV. This is consistent with the analysis of time-of-flight experiment on Be slabs[10].

As a sample of C/E distribution for high threshold reactions, the result of $^{93}Nb(n,2n)^{92m}Nb$ is shown in Fig. 4. The calculation based on JENDL-3 agrees fairly well with the experiment for high threshold reactions. This observation is corresponding to the status of nuclear data at 14 MeV, i.e., the elastic cross section of JENDL-3 is higher by 4~7% than that of the others. The calculation overestimates the reaction rate of $^{115}In(n,n')^{115m}In$ between 300 and 600mm by 10~20%. This behavior corresponds to the spectrum measurement mentioned above.

The calculated integral flux between 0.16 and 0.5 MeV based on JENDL-3 agrees fairly well with the measured one (see Fig. 5), while the calculation underestimates the flux by 10~15% for LANL and JENDL-3PR1, and by 20% for ENDF/B-IV. This feature is consistent with the time-of-flight experiment on Be slabs[10]. In the cases of low-energy sensitive reactions, the C/Es are around 1.2 for all files. This is consistent with the C/Es of integral flux between 2 and 160 keV shown in Fig. 5.

This observation and the discrepancy of neutron spectrum of 2 ~ 10 MeV call for some minor changes of both ^{9}Be(n,2n) cross section itself and secondary neutron energy distribution.

C assembly

Figure 6 shows C/E distributions of ^{238}U(n,f), ^{58}Ni(n,p)^{58}Co and integrated flux above 5 MeV. The calculation was done by DOT3.5. The calculation agrees well with the experiment within 10%. The agreement for the other reactions are almost the same as those shown above. The status of ^{12}C neutron data in JENDL-3 seems to be fine.

Fe assembly

Figures 7 and 8 show the neutron spectrum in the Fe assembly at 610 and 1010mm from the target, respectively. The spectrum calculated by MCNP agrees well with measured one, but that by DOT3.5 deviates from the experiment. The same results were obtained for the other points measured. From the comparison, the following observations are reduced for the DOT3.5 calculation:

1) In the front region, the calculated spectra agree with the measured ones above 400 keV, but the calculation overestimates by a factor of about 2 below 400 keV.
2) On the contrary, the tendency in the rear region is quite different from that in the front region. A good agreement is observed below 100 keV, however, the calculation underestimates by a factor of about 0.2 above 100 keV.

The self-shielding effect was not considered in the DOT3.5 calculation. Above discrepancies suggest that the self-shielding effect is essential for the neutron transport calculation in a medium with much amount of resonance such as iron.

From the analysis by MCNP, the status of neutron data for Fe in JENDL-3 seems to be enough for applying to the fusion neutronics.

5. Summary

From the present data test through the analyses of integral benchmark experiments on lithium-oxide, beryllium, graphite and iron assemblies, neutron nuclear data of ^{7}Li, ^{9}Be, ^{12}C and Fe in JENDL-3 have enough accuracy for the fusion neutronics application.

References

1) Maekawa H., et al., "Fusion Blanket Benchmark Experiments on a 60 cm-Thick Lithium-Oxide Cylindrical Assembly," JAERI-M 86-182 (1986).
2) Maekawa H., et al., "Benchmark Experiments on a 60 cm-Thick Graphite Cylindrical Assembly," JAERI-M 88-034 (1988).
3) Maekawa H., et al., "Benchmark Experiment and Analysis of a Beryllium Cylindrical Assembly," 9th ANS Topical Mtg. on Technol. of Fusion Energy, Oct. 7-11, 1990, Oak Brook, Illinois.
4) Konno C., et al., "Measurements and Analyses of Low Energy Neutron Spectrum in a Large Cylindrical Iron Assembly Bombarded by D-T Neutrons," ISFNT-2, June 2-7, 1991, Karlsruhe, FRG.
5) Maekawa H., "Clean Benchmark Experiments and Analyses at FNS," JAERI-M 86-029 pp171-182 (1986).
6) Maekawa H., "Fusion Neutronics Integral Test for JENDL-3T," JAERI-M 88-065, pp198-211 (1988).
7) Maekawa H., et al., Fusion Technology 15 1283 (1989).
8) Maekawa H., "Benchmark Test of JENDL-3," JAERI-M 90-025, pp69-87 (1990).
9) Kosako K., et al., "Cross Section Libraries Based on JENDL-3 for Fusion Neutronics Analysis," JAERI-M 90-149, pp11-13 (1990).
10) Oyama Y. and Maekawa H., Nucl. Sci. Eng., 97, 220 (1987).

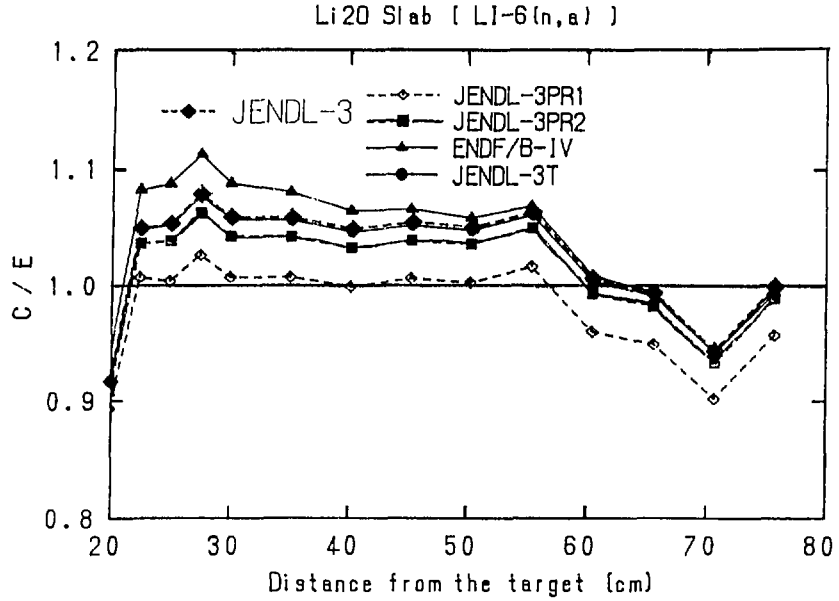

Fig. 1 Comparison of C/E values for the ^{6}Li tritium production rate in Li_2O assembly.

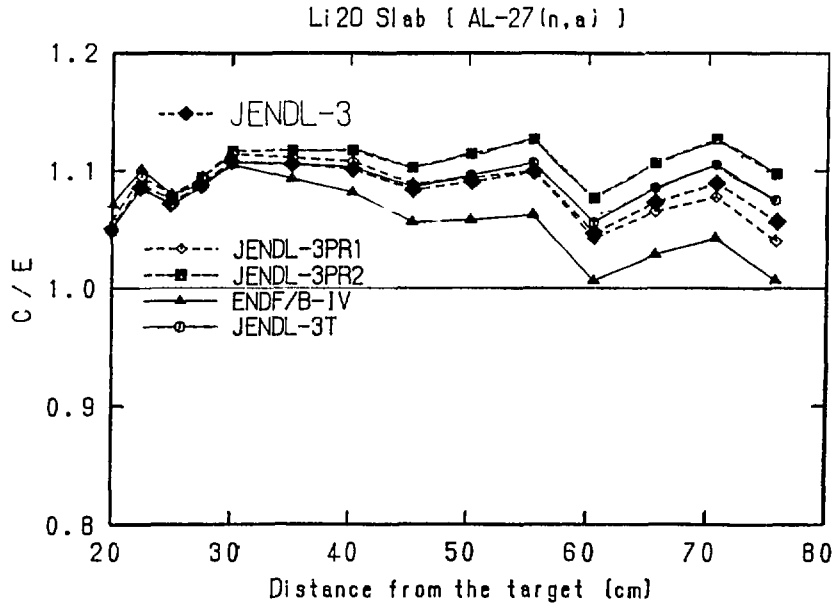

Fig. 2 Comparison of C/E values for the reaction rate of $^{27}Al(n,\alpha)^{24}Na$ in Li_2O assembly.

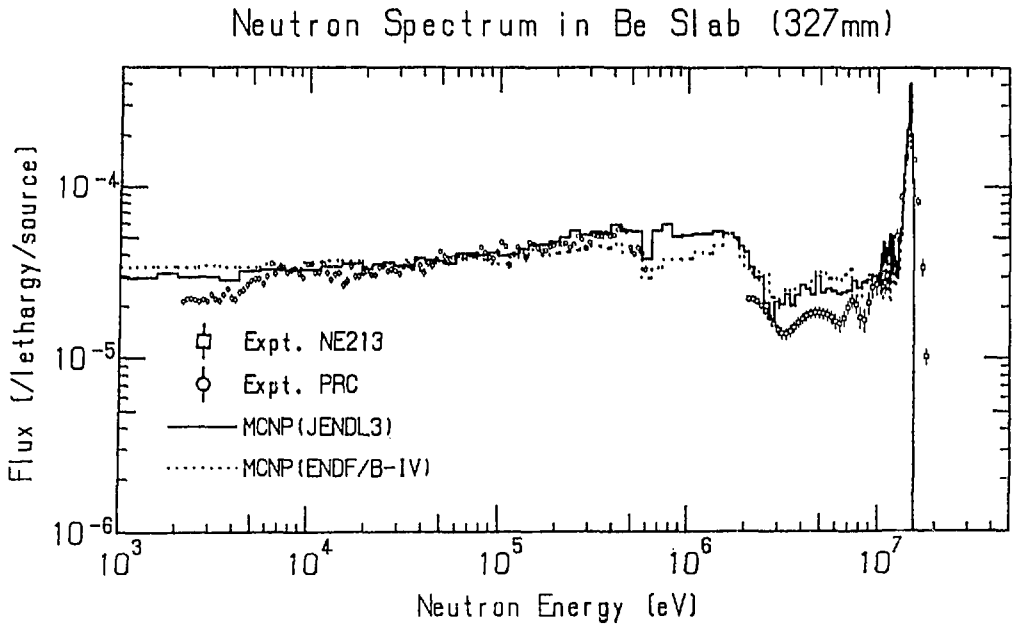

Fig. 3 Measured and calculated neutron spectra in Be assembly at 327mm from the target.

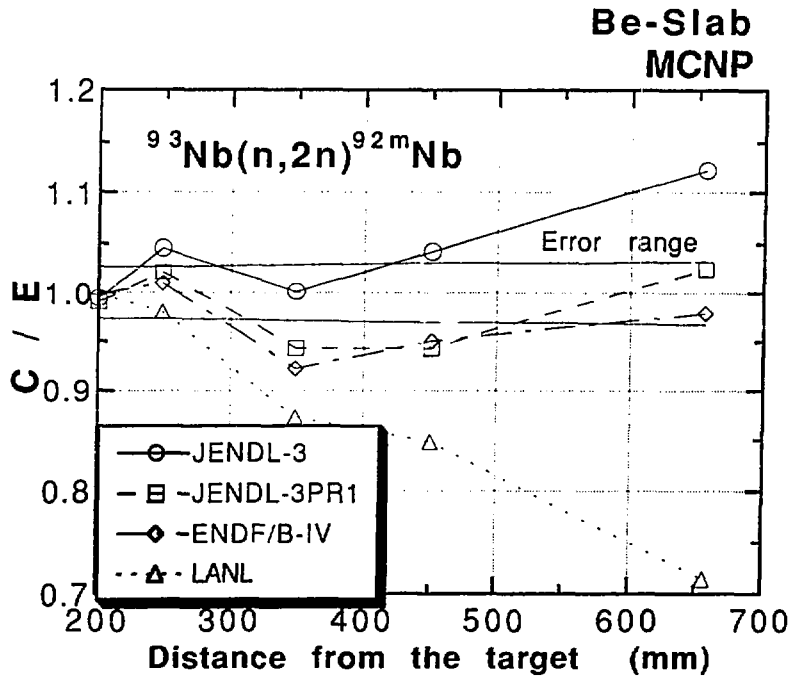

Fig. 4 Comparison of C/E values for the reaction rate of $^{93}Nb(n,2n)^{92m}Nb$ in Be assembly.

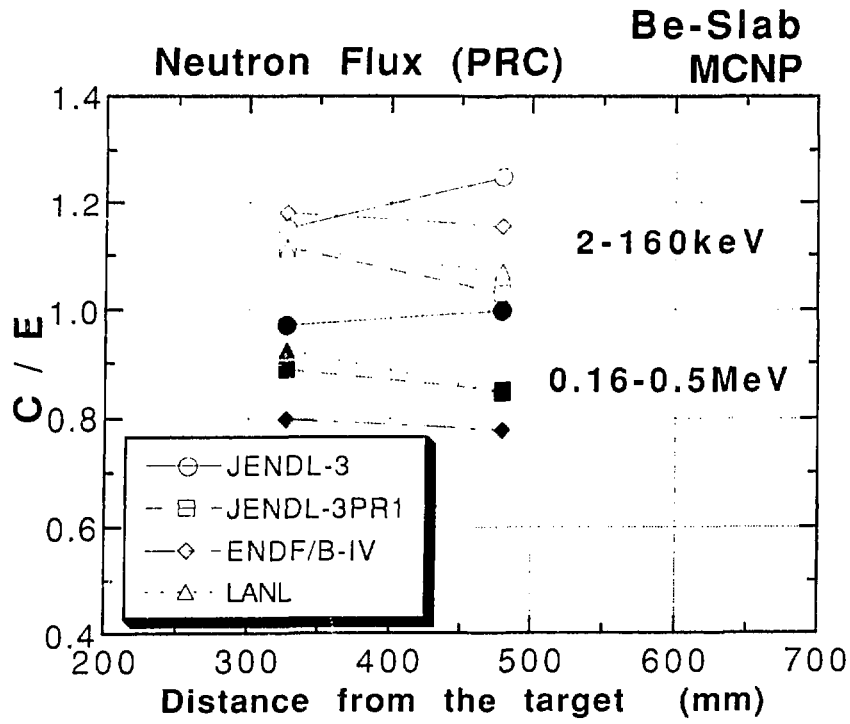

Fig. 5 Comparison of C/E values for integral flux in Be assembly.

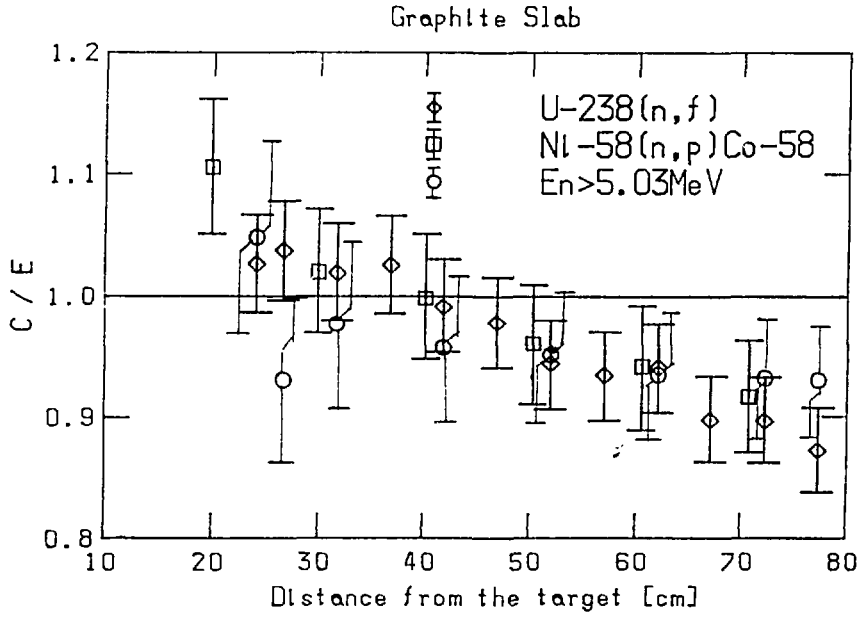

Fig. 6 Comparison of C/E values for $^{238}U(n,f)$, $^{58}Ni(n,p)^{58}Co$ and integrated flux above 5 MeV in C assembly.

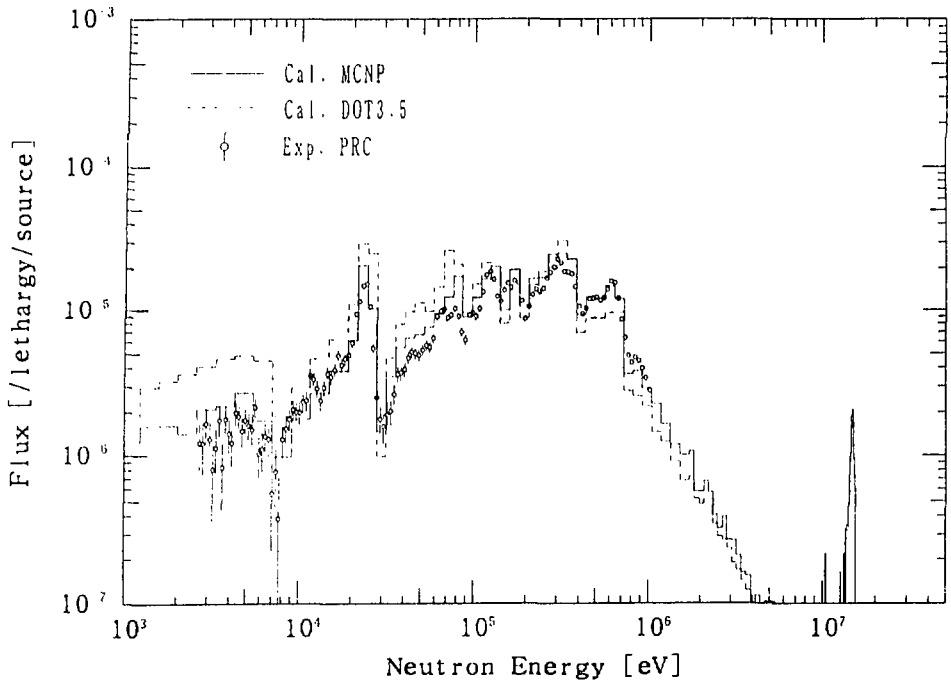

Fig. 7 Measured and calculated neutron spectra in Fe assembly at 610mm from the target.

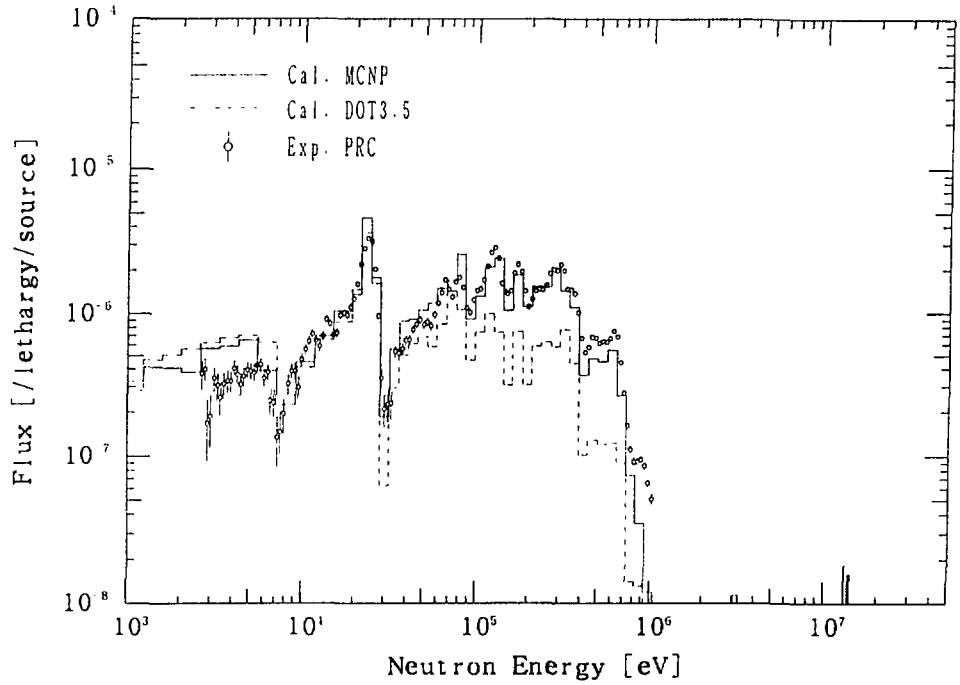

Fig. 8 Measured and calculated neutron spectra in Fe assembly at 1010mm from the target.

11.5 Measurement of Leakage Neutron Spectra from Various Sphere Piles for Fusion Reactor Related Materials with 14 MeV Neutrons

Chihiro Ichihara, Shu A. Hayashi, Katsuhei Kobayashi
Research Reactor Institute, Kyoto University
Kumatori-cho, Sennan-gun, Osaka 590-04

Itsuro Kimura
Dept. Nuclear Engineering, Kyoto University
Yoshida-honmachi, Sakyo-ku, Kyoto 606

Junji Yamamoto, and Akito Takahashi
Dept. Nuclear Engineering, Osaka University
2-1 Yamada-oka, Suita, Osaka 565

Abstract

In order to examine the existing nuclear data files related to the fusion reactor materials, neutron leakage current from the sphere piles of various kinds of samples have been measured using the intense pulsed 14 MeV neutron source, OKTAVIAN and a time-of-flight technique. Measured samples include 1) fluorine-related samples, i.e. LiF, and TEFLON:$(CF_2)_n$, 2) fusion reactor structural materials and others, Li, Aℓ, Si, Ti, Cr, Mn, Co, Cu, Zr, Nb, Mo, and W. The thickness of the piles were from 0.5 to 4.7 mean free paths for 14 MeV neutrons. The neutron energy spectra from the above piles were obtained in the energy range from 0.1 to 14 MeV. The obtained data were compared with the theoretical calculations using MCNP and ANISN transport codes and the evaluated data files, JENDL-3 and others. For each pile, some discussions and comments were presented in the integral assessment.

1. Introduction

An integral experiment is useful for the examination of the existing data files and calculation method. We have measured the angular flux in the fission reactor candidate materials using time-of-flight techniques and photoneutrons from the electron linac at Kyoto University Research Reactor Institute. The results were analyzed using one-dimensional Sn codes, mainly ANISN and multi-group constants from JENDL-2 or ENDF/B-IV nuclear data [1)-3)]. The design study of the fusion reactor or fusion-fission hybrid reactors needs the evaluated data at higher energy region.

The new version of Japanese Evaluated Nuclear data (JENDL-3)[4)] were published and are expected to respond these requirements. The present paper describes the results of the integral experiments performed at the OKTAVIAN facility and the calculation obtained by

using MCNP[5] and ANISN[6] codes with JENDL-3 and other evaluated nuclear data files for the comparison.

2. Experiment

2.1 Sample piles

The samples were formed as spherical piles so as to place the tritium neutron producing target at their centers. The samples include lithium, lithium fluoride, TEFLON: $(CF_2)_n$, aluminum, silicon, titanium, chromium, manganese, cobalt, copper, zirconium, niobium, molybdenum, and tungsten. Powdered or flaked samples were packed into spherical shells made of stainless steel or carbon steel. The detail of the samples are listed in **Table 1**, where pile diameters, sample thicknesses (both in centimeters and in mean free paths for 14 MeV neutrons) are given. The geometries of the piles are shown in **Fig.1** to **4**.

2.2 Experimental setup

The experiment has been performed by the time-of-flight (TOF) technique using the intense 14 MeV neutron source facility OKTAVIAN[7] at Osaka University. The experimental arrangement in the OKTAVIAN facility is shown in **Fig.5**. A tritium neutron producing target was placed at the center of the pile. The energy of the incident deuterons was about 250 keV. A cylindrical liquid organic scintillator NE-218 (12.7 cm-diam × 5.1 cm-long) was used as a neutron detector, which was located about 11 m from the tritium target, and 55° with respect to the deuteron beam axis. A pre-collimator made of polyethylene-iron multi-layers was set between the pile and the detector in order to reduce the background neutrons. The aperture size of this collimator was determined so that the whole surface of the piles facing the detector could be viewed.

3. Data Processing

The detector efficiency was determined by combining, 1) the Monte Carlo calculation, 2) the measured efficiency derived from the TOF measurement of ^{252}Cf spontaneous fission spectrum, and 3) the measured efficiency from the leakage spectrum from a graphite sphere, 30 cm in diameter with the similar detection system.

To monitor the absolute number of the source neutrons during each run, a cylindrical niobium foil was set in front of the tritium target and irradiated during the TOF experiment.

From the γ-ray intensity of the induced activity, ^{92m}Nb and the integrated counts of the source neutron spectrum, the absolute neutron leakage spectrum can be obtained. The formulation of this procedure is stated elsewhere[8].

4. Calculations

The theoretical calculations were performed using mostly MCNP, which is a three-dimensional continuous energy Monte Carlo transport code. The continuous libraries for MCNP were FSXLIB[9] derived from JENDL-3. For some samples the libraries from JENDL-3T, the test version of JENDL-3 were used. In addition to these JENDL-3 based libraries, BMCCS, and ENDL-85 attached with MCNP code were also used for the reference. For Mn pile, one-dimensional Sn transport code, ANISN was used. The 125-group cross section library FUSION-J3[10] (P5S16) was used for this calculation.

In the Table-1, the calculation code and the data libraries are summarized.

5. Results

The measured and calculated spectra are shown in Fig.6 through 19.

5.1 LiF and lithium

The neutron leakage spectrum from the LiF 61 cm pile was measured for the examination of the cross section data of fluorine. A leakage spectrum from a lithium 40 cm pile spectrum was measured by Sugiyama, et al. using the Time-of-flight technique at OKTAVIAN before[11]. We also measured the leakage spectrum from this lithium pile in order to presume the fluorine data by comparing LiF and Li results. The predicted spectra for LiF using JENDL-3(Li,F), and LASL-subset(Li) and ENDF/B-IV(F) show considerable underestimation in almost whole energy range (**Fig.6**). The discrepancy is especially large between 4 and 14 MeV, and below 2 MeV. In 4 MeV<En<12 MeV energy range, the JENDL-3 calculation gives lower value than the other one does. In **Fig.7** are given the experimental and calculated leakage spectra from the 40 cm lithium sphere in a similar manner and using the same data libraries as the LiF sphere for the reference. In this result, the difference between measured and calculated spectra is not so large as the LiF results. Especially, the experimental and calculated spectra below 3 MeV agree with each other within experimental errors. Therefore, the cause of the large difference in the experimental and calculated spectra will principally be attributed to the cross sections of fluorine of both

JENDL-3 and ENDF/B-IV.

The calculated spectra for Li with JENDL-3 and LASL-subset below 10 MeV is almost equivalent, and the only difference appears between 10 MeV and 13 MeV. On the other hand, the calculated spectra for LiF pile with JENDL-3 and the other data differ between 6 and 13 MeV. This implies that the fluorine data in JENDL-3 gives the principal difference between 6 and 10 MeV in the LiF calculation, and the discrepancy in the LiF calculation between 10 MeV and 13 MeV will be due to the lithium data in both JENDL-3 and LASL-subset.

5.2 TEFLON

For a TEFLON 40 cm pile, the two calculation badly underestimate the measurement (**Fig.8**). Both calculation give almost same calculated spectra. Since the calculations for the LiF pile give underestimation similar to the TEFLON pile, the difference between the experiment and calculation for TEFLON can be attributed to the fluorine data, possibly inelastic scattering cross sections.

5.3 Aluminum

Though the general shape of the experimental spectrum can be predicted with both JENDL-3 and ENDF/B-IV libraries, the discrepancies in the range from 4 MeV to the elastic scattering peak are observed for the Aℓ 40 cm pile (**Fig.9**). The underestimation with ENDF/B-IV between 9 and 12 MeV probably comes from the problem as to the inelastic level scattering cross sections of aluminum. On the other hand, the prediction with JENDL-3 underestimates the experiment in wider energy range e.g. between 4 and 10 MeV. However, the calculated spectrum except for this range is almost same as the ENDF/B-IV calculation. The aluminum data in JENDL-3 might have further problem such as the $(n,2n)$ and inelastic level scattering cross sections.

5.4 Silicon

The **Figure 10** shows the experimental and calculated leakage neutron spectra from a silicon 60 cm pile. The calculation with JENDL-3 is in fair agreement with the experiment in general compared with the old ENDL-III calculation. However, there still exists some amount of discrepancies in the energy range 0.2 MeV<En<2 MeV and around 10 MeV. This

fact implies the problems in the cross section data, possibly the inelastic continuum scattering, and inelastic level scattering, respectively.

5.5 Titanium

Though the calculated spectra with JENDL-3T and ENDF/B-IV for a Ti 40 cm pile well predict the elastic scattering peak, the other part of the spectra differs considerably (**Fig.11**). The discrepancies below 8 MeV in both calculated spectra can be attributed to the problem of continuum inelastic scattering and/or $(n,2n)$ cross sections. The underestimation of JENDL-3T spectrum in the energy range 8 MeV<En<12 MeV will be due to the inelastic level scattering cross sections.

5.6 Chromium

For a Cr 40 cm pile, a quite different spectrum from the experiment was obtained by the calculation using ENDF/B-IV data (**Fig.12**). It seems that the inelastic level scattering cross sections of chromium in ENDF/B-IV is far inadequate. JENDL-3 data give a good prediction, being in almost good agreement with the experiment in the whole energy range. The JENDL-3 data for Cr can be considered as satisfactory.

5.7 Manganese

For a Mn 61 cm pile, the ENDF/B-IV prediction gives an erroneous spectrum for the energy range 1 MeV<En<14 MeV (**Fig.13**). The JENDL-3 data give a greatly improved prediction, but there still exists a little discrepancy above 5 MeV probably due to the $(n,2n)$ and/or inelastic level scattering cross sections.

5.8 Cobalt

The calculated spectra for a 40 cm Co pile show large underestimation to the experiment in general (**Fig.14**). The JENDL-3 spectrum agrees well with the experiment above 11 MeV, though it disagrees badly between 8 MeV and 11 MeV, where the inelastic level scattering are still dominant. This fact implies that the inelastic scattering cross sections to the higher levels have been ignored. The calculated spectrum with JENDL-3 below 8 MeV are slightly better than the ENDL-85 spectrum. However, the discrepancy from the experimental result is very large in both cases, which suggests the continuum part of the inelastic scattering

and/or $(n,2n)$ cross sections are suspicious.

5.9 Copper

The spectrum calculated with ENDF/B-IV considerably underestimates the experimental one around 10 MeV for a Cu 61 cm pile (**Fig.15**). However, other part of the calculation seems fair. The calculation using JENDL-3 data predicts the experiment quite well. It can be concluded that JENDL-3 data are quite satisfactory for copper.

5.10 Zirconium

For the Zr 61 cm pile, the calculated spectrum with JENDL-3 gives an improved prediction compared with the ENDL-85 spectrum (**Fig.16**). However, the JENDL-3 calculation gives a slight overestimation (10 to 30 % of the spectral values) throughout the whole energy range below the elastic peak, which is probably due to the problem of the inelastic scattering and/or $(n,2n)$ cross sections. Also, a considerable underestimation appears at the lower part of the elastic peak (10 MeV<En<13 MeV), which is probably due to the ignorance or inadequate evaluation of the inelastic scattering cross sections to the discrete levels.

5.11 Niobium

The calculated spectrum with JENDL-3 for a Nb 28 cm pile gives much improved prediction compared with the ENDF/B-IV one (**Fig.17**). The agreement is excellent for the elastic scattering peak and in the energy region 0.4 Mev<En<6 MeV. There exists some overestimation below the elastic scattering peak and considerable overestimation below 0.4 MeV. The former is probably due to unreasonably high inelastic level scattering cross section to the excited levels. The latter overestimation might be due to the continuum part of the inelastic scattering cross sections, and/or secondary neutron energy distribution.

5.12 Molybdenum

The calculated spectrum with ENDL-85 gives considerable discrepancy for a Mo 61 cm pile (**Fig.18**). On the other hand, the Mo data in JENDL-3 can be considered much improved as the JENDL-3 calculated spectrum agrees pretty well except for the region 3 MeV<E_n<13 MeV, where considerable underestimation is given. It can be estimated that the inelastic scattering cross sections to the excited levels have been ignored or inadequate.

5.13 Tungsten

The calculated spectrum for a W 40 cm pile using the data from JENDL-3 gives an improved prediction compared with the ENDL-85 one (**Fig.19**). The JENDL-3 calculation roughly agrees below 3 MeV, but for 0.5 MeV<En<1.3 MeV range, it gives a considerable underestimation. It also gives a severe underestimation in the region 3 MeV<En<13 MeV. The $(n,2n)$ cross section should be checked for the cause of the former discrepancy. For the latter cause, the inelastic scattering cross sections for the higher excited levels of the tungsten isotopes should be examined.

Acknowledgement

Part of this work has been supported by a Grant-in-Aid for Scientific Research from the Ministry of Education, Science and Culture, Japan. This is also undertaken with the framework of the co-operative research program of the OKTAVIAN facility. We express sincere thanks to the joint study group of university faculties directed by Prof. Kazunori Sugiyama of Tohoku University for providing the lithium sample pile. We are very much grateful to Prof. Kenji Sumita of Osaka University for his continuous support for this work.

References

1) I. Kimura, et al.: *Nucl. Data for Science and Technology*, 98(1983)
2) T. Mori, et al.: *ibid.*, 22[9], 708(1983)
3) S. A. Hayashi, et al.: *J. Nucl. Sci. Technol*, 24[9], 702(1987)
4) K. Shibata, et al.: *Japanese Evaluated Nuclear Data Library, Version-3 - JENDL-3 -*, JAERI 1319(1990)
5) J. F. Briesmeister ed.: *MCNP-A General Monte Carlo Code for Neutron and Photon Transport, LA-73966-M*, Rev.2, (1986)
6) W. W. Engle, Jr.: *K-1693*, (1967)
7) K. Sumita, et al.: *Proc. 12th SOFT*, Vol.1, 687(1982)
8) A. Takahashi, et el.: *OKTAVIAN Report*, C-8302(1983)
9) K. Kosako, et al.: *private communication*
10) K. Maki, et al.: *private communication*
11) K. Sugiyama, et al.: *OKTAVIAN Report*, C-86-02(1986)

Table 1 Characteristic parameters of the sample piles.

Pile	Dia. (cm)	Sample-Thick. (cm)	(MFPs)	Calc. Code	Data Library
Li	40	9.8	0.6	MCNP	^{6}Li,^{7}Li,F:J3 ^{6}Li:LASL ^{7}Li:B-Ⅳ
LiF	61	27.5	3.5	MCNP	6Li,7Li:J3 F:J3 ^{6}Li:LASL ^{7}Li:B-Ⅳ F:B-Ⅳ
TEFLON	40	9.8	0.7	MCNP	C,F:J3 C:LASL F:B-Ⅳ
Al	40	9.8	0.5	MCNP	J3, B-Ⅳ
Si	60	20.0	1.1	MCNP	J3, B-Ⅲ
Ti	40	9.8	0.5	MCNP	J3T, B-Ⅳ
Cr	40	9.8	0.7	MCNP	J3, B-Ⅳ
Mn	60	27.5	3.4	ANISN	J3T, B-Ⅳ
Co	40	9.8	0.5	MCNP	J3, E-85
Cu	61	27.5	4.7	MCNP	J3T, B-Ⅳ
Zr	61	27.5	2.0	MCNP	J3, E-85
Nb	28	11.2	1.1	MCNP	J3, B-Ⅳ
Mo	61	27.5	1.5	MCNP	J3, E-85
W	40	9.8	0.8	MCNP	J3, E-85

J3: JENDL-3, J3T: JENDL-3T, LASL: LASL subset
B-Ⅳ: ENDF/B-Ⅳ, B-Ⅲ: ENDF/B-Ⅲ, E85: ENDL-85

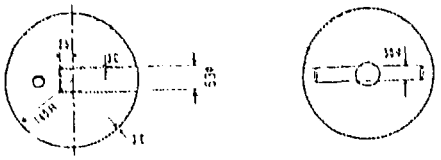

Fig. 1 28 cm diameter pile for Nb

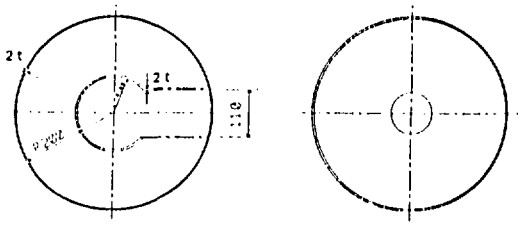

Fig. 2 40 cm diameter pile for Li, TEFLON, Aℓ, Ti, Cr, Co, and W

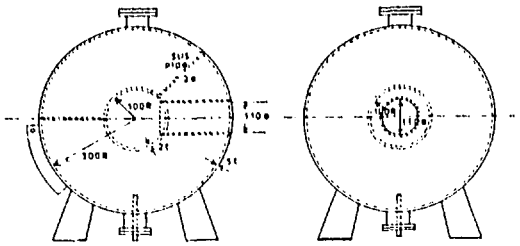

Fig. 3 60 cm diameter pile for Si

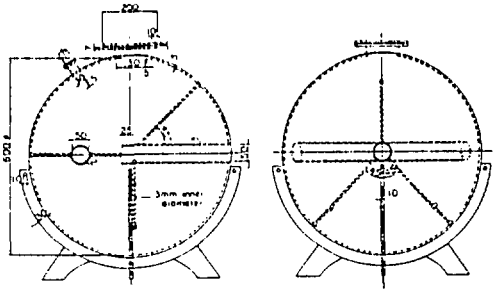

Fig. 4 61 cm diameter pile for LiF, Mn, Cu, and Mo

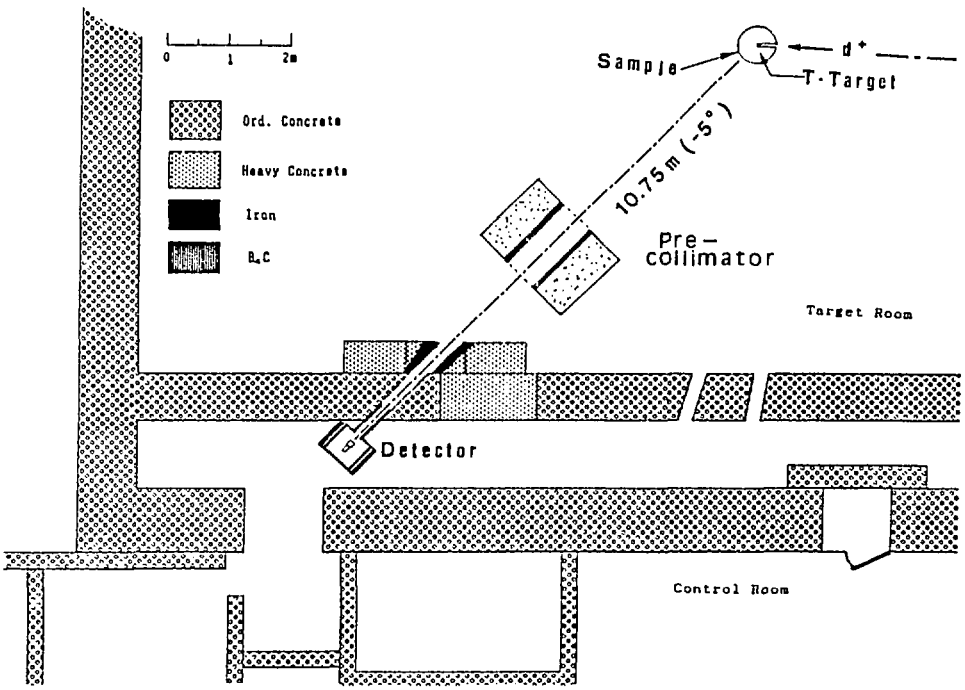

Fig. 5 Experimental arrangement in the OKTAVIAN Facility

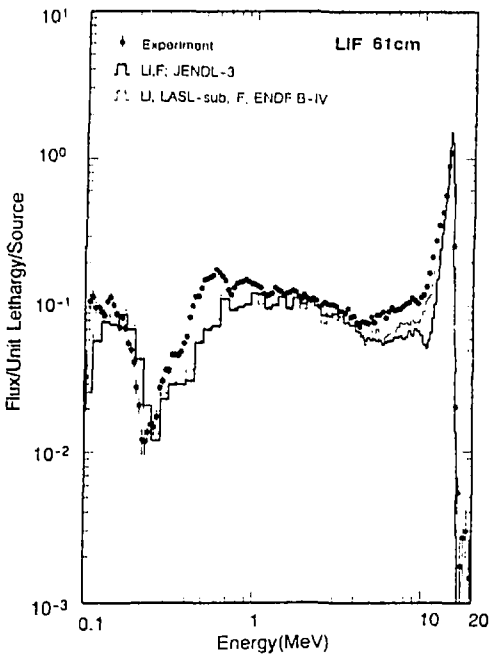

Fig. 6 Experimental and calculated spectra from LiF 61 cm pile

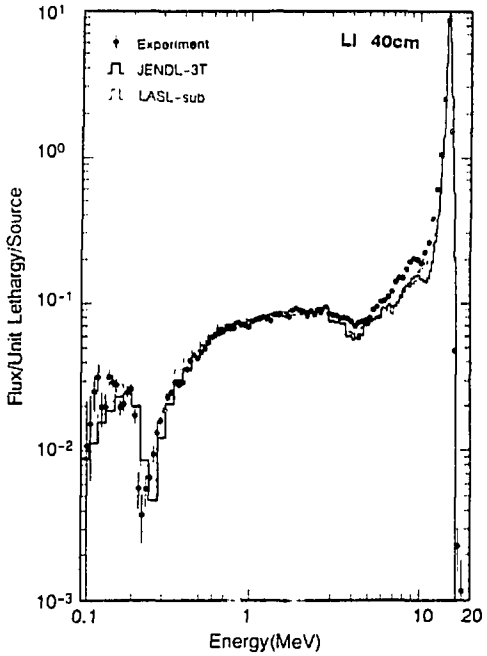

Fig. 7 Experimental and calculated spectra from Li 40 cm pile

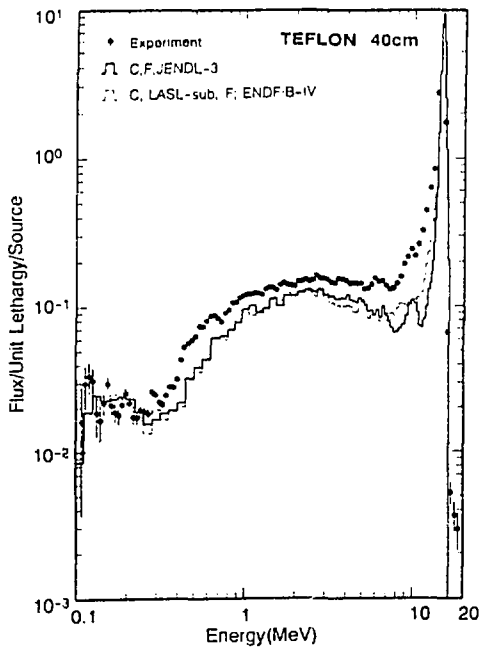

Fig. 8 Experimental and calculated spectra from TEFLON 40 cm pile

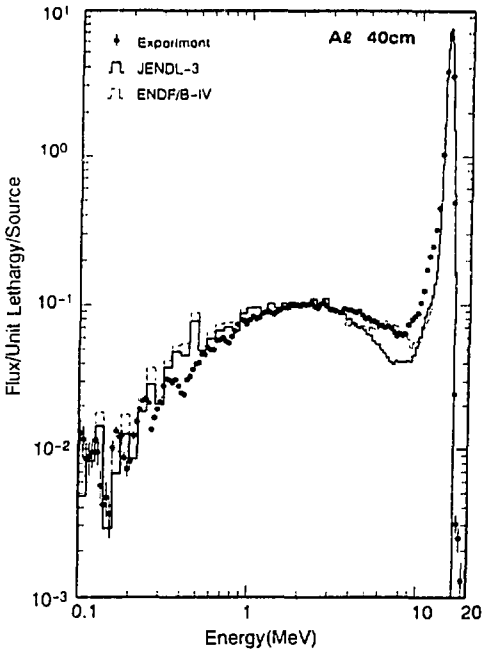

Fig. 9 Experimental and calculated spectra from Aℓ 40 cm pile

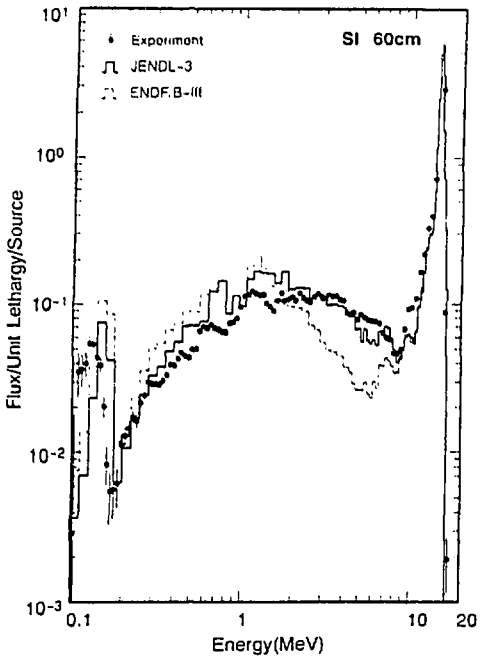

Fig. 10 Experimental and calculated spectra from Si 60 cm pile

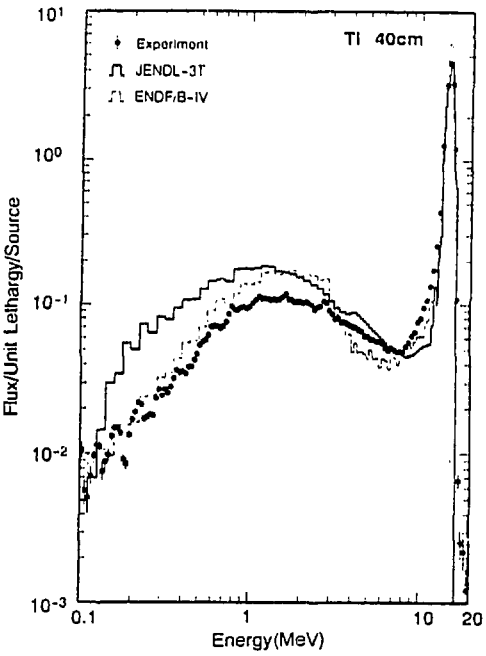

Fig. 11 Experimental and calculated spectra from Ti 40 cm pile

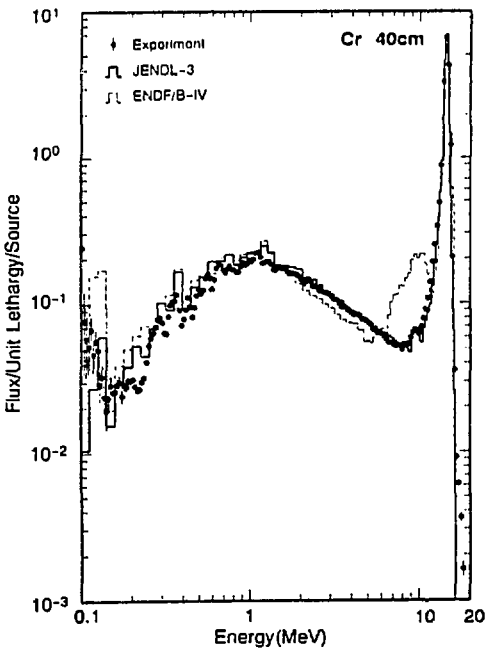

Fig. 12 Experimental and calculated spectra from Cr 40 cm pile

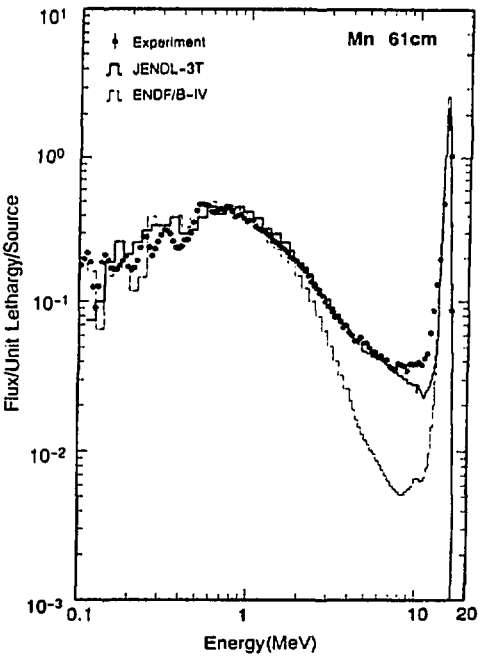

Fig. 13 Experimental and calculated spectra from Mn 61 cm pile

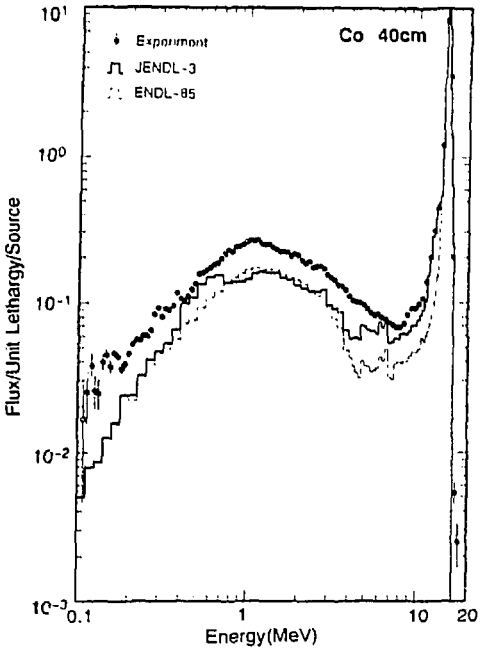

Fig. 14 Experimental and calculated spectra from Co 40 cm pile

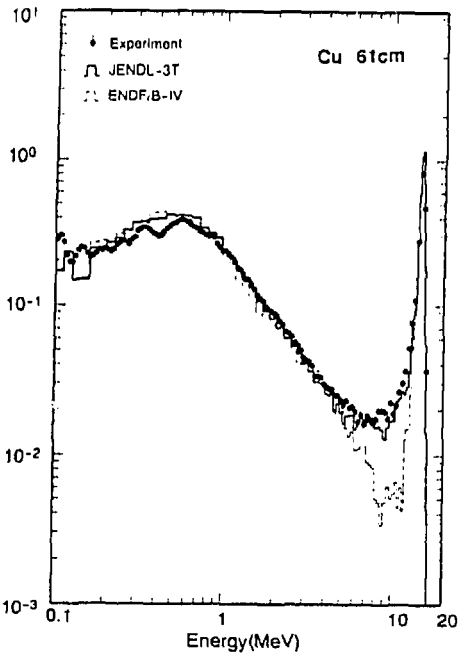

Fig. 15 Experimental and calculated spectra from Cu 61 cm pile

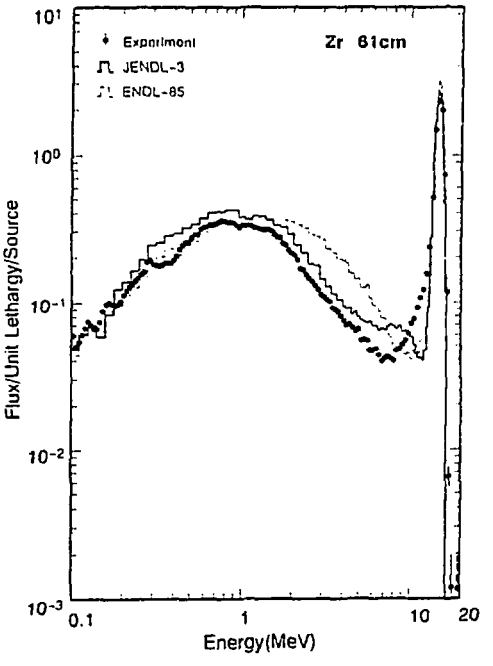

Fig. 16 Experimental and calculated spectra from Zr 61 cm pile

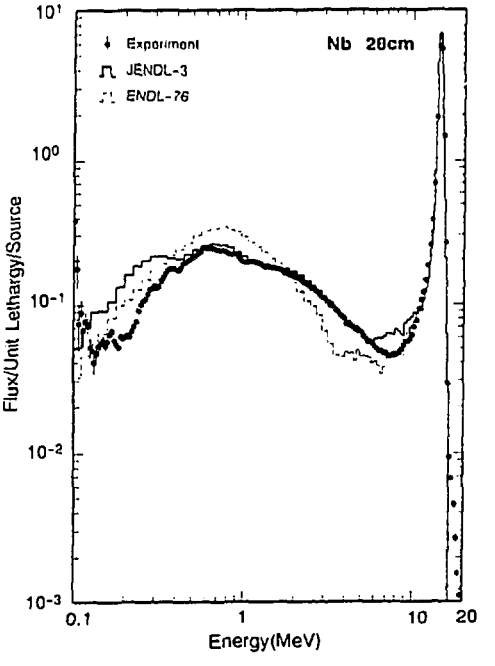

Fig. 17 Experimental and calculated spectra from Nb 28 cm pile

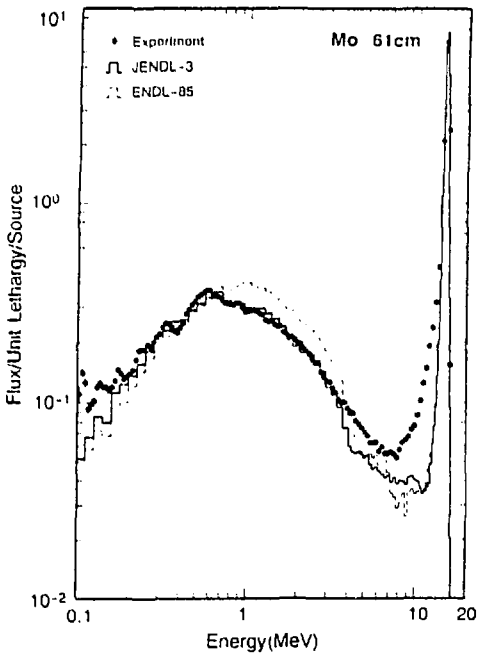

Fig. 18 Experimental and calculated spectra from Mo 61 cm pile

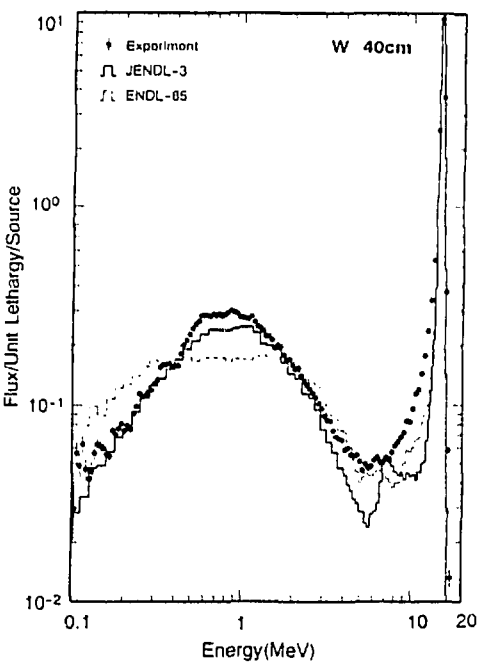

Fig. 19 Experimental and calculated spectra from W 40 cm pile

Appendix I The Program of the Second Specialists' Meeting on Nuclear Data for Fusion Reactors

December 20 (Thuirsday)

	Speaker	
10:30 - 10:35		
1. Opening Address	M. ISHII(JAERI)	(5 min)
10:35 - 11:20		
2. Nuclear Data for Fusion Reactors and Development of JENDL-3	Chairman: Y. NAKAJIMA(JAERI)	
2. 1 Plan and Objective of the Meeting	H. MAEKAWA(JAERI)	(15 min)
2. 2 Review of JENDL-3 Evaluation Work	T. NAKAGAWA(JAERI)	(25 min)
11:20 - 12:00		
3. Preparation of Reactor Constants	Chairman: N. YAMANO(SAEI)	
3. 1 Production of JSSTDL295 Standard Library	A. HASEGAWA(JAERI)	(20 min)
3. 2 MCNP Cross Section Library Based on JENDL-3	K. KOSAKO(JAERI)	(15 min)
12:00 - 13:00 Lunch		
13:00 - 14:50		
4. Nuclear Data Relevant to Blankets of Fusion Reactors (Mainly Light Nuclides)	Chairman: M. BABA(Tohoku U.)	
4. 1 Review of JENDL-3 Data Relevant to Blankets	S. CHIBA(JAERI)	(20 min)
4. 2 Results of Benchmark Tests (Speakers are given in Appendix II) and Discussion		(90 min)
14:50 - 15:05 Coffee Break		
15:05 - 16:35		
5. Nuclear Data Relevant to Structural Materials (Mainly Medium Weight Nuclides)	Chairman: Y. KANDA(Kyushu U.)	
5. 1 Review of JENDL-3 Data Relevant to Structural Materials	S. IIJIMA(Toshiba) and T. ASAMI(NEDAC)	(20 min)
5. 2 Results of Benchmark Tests (Speakers are given in Appendix II) and Discussion		
16:35 - 17:30		
6. Analyses of Engineering Benchmark Experiments	Chairman: Y. IKEDA(JAERI)	
6. 1 Integral Test of JENDL-3 Through Analysis of Fusion Blanket Experiment Phase IIB	M. NAKAGAWA(JAERI)	(20 min)
6. 2 Experiment of Multi-layer Li Sphere(Evaluation on Tritium Breeding Ratio)	J. CETNAR and T. IGUCHI(U. of Tokyo)	(15 min)
6. 3 Experiment of Multi-layer Li Sphere(Distribution of Time Dependent Tritium Production Rate)	A. TAKAHASHI(Osaka U.)	(15 min)
18:00 - 20:00 Reception at Akogigaura Club		

December 21 (Friday)

9:10 - 10:50
7. Nuclear Data Relevant to Gamma Rays
Chairman: K. SHIN(Kyoto U.)
7. 1 Review of Photon Production Data in JENDL-3 M. IGASHIRA(TIT) (20 min)
7. 2 Experiments of Nuclear Heating by Gamma-Rays at FNS
Y. OYAMA(JAERI) (25 min)
7. 3 Integral Experiments on Gamma-Ray Production at OKTAVIAN
J. YAMAMOTO(Osaka U.) (25 min)
7. 4 Analysis of ORNL 14 MeV SUS304 Benchmark Experiment
K. SAKURAI(JAERI) and K. UEKI(Ship Research Inst.) (20 min)

10:50 - 11:00 Coffee Break

11:00 - 12:05
8. Activation Cross Section Data
Chairman: Y. NAKAJIMA(JAERI)
8. 1 Review of Activation Cross Section Data in JENDL
N. YAMAMURO(Data Eng.) (20 min)
8. 2 Activation Cross Sections of Fusion Structural Materials
Y. IKEDA(JAERI) (20 min)
8. 3 Estimation of Accuracy of Data in JENDL-3 Dosimetry File
T. IGUCHI(U. of Tokyo) (20 min)

13:10 - 13:35
9. KERMA, PKA and DPA Files
Chairman: S. IWASAKI(Tohoku U.)
9. 1 Evaluation and Compilation of KERMA, PKA and DPA File
M. KAWAI(Toshiba) (20 min)

13:35 - 14:30
10. Requirements and Comments from Fusion Reactor Design
Chairman: S. MORI(KHI)
10. 1 Nuclear Data Needs from Fusion Reactor Safety Analysis
Y. SEKI(JAERI) (20 min)
10. 2 Requirements for Nuclear Data from ITER/EFR Nuclear Design
K. MAKI(JAERI) (20 min)

14:30 - 14:40 Coffee Bre k

14:40 - 16:10
11. Discussion
Chairman: A. TAKAHASHI(Osaka U.)
11. 1 Summary Talk (Priority, Strategy, etc) H. MAEKAWA(JAERI) (15 min)
11. 2 Discussion (75 min)

16:10 - 16:15
12. Closing Address Y. KANEKO(JAERI) (5 min)

Appendix II Presentations of the Analysis of Benchmark Experiments

1. Nuclear Data Relevant to the Blanket Materials of Fusion Reactors (Session 4)

Nuclides	Benchmark Experiments	Speaker
^{6}Li	LLNL Pulsed Sphere Program	K. UEKI and M. KAWAI
	〃	M. NAKAGAWA
^{7}Li	LLNL Pulsed Sphere Program	K. UEKI and M. KAWAI
	〃	M. NAKAGAWA
	FNS TOF Experiment(Li_2O)	Y. OYAMA
	FNS Integral Experiment(Li_2O)	H. MAEKAWA
^{9}Be	LLNL Pulsed Sphere Program	K. UEKI and M. KAWAI
	〃	M. NAKAGAWA
	FNS TOF Experiment	Y. OYAMA
	FNS Integral Experiment	H. MAEKAWA
	Kurchatov Multplication Experiment	M. NAKAGAWA
^{12}C	LLNL Pulsed Sphere Program	K. UEKI and M. KAWAI
	FNS TOF Experiment	Y. OYAMA
	FNS Integral Experiment	H. MAEKAWA
^{14}N	FNS TOF Experiment	H. MAEKAWA
^{16}O	FNS TOF Experiment	H. MAEKAWA
	LLNL Pulsed Sphere Program	K. UEKI and M. KAWAI
^{19}F	OKTAVIAN TOF Experiment(LiF, CF_2)	C. ICHIHARA
Pb	LLNL Pulsed Sphere Program	M. NAKAGAWA
	FNS TOF Experiment	H. MAEKAWA

2. Nuclear Data Relevant to the Structural Materials of Fusion Reactors(Session 5)

Nuclides	Benchmark Experiments	Speaker
Al	OKTAVIAN TOF Experiment	C. ICHIHARA
Si	OKTAVIAN TOF Experiment	C. ICHIHARA
Cr	OKTAVIAN TOF Experiment	C. ICHIHARA
Mn	OKTAVIAN TOF Experiment	C. ICHIHARA
Fe	FNS TOF Experiment	Y. OYAMA
	FNS Integral Experiment	C. KONNO
	LLNL Pulsed Sphere Program	K. UEKI and M. KAWAI
Co	OKTAVIAN TOF Experiment	C. ICHIHARA
Cu	OKTAVIAN TOF Experiment	C. ICHIHARA
Zr	OKTAVIAN TOF Experiment	C. ICHIHARA
Nb	OKTAVIAN TOF Experiment	C. ICHIHARA
Mo	OKTAVIAN TOF Experiment	C. ICHIHARA
W	OKTAVIAN TOF Experiment	C. ICHIHARA

Appendix III List of Participants for the Second Specialists' Meeting on Nuclear Data for Fusion Reactors

Participant		Affiliation
Takeo	ARUGA	Japan Atomic Energy Research Institute
Tetsuo	ASAMI	Nuclear Energy Data Center
Mamoru	BABA	Tohoku University
Jerzy	CETNAR	University of Tokyo
Satoshi	CHIBA	Japan Atomic Energy Research Institute
Tokio	FUKAHORI	Japan Atomic Energy Research Institute
Hiroyuki	HANDA	Hitachi Engineering Co. Ltd.
Akira	HASEGAWA	Japan Atomic Energy Research Institute
Chihiro	ICHIHARA	Kyoto University, Research Reactor Institute
Sin-iti	IGARASI	Nuclear Energy Data Center
Masayuki	IGASHIRA	Tokyo Institute of Technology, Institute of Reactor Technology
Tetsuo	IGUCHI	University of Tokyo
Yujiro	IKEDA	Japan Atomic Energy Research Institute
Mitsuhiko	ISHII	Japan Atomic Energy Research Institute
Shikoh	ITOH	Nagoya University
Shin	IWASAKI	Tohoku University
Yukinori	KANDA	Kyushu University
Yoshihiko	KANEKO	Japan Atomic Energy Research Institute
Masayoshi	KAWAI	Toshiba Corp.
Yasuyuki	KIKUCHI	Japan Atomic Energy Research Institute
Chikara	KONNO	Japan Atomic Energy Research Institute
Kazuaki	KOSAKO	Japan Atomic Energy Research Institute
Fujio	MAEKAWA	Japan Atomic Energy Research Institute
Hiroshi	MAEKAWA	Japan Atomic Energy Research Institute
Koichi	MAKI	Japan Atomic Energy Research Institute
Motoharu	MIZUMOTO	Japan Atomic Energy Research Institute
Seiji	MORI	Kawasaki Heavy Industries Ltd.
Takamasa	MORI	Japan Atomic Energy Research Institute
Masayuki	NAKAGAWA	Japan Atomic Energy Research Institute
Tsuneo	NAKAGAWA	Japan Atomic Energy Research Institute
Yutaka	NAKAJIMA	Japan Atomic Energy Research Institute
Hiroshi	NAKASHIMA	Japan Atomic Energy Research Institute
Yukio	OYAMA	Japan Atomic Energy Research Institute
Yasushi	SEKI	Japan Atomic Energy Research Institute
Kazuo	SHIN	Kyoto university
Akito	TAKAHASHI	Osaka University
Tooru	TATENO	Mitsubishi Atomic Power Industries Inc.
Kohtaro	UEKI	Ship Research Institute
Takashi	WATANABE	Kawasaki Heavy Industries Ltd.
Junji	YAMAMOTO	Osaka University
Nobuhiro	YAMAMURO	Data Engineering Inc.
Naoki	YAMANO	Sumitomo Atomic Energy Industries Ltd.
Baosheng	YU	Japan Atomic Energy Research Institute/IAE (China)

国際単位系(SI)と換算表

表1　SI基本単位および補助単位

量	名称	記号
長さ	メートル	m
質量	キログラム	kg
時間	秒	s
電流	アンペア	A
熱力学温度	ケルビン	K
物質量	モル	mol
光度	カンデラ	cd
平面角	ラジアン	rad
立体角	ステラジアン	sr

表2　SIと併用される単位

名称	記号
分，時，日	min, h, d
度，分，秒	°, ′, ″
リットル	l, L
トン	t
電子ボルト	eV
原子質量単位	u

1 eV = 1.60218×10^{-19} J
1 u = 1.66054×10^{-27} kg

表5　SI接頭語

倍数	接頭語	記号
10^{18}	エクサ	E
10^{15}	ペタ	P
10^{12}	テラ	T
10^{9}	ギガ	G
10^{6}	メガ	M
10^{3}	キロ	k
10^{2}	ヘクト	h
10^{1}	デカ	da
10^{-1}	デシ	d
10^{-2}	センチ	c
10^{-3}	ミリ	m
10^{-6}	マイクロ	μ
10^{-9}	ナノ	n
10^{-12}	ピコ	p
10^{-15}	フェムト	f
10^{-18}	アト	a

表3　固有の名称をもつSI組立単位

量	名称	記号	他のSI単位による表現
周波数	ヘルツ	Hz	s^{-1}
力	ニュートン	N	$m\cdot kg/s^2$
圧力，応力	パスカル	Pa	N/m^2
エネルギー，仕事，熱量	ジュール	J	$N\cdot m$
工率，放射束	ワット	W	J/s
電気量，電荷	クーロン	C	A·s
電位，電圧，起電力	ボルト	V	W/A
静電容量	ファラド	F	C/V
電気抵抗	オーム	Ω	V/A
コンダクタンス	ジーメンス	S	A/V
磁束	ウェーバ	Wb	V·s
磁束密度	テスラ	T	Wb/m^2
インダクタンス	ヘンリー	H	Wb/A
セルシウス温度	セルシウス度	°C	
光束	ルーメン	lm	cd·sr
照度	ルクス	lx	lm/m^2
放射能	ベクレル	Bq	s^{-1}
吸収線量	グレイ	Gy	J/kg
線量当量	シーベルト	Sv	J/kg

表4　SIと共に暫定的に維持される単位

名称	記号
オングストローム	Å
バーン	b
バール	bar
ガル	Gal
キュリー	Ci
レントゲン	R
ラド	rad
レム	rem

1 Å = 0.1 nm = 10^{-10} m
1 b = 100 fm^2 = 10^{-28} m^2
1 bar = 0.1 MPa = 10^{5} Pa
1 Gal = 1 cm/s^2 = 10^{-2} m/s^2
1 Ci = 3.7×10^{10} Bq
1 R = 2.58×10^{-4} C/kg
1 rad = 1 cGy = 10^{-2} Gy
1 rem = 1 cSv = 10^{-2} Sv

(注)

1. 表1－5は「国際単位系」第5版，国際度量衡局 1985年刊行による。ただし，1 eV および 1 u の値は CODATA の1986年推奨値によった。
2. 表4には海里，ノット，アール，ヘクタールも含まれているが日常の単位なのでここでは省略した。
3. barは，JISでは流体の圧力を表わす場合に限り表2のカテゴリーに分類されている。
4. EC閣僚理事会指令ではbar，barnおよび「血圧の単位」mmHgを表2のカテゴリーに入れている。

換算表

力	N(=10^5 dyn)	kgf	lbf
	1	0.101972	0.224809
	9.80665	1	2.20462
	4.44822	0.453592	1

粘度　1 Pa·s($N\cdot s/m^2$) = 10 P(ポアズ)(g/(cm·s))

動粘度　1 m^2/s = 10^4 St(ストークス)(cm^2/s)

圧	MPa(=10 bar)	kgf/cm^2	atm	mmHg(Torr)	lbf/in^2(psi)
	1	10.1972	9.86923	7.50062×10^{3}	145.038
力	0.0980665	1	0.967841	735.559	14.2233
	0.101325	1.03323	1	760	14.6959
	1.33322×10^{-4}	1.35951×10^{-3}	1.31579×10^{-3}	1	1.93368×10^{-2}
	6.89476×10^{-3}	7.03070×10^{-2}	6.80460×10^{-2}	51.7149	1

エネルギー・仕事・熱量	J(=10^7 erg)	kgf·m	kW·h	cal(計量法)	Btu	ft·lbf	eV
	1	0.101972	2.77778×10^{-7}	0.238889	9.47813×10^{-4}	0.737562	6.24150×10^{18}
	9.80665	1	2.72407×10^{-6}	2.34270	9.29487×10^{-3}	7.23301	6.12082×10^{19}
	3.6×10^{6}	3.67098×10^{5}	1	8.59999×10^{5}	3412.13	2.65522×10^{6}	2.24694×10^{25}
	4.18605	0.426858	1.16279×10^{-6}	1	3.96759×10^{-3}	3.08747	2.61272×10^{19}
	1055.06	107.586	2.93072×10^{-4}	252.042	1	778.172	6.58515×10^{21}
	1.35582	0.138255	3.76616×10^{-7}	0.323890	1.28506×10^{-3}	1	8.46233×10^{18}
	1.60218×10^{-19}	1.63377×10^{-20}	4.45050×10^{-26}	3.82743×10^{-20}	1.51857×10^{-22}	1.18171×10^{-19}	1

1 cal = 4.18605 J(計量法)
　　= 4.184 J(熱化学)
　　= 4.1855 J(15°C)
　　= 4.1868 J(国際蒸気表)

仕事率　1 PS(仏馬力)
　　= 75 kgf·m/s
　　= 735.499 W

放射能	Bq	Ci
	1	2.70270×10^{-11}
	3.7×10^{10}	1

吸収線量	Gy	rad
	1	100
	0.01	1

照射線量	C/kg	R
	1	3876
	2.58×10^{-4}	1

線量当量	Sv	rem
	1	100
	0.01	1

(86年12月26日現在)